



National Library  
of Canada

Acquisitions and  
Bibliographic Services Branch

395 Wellington Street  
Ottawa, Ontario  
K1A 0N4

Bibliothèque nationale  
du Canada

Direction des acquisitions et  
des services bibliographiques

395, rue Wellington  
Ottawa (Ontario)  
K1A 0N4

*Your file - Votre référence*

*Our file - Notre référence*

## NOTICE

The quality of this microform is heavily dependent upon the quality of the original thesis submitted for microfilming. Every effort has been made to ensure the highest quality of reproduction possible.

If pages are missing, contact the university which granted the degree.

Some pages may have indistinct print especially if the original pages were typed with a poor typewriter ribbon or if the university sent us an inferior photocopy.

Reproduction in full or in part of this microform is governed by the Canadian Copyright Act, R.S.C. 1970, c. C-30, and subsequent amendments.

## AVIS

La qualité de cette microforme dépend grandement de la qualité de la thèse soumise au microfilmage. Nous avons tout fait pour assurer une qualité supérieure de reproduction.

S'il manque des pages, veuillez communiquer avec l'université qui a conféré le grade.

La qualité d'impression de certaines pages peut laisser à désirer, surtout si les pages originales ont été dactylographiées à l'aide d'un ruban usé ou si l'université nous a fait parvenir une photocopie de qualité inférieure.

La reproduction, même partielle, de cette microforme est soumise à la Loi canadienne sur le droit d'auteur, SRC 1970, c. C-30, et ses amendements subséquents.

UNIVERSITY OF ALBERTA

THERMAL WELL TEST ANALYSIS AND EVALUATION OF  
RESERVOIR CHARACTERIZATION METHODS USING AN  
ANALYTICAL MULTI-REGION COMPOSITE RESERVOIR MODEL

BY



LUIS GUILLERMO ACOSTA

A THESIS

SUBMITTED TO THE FACULTY OF GRADUATE STUDIES AND RESEARCH IN  
PARTIAL FULFILMENT OF THE REQUIREMENTS FOR THE DEGREE OF

MASTER OF SCIENCE

IN

PETROLEUM ENGINEERING

DEPARTMENT OF MINING, METALLURGICAL AND PETROLEUM  
ENGINEERING

EDMONTON, ALBERTA

SPRING, 1994



National Library  
of Canada

Acquisitions and  
Bibliographic Services Branch

395 Wellington Street  
Ottawa, Ontario  
K1A 0N4

Bibliothèque nationale  
du Canada

Direction des acquisitions et  
des services bibliographiques

395, rue Wellington  
Ottawa (Ontario)  
K1A 0N4

Your file / Votre référence

Your file / Votre référence

**The author has granted an irrevocable non-exclusive licence allowing the National Library of Canada to reproduce, loan, distribute or sell copies of his/her thesis by any means and in any form or format, making this thesis available to interested persons.**

**L'auteur a accordé une licence irrévocable et non exclusive permettant à la Bibliothèque nationale du Canada de reproduire, prêter, distribuer ou vendre des copies de sa thèse de quelque manière et sous quelque forme que ce soit pour mettre des exemplaires de cette thèse à la disposition des personnes intéressées.**

**The author retains ownership of the copyright in his/her thesis. Neither the thesis nor substantial extracts from it may be printed or otherwise reproduced without his/her permission.**

**L'auteur conserve la propriété du droit d'auteur qui protège sa thèse. Ni la thèse ni des extraits substantiels de celle-ci ne doivent être imprimés ou autrement reproduits sans son autorisation.**

ISBN 0-612-11140-7

**Canada**

**UNIVERSITY OF ALBERTA  
RELEASE FORM**

**NAME OF AUTHOR:** Luis Guillermo Acosta

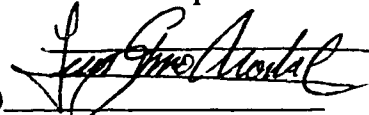
**TITLE OF THESIS:** Thermal Well Test Analysis and Evaluation of  
Reservoir Characterization Methods Using an  
Analytical Multi-Region Composite Reservoir Model

**DEGREE FOR WHICH THESIS WAS PRESENTED:** Master of Science

**YEAR THE DEGREE WAS GRANTED:** Spring, 1994

Permission is hereby granted to THE UNIVERSITY OF ALBERTA LIBRARY to reproduce single copies of this thesis and to lend or sell such copies for private, scholarly or scientific research purposes only.

The author reserves other publication rights, and neither the thesis nor extensive extracts from it may be printed or otherwise reproduced without the author's written permission.

(SIGNED) 


**PERMANENT ADDRESS:**  
250 Hillington Court  
Edmonton, Alberta  
CANADA T5R-5X5

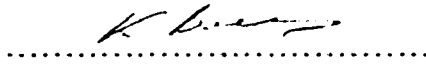
**DATED:** March 16, 1994.

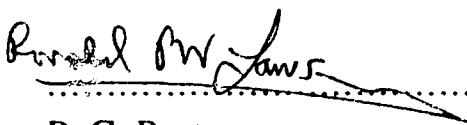



THE UNIVERSITY OF ALBERTA  
FACULTY OF GRADUATE STUDIES AND RESEARCH

The undersigned certify that they have read, and recommend to the Faculty of Graduate Studies and Research for acceptance, a thesis called " THERMAL WELL TEST ANALYSIS AND EVALUATION OF RESERVOIR CHARACTERIZATION METHODS USING AN ANALYTICAL MULTI-REGION COMPOSITE RESERVOIR MODEL " submitted by LUIS GUILLERMO ACOSTA in partial fulfilment of the requirements for the degree of MASTER OF SCIENCE in PETROLEUM ENGINEERING.

  
A. K. Ambastha (Supervisor)

  
K. Barron

  
R. G. Bentsen

  
K. Nandakumar

DATED: February 25, 1994.

## **ABSTRACT**

To monitor the progress of a thermal recovery project, such as a steam injection operation, it is important to have a knowledge of the volume swept by the injecting fluid. Well testing offers a comparatively rapid and economical way of estimating the swept volume. Well tests conducted on wells undergoing a thermal recovery process typically have been idealized using a two or three-region composite reservoir model. Each of these regions has different rock and fluid properties. However, for continuous variations of mobility and storativity within the swept region, a simple two- or three-region model may not be appropriate.

A multi-region, composite reservoir model has been developed to study the effects of various trends of mobility and storativity variations, within the swept region, on well tests for composite reservoirs. This study has been designed to address analytically the problem of multi-region composite reservoir by using the Laplace transformation technique. The solution to the problem in Laplace space is inverted numerically to real space by means of the Stehfest algorithm.

The multi-region composite reservoir model has been used to analyze drawdown tests from reservoirs undergoing a thermal recovery process such as steam injection or in-situ combustion. Based on the mobility and/or storativity of these reservoirs, three zones may be identified for a reservoir undergoing a thermal recovery process. These zones are: a swept zone with the highest mobility and/or storativity, a transition zone with continuously

changing mobility and/or storativity, and an unswept zone with the lowest values for mobility and/or storativity. This study is intended to investigate how representing these reservoirs by different numbers of regions affects the pressure behaviour analysis. It has been found that representing the transition zone by one region may generate pressure behaviours which may show higher contrasts in physical properties than what actually exist. Using various regions to represent the transition zone will avoid these apparently high or non-existing property contrasts.

The purpose of investigating how these factors change the reservoir pressure behaviour is to ascertain what effect these factors will have on the estimation of swept volume and effective properties of the reservoir. This study presents an evaluation of the applicability, utility and accuracy of the pseudosteady state method to estimate the swept volume in a steam injection project.

Finally, this work is intended to demonstrate how storativity variation can affect significantly the results obtained from some reservoir characterization methods. It has been shown that reservoir characterization methods, in which mobility is considered to be the only variable affecting the pressure behaviour from a reservoir, will fail when there is a storativity variation in the reservoir. This is consistent with the well known fact that the pressure behaviour from a reservoir is affected by both mobility and storativity.

## **ACKNOWLEDGEMENTS**

I sincerely wish to express my gratitude and appreciation to Professor A.K. Ambastha for his excellent guidance and encouragement throughout this study. I also gratefully acknowledge Professor K. Nandakumar for letting me use one of his research computers. Miscellaneous help from Mr. Paul A. Barrow and Mr. Rob L. Barton, concerning the use of computer accounts, is greatly appreciated. I would also like to thank my friend Ben Issaka for his helpful suggestions throughout this study. Financial support for this work was provided by Energy, Mines and Resources (E.M.R), and Alberta Oil Sands Technology and Research Authority (AOSTRA), for which I am very thankful. I also wish to acknowledge the use of the work station as well as other computer facilities from the Chemical Engineering and Mining, Metallurgical and Petroleum Engineering departments, respectively, of the University of Alberta. I am indebted to my parents, Guillermo and Dorita, and my sister, Elena, for their unlimited love, patience, understanding and support during my graduate studies.

## TABLE OF CONTENTS

	<u>Page</u>
LIST OF TABLES	
LIST OF FIGURES	
NOMENCLATURE	
1. INTRODUCTION .....	1
2. LITERATURE REVIEW .....	3
2.1 Two-region Composite Models .....	5
2.1.1 Analytical Approach .....	5
2.1.2 Numerical Approach .....	12
2.2 Three-region Composite Models .....	15
2.2.1 Analytical Approach .....	15
2.2.2 Numerical Approach .....	16
2.3 Multi-region Composite Models .....	17
2.3.1 Analytical Approach .....	18
2.3.2 Numerical Approach .....	19
2.4 Drawdown Analysis .....	20
2.5 Estimating Swept Volume in Thermal Recovery Projects .....	21
2.5.1 Deviation Time Method .....	21
2.5.2 Intersection Time Method .....	22
2.5.3 Type-Curve Matching Method .....	23
2.5.4 Pseudosteady State Method .....	24
2.6 Mobility and Storativity Profiles .....	26
2.7 Discontinuity Radii .....	27

3.	STATEMENT OF THE PROBLEM .....	30
4.	MATHEMATICAL MODEL FOR A MULTI-REGION COMPOSITE RESERVOIR WITH SKIN AT THE DISCONTINUITIES .....	32
4.1	Mathematical Development.....	33
4.1.1	Governing Equations .....	33
4.1.2	Inner Boundary Conditions .....	33
4.1.3	Conditions at the Discontinuities .....	34
4.1.4	Outer Boundary Conditions .....	34
4.1.5	Initial Condition .....	35
4.1.6	Dimensionless Variables .....	35
4.1.7	General Solution .....	37
4.1.8	Solution's Constants.....	38
4.2	Verification of Solution .....	42
5.	DRAWDOWN TEST ANALYSIS FOR MULTI-REGION COMPOSITE RESERVOIRS .....	49
5.1	Description of a Reservoir undergoing Steam Injection .....	49
5.2	Steam Injection Pressure Transient Behaviour .....	58
5.3	Analyzing Pressure Transient Responses for a Multi-region Composite Reservoir .....	61
5.4	Analyzing Characterization Methods.....	92
6	CONCLUSIONS AND RECOMMENDATIONS .....	102
6.1	CONCLUSIONS .....	102
6.2	RECOMMENDATIONS .....	106
	REFERENCES .....	107

APPENDIX A	Development of expressions for effective physical properties for multi-region composite reservoirs .....	114
APPENDIX B	Development of the dimensionless form of Yeh and Agarwal's (1989) equations .....	119
APPENDIX C	Data used to analyze the transient pressure response for a multi-region composite reservoir .....	126
APPENDIX D	Program to obtain the transient pressure response for a multi- region composite reservoir. A reservoir characterization subroutine is also included .....	133
APPENDIX E	Overcoming the matrix singularity problem .....	160
APPENDIX F	Transient pressure response for a multi-region composite reservoir (sample results for a particular run) .....	163
APPENDIX G	Figures for transient pressure responses for multi-region composite reservoirs .....	171

## LIST OF TABLES

	<u>Page</u>
Table C1	Discontinuity radii data for a multi-region composite reservoir visualized as a three-region composite reservoir ..... 127
Table C2	Physical properties data for a multi-region composite reservoir visualized as a three-region composite reservoir ..... 127
Table C3	Discontinuity radii data for a multi-region composite reservoir visualized as a four-region composite reservoir ..... 128
Table C4	Physical properties data for a multi-region composite reservoir visualized as a four-region composite reservoir ..... 128
Table C5	Discontinuity radii data for a multi-region composite reservoir visualized as a six-region composite reservoir ..... 129
Table C6	Physical properties data for a multi-region composite reservoir visualized as a six-region composite reservoir ..... 129
Table C7	Discontinuity radii data for a multi-region composite reservoir visualized as an eight-region composite reservoir ..... 130
Table C8	Physical properties data for a multi-region composite reservoir visualized as an eight-region composite reservoir ..... 130
Table C9	Discontinuity radii data for a multi-region composite reservoir visualized as a ten-region composite reservoir ..... 131
Table C10	Physical properties data for a multi-region composite reservoir visualized as a ten-region composite reservoir ..... 131
Table C11	Physical properties data for a multi-region composite reservoir for a particular ten-region case (Figures 5.29 and 5.30) ..... 132



## LIST OF FIGURES

	<u>Page</u>
Figure 2.1      Top view of a multi-region composite reservoir .....	4
Figure 4.1      Comparison between this study and Agarwal et al.'s (1970) work for $s = 0$ .....	43
Figure 4.2      Comparison between this study and Agarwal et al.'s (1970) work for $s = 20$ .....	43
Figure 4.3      Comparison between this study and Wattenbarger and Ramey's (1970) work for $s = 5$ .....	45
Figure 4.4      Comparison between this study and Wattenbarger and Ramey's (1970) work for $s = 20$ .....	45
Figure 4.5      Comparison between this study and Ambastha's (1992) work for $C_D = 0$ .....	46
Figure 4.6      Comparison between this study and Ambastha's (1992) work for $C_D = 5000$ .....	46
Figure 4.7      Comparison between this study and Ambastha and Ramey's (1992) work for various $M_{12}$ .....	48
Figure 4.8      Comparison between this study and Ambastha and Ramey's (1992) work for non-unit $F_{s12}$ and $F_{s13}$ .....	48
Figure 5.1      Mobility ratio or storativity ratio versus dimensionless radius in a multi- region composite reservoir in which mobility ratio or storativity ratio is a linear function of dimensionless radius .....	51
Figure 5.2      Mobility ratio or storativity ratio as a linear function of dimensionless radius with different discontinuity radii .....	53

Figure 5.3	Mobility ratio or storativity ratio as a linear function of dimensionless radius with different transition region's slopes .....	53
Figure 5.4	Mobility ratio or storativity ratio as a linear function of dimensionless radius for a three-region composite reservoir .....	54
Figure 5.5	Mobility ratio or storativity ratio as a linear function of dimensionless radius for a four-region composite reservoir .....	54
Figure 5.6	Mobility ratio or storativity ratio as a linear function of dimensionless radius for a six-region composite reservoir .....	55
Figure 5.7	Mobility ratio or storativity ratio as a linear function of dimensionless radius for an eight-region composite reservoir .....	55
Figure 5.8	Mobility ratio or storativity ratio as a linear function of dimensionless radius for a ten-region composite reservoir .....	56
Figure 5.9	Dimensionless semilog pressure derivative for $R_{D1} = 100$ , $R_{Dn-1} = 1000$ , $m_{tr} = 0.02$ , and $F_{s1i} = 1$ .....	62
Figure 5.10	Dimensionless Cartesian pressure derivative for $R_{D1} = 100$ , $R_{Dn-1} = 1000$ , $m_{tr} = 0.02$ , and $F_{s1i} = 1$ .....	64
Figure 5.11	Dimensionless semilog pressure derivative for $R_{D1} = 500$ , $R_{Dn-1} = 1400$ , $m_{tr} = 0.02$ , and $F_{s1i} = 1$ .....	66
Figure 5.12	Dimensionless Cartesian pressure derivative for $R_{D1} = 500$ , $R_{Dn-1} = 1400$ , $m_{tr} = 0.02$ , and $F_{s1i} = 1$ .....	68
Figure 5.13	Effect of first discontinuity radius on dimensionless semilog pressure derivative for a ten-region composite reservoir with $F_{s1i} = 1$ .....	70
Figure 5.14	Effect of first discontinuity radius on dimensionless Cartesian pressure derivative for a ten-region composite reservoir with $F_{s1i} = 1$ .....	70

Figure 5.15	Dimensionless semilog pressure derivative for $R_{D1} = 100$ , $R_{Dn-1} = 1000$ , $m_{tr} = 0.50$ , and $F_{s1i} = 1$ .....	71
Figure 5.16	Dimensionless Cartesian pressure derivative for $R_{D1} = 100$ , $R_{Dn-1} = 1000$ , $m_{tr} = 0.50$ , and $F_{s1i} = 1$ .....	73
Figure 5.17	Effect of transition region's slope on dimensionless semilog pressure derivative for a ten-region composite reservoir with $F_{s1i} = 1$ .....	74
Figure 5.18	Effect of transition region's slope on dimensionless Cartesian pressure derivative for a ten-region composite reservoir with $F_{s1i} = 1$ .....	74
Figure 5.19	Dimensionless semilog pressure derivative for $R_{D1} = 100$ , $R_{Dn-1} = 1000$ , $m_{tr} = 0.02$ , and $M_{1i} = 1$ .....	76
Figure 5.20	Dimensionless Cartesian pressure derivative for $R_{D1} = 100$ , $R_{Dn-1} = 1000$ , $m_{tr} = 0.02$ , and $M_{1i} = 1$ .....	76
Figure 5.21	Effective dimensionless Cartesian pressure derivative for $R_{D1} = 100$ , $R_{Dn-1} = 1000$ , $m_{tr} = 0.02$ , and $M_{1i} = 1$ .....	78
Figure 5.22	Dimensionless semilog pressure derivative for $R_{D1} = 500$ , $R_{Dn-1} = 1400$ , $m_{tr} = 0.02$ , and $M_{1i} = 1$ .....	81
Figure 5.23	Dimensionless Cartesian pressure derivative for $R_{D1} = 500$ , $R_{Dn-1} = 1400$ , $m_{tr} = 0.02$ , and $M_{1i} = 1$ .....	84
Figure 5.24	Effect of first discontinuity radius on dimensionless semilog pressure derivative for a ten-region composite reservoir with $M_{1i} = 1$ .....	86
Figure 5.25	Dimensionless semilog pressure derivative for $R_{D1} = 100$ , $R_{Dn-1} = 1000$ , $m_{tr} = 0.50$ , and $M_{1i} = 1$ .....	86
Figure 5.26	Dimensionless Cartesian pressure derivative for $R_{D1} = 100$ , $R_{Dn-1} = 1000$ , $m_{tr} = 0.50$ , and $M_{1i} = 1$ .....	88

Figure 5.27	Effect of transition region's slope on dimensionless semilog pressure derivative for a ten-region composite reservoir with $M_{1i} = 1$ .....	88
Figure 5.28	Dimensionless Cartesian pressure derivative for linear variation of mobility ratio and storativity ratio with dimensionless radius .....	89
Figure 5.29	Effect of storativity ratio profile on dimensionless semilog pressure derivative for a ten-region composite reservoir .....	91
Figure 5.30	Effect of storativity ratio profile on dimensionless Cartesian pressure derivative for a ten-region composite reservoir .....	91
Figure 5.31	Mobility ratio versus dimensionless radius of investigation for a five-region composite reservoir with $F_{s1i} = 1$ and $M_{15} = 0.5$ .....	96
Figure 5.32	Mobility ratio versus dimensionless radius of investigation for a five-region composite reservoir with $F_{s1i} = 1$ and $M_{15} = 2.0$ .....	96
Figure 5.33	Mobility ratio versus dimensionless radius of investigation for a reservoir with $F_{s1i} = 1$ and an asymptotical mobility ratio profile .....	98
Figure 5.34	Mobility ratio versus dimensionless radius of investigation for a thermal recovery reservoir with $F_{s1i} = 1$ .....	98
Figure 5.35	Mobility ratio versus dimensionless radius of investigation for a five-region composite thermal recovery reservoir with $M_{15} = 0.5$ .....	100
Figure 5.36	Mobility ratio versus dimensionless radius of investigation for a five-region composite thermal recovery reservoir with $M_{15} = 2.0$ .....	100
Figure 5.37	Mobility ratio versus dimensionless radius of investigation for a thermal recovery reservoir with an asymptotical mobility ratio profile..	101
Figure 5.38	Mobility ratio versus dimensionless radius of investigation for a thermal recovery reservoir with changing storativity ratio.....	101

Figure G.1	Dimensionless wellbore pressure for $R_{D1} = 100$ , $R_{Dn-1} = 1000$ , $m_{tr} = 0.02$ , and $F_{s1i} = 1$ .....	172
Figure G.2	Dimensionless wellbore pressure for $R_{D1} = 500$ , $R_{Dn-1} = 1400$ , $m_{tr} = 0.02$ , and $F_{s1i} = 1$ .....	172
Figure G.3	Dimensionless wellbore pressure for $R_{D1} = 1000$ , $R_{Dn-1} = 1900$ , $m_{tr} = 0.02$ , and $F_{s1i} = 1$ .....	173
Figure G.4	Dimensionless semilog pressure derivative for $R_{D1} = 1000$ , $R_{Dn-1} = 1900$ , $m_{tr} = 0.02$ , and $F_{s1i} = 1$ .....	173
Figure G.5	Dimensionless Cartesian pressure derivative for $R_{D1} = 1000$ , $R_{Dn-1} = 1900$ , $m_{tr} = 0.02$ , and $F_{s1i} = 1$ .....	174
Figure G.6	Dimensionless wellbore pressure for $R_{D1} = 2000$ , $R_{Dn-1} = 2900$ , $m_{tr} = 0.02$ , and $F_{s1i} = 1$ .....	174
Figure G.7	Dimensionless semilog pressure derivative for $R_{D1} = 2000$ , $R_{Dn-1} = 2900$ , $m_{tr} = 0.02$ , and $F_{s1i} = 1$ .....	175
Figure G.8	Dimensionless Cartesian pressure derivative for $R_{D1} = 2000$ , $R_{Dn-1} = 2900$ , $m_{tr} = 0.02$ , and $F_{s1i} = 1$ .....	175
Figure G.9	Effect of first discontinuity radius on dimensionless wellbore pressure for a ten-region composite reservoir with $F_{s1i} = 1$ .....	176
Figure G.10	Dimensionless wellbore pressure for $R_{D1} = 100$ , $R_{Dn-1} = 1000$ , $m_{tr} = 0.10$ , and $F_{s1i} = 1$ .....	176
Figure G.11	Dimensionless semilog pressure derivative for $R_{D1} = 100$ , $R_{Dn-1} = 1000$ , $m_{tr} = 0.10$ , and $F_{s1i} = 1$ .....	177
Figure G.12	Dimensionless Cartesian pressure derivative for $R_{D1} = 100$ , $R_{Dn-1} = 1000$ , $m_{tr} = 0.10$ , and $F_{s1i} = 1$ .....	177

Figure G.13	Dimensionless wellbore pressure for $R_{D1} = 100$ , $R_{Dn-1} = 1000$ , $m_{tr} = 0.50$ , and $F_{s1i} = 1$ .....	178
Figure G.14	Dimensionless wellbore pressure for $R_{D1} = 100$ , $R_{Dn-1} = 1000$ , $m_{tr} = 1.00$ , and $F_{s1i} = 1$ .....	178
Figure G.15	Dimensionless semilog pressure derivative for $R_{D1} = 100$ , $R_{Dn-1} = 1000$ , $m_{tr} = 1.00$ , and $F_{s1i} = 1$ .....	179
Figure G.16	Dimensionless Cartesian pressure derivative for $R_{D1} = 100$ , $R_{Dn-1} = 1000$ , $m_{tr} = 1.00$ , and $F_{s1i} = 1$ .....	179
Figure G.17	Effect of transition region's slope on dimensionless wellbore pressure for a ten-region composite reservoir with $F_{s1i} = 1$ .....	180
Figure G.18	Dimensionless wellbore pressure for $R_{D1} = 100$ , $R_{Dn-1} = 1000$ , $m_{tr} = 0.02$ , and $M_{1i} = 1$ .....	180
Figure G.19	Dimensionless wellbore pressure for $R_{D1} = 500$ , $R_{Dn-1} = 1400$ , $m_{tr} = 0.02$ , and $M_{1i} = 1$ .....	181
Figure G.20	Dimensionless wellbore pressure for $R_{D1} = 1000$ , $R_{Dn-1} = 1900$ , $m_{tr} = 0.02$ , and $M_{1i} = 1$ .....	181
Figure G.21	Dimensionless semilog pressure derivative for $R_{D1} = 1000$ , $R_{Dn-1} = 1900$ , $m_{tr} = 0.02$ , and $M_{1i} = 1$ .....	182
Figure G.22	Dimensionless Cartesian pressure derivative for $R_{D1} = 1000$ , $R_{Dn-1} = 1900$ , $m_{tr} = 0.02$ , and $M_{1i} = 1$ .....	182
Figure G.23	Dimensionless wellbore pressure for $R_{D1} = 2000$ , $R_{Dn-1} = 2900$ , $m_{tr} = 0.02$ , and $M_{1i} = 1$ .....	183
Figure G.24	Dimensionless semilog pressure derivative for $R_{D1} = 2000$ , $R_{Dn-1} = 2900$ , $m_{tr} = 0.02$ , and $M_{1i} = 1$ .....	183

Figure G.25	Dimensionless Cartesian pressure derivative for $R_{D1} = 2000$ , $R_{Dn-1} = 2900$ , $m_{tr} = 0.02$ , and $M_{1i} = 1$ .....	184
Figure G.26	Effect of first discontinuity radius on dimensionless wellbore pressure for a ten-region composite reservoir with $M_{1i} = 1$ .....	184
Figure G.27	Effect of first discontinuity radius on dimensionless Cartesian pressure derivative for a ten-region composite reservoir with $M_{1i} = 1$ .....	185
Figure G.28	Dimensionless wellbore pressure for $R_{D1} = 100$ , $R_{Dn-1} = 1000$ , $m_{tr} = 0.10$ , and $M_{1i} = 1$ .....	185
Figure G.29	Dimensionless semilog pressure derivative for $R_{D1} = 100$ , $R_{Dn-1} = 1000$ , $m_{tr} = 0.10$ , and $M_{1i} = 1$ .....	186
Figure G.30	Dimensionless Cartesian pressure derivative for $R_{D1} = 100$ , $R_{Dn-1} = 1000$ , $m_{tr} = 0.10$ , and $M_{1i} = 1$ .....	186
Figure G.31	Dimensionless wellbore pressure for $R_{D1} = 100$ , $R_{Dn-1} = 1000$ , $m_{tr} = 0.50$ , and $M_{1i} = 1$ .....	187
Figure G.32	Dimensionless wellbore pressure for $R_{D1} = 100$ , $R_{Dn-1} = 1000$ , $m_{tr} = 1.00$ , and $M_{1i} = 1$ .....	187
Figure G.33	Dimensionless semilog pressure derivative for $R_{D1} = 100$ , $R_{Dn-1} = 1000$ , $m_{tr} = 1.00$ , and $M_{1i} = 1$ .....	188
Figure G.34	Dimensionless Cartesian pressure derivative for $R_{D1} = 100$ , $R_{Dn-1} = 1000$ , $m_{tr} = 1.00$ , and $M_{1i} = 1$ .....	188
Figure G.35	Effect of transition region's slope on dimensionless wellbore pressure for a ten-region composite reservoir with $M_{1i} = 1$ .....	189
Figure G.36	Effect of transition region's slope on dimensionless Cartesian pressure derivative for a ten-region composite reservoir with $M_{1i} = 1$ .	189

Figure G.37	Dimensionless wellbore pressure for a reservoir in which mobility ratio and storativity ratio are linear functions of dimensionless radius .....	190
Figure G.38	Dimensionless semilog pressure derivative for both linearly changing mobility ratio and storativity ratio profiles with dimensionless radius ..	190
Figure G.39	Effect of storativity ratio profile on dimensionless wellbore pressure for a ten-region composite reservoir .....	191
Figure G.40	Mobility ratio versus conventional dimensionless radius of investigation for a five-region composite reservoir with $F_{s1i} = 1$ and $M_{15} = 0.5$ .....	192
Figure G.41	Mobility ratio versus conventional dimensionless radius of investigation for a five-region composite reservoir with $F_{s1i} = 1$ and $M_{15} = 2.0$ .....	192
Figure G.42	Mobility ratio versus dimensionless radius of investigation for a thermal recovery process with $F_{s1tr} = 100$ and $F_{s1n} = 1000$ .....	193
Figure G.43	Mobility ratio versus dimensionless radius of investigation for a thermal recovery process with $F_{s1tr} = F_{s1n} = 1000$ .....	193



## NOMENCLATURE

$A$	=	Area, $\pi R^2$ or $\pi r_e^2$ , $m^2$
$A$	=	Matrix of coefficients
$a_D$	=	Dimensionless observation well distance, $a/r_w$
$b$	=	Vector of known terms
$c$	=	Vector of unknown constants
$C$	=	Wellbore storage coefficient, $m^3/Pa$
$C_D$	=	Dimensionless wellbore storage coefficient
$C_j$	=	Arbitrary constants
$c_t$	=	Total system compressibility, $Pa^{-1}$
$F_s$	=	Storativity ratio between two regions as defined in Figures 4.5, 4.6, G.42 and G.43
$F_{s1i}$	=	Storativity ratio between regions 1 and i, $(\phi c_D)_1/(\phi c_D)_i$ for $i = 1, 2, \dots, n$
$h$	=	Formation thickness, $m$
$I_j$	=	Modified Bessel function of the first kind of order $j$
$k$	=	Permeability, $m^2$
$K_j$	=	Modified Bessel function of the second kind of order $j$
$m_c$	=	Cartesian line slope, $Pa/sec$
$m_{cD}$	=	Dimensionless Cartesian line slope
$m_s$	=	Semi-log line slope, $Pa/cycle$
$n$	=	The last region of a multi-region composite reservoir
$M$	=	Mobility ratio between two regions as defined in Figures 4.5 and 4.6
$M$	=	Actual reservoir mobility ratio, as defined in Equations 5.5b and 5.6b

$\bar{M}$	=	Reservoir instantaneous mobility ratio, as defined in Equation 5.3b	
$M_i$	=	Mobility ratio between two regions, $(k/\mu)_i/(k/\mu)_{i+1}$	for $i = 1, 2, \dots, n-1$
$M_{1i}$	=	Mobility ratio between regions 1 and i, $(k/\mu)_1/(k/\mu)_i$	for $i = 1, 2, \dots, n$
$m_{tr}$	=	Dimensionless slope of the transition region	
$p$	=	Pressure, Pa	
$p_D$	=	Dimensionless pressure drop	
$p_o$	=	Initial reservoir pressure, Pa	
$\bar{p}_D$	=	Dimensionless pressure drop in Laplace space	
$q$	=	Flow rate, $\text{sm}^3/\text{sec}$	
$r$	=	Radius, m	
$r_e$	=	Reservoir outer radius, m	
$r_{eD}$	=	Dimensionless reservoir outer radius	
$r_i$	=	Radius of investigation, m, as defined in Equation 5.4a	
$r_{iD}$	=	Dimensionless radius of investigation as defined in Equation 5.4b	
$r_w$	=	Wellbore radius, m	
$R$	=	Discontinuity radius in a composite reservoir, m	
$R_{Di}$	=	Dimensionless discontinuity radius in a composite reservoir, $R_i/r_w$	for $i = 1, 2, \dots, n-1$
$s$	=	Skin effect at the wellbore, dimensionless	
$s_{fi}$	=	Skin effect at the front (or discontinuity), dimensionless	for $i = 1, 2, \dots, n-1$
$t$	=	Time, seconds	
$t_D$	=	Dimensionless time	
$t_{DA}$	=	Dimensionless time based on the area, $(\pi R_{Dn-1}^2)$	
$t_{De}$	=	Dimensionless time based on the radius $R_{D1}$	

$V$	=	Reservoir volume, $m^3$
$V_s$	=	Swept volume, $m^3$
$z$	=	Laplace parameter

## Greek Symbols

$\alpha_{(i,j)}$	=	Coefficients in Equations 4.26 through 4.29
$\beta$	=	Formation volume factor, $m^3/sm^3$
$\partial$	=	Partial
$\overline{\lambda}_i$	=	Reservoir instantaneous mobility, as defined in Equation 5.3a
$\Delta p_s$	=	Pressure drop across skin, psi
$\Delta p_{sf}$	=	Pressure drop across skin at the discontinuity, Pa
$\Delta t$	=	Shut-in time, seconds
$\eta_i$	=	Diffusivity ratio between between between regions 1 and i, $(k/\mu\phi c_D)_1/(k/\mu\phi c_D)_i$ for $i = 1, 2, \dots, n$
$\mu$	=	Viscosity, Pa-sec
$\phi$	=	Porosity, fraction
$(\phi c_D)_{eff}$	=	Effective storativity corresponding to the volume up to $R_D$ as defined for Equation 5.1

## Subscripts

$c$	=	Cartesian
-----	---	-----------

<i>D</i>	=	Dimensionless
<i>e</i>	=	Exterior
<i>eff</i>	=	Effective
<i>f</i>	=	Front or flowing
<i>i</i>	=	A general term
<i>o</i>	=	Initial
<i>pss</i>	=	Pseudosteady state
<i>s</i>	=	Swept or shut-in
<i>ss</i>	=	Steady state
<i>t</i>	=	Total
<i>w</i>	=	Wellbore
<i>1</i>	=	Inner region in a multi-region composite reservoir
<i>2,3..n</i>	=	Regions of a multi-region composite reservoir

## CHAPTER 1

### INTRODUCTION

Over the years, thermal oil recovery methods have gained considerable interest and much use. Two of the most important thermal processes are in-situ combustion and steamflooding. Currently, thermal recovery by steamflooding is the dominant method for producing heavy oil around the world. The determination of the swept volume in thermal recovery processes is important. A knowledge of the steam swept volume provides an estimate of heat losses to the surrounding formation as well as the thermal efficiency of the operation.

In displacement projects, the swept volume has been estimated occasionally by coring and/or temperature observations at wells, during the injection process. These methods of estimating the steam swept volume are very expensive and uncertain due to reservoir heterogeneity. One practical and economical way of estimating the swept volume is by well test analysis, which also provides an estimation of flow capacity and skin factor.

The concept of determining the swept volume by pressure transient techniques has been studied by several authors. The most commonly used thermal well test has been the falloff test developed by *Eggenschwiler et al.* (1980). Their study utilizes a composite system, in which a steamflood or combustion process is represented as a reservoir model with two regions having highly contrasting fluid mobilities. Such a model seems ideally suited for

thermal oil recovery, due to the high mobility contrast between the swept and unswept regions. At early times, a semi-log graph of pressure versus time would generate a straight line corresponding to the inner-region mobility. Following this semi-log straight line, a pseudosteady Cartesian straight line may develop with a slope that can be related to the swept volume.

The pseudosteady state method developed by *Eggenschwiler et al.* (1980) is independent of the geometry of the swept region and has been applied by several investigators to field and simulated cases, with apparent success. However, simulated thermal falloff tests have shown that mobility and storativity may be continuously changing in the swept region. For continuous variations of mobility and storativity within the swept region, a simple two- or three-region model may not be appropriate. In this study, an analytical solution to a multi-region model is presented. Infinitesimally thin skins at the discontinuities are included. This work is intended to study the effects of various trends of mobility and storativity, within the swept region, on well tests for composite reservoirs.

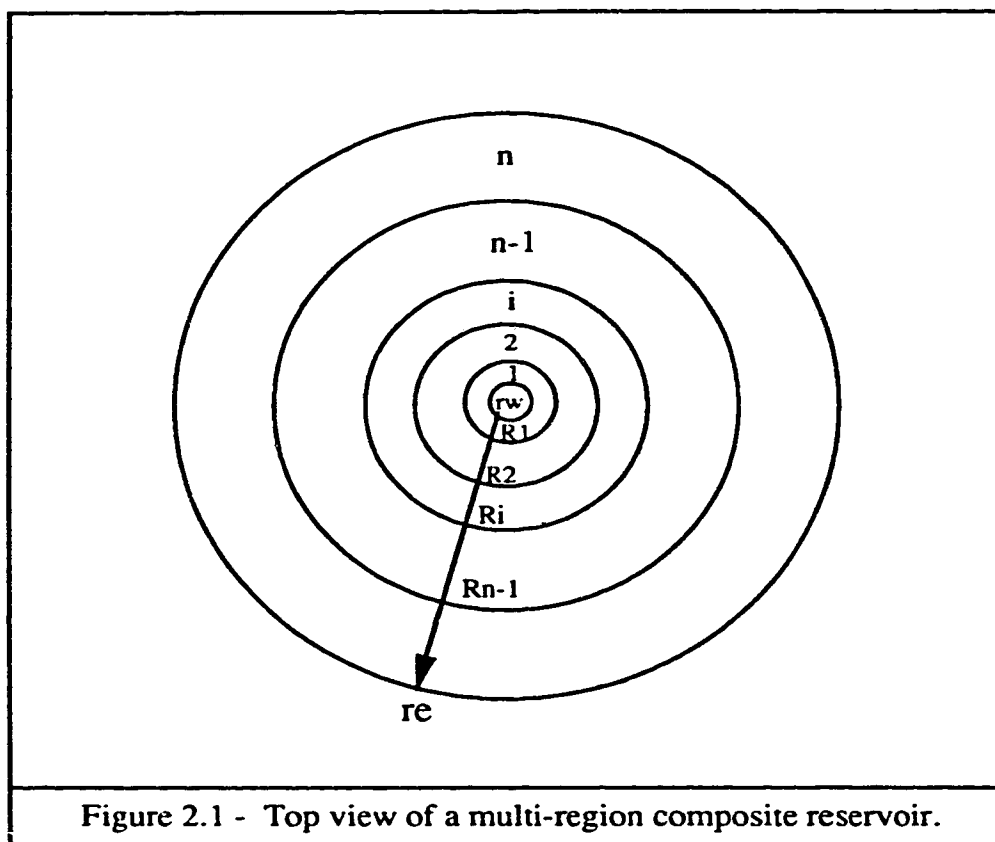
The literature survey conducted for this study is presented in Chapter 2. The statement of the problem and objectives of this study are discussed in Chapter 3. The mathematical model and its validation are presented in Chapter 4. The transient pressure behaviour of multi-region composite reservoirs is discussed in Chapter 5. Finally, Chapter 6 presents conclusions drawn from this study and recommendations for future research.

## CHAPTER 2

### LITERATURE REVIEW

In recent years, the behaviour of composite reservoirs has attracted much attention and many studies have appeared on this subject. A composite reservoir is made up of two or more regions. Rock and fluid properties are different in each region. The origin of composite systems may be natural or artificial. Examples of naturally created multi-zone composite systems include a reservoir with different permeability zones, an oil reservoir in communication with an aquifer, and an oil well with a finite-thickness skin zone surrounding the wellbore. Enhanced oil recovery projects, such as CO<sub>2</sub> miscible flooding, polymer flooding, in-situ combustion and steam injection, are examples of artificially created conditions, wherein the reservoir can be viewed as a multi-region system with different rock and/or fluid properties. A reservoir undergoing a thermal recovery process typically has been idealized as a composite reservoir.

Figure 2.1 schematically illustrates the reservoir model considered in this study. This model represents a radial multi-region composite reservoir in which there are interfaces or discontinuities between each region. In Figure 2.1, the distances  $R_i$  are the different positions where a discontinuity or front can be recognized. Discontinuities are the locations where rock and/or fluid properties have a significant variation. These discontinuity distances are important parameters when analyzing well tests in composite reservoirs. Strictly speaking, fronts in many enhanced oil recovery operations are not cylindrical. The





front's shape may be distorted by gravity and/or viscous fingering effects. Thus, the front radius exists only in some average sense. It is perhaps better to speak of the volume of the inner region, instead of front radius, especially when pseudosteady state data are available.

In general, reservoirs with contrasts in physical properties have been analyzed using analytical or numerical composite reservoir models. The pressure behaviour of composite reservoirs has been considered extensively in many studies. All these studies can be classified in three large groups: two-region composite, three-region composite and multi-region (more than three regions) composite reservoir models. However, the great majority of studies have considered the case of two-region composite reservoirs.

## **2.1 Two-region Composite Models**

The two-region composite model is the most commonly used model in the petroleum industry. There are several publications detailing the application of two-region composite models to describe pressure behaviour in petroleum reservoirs. Numerous two-region composite reservoir studies have defined the general principles to analyze composite reservoirs. Some of these studies will be discussed briefly in this section.

### **2.1.1 Analytical Approach**

*Hazebroek et al.* (1958) developed an analytical method using pressure falloff data from pattern waterflood injection wells. Their method determines the reservoir static pressure by trial and error. By plotting  $\log(p - p_e)$  versus shut-in time, they are able to estimate the

permeability-thickness product and skin factor. However, the permeability-thickness product obtained may be reflecting only a part of the reservoir and the use of trial and error may involve inaccuracies.

*Hurst* (1960) analyzed unsteady flow of fluids through two sands in series with different mobilities in each sand. He used the Laplace transform to obtain a solution for a single well located at the center of concentric sands. *Hurst* (1960) also considered the interference between two oil fields sharing the same aquifer as a two-region system with different physical properties in each region.

*Loucks and Guerrero* (1961) proposed radial composite reservoir solutions, using the Laplace transformation. *Loucks and Guerrero* (1961) studied the pressure distribution in an infinite composite reservoir composed of two adjacent concentric regions of different permeabilities. They found that, under certain conditions, the permeability in both zones, as well as the size of the inner zone, can be determined from transient pressure test data.

*Larkin* (1963) presented solutions to the diffusion equation for a line source located anywhere in a region bounded by a circular discontinuity. He used Green's functions presented by *Jaeger* (1944). *Larkin's* (1963) solution considers different rock and fluid properties on opposite sides of the discontinuity. *Jones* (1962) studied the behaviour of a composite reservoir, using the Laplace transformation. *Jones* (1962) made predictions for the behaviour of wells located near a gas-water contact. He extended the application of *Larkin's* (1963) solution by including mobility and diffusivity terms for several fluid phases in series. However, neither *Larkin* (1963) nor *Jones* (1962) specified the times for which their approximate solutions are valid.

*Carter* (1966) analyzed the pressure transient behaviour of a closed, radial, composite system with a well producing at a constant rate. He stated that in a graph of pressure versus time, an early semilog straight line may be observed. This semilog straight line corresponds to the inner region mobility. After this semilog straight line, a pseudosteady state period may follow. During this period, a Cartesian graph of pressure versus time will yield a straight line. From the slope of this Cartesian line, a volume can be estimated. *Carter* (1966) pointed out that this estimated volume would be greater than the inner region volume.

*Odeh* (1969) analyzed well tests from infinite outer boundary composite reservoirs. He stated that if a large contrast of physical properties exist, the pressure transient behaviour of an infinite outer boundary composite reservoir would be the same as the closed outer boundary case. The reason for this behaviour lies in the effects of the discontinuity being the same as those of a closed outer boundary. However, once the effect of the discontinuity ends, a second semilog straight line may follow the pseudosteady state period. This second semilog straight line will correspond to the outer region mobility.

*Eggenschwiler et al.* (1980) presented an analytical solution in Laplace space for the transient pressure behaviour of a well, producing at a constant rate, from a two-region, radial composite reservoir. Their method is widely used to estimate the swept or burned volume from well tests in thermal recovery projects, such as steamflooding or in-situ combustion. *Eggenschwiler et al.* (1980) modeled the swept volume as a radial region adjacent to the injection well. Wellbore storage and skin effects were also considered. Reservoir and fluid properties, such as permeability, porosity and compressibility of the reservoir fluid, were considered to be different in the inner (swept zone) and the outer

region (unswept zone). *Horne et al.* (1980) extended the *Eggenschwiler et al.* (1980) solution to finite composite reservoirs. *Tang* (1982) used the *Eggenschwiler et al.* (1980) method to calculate a front radius on the basis of a theoretical deviation time. *Tang* (1982) analyzed an in-situ combustion case. He found that the error involved in the estimated radius of the burned zone increases with an increase in the diffusivity ratio.

*Walsh et al.* (1981) used the *Eggenschwiler et al.* (1980) model to analyze falloff test data from in-situ combustion and steam injection projects. They observed that a long transition zone between the two semilog straight lines, for the swept and unswept regions, contains an approximate pseudosteady state region that may provide the information required to estimate the inner zone volume. To compute the swept zone volume, the mean temperature and pressure of the swept zone are required. *Walsh et al.* (1981) explained that, since the concept of pseudosteady state is based on material balance principles, the estimated volume of the swept zone is independent of the shape of the actual swept volume.

*Satman* (1981) analyzed transient flow in multi-layer, radial, and infinitely large composite reservoirs with fluid banks. *Satman* (1981) studied how the swept volume can be estimated by using a Cartesian graph of well test data, taken after the end of the first semilog straight line of a falloff test. He concluded that the average properties of the swept zone in a multi-layer system can be determined from the first semilog straight line of the well test data. *Satman* (1981) also stated that the first discontinuity radius can be found by using the time at which pressure data deviate from the first semilog straight line. *Satman and Oskay* (1985) studied the effects of a tilted front on well test analysis for multi-layer radial composite reservoirs. Their study suggests that if a sharp front model is used to

estimate the front radius from a tilted front reservoir, the estimated front radius will be lower than the actual front radius.

*Rosa and Horne* (1983) developed a solution applicable to composite reservoirs. They used the Laplace transform technique to develop their model. *Rosa and Horne* (1983) showed that the *Stehfest* (1970) numerical inversion scheme could be used to invert exact solutions from Laplace space to real space. Their study also showed a way to broaden the application of automated type-curve matching in well test analysis.

*Da Prat et al.* (1985) used the *Eggenschwiler et al.* (1980) composite model to determine the burned volume and the location of the fire-front in an in-situ combustion project. *Da Prat et al.* (1985) reported that the real pressure profile from the project matched quite well with the predictions made with the composite model. They also stated that the values obtained for the burned volume and the location of the burning front were reliable and simple to interpret.

*Brown* (1985) analyzed the drawdown pressure derivative behaviour of two region, radial and infinitely-large composite reservoirs. He studied the nature and duration of the transition region between the two semilog straight lines observed on a composite reservoir's pressure profile. He concluded that storativity influences only the timing and shape of the transition region, but does not affect the slope of the two semilog straight lines. *Brown* (1985) also discussed how the transition region shape is affected by the mobility ratio between regions.

*Barua and Horne* (1987) discussed the application of automated type-curve matching to analyze well tests from reservoirs undergoing a thermal recovery process. *Barua and Horne* (1987) used the *Eggenschwiler et al.* (1980) analytical model in their automated type-curve analysis. *Rosa and Horne's* (1983) solution was also considered in their study. With their automated type-curve matching method, an average radius of the swept zone can be obtained. The *Barua and Horne* (1987) method might give good estimates for the inner zone properties, even when the mobility ratio is not high or when the falloff test has been preceded by a short injection period. However, a lot of computer operations are required and the estimated outer zone properties might be unrealistic.

*Olarewaju and Lee* (1987) proposed an analytical solution in Laplace space for two-region, radial composite reservoirs produced either at a constant bottomhole pressure or at a constant rate. Their solution includes wellbore phase redistribution as suggested by *Fair* (1981). However, their study did not consider storativity variation. *Olarewaju and Lee's* (1987) study indicates that the phase redistribution effect is larger for a damaged system than for a stimulated one. They concluded that when the effect of phase redistribution is not severe enough to cause the characteristic pressure distortion (hump), it could lead to a misinterpretation of the reservoir pressure behaviour.

*Olarewaju and Lee* (1989) developed a two-region composite model to determine reservoir parameters, such as permeabilities of the inner and outer zones, radius of the inner zone, and wellbore storage. *Olarewaju and Lee* (1989) stated that for radial flow in an infinite-acting reservoir, the value of the semilog pressure derivative is shifted from 0.5 by a factor equal to the mobility ratio between the outer and the inner zones.

*Ambastha* (1988) presented an analytical study of the transient pressure derivative behaviour of a well in a two-region composite reservoir with a thin skin at the front. *Ambastha* (1988) found that the transition period between the end of the first semilog straight line and the beginning of the second semilog straight line is longer for larger mobility ratios. However, the effect of the storativity ratio on the timing of the semilog straight lines can be assumed as negligible. *Ambastha* (1988) found that the time to the maximum semilog pressure derivative and the magnitude of the maximum pressure derivative are affected by the mobility ratio. He also showed that, although the storativity ratio mildly affects the time to the maximum semilog pressure derivative, the magnitude of the maximum pressure derivative is affected significantly by the storativity ratio.

*Ambastha and Ramey* (1990) investigated the effect of skin at the front on composite reservoirs well tests. They showed how the effects of skin at the front on the transient pressure derivative behaviour are similar to the effects of storativity ratio. *Ambastha and Ramey* (1990) explained how skin at the front may be the cause of a short duration pseudosteady state period corresponding to the inner swept volume, for small mobility and storativity contrasts.

*Olarewaju et al.* (1991) presented type curves from a two-region composite model. They analyzed radially-damaged or -stimulated wells. Their type curves can be used to analyze the extent and magnitude of impairment in a damaged system or the extent or quality of improvement achieved from stimulation. The effect of phase redistribution was also included in their type curves. However, storativity variation was not considered.

### 2.1.2 Numerical Approach

*Bixel and van Poolen* (1967) numerically solved a two-region infinite system in which a well was located at the center of a circular region surrounded by a radial discontinuity. They showed how to estimate the inner region transmissibility by using the slope of the early straight line segment of the drawdown curve. *Bixel and van Poolen* (1967) studied the effect of mobility ratio on transient pressure behaviour. Each set of type curves had a fixed value of storativity ratio. However, the effect of storativity ratio on pressure behaviour was not discussed.

A finite thickness skin zone was treated by *Wattenbarger and Ramey* (1970) as a composite system. They used a numerical technique to obtain pressure transient behaviour for such systems. They concluded that the infinitesimally thin skin concept is applicable for damaged zone dimensionless radii from 1 to about 10. Their work suggested that if the damaged zone dimensionless radius is equal to or larger than 10, two straight lines will be evident on a semi-logarithmic plot.

In 1972, *Kazemi et al.* analyzed simulated pressure falloff tests in reservoirs with fluid banks. They emphasized how wellbore storage can mask the information that can be obtained from the early data of a falloff test. *Kazemi et al.* (1972) studied the two straight lines that can be observed on a falloff test pressure profile. They concluded that the slope ratio of the second straight line to that of the first straight line segment approximates the mobility ratio for the two zones, only when the storativity ratio is near unity. *Kazemi et al.* (1972) stated that when the storativity ratio is greater than one, the ratio of the slopes is



usually greater than the mobility ratio, whereas if the storativity ratio is less than unity, the ratio of the slopes is less than the mobility ratio.

In 1974, *Merrill et al.*, using the same type of simulator as *Kazemi et al.* (1972), investigated the pressure behaviour of two-zone composite systems. *Merrill et al.* (1974) defined what type of information can be obtained from a falloff test, depending on the conditions of the system tested. They concluded that proper analysis of falloff tests from waterflood systems with two contrasting fluid zones can yield information about mobilities and saturations on both sides of the front as well as the distance to the front. Analysis of gas injection systems can give information about the mobility of the first zone and the distance to the front.

*Sosa et al.* (1981) considered the effect of saturation distribution in the swept region on waterflood falloff tests. They used a radial numerical simulator to account for the relative permeability characteristics of the system. Their study showed how the transition region between the water and oil regions affects significantly the falloff test data. *Sosa et al.*'s (1981) analysis provides some qualitative information about waterflooding processes.

*Messner and Williams* (1982) applied the *Walsh et al.* (1981) procedure and used an implicit thermal simulator to analyze falloff data from steam injection projects. The swept volume comparison between the results from the two methods appeared to be favourable. However, thermal efficiencies calculated by the pseudosteady state method tended to be very low, indicating larger than expected overburden heat losses and excessive channelling. *Messner and Williams* (1982) stated that the low thermal efficiencies could also be due to

the inability of the method to accurately assess the reservoir heat content, ahead of the steam zone.

*Fassihi* (1988) numerically simulated falloff tests of steamflood and in-situ combustion processes using areal and radial models. He analyzed whether the swept volume estimated by applying the *Eggenschwiler et al.* (1980) analytical model agreed with the simulated swept volume. In this comparison, the effects of several parameters were studied. These parameters included reservoir and operational characteristics, such as wellbore gridblock size, non-uniform permeability, layering, flowing non-condensable gas, and oil vaporization. *Fassihi* (1988) concluded that, in reservoirs with highly contrasting homogeneous zones, estimated swept volumes from steam falloff tests, using the analytical model, were in good agreement with simulated swept volumes. However, continuously changing the reservoir's physical characteristics may mask the pseudosteady state period, making the analysis impossible. *Fassihi* (1988) also observed that in some in-situ combustion processes, the high mobility of the gases ahead of the front tends to distort the pseudosteady state period, making estimation of the burned volume inaccurate.

*Ziegler* (1990) analyzed pressure falloff data from a steam injection project. He compared results from the *Eggenschwiler et al.* (1980) analytical model and a simulator. *Ziegler* (1990) concluded that the analytical model yields results which are in good agreement with numerical simulation predictions. *Ziegler* (1990) recommended the use of the analytical model to determine reservoir parameters from steam injection falloff tests.

## 2.2 Three-region Composite Models

Solutions for a well located in a radial, three-region reservoir are available. However, very few studies have investigated the transient pressure response from these reservoirs. This section will present some of the most important analysis in this area of well testing.

### 2.2.1 Analytical Approach

*Onyekonwu and Ramey* (1986) developed an analytical solution for three-region, radially infinite, composite reservoirs. They showed, how in a two-region reservoir model, the assumption of a sharp mobility contrast between the zones is not exactly correct. *Onyekonwu and Ramey* (1986) discussed the existing gradation in fluid properties from the swept zone to the unswept zone. They explained that, in a three-region model, the middle zone is used to represent the region where the gradual change in fluid properties between the swept and unswept zones occurs. In their study, *Onyekonwu and Ramey* (1986) also analyzed the effect of the transition zone, mobility ratio and storativity ratio on pressure behaviour. The transition zone causes a departure from pseudosteady state behaviour. This departure is directly proportional to the size of the transition zone. The time of departure from pseudosteady state behaviour is directly proportional to the mobility ratio between the swept and the unswept zones. However, the time of departure from pseudosteady state is independent of the storativity ratio.

*Barua and Horne* (1985) compared analytical solutions for two-region and three-region, radially infinite, composite reservoirs. The three-region model included a transition region between the swept and unswept regions. *Barua and Horne* (1985) used automated type-

curve matching in their analysis. When trying to match the two-region model to the three-region model, they found several data points did not match. They concluded that this failure to match indicated the presence of an intermediate zone between the swept and the unswept zones. *Barua and Horne* 's (1985) work suggests that, by including the intermediate zone in the analysis, the estimates of the discontinuity radii will improve.

*Ambastha and Ramey* (1992) studied the transient pressure response of a well in a three-region composite reservoir. They discussed in detail the effective physical properties of a three-region composite reservoir. *Ambastha and Ramey* (1992) showed how the deviation time method would yield a front radius  $R_1$ , if the mobility ratio and the storativity ratio, at the first discontinuity, are balanced in such a way that a correct deviation time is observed. They also concluded that the pseudosteady state method will yield the second front radius  $R_2$ , if the effective storativity is used in the analysis. *Ambastha and Ramey* (1992) defined a criterion to distinguish apparent pseudosteady state from real pseudosteady state. This criterion uses the effective time to the start of pseudosteady state. When an apparent pseudosteady state is developed, the analysis yields an overestimated value for the second front radius  $R_2$ .

### 2.2.2 Numerical Approach

*Merrill et al.* (1974) used a simulator to study the application of a three-region composite model when analyzing well tests from enhanced oil recovery projects. They used the deviation time concept in their analysis. *Merrill et al.*'s (1974) work includes a tabulation of deviation times for different conditions of three-zone reservoirs. From this table, they obtained an averaged deviation time. They concluded that for three-zone systems, the

average dimensionless deviation time is 0.485. This value of time can be used to estimate the distance to the first discontinuity in the reservoir.

*Onyekonwu et al.* (1984) analyzed in-situ combustion falloff data by using two thermal simulators. He studied how to determine the proper average temperature when using the pseudosteady state concept to estimate the swept volume. *Onyekonwu et al.* (1984) found that the swept volume, determined from pressure analysis, includes both a burned volume and a high gas saturation zone ahead of the front. They emphasized that an effective value of temperature is required for evaluation of compressibility and the formation volume factor. These variables are important for accurate interpretation of falloff data. In their work, *Onyekonwu et al.* (1984) show how the effective temperature is strongly dependent on the wellbore and peak temperatures. They also concluded that this effective temperature is usually lower than the average temperature based on an energy balance.

### **2.3 Multi-region Composite Models**

Very little research has been reported about multi-region (more than three regions) composite reservoir models. Normally, multi-region composite models are used to characterize reservoirs with different permeability zones. However, very few studies have investigated the transient pressure response from these reservoirs. The application of multi-region composite models in reservoir characterization will be addressed briefly.

### 2.3.1 Analytical Approach

*Nanba and Horne* (1989) presented a method to estimate water and oil relative permeabilities from pressure transient analysis of water injection well data. In their work, a nonlinear regression algorithm was implemented. *Nanba and Horne's* (1989) solutions were derived based on analytical multicomposite and stepwise(numerical) multicomposite systems. These solutions were compared with the line source moving bank solution and with numerical results. The comparison indicated that multicomposite analytical solutions are appropriate for the analysis of water injection problems. Field examples supported the practicality of the proposed interpretation procedure.

*Abbaszadeh-Dehghani and Kamal* (1989) analyzed pressure transient tests of water injection wells using two-region and multi-region composite reservoir models. They found that the assumption of a stationary front during falloff is generally acceptable, and that waterflooding is better represented by a multi-region composite reservoir. *Abbaszadeh-Dehghani and Kamal* (1989) also studied how the duration of the transition region is increased by storativity contrast between regions.

*Oliver* (1990) presented a process of estimating a permeability distribution from well-test data. He described the relative contribution of the permeability of various regions to the estimate of the average permeability. *Oliver* (1990) showed that permeability estimates using the semilog pressure derivative are some type of volume-averaged reservoir permeability. He concluded that the instantaneous semilog pressure derivative from drawdown pressure data depends upon a weighted average of the permeability within the annular region of the reservoir. *Oliver's* (1990) work only considered the unit storativity

ratio case and the variation of mobility was very small. The maximum mobility ratio considered was five.

### 2.3.2 Numerical Approach

In 1989, *Yeh and Agarwal* simulated a multicomposite model to study how a reservoir mobility profile can be obtained from the reservoir transient pressure behaviour. They defined a term called "instantaneous mobility" which is inversely related to the instantaneous value of the semilog pressure derivative. *Yeh and Agarwal* (1989) also established a relation between instantaneous mobility and the radius of investigation. From simulation runs, they concluded that the instantaneous mobility represents a volumetric average of the true reservoir mobility. They developed an equation to relate the instantaneous mobility to the real reservoir mobility. The theoretical basis for their equations was not explained. *Yeh and Agarwal*'s (1989) characterization method apparently yields satisfactory results when there are low mobility contrasts and storativity is constant within the reservoir.

Using *Oliver*'s (1990) results, *Feitosa et al.* (1993a) expanded *Yeh and Agarwal*'s (1989) algorithm. *Feitosa et al.* (1993a) concluded that *Yeh and Agarwal*'s (1989) method can be improved by establishing a different relationship between instantaneous mobility and the actual reservoir mobility. They considered that the instantaneous mobility represents the harmonic volumetric average of the reservoir's real mobility. *Feitosa et al.*'s (1993a) characterization method seems to yield slightly better results than *Yeh and Agarwal*'s (1989) algorithm. *Feitosa et al.* (1993a) also developed a new characterization method called the inverse solution algorithm (ISA). This algorithm yields similar results to those

obtained from the modified version of *Yeh and Agarwal*'s (1989) method. In all the cases studied, the mobility contrasts were low and storativity remained constant within the reservoir. In the same year, with the purpose of expanding their previous work, *Feitosa et al.* (1993b) included porosity variation in their analysis. They studied porosity variation cases by using the inverse solution algorithm (ISA). *Feitosa et al.* (1993b) concluded that since, in real situations, porosity variations are small compared to permeability variations, the ISA can be applied to obtain a reasonably good approximation to the actual permeability distribution.

## 2.4 Drawdown Analysis

Drawdown tests may provide information about formation permeability, skin factor, and the reservoir volume communicating with the well. Thus, obtaining information from a drawdown test is of great importance. In 1988, *Ambastha* investigated the drawdown pressure derivative response of a two-region composite reservoir. In his work, *Ambastha* (1988) defined the parameters used in a pressure derivative drawdown analysis. When wellbore storage is negligible, the drawdown pressure derivative is not affected by skin at the wellbore. In the absence of wellbore storage, the parameters for the drawdown pressure derivative are the mobility ratio and the storativity ratio. A consideration of wellbore storage introduces two additional parameters: the dimensionless wellbore storage coefficient and the skin factor.



After obtaining drawdown data from a composite reservoir, a dimensionless graph of  $p_{wD}$  versus  $\ln t_D$  may yield two semilog straight lines with a transition period in between. The first semilog straight line develops in an early period and it is related to the inner region mobility. The second semilog straight line develops in a late period and it is related to the outer region mobility. Wellbore storage effects may mask the semilog line corresponding to the inner region mobility. Thus, in composite reservoir well tests, wellbore storage should be minimized. As for the second semilog straight line, this line may be observed as long as the test is run long enough to see the effects of the outer region. However, outer boundary effects may mask the second semilog line.

## **2.5 Estimating Swept Volume in Thermal Recovery Projects**

Many authors have applied different methods to estimate the swept or burned volume from pressure transient analysis. These methods include the deviation time method, the intersection time method, the type-curve matching method and the pseudosteady state method. The correct use of these methods will depend on the conditions of the well test and the reservoir characteristics.

### **2.5.1 Deviation Time Method**

This method states that when falloff test data are being plotted, a graph of pressure vs. time would generate an early semilog straight line corresponding to the inner-region (swept zone) mobility. When the effects of the interface (or front) are felt, a deviation from the straight line can be observed. The time at the end of the semilog straight line is used to

calculate a front radius on the basis of a theoretical dimensionless deviation time. The deviation time method was first used by *van Poolen* (1964) to locate the flood front in an in-situ combustion process.

*Bixel and van Poolen* (1967) found a value of 0.25 for the dimensionless deviation time. *Merrill et al.* (1974), after running several simulation cases, found that the dimensionless deviation time should lie in a range between 0.13 and 1.39. The arithmetic average of this range was 0.389. *Tang* (1982) obtained an approximated value of dimensionless deviation time equal to 0.4. *Ambastha and Ramey* (1989), based on the semilog pressure derivative behaviour, found a value of 0.18 for the dimensionless deviation time.

Many authors have studied the deviation time method obtaining significantly different values for the dimensionless deviation time. This significant difference in values for dimensionless deviation time indicates that an accurate and reliable specification for dimensionless deviation time is required to obtain meaningful results from this method. Another disadvantage of the deviation time method is that the flood front is considered to be cylindrical, which is often not the case for thermal recovery projects, since gravity and/or viscous fingering effects distort the front's shape. Furthermore, it is possible for wellbore storage effects to mask the initial semilog straight line, making the method incapable of producing any results.

### **2.5.2 Intersection Time Method**

Following the end of the early semilog straight line, falloff data deviates for a period of time, known as the transition period. After this interval of time, it may be possible to

observe a second semilog straight line, characteristic of the fluid mobility in the outer (unswept) zone. The time at which the two semilog straight lines intersect can be used to estimate a front radius, by using a theoretical dimensionless intersection time as a basis. *Bixel and van Poollen* (1967) proposed this method when discussing the effects of linear and radial discontinuities in composite reservoirs on pressure transient behaviour.

*Odeh* (1969) presented an equation relating the dimensionless discontinuity (or front) radius with the dimensionless intersection time, for equal storativity in both regions. *Merrill et al.* (1974) presented a graphical correlation using a simulator. They showed that for mobility ratios close to or less than unity, the dimensionless intersection time is a constant. However, *Merrill et al.* (1974) observed that for mobility ratios much greater than unity, the dimensionless intersection time is affected by both the mobility ratio and the storativity ratio. *Sosa et al.* (1981) used the intersection method to analyze the effects of mobility ratio on simulated falloff tests. *Ambastha and Ramsey* (1989) provided a number of reasons as to why the intersection time method is not suitable for thermal recovery well test analysis. They stated that in most thermal well test cases, the falloff test will not be run long enough to see the second semilog straight line, or the outer boundary effects may mask the second semilog straight line, or wellbore storage and skin may mask the first semilog line.

### 2.5.3 Type-Curve Matching Method

Type curves are dimensionless functions of pressure or pressure derivatives versus time, with mobility and storativity ratios as parameters. Generally, theoretical dimensionless type curves are generated by a mathematical model. The type-curve matching procedure involves fitting the entire well test data to a set of type curves. Once a match is obtained, an

arbitrary point of the data is selected and related to the definition of dimensionless variables of the type curve. By relating data and dimensionless variables definitions, unknown variables are obtained. These variables include important reservoir information, such as permeability, wellbore storage, wellbore skin factor and discontinuity radii. However, the non-uniqueness of the match is still the major disadvantage of type curve matching methods.

Several type curves were developed by *Bixel and van Poollen* (1967) with mobility ratio as a correlating parameter. *Barua and Horne* (1987) successfully used automated type-curve matching to analyze thermal recovery well tests. *Olarewaju and Lee* (1987) used their type curves to analyze field tests exhibiting composite reservoir behaviour. *Olarewaju and Lee's* (1987) type curves include *Fair's* (1981) phase- redistribution parameter. *Ambastha and Ramey* (1989) presented pressure derivative type curves applicable for all front radii, with mobility and storativity ratios as parameters for infinitely-large composite reservoirs. The time match point is used to calculate the front radius, while the pressure derivative match point yields the mobility of the inner (swept) region. Wellbore storage was not considered. *Ambastha and Ramey* (1989) explained that because of enhancement of detail in a pressure derivative graph, improved type-curve matching may be possible by using a pressure derivative type curve.

#### 2.5.4 Pseudosteady State Method

*Eggenschwiler et al.* (1980) proposed a pseudosteady state method to calculate the inner swept volume for composite reservoirs with large mobility and storativity contrasts

between the swept and unswept regions. They observed that due to these contrasts, the swept region can behave like a closed system for a short duration after the end of the semilog line corresponding to the inner zone mobility. During this time, a pseudosteady Cartesian straight line may originate. The slope of this Cartesian line is inversely proportional to the swept volume. As the pseudosteady state method is independent of the geometry of the swept region, it is not necessary for the flood front to be cylindrical to get a good estimate of the swept volume. *Eggenschwiler et al.* (1980) successfully validated their work against *van Poolen* (1965) and *Kazemi* (1966) falloff data.

*Walsh et al.* (1981) applied the pseudosteady state method to determine swept volume and heat distribution in steamflooding and in-situ combustion wells. They emphasized the use of a two-phase effective compressibility when applying the pseudosteady state method to estimate the swept volume in a steam injection process. The two-phase compressibility accounts for volumetric changes caused by steam condensation. *Satman et al.* (1980) and *Tang* (1982) extended the pseudosteady state method to cases where the pseudosteady state did not develop completely due to insufficient mobility and storativity contrasts between the two regions.

*Onyekonwu et al.* (1984) used the pseudosteady state concept to interpret combustion falloff data. The swept volume calculated by using the pseudosteady state method and simulated swept volume showed a good agreement. *Onyekonwu et al.* (1984) developed correction graphs to relate the burned and swept volumes. *Da Prat et al.* (1985) applied the pseudosteady state method to locate the burning front in an in-situ combustion project. They concluded that the estimated front radius (assuming the front to be cylindrical) was in good agreement with the actual locations of the injection and production wells.

*Issaka and Ambastha* (1992) simulated steam injection falloff tests for a horizontal well. The effects on falloff data of various parameters, such as wellbore grid block sizes, injection time, permeability anisotropy, injection rate and front shape were investigated. Their study showed that swept volume might be overestimated, by 5% to 60%, for horizontal wells. *Issaka and Ambastha* (1992) indicated that longer injection times prior to shut-in may have an adverse effect on the estimated swept volume. The reason for this adverse effect is that for longer injection times, the shape of the swept region is more irregular.

*Sheng* (1992) applied the pseudosteady state method to analyze thermal recovery projects by using the *Stanislav et al.* (1989) approach. He simulated falloff data and studied the effects of parameters such as gravity, dip, permeability anisotropy and irregular shape of the swept volume. *Sheng* (1992) found that all these parameters do not affect the results significantly. He also concluded that, although the estimated swept volume and skin are reasonably calculated by the pseudosteady state method, the permeability might be overestimated by 30% to 40%. His study showed how the estimation of permeabilities and swept volumes depends on the vertical position of a pressure recorder, where pressure falloff data are measured.

## 2.6 Mobility and Storativity Profiles

Previous simulation studies have reported profiles of mobility ratio and storativity ratio, most commonly observed in thermal recovery projects. The mobility ratio and the storativity ratio values used in this study are in a range from 1 to 1000. The characteristic

profiles used in this study are within the range of values given in previous studies from the literature. We refer to some of these studies in this section.

*Fassihi* (1988) simulated several falloff tests to analyze the pressure transient behaviour in steamflood and in-situ combustion processes. His table of estimated physical properties includes values of mobility ratio from 7 to 600 and values of storativity ratio from 23 to 33000.

*Onyekonwu et al.* (1984) made a comparison between analytical and numerical composite reservoir models. They used a three-zone model in the comparison. The estimated value of mobility ratio between the inner region and the transition region was 16 and the estimated value for mobility ratio between the first and the third region was 1840. The storativity ratio between the first and the transition region was 4, while the storativity ratio between the first and the third region was 110.

*Onyekonwu and Ramey* (1986) studied the effect of the transition region on the pressure behaviour of a three-region composite system. The mobility ratio between the first zone and the transition zone was 25, while the mobility ratio between the first and last zone was 1000. Storativity ratios for the first and second discontinuities were 5 and 35, respectively.

## 2.7 Discontinuity Radii

Previous studies have analyzed well tests in enhanced oil recovery operations. These studies have considered cases of injection of fluids to displace and produce oil. Some other

well test analyses have considered cases in which a fraction of oil is burned creating a heat gradient to mobilize and produce oil. Normally, all these types of well test analysis consider the reservoir as a system with multiple banks. Three main banks are considered in these systems. A bank, which represents the injected fluid, is also known as the swept zone. A bank, in which the injected fluid and oil are present, is also known as the transition zone. A bank, which represents the oil region, is termed the unswept zone. Two discontinuities are distinguished within these three banks: a discontinuity between the swept zone and the start of the transition zone, and a discontinuity between the end of transition zone and the unswept zone. The distances from the wellbore to the discontinuities are known as the first and last discontinuity radii, respectively. Although a multi-region composite reservoir may have several discontinuity radii, whenever a ratio of discontinuity radii is mentioned in this study, it will be referring to the ratio between the last and the first discontinuity radii.

Several studies have reported the ratios of discontinuity radii most commonly observed in thermal recovery projects. Some of the ratios of discontinuity radii used in this analysis are: 1.4, 1.9, 2.8 and 10. The ratios of discontinuity radii used in this study are within the range of values given in the studies to be discussed subsequently.

*Merrill et al. (1974)* simulated the pressure behaviour of three-zone composite systems. They analyzed gas injection processes. In their analysis, *Merrill et al. (1974)* used ratios of discontinuity radii of 1.6 and 2.

In 1984, *Onyekonwu et al.* simulated falloff tests to analyze an in-situ combustion project. *Onyekonwu et al. (1984)* reported a table with simulation results. They showed how the



discontinuity radii depend on fluid saturation, temperature and reservoir physical characteristics, such as mobility and storativity. Depending on the interpretation applied to their simulation results, the ratios of discontinuity radii range from 1.6 to 5.6.

*Onyekonwu and Ramey* (1986) simulated an in-situ combustion project to generate data for an analytical model. Their data included a range of ratios of discontinuity radii from 1.1 to 1.4.

In 1989, *Yeh and Agarwal* analyzed injection well test pressure data from reservoirs with multiple fluid banks. They studied reservoirs undergoing a waterflood or chemical injection. They generated simulation results by using a two-phase, two-dimensional numerical model. *Yeh and Agarwal* 's (1989) study used more than 20 sets of relative permeability data and some field tests. Their study included ratios of discontinuity radii of 4.4, 4.8, 10.5 and 20.

## CHAPTER 3

### STATEMENT OF THE PROBLEM

As discussed in the literature review, over the years, the pressure behaviour of composite reservoirs has gained considerable interest and many studies have appeared on this subject. A composite reservoir represents a number of well testing scenarios. Well test scenarios in thermal recovery operations have been typically represented by the use of a two- or three-region composite reservoir model. In some cases, the two- or three-region composite models may not be adequate to describe systems in which the mobility and storativity change continuously within the swept region. For these reservoirs, a multi-region composite model is more suitable. Therefore, this study investigates the pressure and pressure derivative responses of a multi-region, radial composite system. Thus, the main objectives of this study are:

1. To develop an analytical solution, similar to the *Eggenschwiler et al.* (1980) solution, for multi-region, radial composite reservoirs with infinitesimally thin skin at the discontinuities.
2. To develop new pressure derivative type curves for type-curve matching analysis of well tests in either homogeneous or multi-region composite reservoirs.

3. To analyze how previous two-region and three-region composite reservoir solutions compare with the multi-region composite solution.
4. To analyze effective mobility and storativity behaviour in multi-region composite reservoirs.
5. To study how mobility and storativity variations affect the swept volume estimation using the pseudosteady state method.
6. To analyze the possibility of improving previous composite reservoir analysis by means of the multi-region composite model.
7. To study briefly some reservoir characterization methods from the literature.

## **CHAPTER 4**

### **MATHEMATICAL MODEL FOR A MULTI-REGION COMPOSITE RESERVOIR WITH SKIN AT THE DISCONTINUITIES**

A mathematical model developed in this study is presented. This model considers a multi-region radial composite reservoir with wellbore storage and skin at the active (injection or production) well and infinitesimally thin skin at the discontinuities. The surface production (or injection) rate is assumed to be constant. The outer boundary may be infinite, closed or at a constant pressure. The solution for this model is obtained by using the Laplace transformation technique.

Some other assumptions in this model are:

- (1) The formation is homogeneous, horizontal and of uniform thickness.
- (2) The front is of infinitesimal thickness in the radial direction.
- (3) The fluid flowing is considered to be of slight, but constant, compressibility.
- (4) The front can be considered stationary throughout the few hours of a testing period.
- (5) Flow is considered to be single phase, radial and laminar.
- (6) Gravity and capillarity effects are considered negligible.

## 4.1 Mathematical Development

The governing equations and boundary conditions in dimensionless form for a multi-region radial composite reservoir are:

### 4.1.1 Governing Equations:

*first (1) region*

$$\frac{1}{r_D} \frac{\partial}{\partial r_D} \left( r_D \frac{\partial p_{D1}}{\partial r_D} \right) = \frac{\partial p_{D1}}{\partial t_D} \quad \text{for } 1 \leq r_D \leq R_{D1} \quad (4.1)$$

*any (i) region*

for  $i = 2, 3, \dots, n$

$$\frac{1}{r_D} \frac{\partial}{\partial r_D} \left( r_D \frac{\partial p_{Di}}{\partial r_D} \right) = \eta_{i-1} \frac{\partial p_{Di}}{\partial t_D} \quad \text{for } R_{D,i-1} \leq r_D \leq R_{Di} \text{ or } r_{eD} (\text{or } \infty) \quad (4.2)$$

### 4.1.2 Inner Boundary Conditions:

$$C_D \frac{dp_{wD}}{dt_D} - \left( \frac{\partial p_{D1}}{\partial r_D} \right)_{r_D=1} = 1 \quad (4.3)$$

$$p_{wD} = p_{D1} - s \left( \frac{\partial p_{D1}}{\partial r_D} \right)_{r_D=1} \quad (4.4)$$

#### 4.1.3 Conditions at the Discontinuities:

*any discontinuity - regions (i) and (i+1)*

$$r_D \frac{\partial p_{D_i}}{\partial r_D} = - \frac{1}{s_i} (p_{D_i} - p_{D_{i+1}}) \quad \text{for } r_D = R_{D_i} \text{ and } t_D > 0$$

for  $i = 1, 2, \dots, n-1$  (4.5)

$$\frac{\partial p_{D_{i+1}}}{\partial r_D} = M_i \frac{\partial p_{D_i}}{\partial r_D} \quad \text{for } r_D = R_{D_i} \text{ and } t_D > 0$$

for  $i = 1, 2, \dots, n-1$  (4.6)

#### 4.1.4 Outer Boundary Conditions:

*Infinite:*

$$p_{D_n}(r_D, t_D)_{r_D \rightarrow \infty} = 0$$

(4.7)

*Closed:*

$$\left( \frac{\partial p_{D_n}}{\partial r_D} \right)_{r_D = r_{cD}} = 0$$

(4.8)

*Constant pressure:*

$$p_{D_n}(r_{cD}, t_D) = 0$$

(4.9)

#### 4.1.5 Initial Condition:

$$p_{D_i}(r_D, 0) = 0 \quad \text{for } i = 1, 2, \dots, n \quad (4.10)$$

#### 4.1.6 Dimensionless Variables:

Dimensionless variables used in Equations 4.1 through 4.10 are defined as:

*Dimensionless pressure:*

$$p_{D_i} = \frac{2\pi k_1 h}{q \beta \mu_1} (p_o - p_i) \quad \text{for } i = 1, 2, \dots, n \quad (4.11)$$

*Dimensionless pressure at the wellbore*

$$p_{wD} = \frac{2\pi k_1 h}{q \beta \mu_1} (p_o - p_w) \quad (4.12)$$

*Diffusivity ratios:*

$$\eta_i = \frac{(k / \phi \mu c_l)_1}{(k / \phi \mu c_l)_{i+1}} \quad \text{for } i = 1, 2, \dots, n-1 \quad (4.13)$$

**Mobility ratios:**

$$M_i = \frac{(k/\mu)_i}{(k/\mu)_{i+1}} \quad \text{for } i = 1, 2, \dots, n-1 \quad (4.14)$$

**Dimensionless radii:**

$$r_D = \frac{r}{r_w} \quad (4.15)$$

$$r_{eD} = \frac{r_e}{r_w} \quad (4.16)$$

$$R_{Di} = \frac{R_i}{r_w} \quad \text{for } i = 1, 2, \dots, n-1 \quad (4.17)$$

**Dimensionless time:**

$$t_D = \frac{k_1 t}{(\phi \mu c_1)_1 r_w^2} \quad (4.18)$$

**Dimensionless wellbore storage coefficient:**

$$C_D = \frac{C}{2\pi(\phi c_1)_1 h r_w^2} \quad (4.19)$$

**Wellbore skin factor:**

$$s = \frac{2\pi k_1 h}{q \beta \mu_1} \Delta p_s \quad (4.20)$$



**Discontinuity skin factor:**

$$s_{fi} = \frac{2\pi k_i h}{q_f \beta \mu_1} \Delta p_{s_{fi}} \quad \text{for } i = 1, 2, \dots, n-1 \quad (4.21)$$

#### 4.1.7 General Solution

A general solution for the governing equations (Equations 4.1 and 4.2) was obtained by using the Laplace transformation technique with the appropriate initial and boundary conditions. The general solution in Laplace space for each region is:

*first (1) region*

$$\overline{p}_{D1}(r_D, z) = C_1 I_0(r_D \sqrt{z}) + C_2 K_0(r_D \sqrt{z}) \quad \text{for } 1 \leq r_D \leq R_{D1} \quad (4.22)$$

*any (i) region*

for  $i = 2, 3, \dots, n$

$$\overline{p}_{Di}(r_D, z) = C_{2i-1} I_0(r_D \sqrt{\eta_{i-1} z}) + C_{2i} K_0(r_D \sqrt{\eta_{i-1} z}) \quad \text{for } R_{D,i-1} \leq r_D \leq R_{Di} \text{ or } r_{eD} \text{ (or } \infty) \quad (4.23)$$

In Equations 4.22 and 4.23 and in all subsequent equations, the transformed time variable is identified by the symbol  $z$ . The dimensionless wellbore pressure drop in Laplace space is:

$$\overline{p}_{wD}(z) = C_1 [I_0(\sqrt{z}) - s\sqrt{z} I_1(\sqrt{z})] + C_2 [K_0(\sqrt{z}) + s\sqrt{z} K_1(\sqrt{z})] \quad (4.24)$$

#### 4.1.8 Solution's Constants

All constants  $C_1$  through  $C_{2n}$  are obtained by solving the system of equations resulting from the use of boundary conditions (Equations 4.3 through 4.9) in Laplace space:

For example:

from Equations 4.3 and 4.4

$$\alpha_{(1,1)}C_1 + \alpha_{(1,2)}C_2 = 1/z \quad (4.25)$$

from Equation 4.5

$$\alpha_{(2,2-1)}C_{2-1} + \alpha_{(2,2)}C_2 + \alpha_{(2,2+1)}C_{2+1} + \alpha_{(2,2+2)}C_{2+2} = 0 \quad \text{for } i = 1, 2, \dots, n-1 \quad (4.26)$$

from Equation 4.6

$$\alpha_{(2+1,2-1)}C_{2-1} + \alpha_{(2+1,2)}C_2 + \alpha_{(2+1,2+1)}C_{2+1} + \alpha_{(2+1,2+2)}C_{2+2} = 0 \quad \text{for } i = 1, 2, \dots, n-1 \quad (4.27)$$

from Equations 4.7 or 4.8 or 4.9

$$\alpha_{(2n,2n-1)}C_{2n-1} + \alpha_{(2n,2n)}C_{2n} = 0 \quad (4.28)$$

The term  $\alpha_{(i,j)}$  denotes the coefficient of the  $C_j$  in the  $i$  th equation. Equation 4.25 is the first equation, and Equation 4.28 is the last equation in a composite system of  $n$  -regions. The terms  $\alpha_{(i,j)}$  are:

$$\alpha_{(1,1)} = C_{DZ} \left( I_0(\sqrt{Z}) - s\sqrt{Z} I_1(\sqrt{Z}) \right) - \sqrt{Z} I_1(\sqrt{Z}) \quad (4.29)$$

$$\alpha_{(1,2)} = C_{Dz} (K_0(\sqrt{z}) + s\sqrt{z} K_1(\sqrt{z})) + \sqrt{z} K_1(\sqrt{z}) \quad (4.30)$$

$$\alpha_{(2,1)} = I_0(R_{D1}\sqrt{z}) + s_{f1} R_{D1}\sqrt{z} I_1(R_{D1}\sqrt{z}) \quad (4.31)$$

$$\alpha_{(2,2)} = K_0(R_{D1}\sqrt{z}) - s_{f1} R_{D1}\sqrt{z} K_1(R_{D1}\sqrt{z}) \quad (4.32)$$

$$\alpha_{(3,1)} = M_1\sqrt{z} I_1(R_{D1}\sqrt{z}) \quad (4.33)$$

$$\alpha_{(3,2)} = -M_1\sqrt{z} K_1(R_{D1}\sqrt{z}) \quad (4.34)$$

$$\alpha_{(2i,2i-1)} = I_0(R_{Di}\sqrt{z\eta_{i-1}}) + s_{fi} R_{Di}\sqrt{z\eta_{i-1}} I_1(R_{Di}\sqrt{z\eta_{i-1}}) \quad \text{for } i = 2, 3, \dots, n-1 \quad (4.35)$$

$$\alpha_{(2i,2i)} = K_0(R_{Di}\sqrt{z\eta_{i-1}}) - s_{fi} R_{Di}\sqrt{z\eta_{i-1}} K_1(R_{Di}\sqrt{z\eta_{i-1}}) \quad \text{for } i = 2, 3, \dots, n-1 \quad (4.36)$$

$$\alpha_{(2i,2i+1)} = -I_0(R_{Di}\sqrt{z\eta_i}) \quad \text{for } i = 1, 2, \dots, n-1 \quad (4.37)$$

$$\alpha_{(2i,2i+2)} = -K_0(R_{Di}\sqrt{z\eta_i}) \quad \text{for } i = 1, 2, \dots, n-1 \quad (4.38)$$

$$\alpha_{(2i+1,2i-1)} = M_i\sqrt{z\eta_{i-1}} I_1(R_{Di}\sqrt{z\eta_{i-1}}) \quad \text{for } i = 2, 3, \dots, n-1 \quad (4.39)$$

$$\alpha_{(2i+1,2i)} = -M_i\sqrt{z\eta_{i-1}} K_1(R_{Di}\sqrt{z\eta_{i-1}}) \quad \text{for } i = 2, 3, \dots, n-1 \quad (4.40)$$

$$\alpha_{(2i+1,2i+1)} = -\sqrt{z\eta_i} I_1(R_{Di}\sqrt{z\eta_i}) \quad \text{for } i = 1, 2, \dots, n-1 \quad (4.41)$$

$$\alpha_{(2i+1,2i+2)} = \sqrt{z\eta_i} K_1(R_{Di}\sqrt{z\eta_i}) \quad \text{for } i = 1, 2, \dots, n-1 \quad (4.42)$$

The remaining coefficients depend on the specified outer boundary condition and are defined by:

***Infinite outer boundary:***

A bounded solution for  $p_{Dn}(r_{D \rightarrow \infty}, z)$  is obtained from Equation 4.23 provided that  $C_{2n-1} = 0$ , as  $I_0(r_D \sqrt{\eta_{n-1} z}) \rightarrow \infty$  as  $r_D \rightarrow \infty$ . Therefore,  $\alpha_{(2n-2,2n-1)}$ ,  $\alpha_{(2n-1,2n-1)}$  and  $\alpha_{(2n,2n-1)}$  are set to zero in the system of equations. Also,  $\alpha_{(2n,2n)} = 0$ , as  $K_0(r_D \sqrt{\eta_{n-1} z})$  in Equation 4.23 approaches zero as  $r_D \rightarrow \infty$ . Thus:

$$\alpha_{(2n-2,2n-1)} = \alpha_{(2n-1,2n-1)} = \alpha_{(2n,2n-1)} = \alpha_{(2n,2n)} = 0 \quad (4.43)$$

The values of  $\alpha_{(2n-2,2n-1)}$  and  $\alpha_{(2n-1,2n-1)}$  are to be used based on Equation 4.43 for infinite reservoirs overriding the values corresponding to  $i = n-1$  for these  $\alpha$ 's from Equations 4.37 and 4.41, respectively.

***Closed outer boundary:***

Excepting the coefficients due to the outer boundary condition, all coefficients remain as defined before in Equations 4.29 through 4.42.

$$\alpha_{(2n,2n-1)} = I_1(r_{eD} \sqrt{2\eta_{n-1}}) \quad (4.44)$$

$$\alpha_{(2n,2n)} = -K_1(r_{eD} \sqrt{2\eta_{n-1}}) \quad (4.45)$$

***Constant-pressure outer boundary:***

As in the previous case, the only different coefficients are those due to the outer boundary condition:

$$\alpha_{(2n,2n-1)} = I_o(r_e D \sqrt{z\eta_{n-1}}) \quad (4.46)$$

$$\alpha_{(2n,2n)} = K_o(r_e D \sqrt{z\eta_{n-1}}) \quad (4.47)$$

In this section, the solution to the transient pressure problem for a radial multi-region composite reservoir with skin at the discontinuities has been described. The problem was arranged as a system of  $2n$  equations with  $2n$  unknowns (constants  $C_j$ ). To solve the problem, all the coefficients were grouped in a matrix called  $A$ , all the unknown constants  $C_j$  were grouped in an unknown vector called  $c$  and all right-hand-side terms from Equations 4.25 through 4.28 were arranged in a known vector called  $b$ . Once the system was set in the form  $Ac = b$ , the unknown vector  $c$  was obtained by multiplying the inverse of matrix  $A$  by the known vector  $b$ . After obtaining the values of the constants  $C_j$ , dimensionless transient pressure and dimensionless pressure derivative (semilog and Cartesian) responses in Laplace space were generated. These responses were numerically inverted from the Laplace space to real space by means of the *Stehfest* (1970) algorithm.

Appendix A contains the development of expressions for the physical properties of multi-region composite reservoirs. Appendix B contains the development of the dimensionless form for instantaneous mobility and radius of investigation. Appendix C contains the input

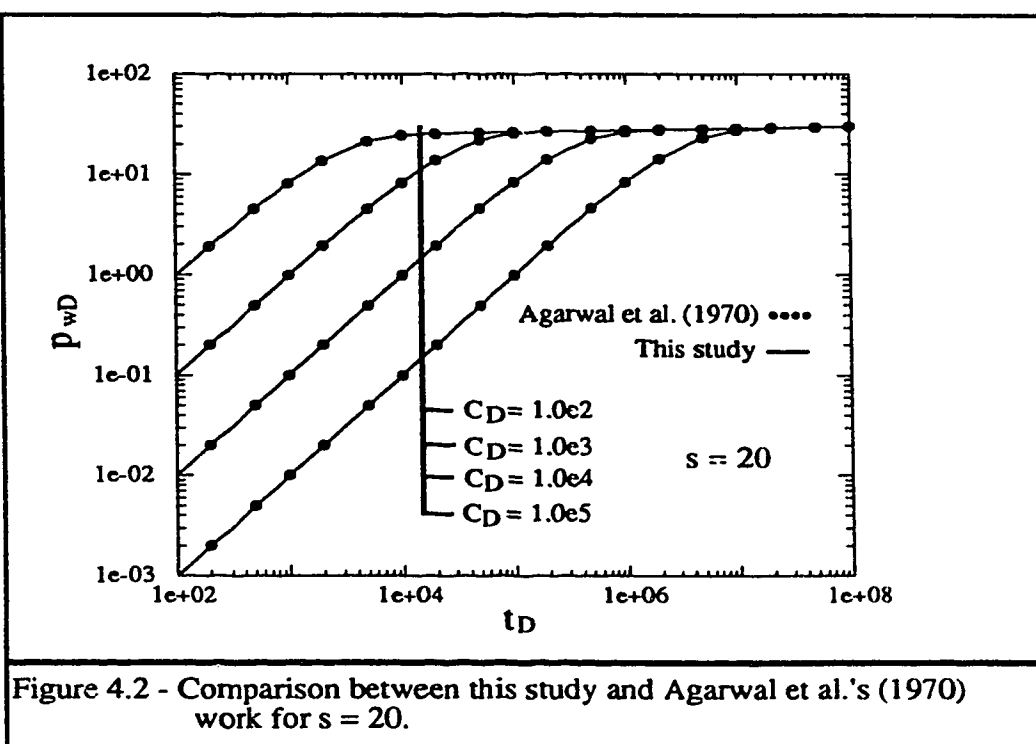
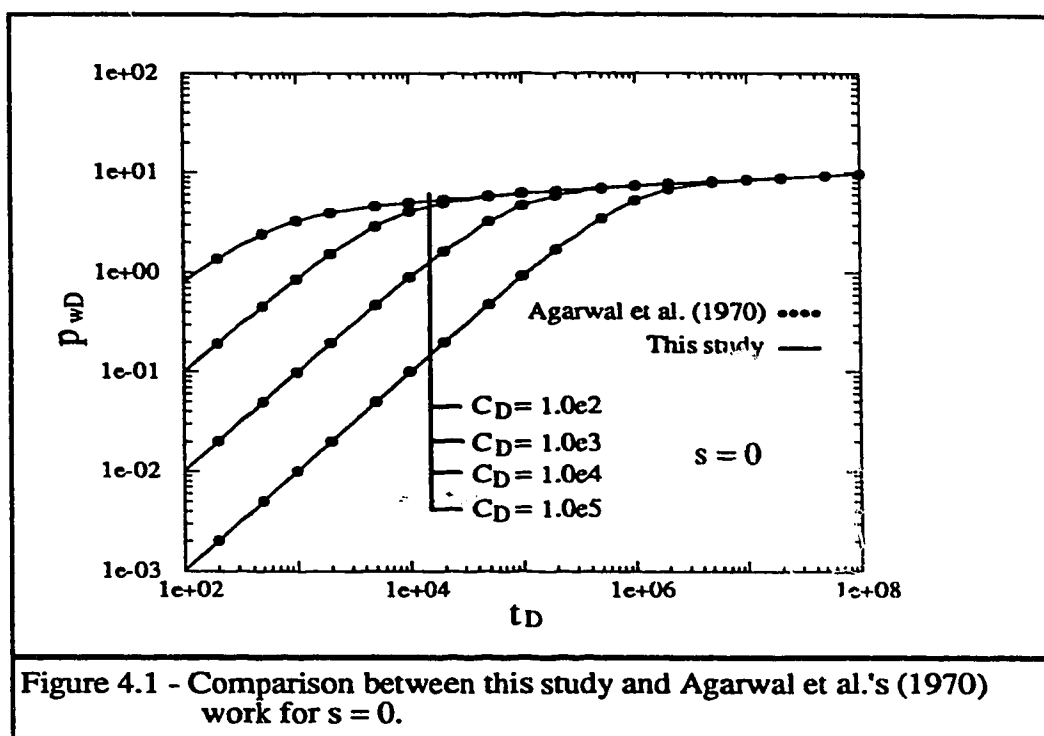
data used to analyze the transient pressure behaviour of multi-region composite reservoirs. Appendix D contains the computer program used in this study.

It is important to note that at very early times ( $t_D = 100$ ), the matrix of coefficients  $A$ , mentioned previously, may become singular or very close to singular (over the working precision limit of the computer). This is because at very early times, there are very small coefficients as well as very large coefficients, which causes the singular behaviour of the matrix. Appendix E explains how the singularity problem was overcome.

Appendix F shows sample results for a particular run of the computer program. Finally, appendix G shows some additional figures for the transient pressure response of multi-region composite reservoirs. These graphs were used during the development of this study, however no discussions have been done about these figures since other figures (Chapter 5) are considered to be more significant for the objectives of this study.

## 4.2 Verification of Solution

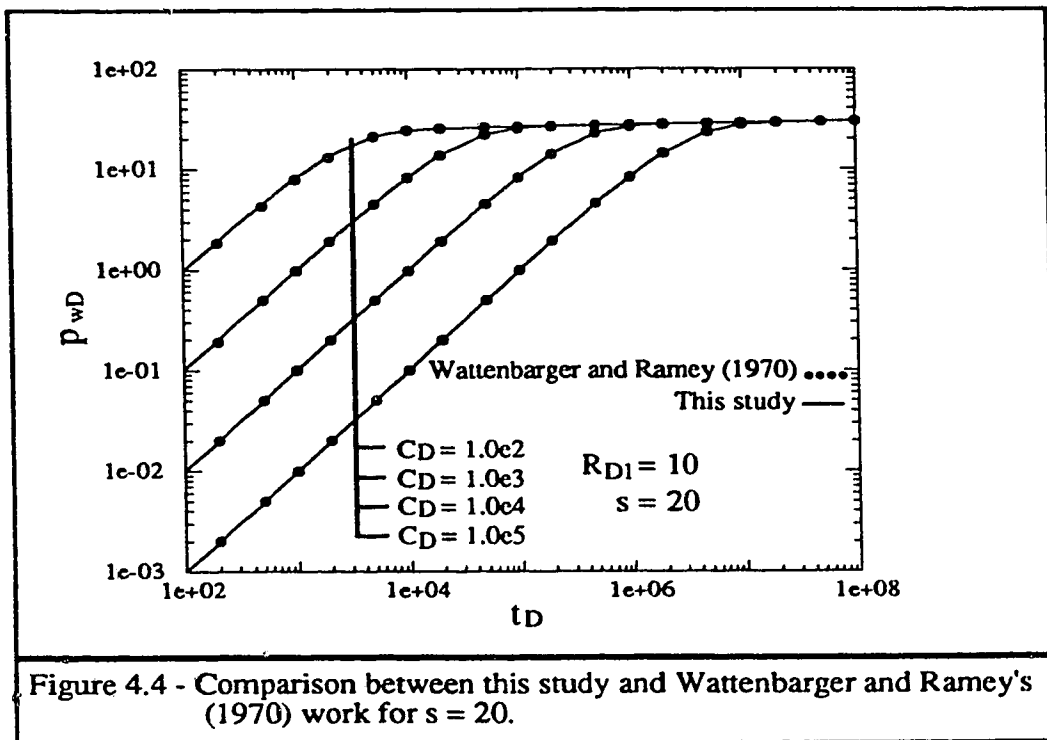
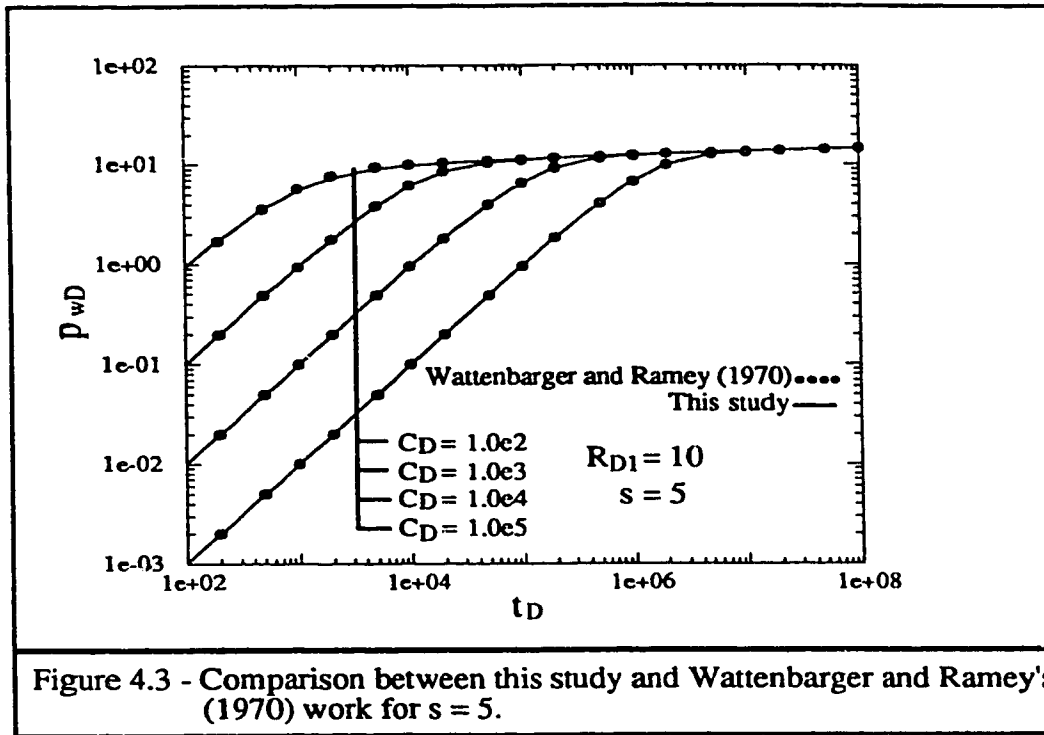
The solution presented in section 4.1 was verified against the *Agarwal et al.* (1970) solution for a well in a homogeneous reservoir with and without skin at the wellbore. To reproduce *Agarwal et al.* (1970) by using this study's solution, the model presented in this work was run as a multi-region (i.e., three, five and ten regions) composite model with no skin at the discontinuities and in which all the mobility and storativity ratios at the discontinuities were equal to unity. The model successfully reproduced the homogeneous reservoir pressure responses (Figures 4.1, 4.2).



The multi-region composite model was also validated against the *Wattenbarger and Ramey* (1970) solution for a well in a homogeneous reservoir with a finite skin zone. *Wattenbarger and Ramey* (1970) showed how the thick skin concept can be visualized as a zone near the wellbore with a permeability lower or higher than the reservoir's permeability. Thus, a homogeneous reservoir with a thick skin zone is a two-region composite reservoir. *Wattenbarger and Ramey* (1970) presented an equation and a table relating thick skin to the mobility ratio between the two zones as well as the discontinuity radius corresponding to that mobility ratio. To verify the multi-region composite reservoir model against the *Wattenbarger and Ramey* (1970) solution, the model was run as a multi-region (ie. three, five and ten regions) composite model with one value of mobility for the region closest to the wellbore and another value of mobility for the rest of the regions beyond the first discontinuity radius. The multi-region composite reservoir model was run with no skin at the discontinuities, and with unit storativity ratios at the discontinuities. It is important to note that the model was run with no skin at the wellbore, and that the values of skin factor observed in Figures 4.3 and 4.4 are values for the thick skin factor. The multi-region composite reservoir model successfully reproduced *Wattenbarger and Ramey's* (1970) dimensionless pressure responses (Figures 4.3, 4.4).

This study was also verified (Figures 4.5 and 4.6) against *Ambastha's* (1992) two-region radial composite model pressure and pressure derivative responses. The multi-region and two-region model solutions were compared with and without skin at the front, with and without wellbore storage and skin. To reproduce *Ambastha's* (1992) results, the multi-region model was run as reservoirs with three, five and ten regions in which all the mobility and storativity ratios at the discontinuities were equal to unity, except one discontinuity at a specified dimensionless radius.





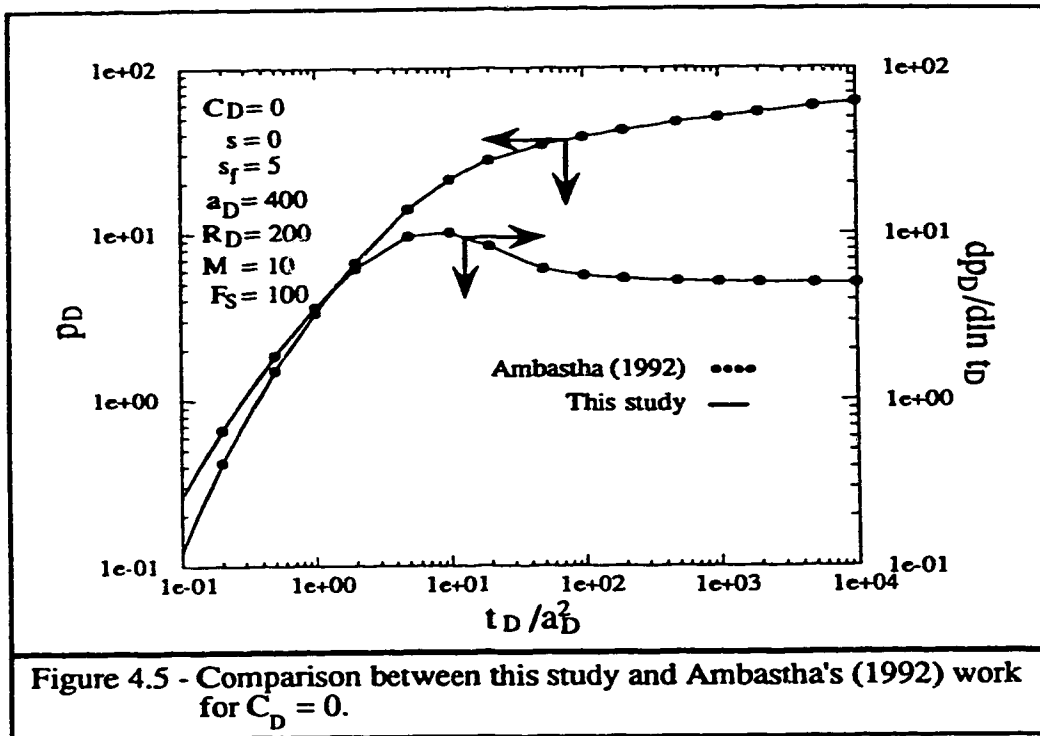


Figure 4.5 - Comparison between this study and Ambastha's (1992) work for  $C_D = 0$ .

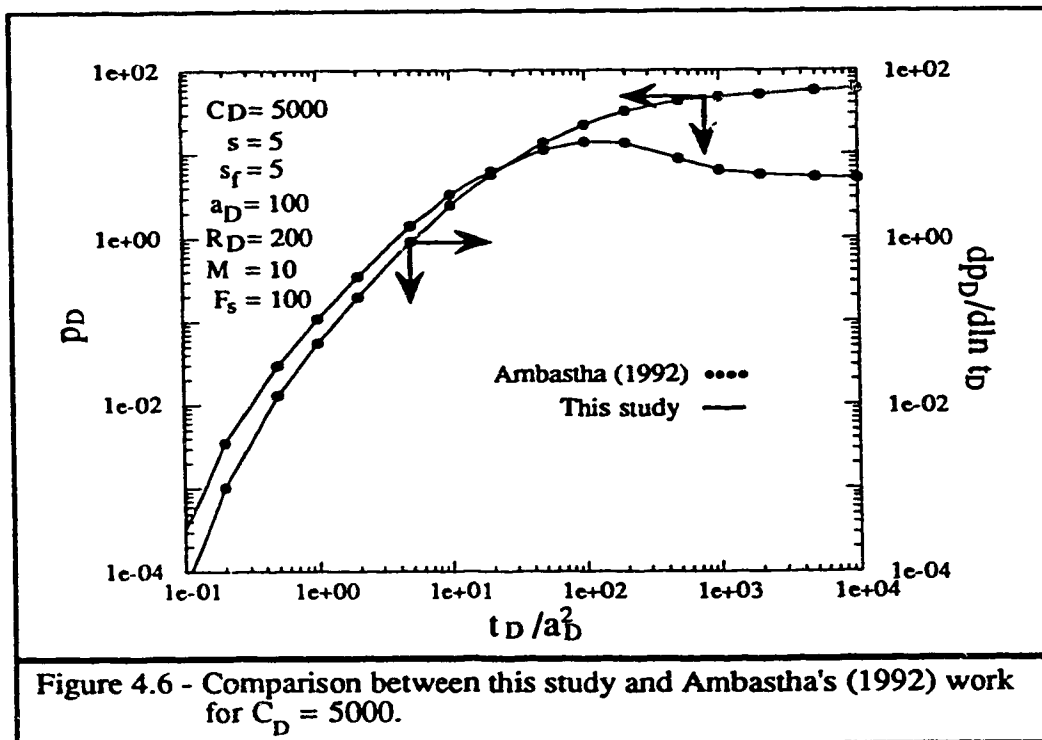


Figure 4.6 - Comparison between this study and Ambastha's (1992) work for  $C_D = 5000$ .

The multi-region composite reservoir model has also been verified against *Ambastha and Ramey* 's (1992) three-region radial composite model pressure and pressure derivative responses. Same type of previous analysis was employed. The comparison between the two studies was also completely satisfactory (Figures 4.7 and 4.8). No further verification seems necessary.

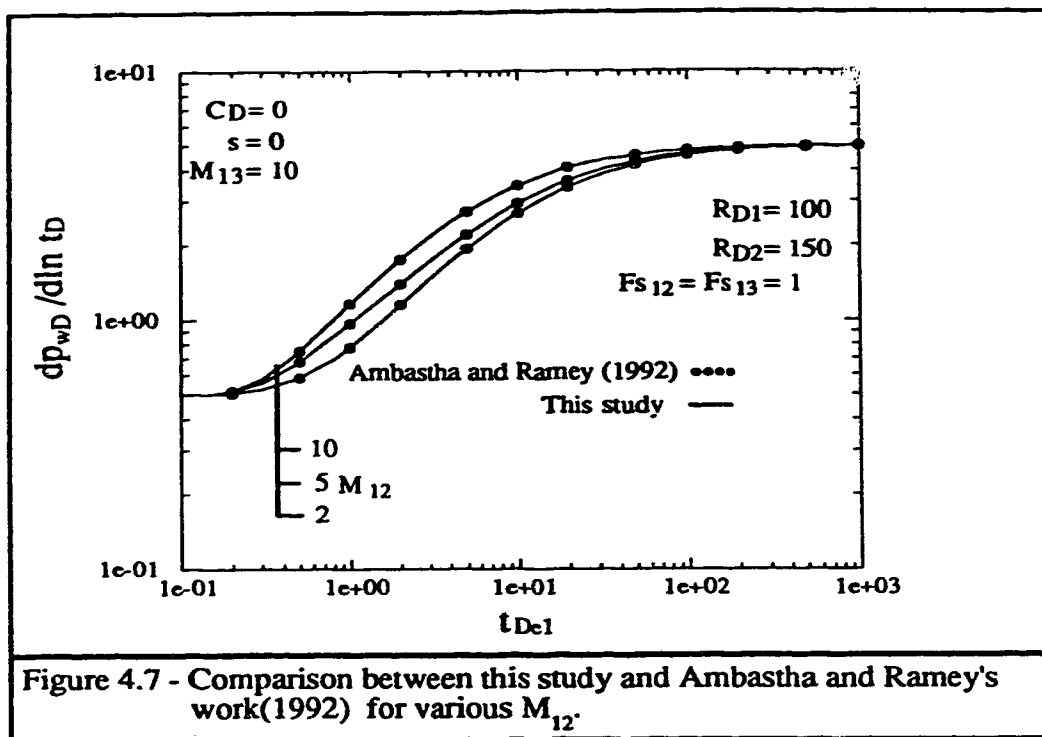


Figure 4.7 - Comparison between this study and Ambastha and Ramey's work(1992) for various  $M_{12}$ .

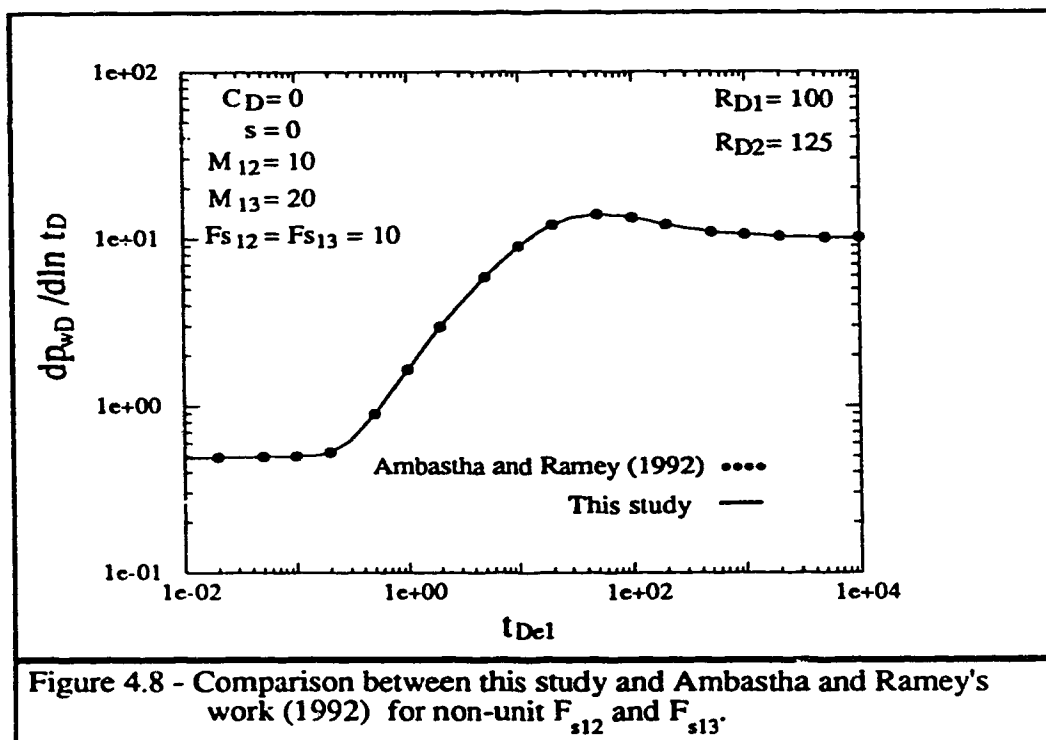


Figure 4.8 - Comparison between this study and Ambastha and Ramey's work (1992) for non-unit  $F_{s12}$  and  $F_{s13}$ .

## **CHAPTER 5**

### **DRAWDOWN TEST ANALYSIS FOR MULTI-REGION COMPOSITE RESERVOIRS**

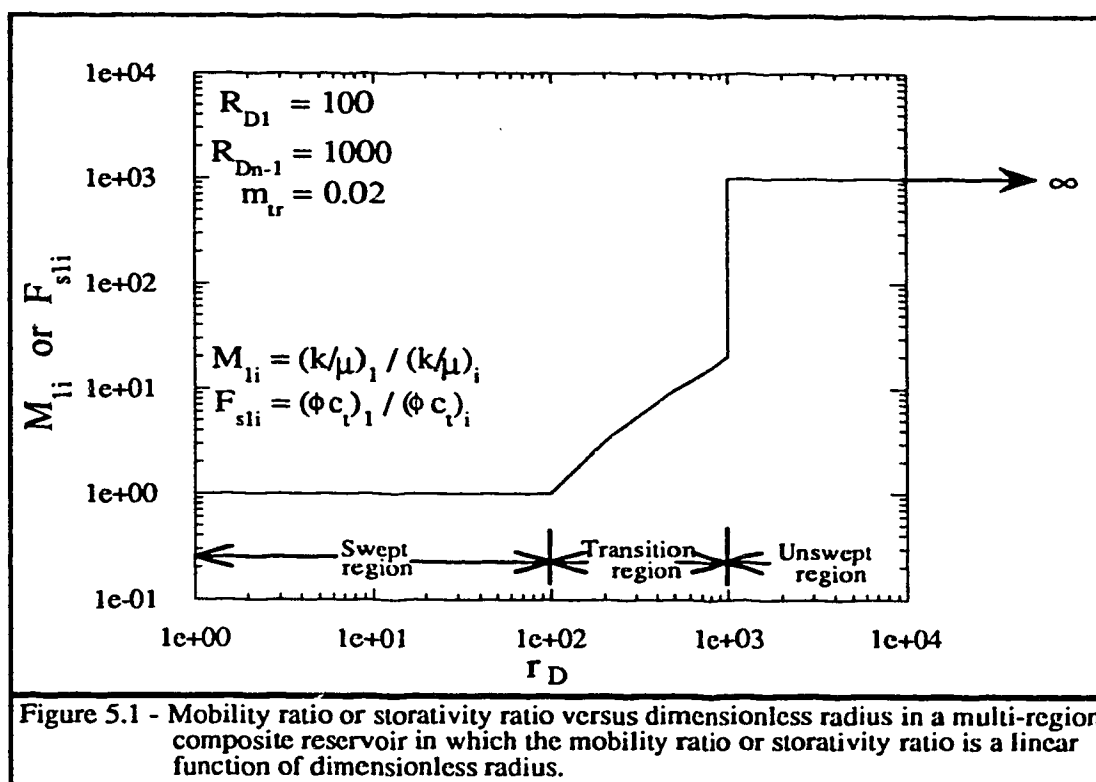
As discussed in Chapter 2, enhanced oil recovery processes, such as in-situ combustion and steam injection, are examples of artificially-created composite systems. In these situations, the reservoir can be viewed as a multi-region system with different rock and/or fluid properties. This study analyzes drawdown test data from a multi-region composite reservoir model representing a reservoir undergoing steam injection.

#### **5.1 Description of a Reservoir undergoing Steam Injection**

A reservoir undergoing steam injection has three characteristic zones. A first inner zone, called the "swept zone", is full of steam and has the greatest values of mobility and storativity. Beyond the inner zone, there exists a second zone in which the mobility and/or the storativity may be continuously changing. This second zone is called the "transition zone". Steam, oil and condensed water are present in the transition zone. At the end of the transition region, towards the reservoir outer boundary, there is a cold heavy oil region called the "unswept zone". This last zone has the lowest mobility and storativity values, and extends as far as the reservoir's outer boundary.

Figure 5.1 represents a mobility ratio and/or storativity ratio profile from a reservoir in which steam is being injected to recover heavy oil. As the pressure transient moves from the swept region to the unswept region, the mobility and storativity will decrease. However, because of the definition of mobility ratio and storativity ratio used in this study, the mobility ratio and the storativity ratio will increase as the pressure transient moves from the swept region to the unswept region. Also, based on the definition, the mobility ratio and storativity ratio of the swept region will be equal to one, while the unswept region will have the largest values for mobility ratio and storativity ratio. The unswept region's mobility ratio and storativity ratio are the overall mobility and storativity ratios. Thus, the swept and unswept regions have well-defined values for mobility ratio and storativity ratio. However, the values for the transition region's mobility ratio or storativity ratio are difficult to define, since mobility and storativity are continuously changing in this region. In the particular case of steam injection, mobility and storativity ratios continuously increase in the transition region. The values for mobility ratio and storativity ratio in the transition region will fall in a range from one to a value lower or equal to the unswept region's ratios.

Though the transition region's mobility and/or storativity ratio profiles can be represented in any suitable manner judged to mimic the real situation, this study analyzes cases in which the transition region's mobility ratio and/or storativity ratio profiles are linear functions of dimensionless radius. Figure 5.1 represents the case of the transition's region linear relationship between mobility and/or storativity ratio versus dimensionless radius. The reason for this transition region's profile not appearing as a straight line is that a Cartesian straight line is being plotted on a log-log scale in Figure 5.1. It is important to note that the definition of mobility ratio in Figure 5.1 is different from the definition in



Equation 4.14. This new definition of mobility ratio will be used with the sole purpose of presenting results. There are not any mathematical implications from this new definition of mobility ratio and the mathematical model remains the same as defined in Chapter 4. In Figure 5.1, an arrow and the symbol for infinity are observed. The purpose of the arrow and the infinity symbol is to represent the fact that the unswept region's outer limit is not defined on the graph, since the reservoir has an infinite outer boundary.

Figures 5.2 and 5.3 are the different mobility and storativity ratio profiles considered in this study. In these figures, three variables should be explained:

- 1       $R_{D1}$  is the radius where the inner region ends and the transition region starts.  
 $R_{D1}$  will be referred to as the first discontinuity radius.
- 2       $R_{Dn-1}$  is the radius where the transition region ends and the unswept region starts.  
 $R_{Dn-1}$  will be referred to as the last discontinuity radius.
3.       $m_{tr}$  is the slope of the line that represents the transition region's relationship between the mobility and/or storativity ratios, and the dimensionless radius.  
 $m_{tr}$  will be referred to as the transition region's slope.

The transition region can be represented by one region with an averaged value for mobility ratio and/or storativity ratio or by several regions with different values of mobility ratio and storativity ratio. Both representations are intended to approximate the transition region's profile. Figures 5.4 through 5.8 show different ways of representing the transition region in this study. The composite models used in this analysis vary from a three-region



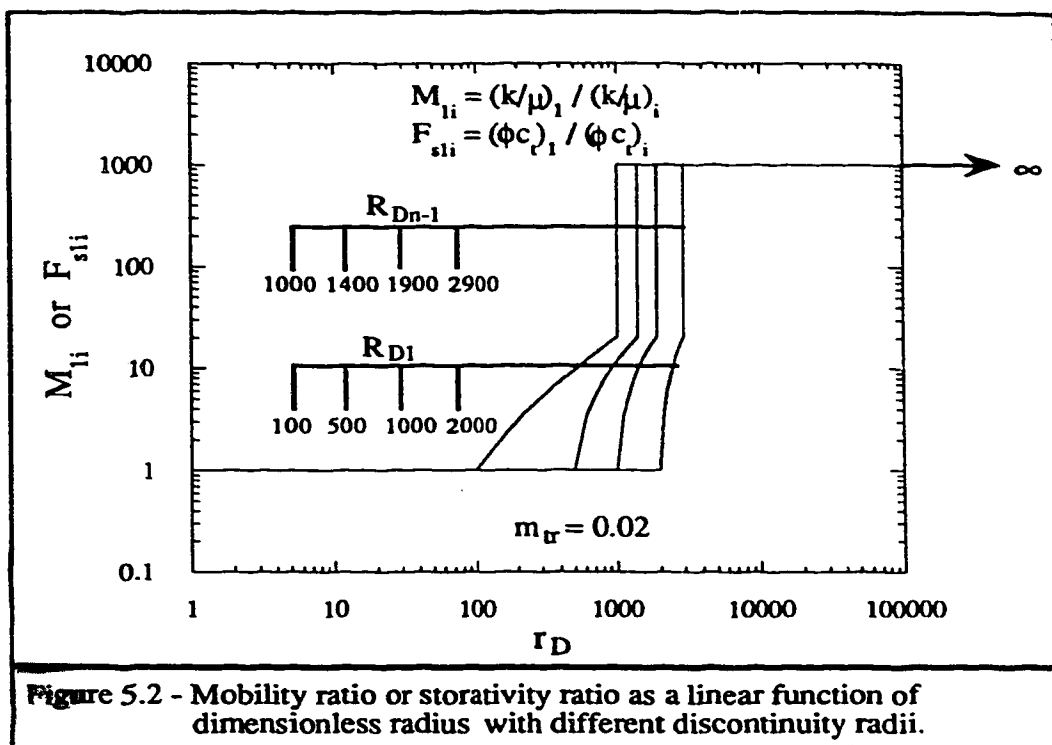


Figure 5.2 - Mobility ratio or storativity ratio as a linear function of dimensionless radius with different discontinuity radii.

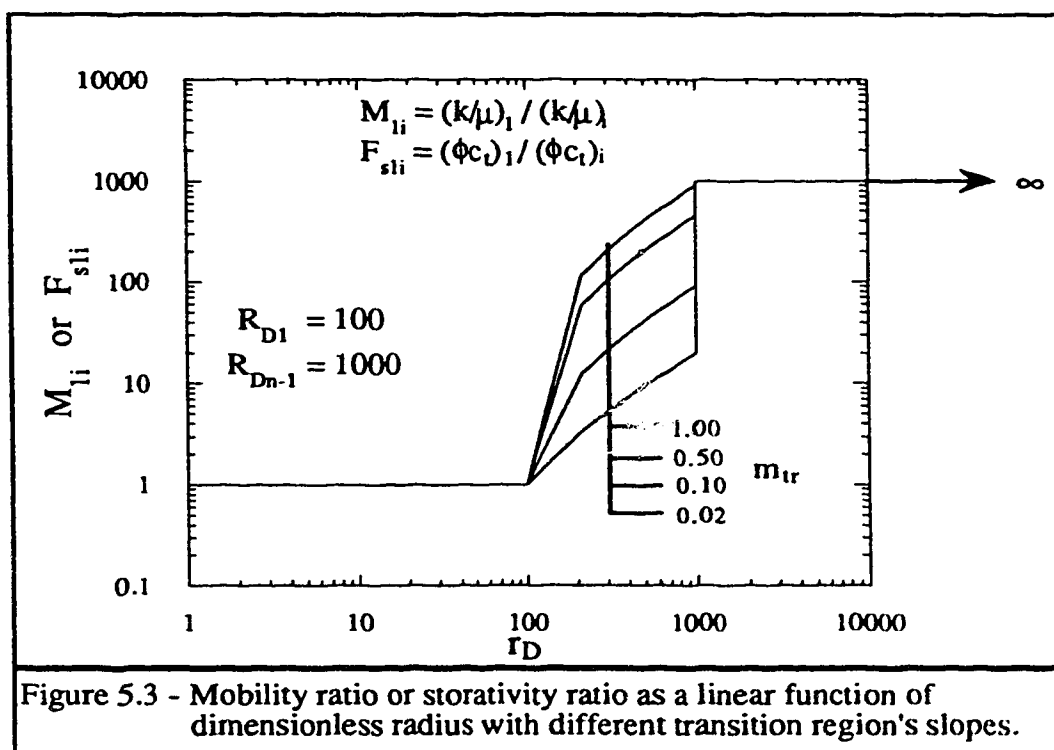
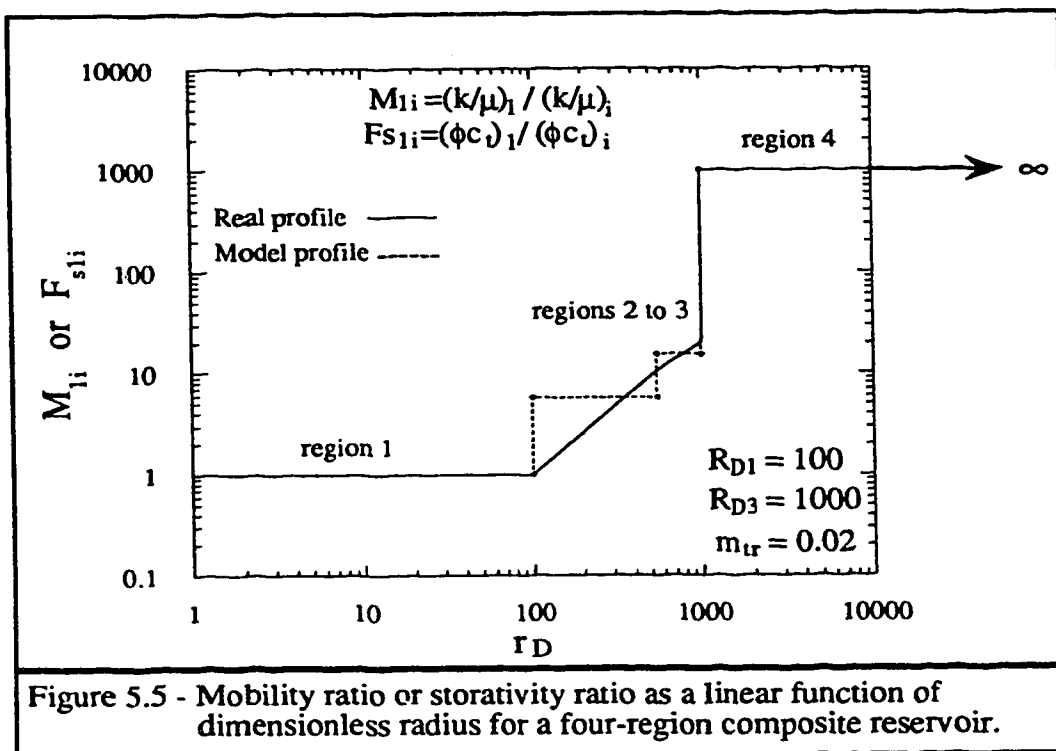
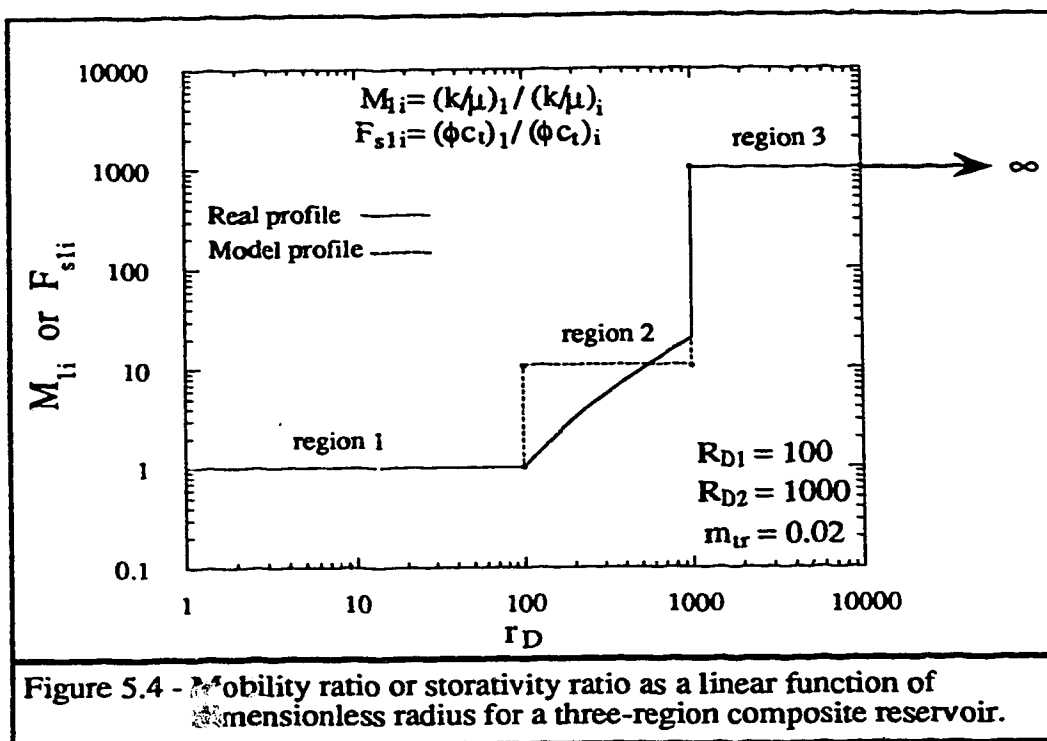


Figure 5.3 - Mobility ratio or storativity ratio as a linear function of dimensionless radius with different transition region's slopes.



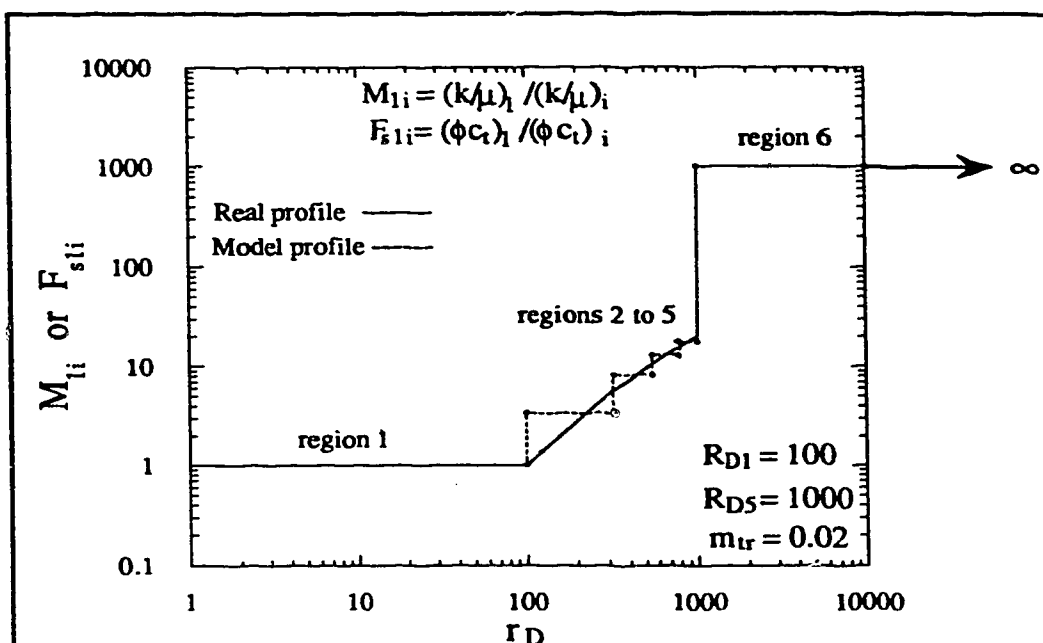


Figure 5.6 - Mobility ratio or storativity ratio as a linear function of dimensionless radius for a six-region composite reservoir.

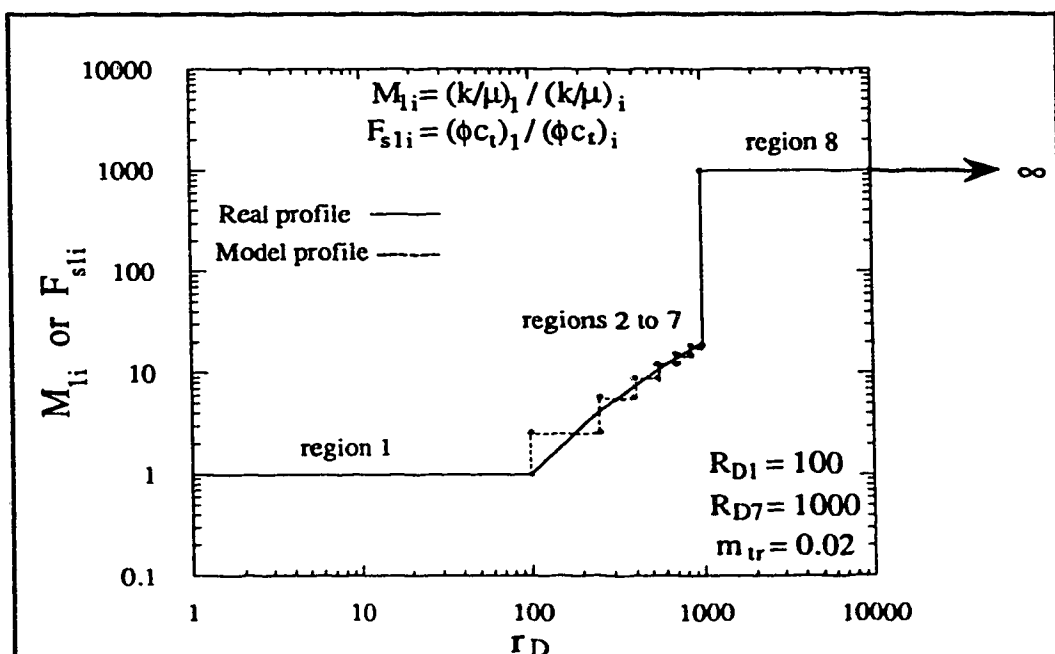
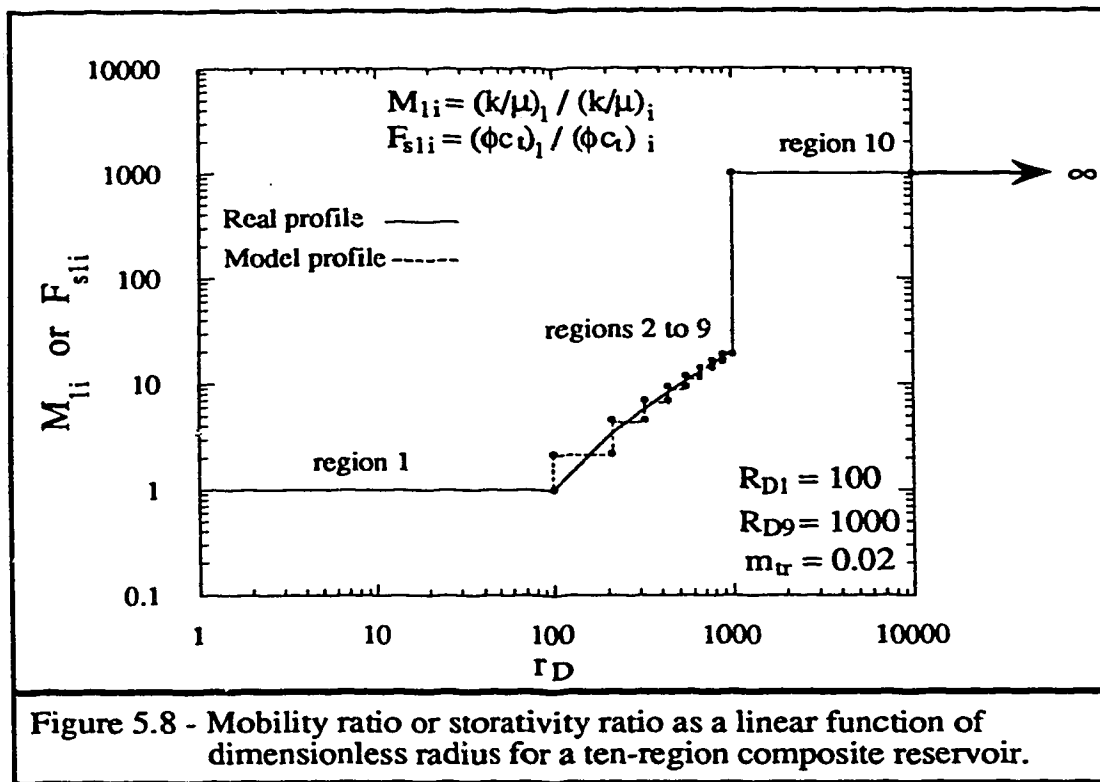


Figure 5.7 - Mobility ratio or storativity ratio as a linear function of dimensionless radius for an eight-region composite reservoir.



composite model to a ten-region composite model. The three-region composite model represents the transition region using one region. The ten-region composite model represents the transition region using eight regions. In all composite models, the swept and the unswept regions are represented by one region each.

The three-region composite model and the ten-region composite model use different values of mobility ratio and/or storativity ratio to represent the transition region's linear profile. To represent this linear profile, a material balance method is used. This method was first proposed by *van Everdingen et al.* (1953) when analyzing the pressure behaviour of an aquifer. Based on this method, there will be two areas between the actual profile line and the value selected. One area is above the actual profile and the other area is under the actual profile line. These areas have triangular shapes (see Figures 5.4 through 5.8). For the case of the three-region composite model, there exists one triangular area above the profile line and one triangular area below the profile line. For the case of a ten-region composite model, there are eight triangular areas above the profile line and eight triangular areas below the profile line. The criterion to select the values representing the transition region is that the areas above the profile should be the same as the areas below the profile line. The smaller the triangular areas, the better is the representation of the straight line profile for mobility and/or storativity variation in the transition region.

Representing a steam injection project by a three-region composite model may yield significantly different pressure transient responses compared to a representation using a ten-region composite model. This study considers such differences in the transient pressure behaviour when the reservoir is represented by a multi-region (three or more regions) composite model.

## 5.2 Steam Injection Pressure Transient Behaviour

Depending on reservoir properties, well conditions and the amount of steam injected, the pressure transient behaviour of a reservoir undergoing steam injection, can be described by different transient flow periods. These periods are:

1. A wellbore storage dominated flow period,
2. An early radial flow period which reflects the mobility of the inner region,
3. An early transition flow period reflecting mobility and/or storativity changes,
4. A pseudosteady state flow period reflecting a large mobility or storativity contrast,
5. A late transition flow period reflecting mobility and/or storativity changes, and
6. A late radial flow period which reflects the mobility of the outer region.

A pressure derivative graph enhances the detail in the information that can be obtained from a well test. Therefore, by using pressure derivative graphs, the pressure transient analysis from a reservoir may be improved. In most of this study, pressure derivative graphs have been used.

A log-log plot of the semilog pressure derivative ( $dp_{wD} / d\ln t_D$ ) versus dimensionless time ( $t_D$ ) may be used to identify the different flow regimes. Various regimes are identified by:

1. A unit slope line for the wellbore dominated period,
2. A zero slope line for for early radial flow in the swept region,
3. A unit slope line for the pseudosteady state flow period, and
4. A zero slope line for the late radial flow in the unswept region.

A log-log plot of the dimensionless Cartesian pressure derivative ( $dp_{wD} / dt_{DA}$ ) versus area-based dimensionless time ( $t_{DA}$ ) may be used to obtain valuable information from a reservoir's pressure transient behaviour. Throughout this study, the area used in the definition of area-based dimensionless time is the area to the last discontinuity radius  $R_{Dn-1}$ . When analyzing a log-log graph of Cartesian pressure derivative versus area-based dimensionless time, various flow regimes are identified by:

1. A zero slope line for the wellbore dominated period,
2. A negative unit slope line for early radial flow in the swept region,
3. A zero slope line for the pseudosteady state flow period, and
4. A negative unit slope line for the late radial flow in the unswept region.

Although the wellbore dominated flow period has been mentioned for completeness sake, this study only considers cases with no wellbore storage. Skin at the wellbore and skin at the discontinuities are also considered to be zero. Since wellbore storage and skin effects have been sufficiently analyzed in previous studies, other features of transient pressure behaviour are considered in this study.

When there is a well defined pseudosteady state period, a log-log graph of the semilog pressure derivative ( $dp_{wD} / d\ln t_D$ ) versus dimensionless time ( $t_D$ ) will exhibit a unit slope line. During the pseudosteady state period, the slope of a Cartesian straight line on a pressure versus time graph is inversely proportional to the volume to the discontinuity at which sharp contrasts in mobility and/or storativity occur. In some cases, after observing the early radial flow and a transition flow period, the semilog pressure derivative data falls

on a straight line, whose slope is less than unity. In such cases, application of the pseudosteady state concept leads to an overestimation of the volume to the last discontinuity radius. *Sheng* (1992) explained that this phenomenon may be caused by a small hot water zone, thermal effects and/or low mobility contrasts between regions. This study further investigates the reasons for this phenomenon.

In a graph of dimensionless Cartesian pressure derivative ( $dp_{wD} / dt_{DA}$ ) versus area-based dimensionless time ( $t_{DA}$ ), a flattening or a zero slope line segment may indicate a pseudosteady state flow period. The condition to be able to see this flattening is a significant mobility and/or storativity contrast between regions. When this flattening occurs at a value of the dimensionless Cartesian pressure derivative equal to  $2\pi$ , the property contrasts observed exist at the radius used to compute the area-based dimensionless time ( $t_{DA}$ ). In this study, the radius used to compute area-based dimensionless time ( $t_{DA}$ ) is the last discontinuity radius  $R_{Dn-1}$ . Thus, if a flattening is observed, when the Cartesian pressure derivative is equal to  $2\pi$ , then there is a significant mobility and/or storativity contrast at the last discontinuity radius  $R_{Dn-1}$ . If a flattening is observed and the value  $m_{cD}$  of the Cartesian pressure derivative is different from  $2\pi$ , then there is a significant mobility and/or storativity contrast at radius  $R_D$  given by:

$$R_D = \frac{R_{Dn-1}}{\sqrt{\frac{m_{cD}}{2\pi}}} \sqrt{\frac{(\phi c_v)_i}{(\phi c_v)_{eff}}} \quad (5.1)$$

For analytical pressure responses shown in this study, Equation 5.1 is useful to check if a correct  $m_{cD}$  occurs with respect to  $R_{D1}$ , as  $R_{Dn-1}$  is an input for data generation



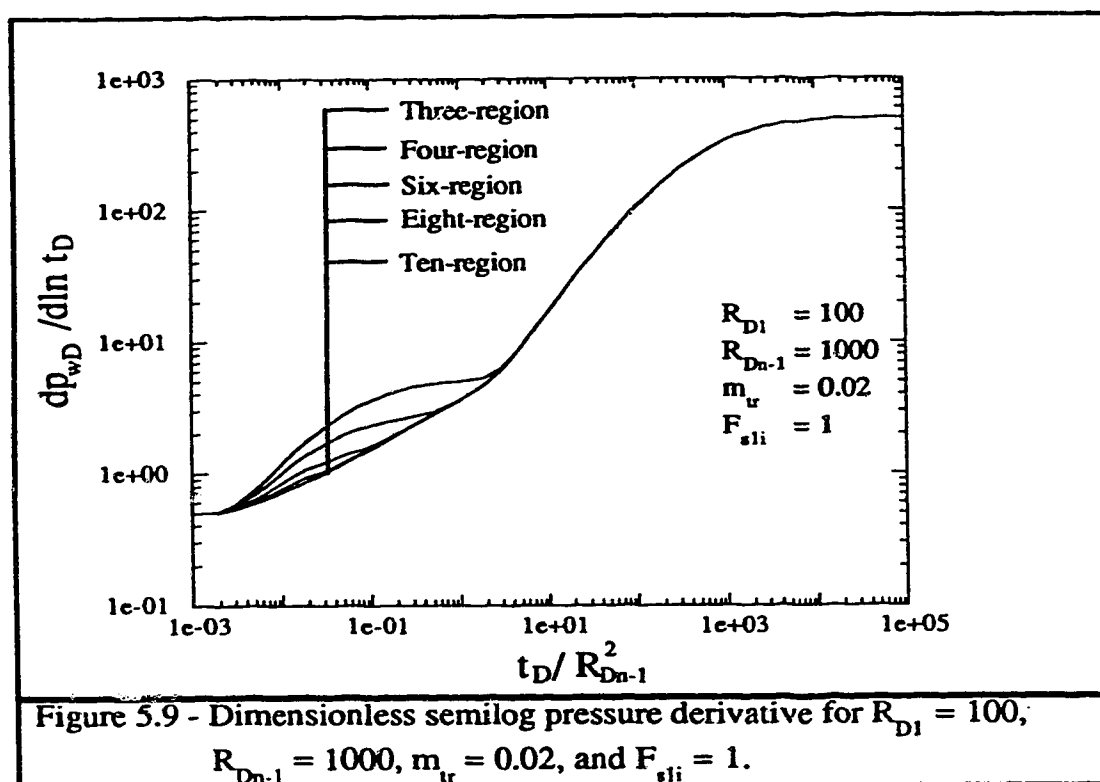
purposes. However, field application of Equation 5.1 is limited because  $R_{Dn-1}$  may not be known accurately. In Equation (5.1), it is important to note that  $(\phi c_L)_{eff}$  is the effective storativity corresponding to the volume up to  $R_D$ .

### 5.3 Analyzing Pressure Transient Responses for a Multi-region Composite Reservoir

This section contains a study of transient pressure responses corresponding to the mobility ratio and storativity ratio profiles shown on Figures 5.4 through 5.8.

Figure 5.9 compares the dimensionless semilog pressure derivative behaviour of several composite models. For all the models, an early and a late radial flow period are observed. The semilog pressure derivative has a value of 0.5 for the early radial flow period and a value of 500 for the late radial flow period. These two values for the semilog pressure derivative represent the swept and unswept region's mobility ratios, respectively. By definition, the mobility ratios of the swept and unswept regions are equal to two times the value of the semilog pressure derivative on the early and late radial flow periods respectively. In our case, the swept region has a mobility ratio of 1, as defined in section 5.2, and the unswept region has a value of 1000.

In Figure 5.9, it can be observed that neither the departure time from the early radial flow period nor the transition region's duration are affected by the number of regions of the composite model. However, the transition region's transient pressure behaviour is affected by the number of regions of the model. Therefore, the information that can be obtained



from the transition region is affected by the number of regions of the model. As observed in Figure 5.9, the transition region's values for the semilog pressure derivative are higher for the three-region composite model than for the ten-region composite model. Thus, this suggests that the value of the transition region's effective mobility ratio for the three-region model is higher than the effective mobility ratio for the ten-region model. Values for the transition region's effective mobility ratio were computed by applying Equation A.9 to the data input values (Tables C2 and C10) of the composite models. A value of 3.07 was obtained for the effective mobility ratio of the ten-region model, while a value of 4.16 was obtained for the effective mobility ratio of the three region composite model. These values confirm the observations from Figure 5.9.

Also, from Figure 5.9, it can be seen that the three-region composite model shows an initial transition period, after the early radial flow, in which the dimensionless semilog pressure derivative falls on a line. This line appears, because of the mobility contrast at the inner region radius. This mobility contrast is the consequence of only one region representing the transition zone. The slope of this line is less than one and suggests a low mobility contrast between regions. The dimensionless Cartesian pressure derivative on Figure 5.10 confirms that there is a low mobility contrast at early times of the pressure transient behaviour. This low mobility contrast is indicated by a deviation of the Cartesian pressure derivative from the negative unit slope line. However, since the mobility contrast is low, the Cartesian pressure derivative does not flatten as it does when there is a high contrast in mobility or storativity. A high contrast in mobility or storativity originates a pseudosteady state period.

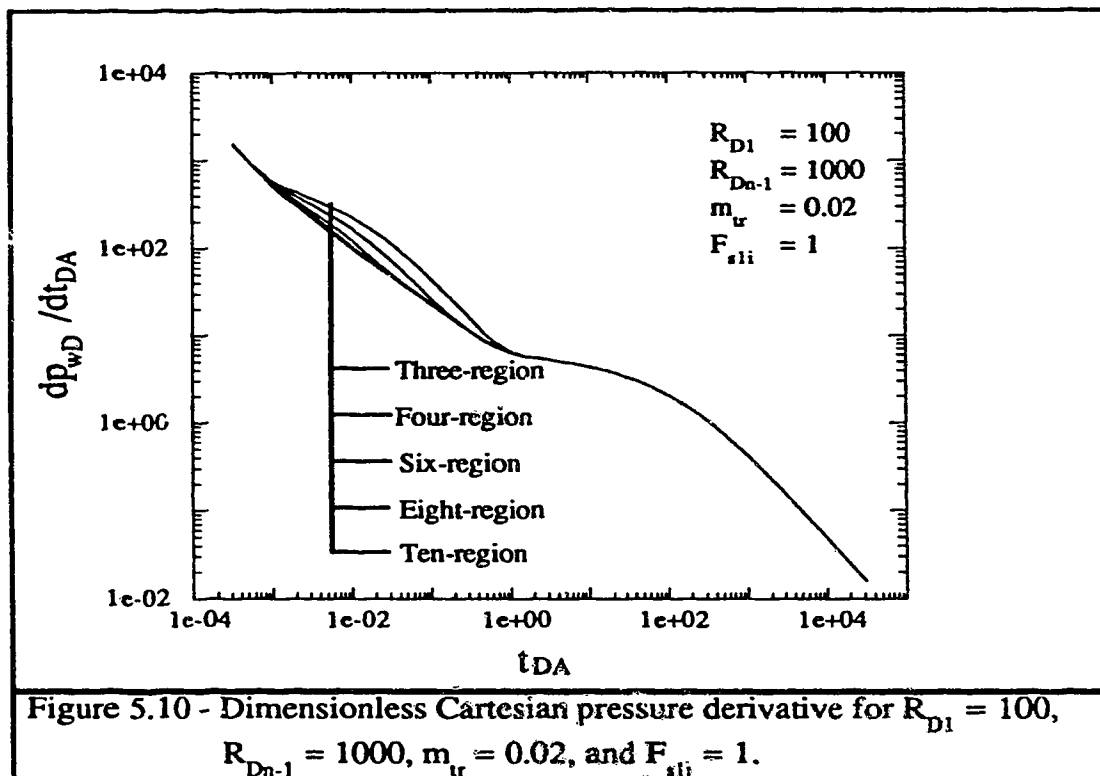
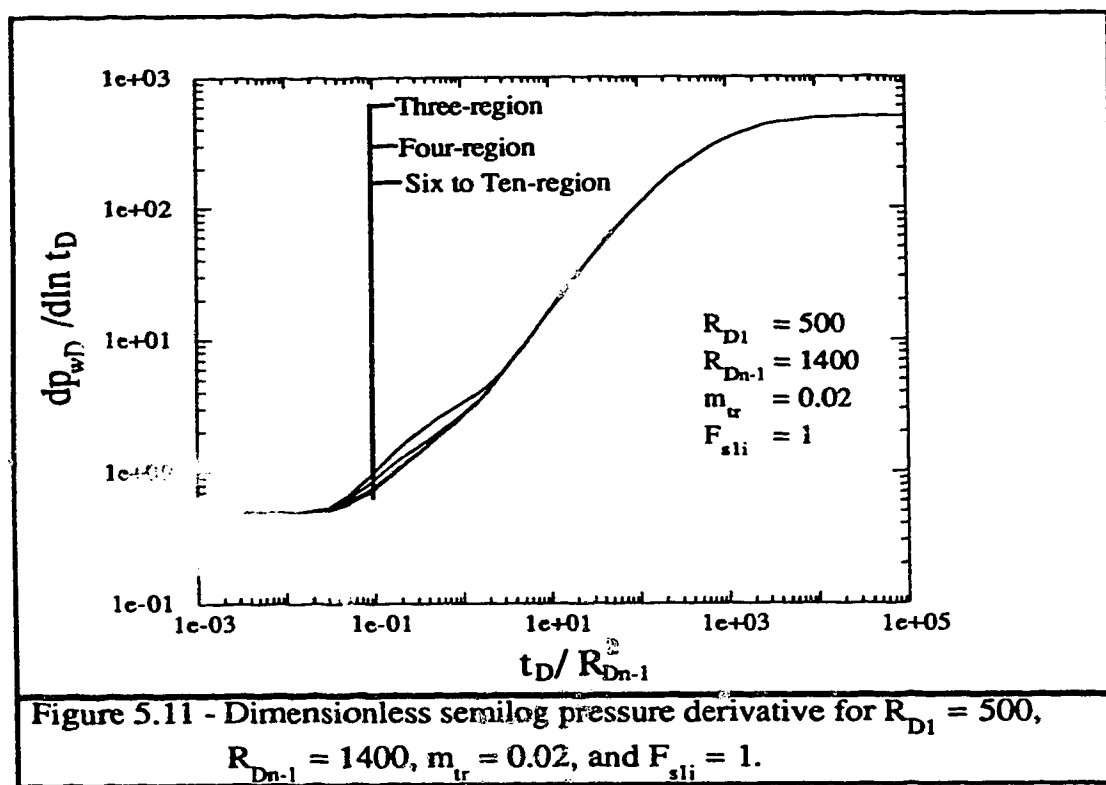


Figure 5.10 shows that all the composite models deviate from the negative unit slope at the same time,  $4 \times 10^{-4}$ , approximately. At this deviation time, the dimensionless Cartesian pressure derivative has a value  $m_{cD}$  of approximately 630. By applying Equation 5.1, a first dimensionless discontinuity radius of approximately 100 was found. This estimated value of first dimensionless discontinuity radius satisfactorily agrees with the input value.

Figure 5.9 shows that there is a time, when, for all of the composite models, the semilog pressure derivative falls on a unit slope straight line. This unit slope straight line indicates a pseudosteady state period due to a high mobility contrast. Figure 5.10 confirms this high contrast by a flattening of the Cartesian pressure derivative. This flattening occurs, when the Cartesian pressure derivative has a value of  $2\pi$ . As explained in Section 5.2, this transient pressure behaviour shows a high mobility contrast at the last discontinuity radius  $R_{Dn-1}$ , as expected.

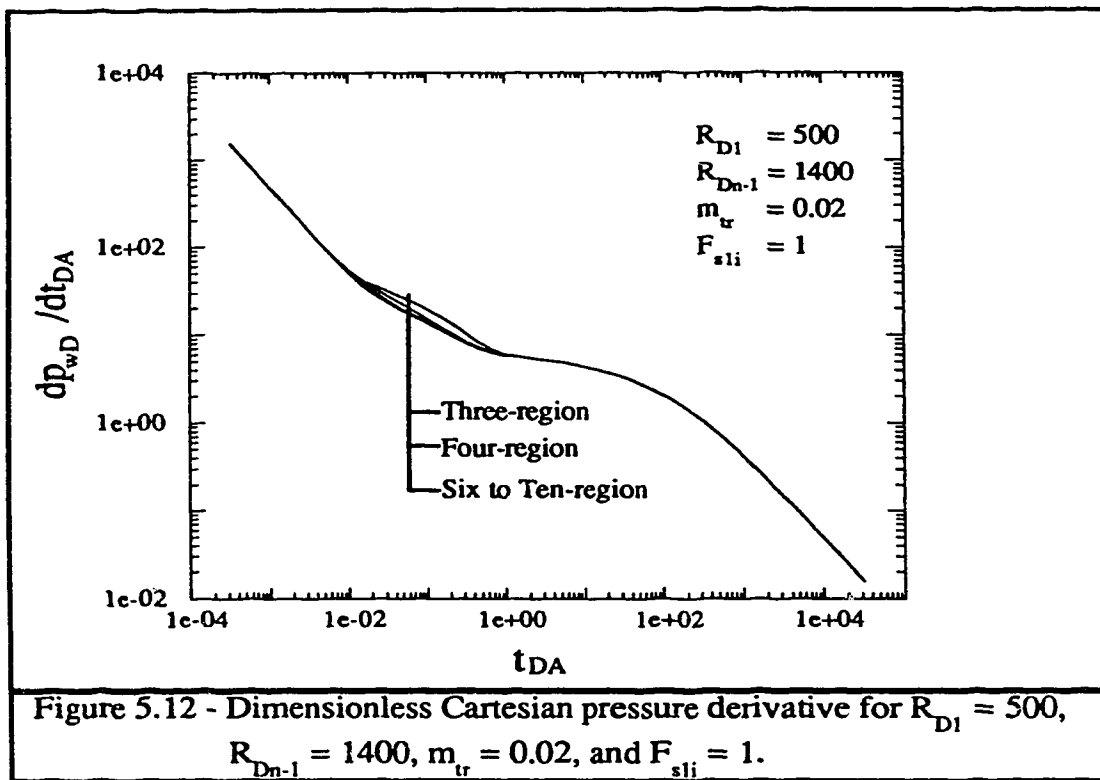
Figure 5.11 shows the effect of increasing the first discontinuity radius on pressure transient behaviour. Although the input mobility ratios are the same as for Figures 5.9 and 5.10, it seems that changing the first and last discontinuity radii affects the effective mobility ratio of the multi-region (three or more regions) composite systems. By applying Equation A.9 to the input mobility ratios of the three-region composite model, an effective mobility ratio of 2.35 was found, while doing the same thing for the ten-region model yielded an effective mobility ratio of 2.12. This is one likely reason as to why the pressure behaviour for all the composite models are closer to each other than those in the previous case of smaller first discontinuity radius (see Figure 5.9 for comparison).



Also, from Figure 5.11, it is observed that the transition region's effects are felt later than the previous case on Figures 5.9 and 5.10, as expected. Thus, increasing the first discontinuity radius increases the deviation time. Another effect of increasing the first discontinuity radius is that the transition region's effects become weaker and the duration of the transition region is shorter.

A general behaviour for all composite models is observed in Figure 5.11. Soon after the end of early radial flow, the semilog pressure derivative falls on a straight line for a short time period. The slope of this straight line is lower than unity. As the number of regions representing the transition region increases, this straight line slope becomes smaller indicating a lower mobility contrast. Thus, more regions in a multi-region composite model, mimicking continuous property variations for an actual reservoir, reduce the possibility of obtaining a unit slope line for the transition pressure behaviour. In theoretical pressure transient models, a unit slope line appears as a consequence of representing a zone with continuously changing mobility or storativity as one region. This one-region representation also erroneously increases the duration of any real pseudosteady state flow period.

At a later period of time in the transition region response, Figure 5.11 shows that all composite models join together and the semilog pressure derivative falls on a straight line. The slope of this straight line is unity, indicating a pseudosteady state period due to a high mobility contrast. Figure 5.12 confirms this high contrast by a flattening of the Cartesian pressure derivative. This flattening occurs, when the Cartesian pressure derivative has a value of  $2\pi$ . This indicates that a large mobility contrast exists at the last discontinuity radius  $R_{Dn-1}$ . By using Equation 5.1, the first dimensionless discontinuity radius can also

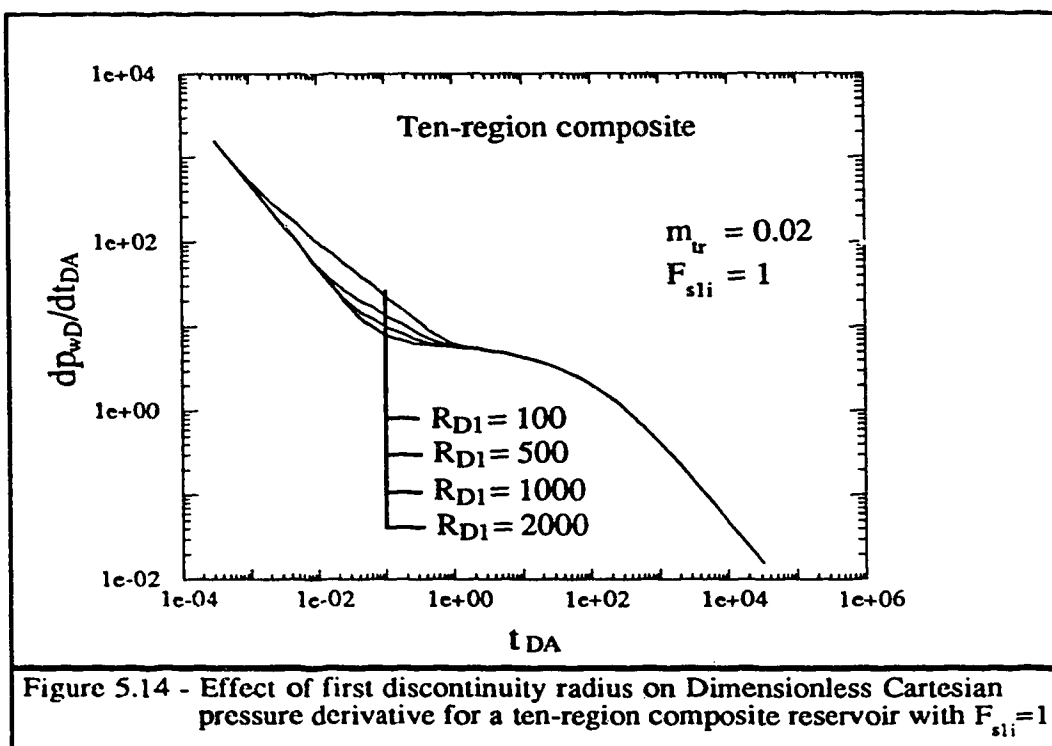
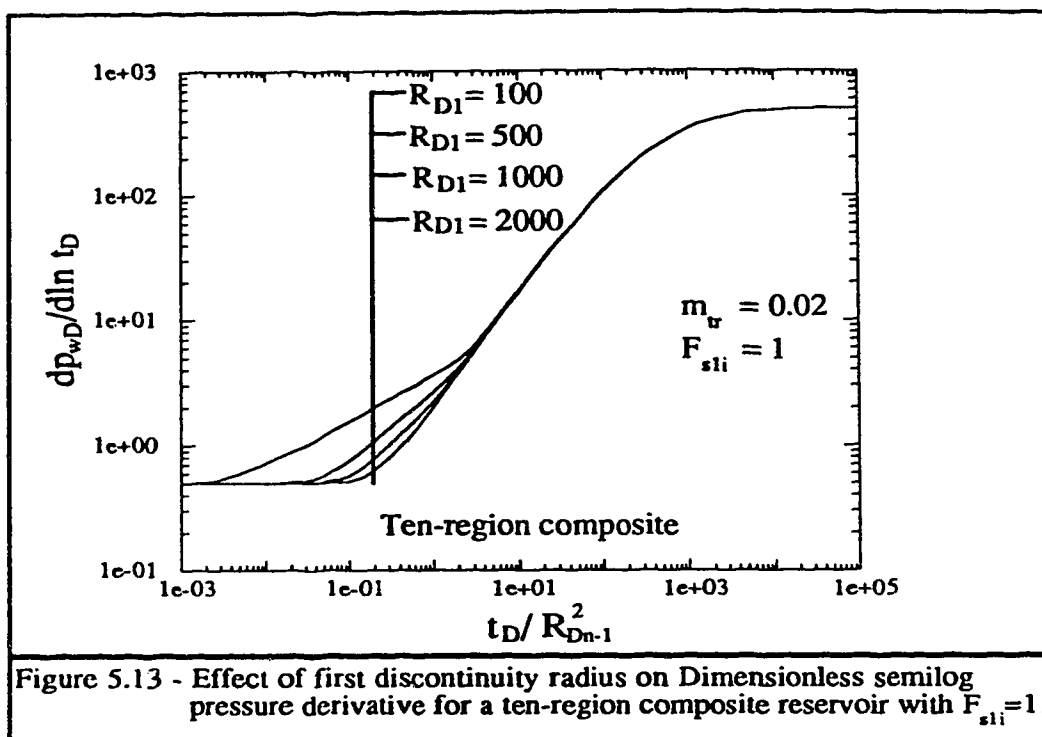


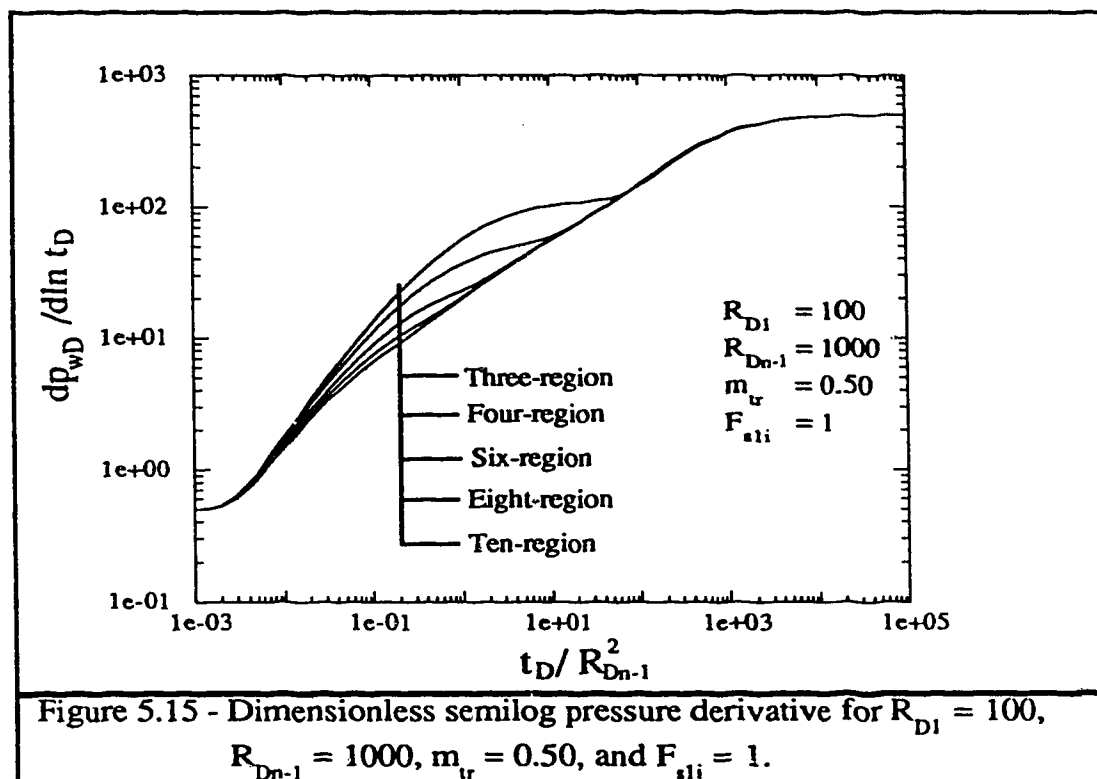


be estimated for the response in Figure 5.12. The first point when the Cartesian pressure derivative deviates from the negative unit slope line indicates a Cartesian pressure derivative value of approximately 49. By applying Equation 5.1 as discussed previously, a value of approximately 500 was obtained for the first dimensionless discontinuity radius. This estimated first dimensionless discontinuity radius is the same as the input value of 500.

Figures 5.13 and 5.14 show the effects of different values of first discontinuity radius on the semilog pressure derivative and the Cartesian pressure derivative behaviour. Figure 5.13 shows that the larger the first discontinuity radius, the larger is the deviation time. Increasing the first discontinuity radius reduces the effects of the transition region on pressure behaviour. The duration of the transition region effects on the pressure behaviour is inversely related to the first discontinuity radius. If the first discontinuity radius is too large compared with the last discontinuity radius, the inner region effects may mask all the transition region effects on the pressure behaviour. Except for the case of totally masked transition region effects, the method based on Equation 5.1 is not affected by the first discontinuity radius.

Figure 5.15 shows the semilog pressure derivative behaviour of another mobility profile. The overall mobility ratio is 1000 as in previous cases. However, a slope( $m_{tr}$ ) of 0.5 is assigned to the transition region's straight line mobility profile. Thus, the mobility ratio at the first discontinuity radius is greater than in previous cases. Increasing the transition region's slope causes a high mobility contrast between the swept region and the transition region. This contrast is observed in Figure 5.15 at the beginning of the transition region effects, when for all the models, the semilog pressure derivative falls on a straight line with a unit slope indicating the pseudosteady state period soon after the end of early radial flow.



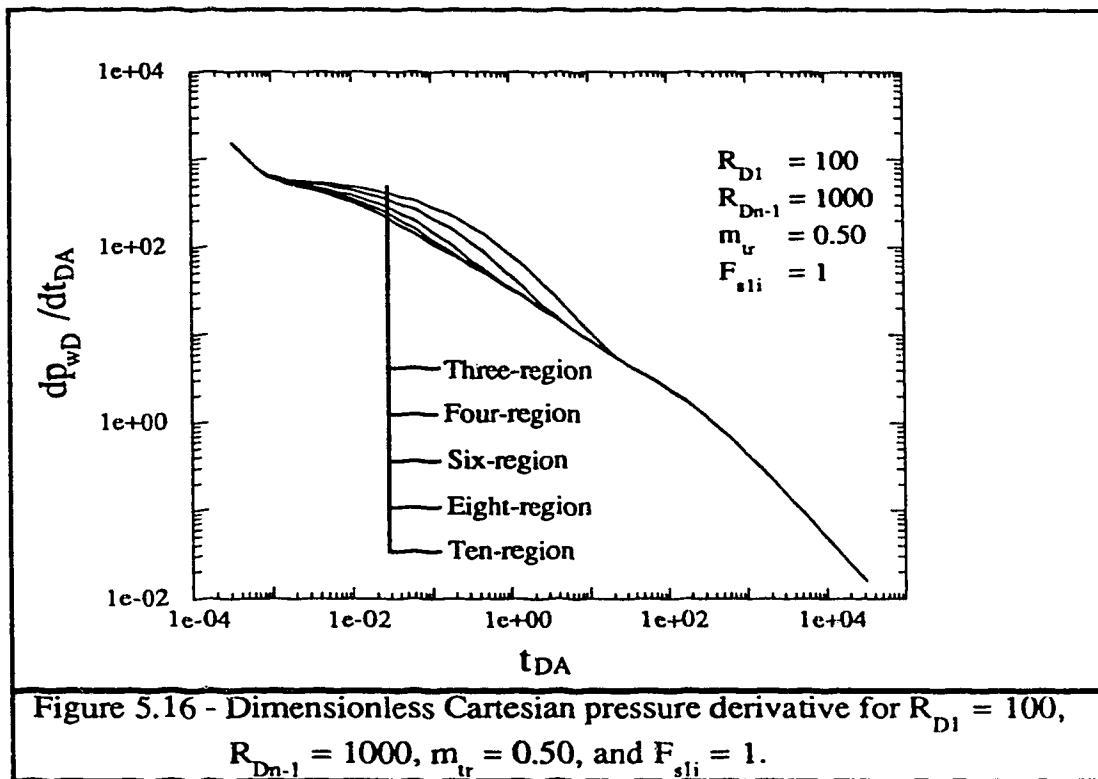


Another effect of increasing the transition region's slope  $m_{tr}$  is that now there is a lower mobility contrast between the transition region and the unswept zone. The effects of this low mobility contrast can be observed in Figure 5.15 at the late transition flow period. This period shows that, for all composite models, the semilog pressure derivative curves fall on a straight line with a slope lower than one. With data from this period of time, the pseudosteady state method may be used to estimate the last discontinuity radius. However, the last discontinuity radius would be overestimated.

Figure 5.16 shows a flattening of the Cartesian pressure derivative, confirming the high contrast in mobility between the swept region and the transition region. Applying Equation 5.1 to the value  $m_{CD}$  of the Cartesian pressure derivative at the first deviation point from the negative unit slope line will yield the first discontinuity radius. The estimated first discontinuity radius is 93, which is slightly lower than the input value of 100.

Figures 5.17 and 5.18 show the effects on the semilog pressure derivative and the Cartesian pressure derivative behaviour of several values of the transition region's slope. In general, increasing the transition region's slope causes an increase in the mobility contrast between the swept and the transition region, while the mobility contrast between the transition region and the unswept region decreases. The higher the mobility contrast, the higher are the chances of existence of a pseudosteady state period.

For low mobility contrasts between the swept and transition regions, Equation 5.1 yields good estimates of the first discontinuity radius. For high mobility contrasts, the pseudosteady state method yields good estimates of the appropriate discontinuity radius, if a correct effective compressibility is used for the analysis. When an adequate flattening in





National Library  
of Canada

Acquisitions and  
Bibliographic Services Branch

395 Wellington Street  
Ottawa, Ontario  
K1A 0N4

Bibliothèque nationale  
du Canada

Direction des acquisitions et  
des services bibliographiques

395, rue Wellington  
Ottawa (Ontario)  
K1A 0N4

Your file - Votre référence

Our file - Notre référence

## NOTICE

The quality of this microform is heavily dependent upon the quality of the original thesis submitted for microfilming. Every effort has been made to ensure the highest quality of reproduction possible.

If pages are missing, contact the university which granted the degree.

Some pages may have indistinct print especially if the original pages were typed with a poor typewriter ribbon or if the university sent us an inferior photocopy.

Reproduction in full or in part of this microform is governed by the Canadian Copyright Act, R.S.C. 1970, c. C-30, and subsequent amendments.

## AVIS

La qualité de cette microforme dépend grandement de la qualité de la thèse soumise au microfilmage. Nous avons tout fait pour assurer une qualité supérieure de reproduction.

S'il manque des pages, veuillez communiquer avec l'université qui a conféré le grade.

La qualité d'impression de certaines pages peut laisser à désirer, surtout si les pages originales ont été dactylographiées à l'aide d'un ruban usé ou si l'université nous a fait parvenir une photocopie de qualité inférieure.

La reproduction, même partielle, de cette microforme est soumise à la Loi canadienne sur le droit d'auteur, SRC 1970, c. C-30, et ses amendements subséquents.

UNIVERSITY OF ALBERTA

THERMAL WELL TEST ANALYSIS AND EVALUATION OF  
RESERVOIR CHARACTERIZATION METHODS USING AN  
ANALYTICAL MULTI-REGION COMPOSITE RESERVOIR MODEL

BY



LUIS GUILLERMO ACOSTA

A THESIS

SUBMITTED TO THE FACULTY OF GRADUATE STUDIES AND RESEARCH IN  
PARTIAL FULFILMENT OF THE REQUIREMENTS FOR THE DEGREE OF

MASTER OF SCIENCE

IN

PETROLEUM ENGINEERING

DEPARTMENT OF MINING, METALLURGICAL AND PETROLEUM  
ENGINEERING

EDMONTON, ALBERTA

SPRING, 1994



National Library  
of Canada

Acquisitions and  
Bibliographic Services Branch

395 Wellington Street  
Ottawa, Ontario  
K1A 0N4

Bibliothèque nationale  
du Canada

Direction des acquisitions et  
des services bibliographiques

395, rue Wellington  
Ottawa (Ontario)  
K1A 0N4

*Vous le trouverez*

*Vous le trouverez*

**The author has granted an irrevocable non-exclusive licence allowing the National Library of Canada to reproduce, loan, distribute or sell copies of his/her thesis by any means and in any form or format, making this thesis available to interested persons.**

**L'auteur a accordé une licence irrévocable et non exclusive permettant à la Bibliothèque nationale du Canada de reproduire, prêter, distribuer ou vendre des copies de sa thèse de quelque manière et sous quelque forme que ce soit pour mettre des exemplaires de cette thèse à la disposition des personnes intéressées.**

**The author retains ownership of the copyright in his/her thesis. Neither the thesis nor substantial extracts from it may be printed or otherwise reproduced without his/her permission.**

**L'auteur conserve la propriété du droit d'auteur qui protège sa thèse. Ni la thèse ni des extraits substantiels de celle-ci ne doivent être imprimés ou autrement reproduits sans son autorisation.**

ISBN 0-612-11140-7

**Canada**



**UNIVERSITY OF ALBERTA**  
**RELEASE FORM**

**NAME OF AUTHOR:** Luis Guillermo Acosta

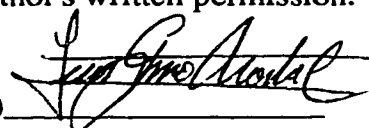
**TITLE OF THESIS:** Thermal Well Test Analysis and Evaluation of  
Reservoir Characterization Methods Using an  
Analytical Multi-Region Composite Reservoir Model

**DEGREE FOR WHICH THESIS WAS PRESENTED:** Master of Science

**YEAR THE DEGREE WAS GRANTED:** Spring, 1994

Permission is hereby granted to THE UNIVERSITY OF ALBERTA LIBRARY to reproduce single copies of this thesis and to lend or sell such copies for private, scholarly or scientific research purposes only.

The author reserves other publication rights, and neither the thesis nor extensive extracts from it may be printed or otherwise reproduced without the author's written permission.

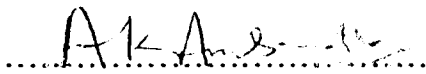
(SIGNED) 

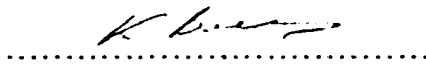
**PERMANENT ADDRESS:**  
250 Hillington Court  
Edmonton, Alberta  
CANADA T5R-5X5

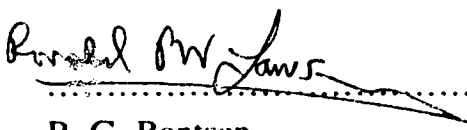
**DATED:** March 16, 1994.


THE UNIVERSITY OF ALBERTA  
FACULTY OF GRADUATE STUDIES AND RESEARCH

The undersigned certify that they have read, and recommend to the Faculty of Graduate Studies and Research for acceptance, a thesis called " THERMAL WELL TEST ANALYSIS AND EVALUATION OF RESERVOIR CHARACTERIZATION METHODS USING AN ANALYTICAL MULTI-REGION COMPOSITE RESERVOIR MODEL " submitted by LUIS GUILLERMO ACOSTA in partial fulfilment of the requirements for the degree of MASTER OF SCIENCE in PETROLEUM ENGINEERING.

  
A. K. Ambastha (Supervisor)

  
K. Barron

  
R. G. Bentsen

  
K. Nandakumar

DATED: February 25, 1994.

## **ABSTRACT**

To monitor the progress of a thermal recovery project, such as a steam injection operation, it is important to have a knowledge of the volume swept by the injecting fluid. Well testing offers a comparatively rapid and economical way of estimating the swept volume. Well tests conducted on wells undergoing a thermal recovery process typically have been idealized using a two or three-region composite reservoir model. Each of these regions has different rock and fluid properties. However, for continuous variations of mobility and storativity within the swept region, a simple two- or three-region model may not be appropriate.

A multi-region, composite reservoir model has been developed to study the effects of various trends of mobility and storativity variations, within the swept region, on well tests for composite reservoirs. This study has been designed to address analytically the problem of multi-region composite reservoir by using the Laplace transformation technique. The solution to the problem in Laplace space is inverted numerically to real space by means of the Stehfest algorithm.

The multi-region composite reservoir model has been used to analyze drawdown tests from reservoirs undergoing a thermal recovery process such as steam injection or in-situ combustion. Based on the mobility and/or storativity of these reservoirs, three zones may be identified for a reservoir undergoing a thermal recovery process. These zones are: a swept zone with the highest mobility and/or storativity, a transition zone with continuously

changing mobility and/or storativity, and an unswept zone with the lowest values for mobility and/or storativity. This study is intended to investigate how representing these reservoirs by different numbers of regions affects the pressure behaviour analysis. It has been found that representing the transition zone by one region may generate pressure behaviours which may show higher contrasts in physical properties than what actually exist. Using various regions to represent the transition zone will avoid these apparently high or non-existing property contrasts.

The purpose of investigating how these factors change the reservoir pressure behaviour is to ascertain what effect these factors will have on the estimation of swept volume and effective properties of the reservoir. This study presents an evaluation of the applicability, utility and accuracy of the pseudosteady state method to estimate the swept volume in a steam injection project.

Finally, this work is intended to demonstrate how storativity variation can affect significantly the results obtained from some reservoir characterization methods. It has been shown that reservoir characterization methods, in which mobility is considered to be the only variable affecting the pressure behaviour from a reservoir, will fail when there is a storativity variation in the reservoir. This is consistent with the well known fact that the pressure behaviour from a reservoir is affected by both mobility and storativity.

## **ACKNOWLEDGEMENTS**

I sincerely wish to express my gratitude and appreciation to Professor A.K. Ambastha for his excellent guidance and encouragement throughout this study. I also gratefully acknowledge Professor K. Nandakumar for letting me use one of his research computers. Miscellaneous help from Mr. Paul A. Barrow and Mr. Rob L. Barton, concerning the use of computer accounts, is greatly appreciated. I would also like to thank my friend Ben Issaka for his helpful suggestions throughout this study. Financial support for this work was provided by Energy, Mines and Resources (E.M.R), and Alberta Oil Sands Technology and Research Authority (AOSTRA), for which I am very thankful. I also wish to acknowledge the use of the work station as well as other computer facilities from the Chemical Engineering and Mining, Metallurgical and Petroleum Engineering departments, respectively, of the University of Alberta. I am indebted to my parents, Guillermo and Dorita, and my sister, Elena, for their unlimited love, patience, understanding and support during my graduate studies.

# TABLE OF CONTENTS

## Page

LIST OF TABLES

LIST OF FIGURES

NOMENCLATURE

1.	INTRODUCTION .....	1
2.	LITERATURE REVIEW .....	3
2.1	Two-region Composite Models .....	5
2.1.1	Analytical Approach .....	5
2.1.2	Numerical Approach .....	12
2.2	Three-region Composite Models .....	15
2.2.1	Analytical Approach .....	15
2.2.2	Numerical Approach .....	16
2.3	Multi-region Composite Models .....	17
2.3.1	Analytical Approach .....	18
2.3.2	Numerical Approach .....	19
2.4	Drawdown Analysis .....	20
2.5	Estimating Swept Volume in Thermal Recovery Projects .....	21
2.5.1	Deviation Time Method .....	21
2.5.2	Intersection Time Method .....	22
2.5.3	Type-Curve Matching Method .....	23
2.5.4	Pseudosteady State Method .....	24
2.6	Mobility and Storativity Profiles .....	26
2.7	Discontinuity Radii .....	27

3.	STATEMENT OF THE PROBLEM .....	30
4.	MATHEMATICAL MODEL FOR A MULTI-REGION COMPOSITE RESERVOIR WITH SKIN AT THE DISCONTINUITIES .....	32
4.1	Mathematical Development.....	33
4.1.1	Governing Equations .....	33
4.1.2	Inner Boundary Conditions .....	33
4.1.3	Conditions at the Discontinuities .....	34
4.1.4	Outer Boundary Conditions .....	34
4.1.5	Initial Condition .....	35
4.1.6	Dimensionless Variables .....	35
4.1.7	General Solution .....	37
4.1.8	Solution's Constants.....	38
4.2	Verification of Solution .....	42
5.	DRAWDOWN TEST ANALYSIS FOR MULTI-REGION COMPOSITE RESERVOIRS .....	49
5.1	Description of a Reservoir undergoing Steam Injection .....	49
5.2	Steam Injection Pressure Transient Behaviour .....	58
5.3	Analyzing Pressure Transient Responses for a Multi-region Composite Reservoir .....	61
5.4	Analyzing Characterization Methods.....	92
6	CONCLUSIONS AND RECOMMENDATIONS .....	102
6.1	CONCLUSIONS .....	102
6.2	RECOMMENDATIONS .....	106
	REFERENCES .....	107

<b>APPENDIX A</b>	<b>Development of expressions for effective physical properties for multi-region composite reservoirs .....</b>	<b>114</b>
<b>APPENDIX B</b>	<b>Development of the dimensionless form of Yeh and Agarwal's (1989) equations .....</b>	<b>119</b>
<b>APPENDIX C</b>	<b>Data used to analyze the transient pressure response for a multi-region composite reservoir .....</b>	<b>126</b>
<b>APPENDIX D</b>	<b>Program to obtain the transient pressure response for a multi- region composite reservoir. A reservoir characterization subroutine is also included .....</b>	<b>133</b>
<b>APPENDIX E</b>	<b>Overcoming the matrix singularity problem .....</b>	<b>160</b>
<b>APPENDIX F</b>	<b>Transient pressure response for a multi-region composite reservoir (sample results for a particular run) .....</b>	<b>163</b>
<b>APPENDIX G</b>	<b>Figures for transient pressure responses for multi-region composite reservoirs .....</b>	<b>171</b>



## LIST OF TABLES

	<u>Page</u>
Table C1	Discontinuity radii data for a multi-region composite reservoir visualized as a three-region composite reservoir ..... 127
Table C2	Physical properties data for a multi-region composite reservoir visualized as a three-region composite reservoir ..... 127
Table C3	Discontinuity radii data for a multi-region composite reservoir visualized as a four-region composite reservoir ..... 128
Table C4	Physical properties data for a multi-region composite reservoir visualized as a four-region composite reservoir ..... 128
Table C5	Discontinuity radii data for a multi-region composite reservoir visualized as a six-region composite reservoir ..... 129
Table C6	Physical properties data for a multi-region composite reservoir visualized as a six-region composite reservoir ..... 129
Table C7	Discontinuity radii data for a multi-region composite reservoir visualized as an eight-region composite reservoir ..... 130
Table C8	Physical properties data for a multi-region composite reservoir visualized as an eight-region composite reservoir ..... 130
Table C9	Discontinuity radii data for a multi-region composite reservoir visualized as a ten-region composite reservoir ..... 131
Table C10	Physical properties data for a multi-region composite reservoir visualized as a ten-region composite reservoir ..... 131
Table C11	Physical properties data for a multi-region composite reservoir for a particular ten-region case (Figures 5.29 and 5.30) ..... 132

## LIST OF FIGURES

	<u>Page</u>
Figure 2.1      Top view of a multi-region composite reservoir .....	4
Figure 4.1      Comparison between this study and Agarwal et al.'s (1970) work for $s = 0$ .....	43
Figure 4.2      Comparison between this study and Agarwal et al.'s (1970) work for $s = 20$ .....	43
Figure 4.3      Comparison between this study and Wattenbarger and Ramey's (1970) work for $s = 5$ .....	45
Figure 4.4      Comparison between this study and Wattenbarger and Ramey's (1970) work for $s = 20$ .....	45
Figure 4.5      Comparison between this study and Ambastha's (1992) work for $C_D = 0$ .....	46
Figure 4.6      Comparison between this study and Ambastha's (1992) work for $C_D = 5000$ .....	46
Figure 4.7      Comparison between this study and Ambastha and Ramey's (1992) work for various $M_{12}$ .....	48
Figure 4.8      Comparison between this study and Ambastha and Ramey's (1992) work for non-unit $F_{s12}$ and $F_{s13}$ .....	48
Figure 5.1      Mobility ratio or storativity ratio versus dimensionless radius in a multi- region composite reservoir in which mobility ratio or storativity ratio is a linear function of dimensionless radius .....	51
Figure 5.2      Mobility ratio or storativity ratio as a linear function of dimensionless radius with different discontinuity radii .....	53

Figure 5.3	Mobility ratio or storativity ratio as a linear function of dimensionless radius with different transition region's slopes .....	53
Figure 5.4	Mobility ratio or storativity ratio as a linear function of dimensionless radius for a three-region composite reservoir .....	54
Figure 5.5	Mobility ratio or storativity ratio as a linear function of dimensionless radius for a four-region composite reservoir .....	54
Figure 5.6	Mobility ratio or storativity ratio as a linear function of dimensionless radius for a six-region composite reservoir .....	55
Figure 5.7	Mobility ratio or storativity ratio as a linear function of dimensionless radius for an eight-region composite reservoir .....	55
Figure 5.8	Mobility ratio or storativity ratio as a linear function of dimensionless radius for a ten-region composite reservoir .....	56
Figure 5.9	Dimensionless semilog pressure derivative for $R_{D1} = 100$ , $R_{Dn-1} = 1000$ , $m_{tr} = 0.02$ , and $F_{s1i} = 1$ .....	62
Figure 5.10	Dimensionless Cartesian pressure derivative for $R_{D1} = 100$ , $R_{Dn-1} = 1000$ , $m_{tr} = 0.02$ , and $F_{s1i} = 1$ .....	64
Figure 5.11	Dimensionless semilog pressure derivative for $R_{D1} = 500$ , $R_{Dn-1} = 1400$ , $m_{tr} = 0.02$ , and $F_{s1i} = 1$ .....	66
Figure 5.12	Dimensionless Cartesian pressure derivative for $R_{D1} = 500$ , $R_{Dn-1} = 1400$ , $m_{tr} = 0.02$ , and $F_{s1i} = 1$ .....	68
Figure 5.13	Effect of first discontinuity radius on dimensionless semilog pressure derivative for a ten-region composite reservoir with $F_{s1i} = 1$ .....	70
Figure 5.14	Effect of first discontinuity radius on dimensionless Cartesian pressure derivative for a ten-region composite reservoir with $F_{s1i} = 1$ .....	70

Figure 5.15	Dimensionless semilog pressure derivative for $R_{D1} = 100$ , $R_{Dn-1} = 1000$ , $m_{tr} = 0.50$ , and $F_{s1i} = 1$ .....	71
Figure 5.16	Dimensionless Cartesian pressure derivative for $R_{D1} = 100$ , $R_{Dn-1} = 1000$ , $m_{tr} = 0.50$ , and $F_{s1i} = 1$ .....	73
Figure 5.17	Effect of transition region's slope on dimensionless semilog pressure derivative for a ten-region composite reservoir with $F_{s1i} = 1$ .....	74
Figure 5.18	Effect of transition region's slope on dimensionless Cartesian pressure derivative for a ten-region composite reservoir with $F_{s1i} = 1$ .....	74
Figure 5.19	Dimensionless semilog pressure derivative for $R_{D1} = 100$ , $R_{Dn-1} = 1000$ , $m_{tr} = 0.02$ , and $M_{1i} = 1$ .....	76
Figure 5.20	Dimensionless Cartesian pressure derivative for $R_{D1} = 100$ , $R_{Dn-1} = 1000$ , $m_{tr} = 0.02$ , and $M_{1i} = 1$ .....	76
Figure 5.21	Effective dimensionless Cartesian pressure derivative for $R_{D1} = 100$ , $R_{Dn-1} = 1000$ , $m_{tr} = 0.02$ , and $M_{1i} = 1$ .....	78
Figure 5.22	Dimensionless semilog pressure derivative for $R_{D1} = 500$ , $R_{Dn-1} = 1400$ , $m_{tr} = 0.02$ , and $M_{1i} = 1$ .....	81
Figure 5.23	Dimensionless Cartesian pressure derivative for $R_{D1} = 500$ , $R_{Dn-1} = 1400$ , $m_{tr} = 0.02$ , and $M_{1i} = 1$ .....	84
Figure 5.24	Effect of first discontinuity radius on dimensionless semilog pressure derivative for a ten-region composite reservoir with $M_{1i} = 1$ .....	86
Figure 5.25	Dimensionless semilog pressure derivative for $R_{D1} = 100$ , $R_{Dn-1} = 1000$ , $m_{tr} = 0.50$ , and $M_{1i} = 1$ .....	86
Figure 5.26	Dimensionless Cartesian pressure derivative for $R_{D1} = 100$ , $R_{Dn-1} = 1000$ , $m_{tr} = 0.50$ , and $M_{1i} = 1$ .....	88

Figure 5.27	Effect of transition region's slope on dimensionless semilog pressure derivative for a ten-region composite reservoir with $M_{1i} = 1$ .....	88
Figure 5.28	Dimensionless Cartesian pressure derivative for linear variation of mobility ratio and storativity ratio with dimensionless radius .....	89
Figure 5.29	Effect of storativity ratio profile on dimensionless semilog pressure derivative for a ten-region composite reservoir .....	91
Figure 5.30	Effect of storativity ratio profile on dimensionless Cartesian pressure derivative for a ten-region composite reservoir .....	91
Figure 5.31	Mobility ratio versus dimensionless radius of investigation for a five-region composite reservoir with $F_{s1i} = 1$ and $M_{15} = 0.5$ .....	96
Figure 5.32	Mobility ratio versus dimensionless radius of investigation for a five-region composite reservoir with $F_{s1i} = 1$ and $M_{15} = 2.0$ .....	96
Figure 5.33	Mobility ratio versus dimensionless radius of investigation for a reservoir with $F_{s1i} = 1$ and an asymptotical mobility ratio profile .....	98
Figure 5.34	Mobility ratio versus dimensionless radius of investigation for a thermal recovery reservoir with $F_{s1i} = 1$ .....	98
Figure 5.35	Mobility ratio versus dimensionless radius of investigation for a five-region composite thermal recovery reservoir with $M_{15} = 0.5$ .....	100
Figure 5.36	Mobility ratio versus dimensionless radius of investigation for a five-region composite thermal recovery reservoir with $M_{15} = 2.0$ .....	100
Figure 5.37	Mobility ratio versus dimensionless radius of investigation for a thermal recovery reservoir with an asymptotical mobility ratio profile..	101
Figure 5.38	Mobility ratio versus dimensionless radius of investigation for a thermal recovery reservoir with changing storativity ratio .....	101

Figure G.1	Dimensionless wellbore pressure for $R_{D1} = 100$ , $R_{Dn-1} = 1000$ , $m_{tr} = 0.02$ , and $F_{s1i} = 1$ .....	172
Figure G.2	Dimensionless wellbore pressure for $R_{D1} = 500$ , $R_{Dn-1} = 1400$ , $m_{tr} = 0.02$ , and $F_{s1i} = 1$ .....	172
Figure G.3	Dimensionless wellbore pressure for $R_{D1} = 1000$ , $R_{Dn-1} = 1900$ , $m_{tr} = 0.02$ , and $F_{s1i} = 1$ .....	173
Figure G.4	Dimensionless semilog pressure derivative for $R_{D1} = 1000$ , $R_{Dn-1} = 1900$ , $m_{tr} = 0.02$ , and $F_{s1i} = 1$ .....	173
Figure G.5	Dimensionless Cartesian pressure derivative for $R_{D1} = 1000$ , $R_{Dn-1} = 1900$ , $m_{tr} = 0.02$ , and $F_{s1i} = 1$ .....	174
Figure G.6	Dimensionless wellbore pressure for $R_{D1} = 2000$ , $R_{Dn-1} = 2900$ , $m_{tr} = 0.02$ , and $F_{s1i} = 1$ .....	174
Figure G.7	Dimensionless semilog pressure derivative for $R_{D1} = 2000$ , $R_{Dn-1} = 2900$ , $m_{tr} = 0.02$ , and $F_{s1i} = 1$ .....	175
Figure G.8	Dimensionless Cartesian pressure derivative for $R_{D1} = 2000$ , $R_{Dn-1} = 2900$ , $m_{tr} = 0.02$ , and $F_{s1i} = 1$ .....	175
Figure G.9	Effect of first discontinuity radius on dimensionless wellbore pressure for a ten-region composite reservoir with $F_{s1i} = 1$ .....	176
Figure G.10	Dimensionless wellbore pressure for $R_{D1} = 100$ , $R_{Dn-1} = 1000$ , $m_{tr} = 0.10$ , and $F_{s1i} = 1$ .....	176
Figure G.11	Dimensionless semilog pressure derivative for $R_{D1} = 100$ , $R_{Dn-1} = 1000$ , $m_{tr} = 0.10$ , and $F_{s1i} = 1$ .....	177
Figure G.12	Dimensionless Cartesian pressure derivative for $R_{D1} = 100$ , $R_{Dn-1} = 1000$ , $m_{tr} = 0.10$ , and $F_{s1i} = 1$ .....	177

Figure G.13	Dimensionless wellbore pressure for $R_{D1} = 100$ , $R_{Dn-1} = 1000$ , $m_{tr} = 0.50$ , and $F_{s1i} = 1$ .....	178
Figure G.14	Dimensionless wellbore pressure for $R_{D1} = 100$ , $R_{Dn-1} = 1000$ , $m_{tr} = 1.00$ , and $F_{s1i} = 1$ .....	178
Figure G.15	Dimensionless semilog pressure derivative for $R_{D1} = 100$ , $R_{Dn-1} = 1000$ , $m_{tr} = 1.00$ , and $F_{s1i} = 1$ .....	179
Figure G.16	Dimensionless Cartesian pressure derivative for $R_{D1} = 100$ , $R_{Dn-1} = 1000$ , $m_{tr} = 1.00$ , and $F_{s1i} = 1$ .....	179
Figure G.17	Effect of transition region's slope on dimensionless wellbore pressure for a ten-region composite reservoir with $F_{s1i} = 1$ .....	180
Figure G.18	Dimensionless wellbore pressure for $R_{D1} = 100$ , $R_{Dn-1} = 1000$ , $m_{tr} = 0.02$ , and $M_{1i} = 1$ .....	180
Figure G.19	Dimensionless wellbore pressure for $R_{D1} = 500$ , $R_{Dn-1} = 1400$ , $m_{tr} = 0.02$ , and $M_{1i} = 1$ .....	181
Figure G.20	Dimensionless wellbore pressure for $R_{D1} = 1000$ , $R_{Dn-1} = 1900$ , $m_{tr} = 0.02$ , and $M_{1i} = 1$ .....	181
Figure G.21	Dimensionless semilog pressure derivative for $R_{D1} = 1000$ , $R_{Dn-1} = 1900$ , $m_{tr} = 0.02$ , and $M_{1i} = 1$ .....	182
Figure G.22	Dimensionless Cartesian pressure derivative for $R_{D1} = 1000$ , $R_{Dn-1} = 1900$ , $m_{tr} = 0.02$ , and $M_{1i} = 1$ .....	182
Figure G.23	Dimensionless wellbore pressure for $R_{D1} = 2000$ , $R_{Dn-1} = 2900$ , $m_{tr} = 0.02$ , and $M_{1i} = 1$ .....	183
Figure G.24	Dimensionless semilog pressure derivative for $R_{D1} = 2000$ , $R_{Dn-1} = 2900$ , $m_{tr} = 0.02$ , and $M_{1i} = 1$ .....	183

Figure G.25	Dimensionless Cartesian pressure derivative for $R_{D1} = 2000$ , $R_{Dn-1} = 2900$ , $m_{tr} = 0.02$ , and $M_{1i} = 1$ .....	184
Figure G.26	Effect of first discontinuity radius on dimensionless wellbore pressure for a ten-region composite reservoir with $M_{1i} = 1$ .....	184
Figure G.27	Effect of first discontinuity radius on dimensionless Cartesian pressure derivative for a ten-region composite reservoir with $M_{1i} = 1$ .....	185
Figure G.28	Dimensionless wellbore pressure for $R_{D1} = 100$ , $R_{Dn-1} = 1000$ , $m_{tr} = 0.10$ , and $M_{1i} = 1$ .....	185
Figure G.29	Dimensionless semilog pressure derivative for $R_{D1} = 100$ , $R_{Dn-1} = 1000$ , $m_{tr} = 0.10$ , and $M_{1i} = 1$ .....	186
Figure G.30	Dimensionless Cartesian pressure derivative for $R_{D1} = 100$ , $R_{Dn-1} = 1000$ , $m_{tr} = 0.10$ , and $M_{1i} = 1$ .....	186
Figure G.31	Dimensionless wellbore pressure for $R_{D1} = 100$ , $R_{Dn-1} = 1000$ , $m_{tr} = 0.50$ , and $M_{1i} = 1$ .....	187
Figure G.32	Dimensionless wellbore pressure for $R_{D1} = 100$ , $R_{Dn-1} = 1000$ , $m_{tr} = 1.00$ , and $M_{1i} = 1$ .....	187
Figure G.33	Dimensionless semilog pressure derivative for $R_{D1} = 100$ , $R_{Dn-1} = 1000$ , $m_{tr} = 1.00$ , and $M_{1i} = 1$ .....	188
Figure G.34	Dimensionless Cartesian pressure derivative for $R_{D1} = 100$ , $R_{Dn-1} = 1000$ , $m_{tr} = 1.00$ , and $M_{1i} = 1$ .....	188
Figure G.35	Effect of transition region's slope on dimensionless wellbore pressure for a ten-region composite reservoir with $M_{1i} = 1$ .....	189
Figure G.36	Effect of transition region's slope on dimensionless Cartesian pressure derivative for a ten-region composite reservoir with $M_{1i} = 1$ .	189



Figure G.37	Dimensionless wellbore pressure for a reservoir in which mobility ratio and storativity ratio are linear functions of dimensionless radius .....	190
Figure G.38	Dimensionless semilog pressure derivative for both linearly changing mobility ratio and storativity ratio profiles with dimensionless radius ..	190
Figure G.39	Effect of storativity ratio profile on dimensionless wellbore pressure for a ten-region composite reservoir .....	191
Figure G.40	Mobility ratio versus conventional dimensionless radius of investigation for a five-region composite reservoir with $F_{s1i} = 1$ and $M_{15} = 0.5$ .....	192
Figure G.41	Mobility ratio versus conventional dimensionless radius of investigation for a five-region composite reservoir with $F_{s1i} = 1$ and $M_{15} = 2.0$ .....	192
Figure G.42	Mobility ratio versus dimensionless radius of investigation for a thermal recovery process with $F_{s1tr} = 100$ and $F_{s1n} = 1000$ .....	193
Figure G.43	Mobility ratio versus dimensionless radius of investigation for a thermal recovery process with $F_{s1tr} = F_{s1n} = 1000$ .....	193

## NOMENCLATURE

$A$	=	Area, $\pi R^2$ or $\pi r_e^2$ , $m^2$
$A$	=	Matrix of coefficients
$a_D$	=	Dimensionless observation well distance, $a/r_w$
$b$	=	Vector of known terms
$c$	=	Vector of unknown constants
$C$	=	Wellbore storage coefficient, $m^3/Pa$
$C_D$	=	Dimensionless wellbore storage coefficient
$C_j$	=	Arbitrary constants
$c_t$	=	Total system compressibility, $Pa^{-1}$
$F_s$	=	Storativity ratio between two regions as defined in Figures 4.5, 4.6, G.42 and G.43
$F_{sli}$	=	Storativity ratio between regions 1 and i, $(\phi c_D)_1/(\phi c_D)_i$ for $i = 1, 2, \dots, n$
$h$	=	Formation thickness, $m$
$I_j$	=	Modified Bessel function of the first kind of order $j$
$k$	=	Permeability, $m^2$
$K_j$	=	Modified Bessel function of the second kind of order $j$
$m_c$	=	Cartesian line slope, $Pa/sec$
$m_{cD}$	=	Dimensionless Cartesian line slope
$m_s$	=	Semi-log line slope, $Pa/cycle$
$n$	=	The last region of a multi-region composite reservoir
$M$	=	Mobility ratio between two regions as defined in Figures 4.5 and 4.6
$M$	=	Actual reservoir mobility ratio, as defined in Equations 5.5b and 5.6b

$\bar{M}$	=	Reservoir instantaneous mobility ratio, as defined in Equation 5.3b	
$M_i$	=	Mobility ratio between two regions, $(k/\mu)_i/(k/\mu)_{i+1}$	for $i = 1, 2, \dots, n-1$
$M_{1i}$	=	Mobility ratio between regions 1 and i, $(k/\mu)_1/(k/\mu)_i$	for $i = 1, 2, \dots, n$
$m_{tr}$	=	Dimensionless slope of the transition region	
$p$	=	Pressure, Pa	
$p_D$	=	Dimensionless pressure drop	
$p_o$	=	Initial reservoir pressure, Pa	
$\bar{p}_D$	=	Dimensionless pressure drop in Laplace space	
$q$	=	Flow rate, $\text{sm}^3/\text{sec}$	
$r$	=	Radius, m	
$r_e$	=	Reservoir outer radius, m	
$r_{eD}$	=	Dimensionless reservoir outer radius	
$r_i$	=	Radius of investigation, m, as defined in Equation 5.4a	
$r_{iD}$	=	Dimensionless radius of investigation as defined in Equation 5.4b	
$r_w$	=	Wellbore radius, m	
$R$	=	Discontinuity radius in a composite reservoir, m	
$R_{Di}$	=	Dimensionless discontinuity radius in a composite reservoir, $R_i/r_w$	for $i = 1, 2, \dots, n-1$
$s$	=	Skin effect at the wellbore, dimensionless	
$s_{fi}$	=	Skin effect at the front (or discontinuity), dimensionless	for $i = 1, 2, \dots, n-1$
$t$	=	Time, seconds	
$t_D$	=	Dimensionless time	
$t_{DA}$	=	Dimensionless time based on the area, $(\pi R_{Dn-1}^2)$	
$t_{De}$	=	Dimensionless time based on the radius $R_{D1}$	

$V$	=	Reservoir volume, m <sup>3</sup>
$V_s$	=	Swept volume, m <sup>3</sup>
$z$	=	Laplace parameter

## Greek Symbols

$\alpha_{(i,j)}$	=	Coefficients in Equations 4.26 through 4.29
$\beta$	=	Formation volume factor, m <sup>3</sup> /sm <sup>3</sup>
$\frac{\partial}{\partial}$	=	Partial
$\lambda_i$	=	Reservoir instantaneous mobility, as defined in Equation 5.3a
$\Delta p_s$	=	Pressure drop across skin, psi
$\Delta p_{sf}$	=	Pressure drop across skin at the discontinuity, Pa
$\Delta t$	=	Shut-in time, seconds
$\eta_i$	=	Diffusivity ratio between between between regions 1 and i, $(k/\mu\phi c_D)_1/(k/\mu\phi c_D)_i$ for $i = 1, 2, \dots, n$
$\mu$	=	Viscosity, Pa-sec
$\phi$	=	Porosity, fraction
$(\phi c_D)_{eff}$	=	Effective storativity corresponding to the volume up to $R_D$ as defined for Equation 5.1

## Subscripts

$c$	=	Cartesian
-----	---	-----------

<i>D</i>	=	Dimensionless
<i>e</i>	=	Exterior
<i>eff</i>	=	Effective
<i>f</i>	=	Front or flowing
<i>i</i>	=	A general term
<i>o</i>	=	Initial
<i>pss</i>	=	Pseudosteady state
<i>s</i>	=	Swept or shut-in
<i>ss</i>	=	Steady state
<i>t</i>	=	Total
<i>w</i>	=	Wellbore
<i>1</i>	=	Inner region in a multi-region composite reservoir
<i>2,3..n</i>	=	Regions of a multi-region composite reservoir

## CHAPTER 1

### INTRODUCTION

Over the years, thermal oil recovery methods have gained considerable interest and much use. Two of the most important thermal processes are in-situ combustion and steamflooding. Currently, thermal recovery by steamflooding is the dominant method for producing heavy oil around the world. The determination of the swept volume in thermal recovery processes is important. A knowledge of the steam swept volume provides an estimate of heat losses to the surrounding formation as well as the thermal efficiency of the operation.

In displacement projects, the swept volume has been estimated occasionally by coring and/or temperature observations at wells, during the injection process. These methods of estimating the steam swept volume are very expensive and uncertain due to reservoir heterogeneity. One practical and economical way of estimating the swept volume is by well test analysis, which also provides an estimation of flow capacity and skin factor.

The concept of determining the swept volume by pressure transient techniques has been studied by several authors. The most commonly used thermal well test has been the falloff test developed by *Eggenschwiler et al.* (1980). Their study utilizes a composite system, in which a steamflood or combustion process is represented as a reservoir model with two regions having highly contrasting fluid mobilities. Such a model seems ideally suited for

thermal oil recovery, due to the high mobility contrast between the swept and unswept regions. At early times, a semi-log graph of pressure versus time would generate a straight line corresponding to the inner-region mobility. Following this semi-log straight line, a pseudosteady Cartesian straight line may develop with a slope that can be related to the swept volume.

The pseudosteady state method developed by *Eggenschwiler et al.* (1980) is independent of the geometry of the swept region and has been applied by several investigators to field and simulated cases, with apparent success. However, simulated thermal falloff tests have shown that mobility and storativity may be continuously changing in the swept region. For continuous variations of mobility and storativity within the swept region, a simple two- or three-region model may not be appropriate. In this study, an analytical solution to a multi-region model is presented. Infinitesimally thin skins at the discontinuities are included. This work is intended to study the effects of various trends of mobility and storativity, within the swept region, on well tests for composite reservoirs.

The literature survey conducted for this study is presented in Chapter 2. The statement of the problem and objectives of this study are discussed in Chapter 3. The mathematical model and its validation are presented in Chapter 4. The transient pressure behaviour of multi-region composite reservoirs is discussed in Chapter 5. Finally, Chapter 6 presents conclusions drawn from this study and recommendations for future research.

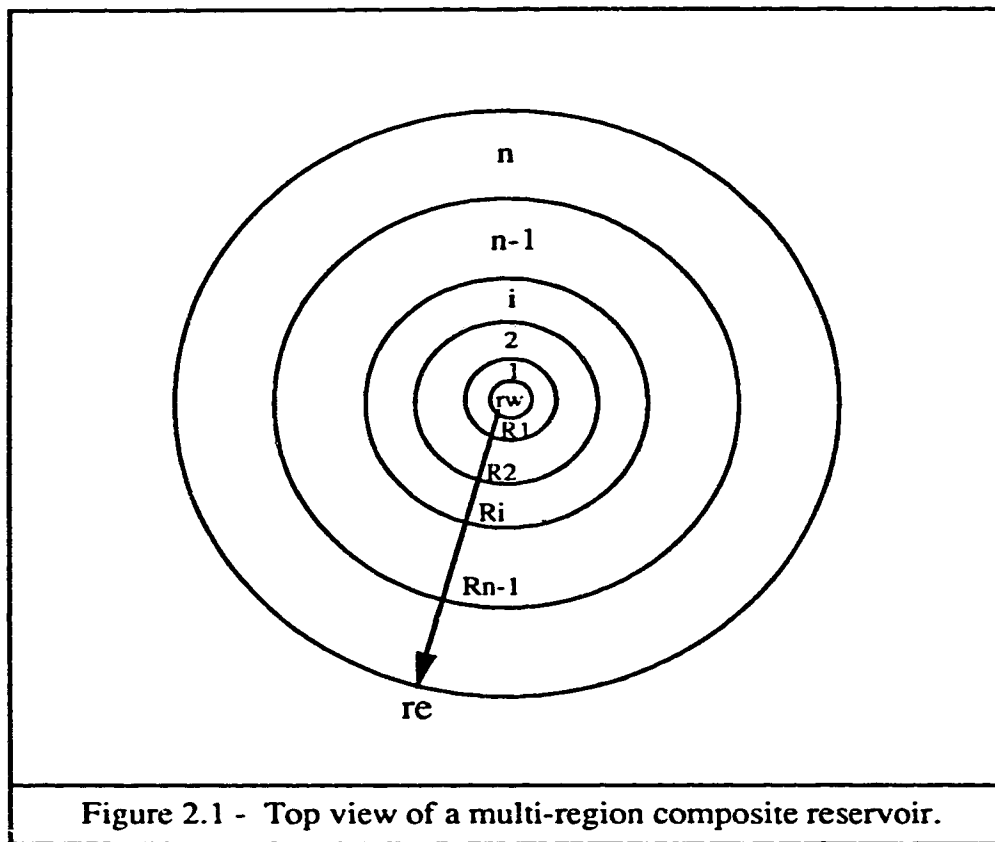
## CHAPTER 2

### LITERATURE REVIEW

In recent years, the behaviour of composite reservoirs has attracted much attention and many studies have appeared on this subject. A composite reservoir is made up of two or more regions. Rock and fluid properties are different in each region. The origin of composite systems may be natural or artificial. Examples of naturally created multi-zone composite systems include a reservoir with different permeability zones, an oil reservoir in communication with an aquifer, and an oil well with a finite-thickness skin zone surrounding the wellbore. Enhanced oil recovery projects, such as CO<sub>2</sub> miscible flooding, polymer flooding, in-situ combustion and steam injection, are examples of artificially created conditions, wherein the reservoir can be viewed as a multi-region system with different rock and/or fluid properties. A reservoir undergoing a thermal recovery process typically has been idealized as a composite reservoir.

Figure 2.1 schematically illustrates the reservoir model considered in this study. This model represents a radial multi-region composite reservoir in which there are interfaces or discontinuities between each region. In Figure 2.1, the distances  $R_i$  are the different positions where a discontinuity or front can be recognized. Discontinuities are the locations where rock and/or fluid properties have a significant variation. These discontinuity distances are important parameters when analyzing well tests in composite reservoirs. Strictly speaking, fronts in many enhanced oil recovery operations are not cylindrical. The





front's shape may be distorted by gravity and/or viscous fingering effects. Thus, the front radius exists only in some average sense. It is perhaps better to speak of the volume of the inner region, instead of front radius, especially when pseudosteady state data are available.

In general, reservoirs with contrasts in physical properties have been analyzed using analytical or numerical composite reservoir models. The pressure behaviour of composite reservoirs has been considered extensively in many studies. All these studies can be classified in three large groups: two-region composite, three-region composite and multi-region (more than three regions) composite reservoir models. However, the great majority of studies have considered the case of two-region composite reservoirs.

## **2.1 Two-region Composite Models**

The two-region composite model is the most commonly used model in the petroleum industry. There are several publications detailing the application of two-region composite models to describe pressure behaviour in petroleum reservoirs. Numerous two-region composite reservoir studies have defined the general principles to analyze composite reservoirs. Some of these studies will be discussed briefly in this section.

### **2.1.1 Analytical Approach**

*Hazebroek et al.* (1958) developed an analytical method using pressure falloff data from pattern waterflood injection wells. Their method determines the reservoir static pressure by trial and error. By plotting  $\log(p - p_e)$  versus shut-in time, they are able to estimate the

permeability-thickness product and skin factor. However, the permeability-thickness product obtained may be reflecting only a part of the reservoir and the use of trial and error may involve inaccuracies.

*Hurst* (1960) analyzed unsteady flow of fluids through two sands in series with different mobilities in each sand. He used the Laplace transform to obtain a solution for a single well located at the center of concentric sands. *Hurst* (1960) also considered the interference between two oil fields sharing the same aquifer as a two-region system with different physical properties in each region.

*Loucks and Guerrero* (1961) proposed radial composite reservoir solutions, using the Laplace transformation. *Loucks and Guerrero* (1961) studied the pressure distribution in an infinite composite reservoir composed of two adjacent concentric regions of different permeabilities. They found that, under certain conditions, the permeability in both zones, as well as the size of the inner zone, can be determined from transient pressure test data.

*Larkin* (1963) presented solutions to the diffusion equation for a line source located anywhere in a region bounded by a circular discontinuity. He used Green's functions presented by *Jaeger* (1944). *Larkin's* (1963) solution considers different rock and fluid properties on opposite sides of the discontinuity. *Jones* (1962) studied the behaviour of a composite reservoir, using the Laplace transformation. *Jones* (1962) made predictions for the behaviour of wells located near a gas-water contact. He extended the application of *Larkin's* (1963) solution by including mobility and diffusivity terms for several fluid phases in series. However, neither *Larkin* (1963) nor *Jones* (1962) specified the times for which their approximate solutions are valid.

*Carter* (1966) analyzed the pressure transient behaviour of a closed, radial, composite system with a well producing at a constant rate. He stated that in a graph of pressure versus time, an early semilog straight line may be observed. This semilog straight line corresponds to the inner region mobility. After this semilog straight line, a pseudosteady state period may follow. During this period, a Cartesian graph of pressure versus time will yield a straight line. From the slope of this Cartesian line, a volume can be estimated. *Carter* (1966) pointed out that this estimated volume would be greater than the inner region volume.

*Odeh* (1969) analyzed well tests from infinite outer boundary composite reservoirs. He stated that if a large contrast of physical properties exist, the pressure transient behaviour of an infinite outer boundary composite reservoir would be the same as the closed outer boundary case. The reason for this behaviour lies in the effects of the discontinuity being the same as those of a closed outer boundary. However, once the effect of the discontinuity ends, a second semilog straight line may follow the pseudosteady state period. This second semilog straight line will correspond to the outer region mobility.

*Eggenschwiler et al.* (1980) presented an analytical solution in Laplace space for the transient pressure behaviour of a well, producing at a constant rate, from a two-region, radial composite reservoir. Their method is widely used to estimate the swept or burned volume from well tests in thermal recovery projects, such as steamflooding or in-situ combustion. *Eggenschwiler et al.* (1980) modeled the swept volume as a radial region adjacent to the injection well. Wellbore storage and skin effects were also considered. Reservoir and fluid properties, such as permeability, porosity and compressibility of the reservoir fluid, were considered to be different in the inner (swept zone) and the outer

region (unswept zone). *Horne et al.* (1980) extended the *Eggenschwiler et al.* (1980) solution to finite composite reservoirs. *Tang* (1982) used the *Eggenschwiler et al.* (1980) method to calculate a front radius on the basis of a theoretical deviation time. *Tang* (1982) analyzed an in-situ combustion case. He found that the error involved in the estimated radius of the burned zone increases with an increase in the diffusivity ratio.

*Walsh et al.* (1981) used the *Eggenschwiler et al.* (1980) model to analyze falloff test data from in-situ combustion and steam injection projects. They observed that a long transition zone between the two semilog straight lines, for the swept and unswept regions, contains an approximate pseudosteady state region that may provide the information required to estimate the inner zone volume. To compute the swept zone volume, the mean temperature and pressure of the swept zone are required. *Walsh et al.* (1981) explained that, since the concept of pseudosteady state is based on material balance principles, the estimated volume of the swept zone is independent of the shape of the actual swept volume.

*Satman* (1981) analyzed transient flow in multi-layer, radial, and infinitely large composite reservoirs with fluid banks. *Satman* (1981) studied how the swept volume can be estimated by using a Cartesian graph of well test data, taken after the end of the first semilog straight line of a falloff test. He concluded that the average properties of the swept zone in a multi-layer system can be determined from the first semilog straight line of the well test data. *Satman* (1981) also stated that the first discontinuity radius can be found by using the time at which pressure data deviate from the first semilog straight line. *Satman and Oskay* (1985) studied the effects of a tilted front on well test analysis for multi-layer radial composite reservoirs. Their study suggests that if a sharp front model is used to

estimate the front radius from a tilted front reservoir, the estimated front radius will be lower than the actual front radius.

*Rosa and Horne* (1983) developed a solution applicable to composite reservoirs. They used the Laplace transform technique to develop their model. *Rosa and Horne* (1983) showed that the *Stehfest* (1970) numerical inversion scheme could be used to invert exact solutions from Laplace space to real space. Their study also showed a way to broaden the application of automated type-curve matching in well test analysis.

*Da Prat et al.* (1985) used the *Eggenschwiler et al.* (1980) composite model to determine the burned volume and the location of the fire-front in an in-situ combustion project. *Da Prat et al.* (1985) reported that the real pressure profile from the project matched quite well with the predictions made with the composite model. They also stated that the values obtained for the burned volume and the location of the burning front were reliable and simple to interpret.

*Brown* (1985) analyzed the drawdown pressure derivative behaviour of two region, radial and infinitely-large composite reservoirs. He studied the nature and duration of the transition region between the two semilog straight lines observed on a composite reservoir's pressure profile. He concluded that storativity influences only the timing and shape of the transition region, but does not affect the slope of the two semilog straight lines. *Brown* (1985) also discussed how the transition region shape is affected by the mobility ratio between regions.

*Barua and Horne* (1987) discussed the application of automated type-curve matching to analyze well tests from reservoirs undergoing a thermal recovery process. *Barua and Horne* (1987) used the *Eggenschwiler et al.* (1980) analytical model in their automated type-curve analysis. *Rosa and Horne's* (1983) solution was also considered in their study. With their automated type-curve matching method, an average radius of the swept zone can be obtained. The *Barua and Horne* (1987) method might give good estimates for the inner zone properties, even when the mobility ratio is not high or when the falloff test has been preceded by a short injection period. However, a lot of computer operations are required and the estimated outer zone properties might be unrealistic.

*Olarewaju and Lee* (1987) proposed an analytical solution in Laplace space for two-region, radial composite reservoirs produced either at a constant bottomhole pressure or at a constant rate. Their solution includes wellbore phase redistribution as suggested by *Fair* (1981). However, their study did not consider storativity variation. *Olarewaju and Lee's* (1987) study indicates that the phase redistribution effect is larger for a damaged system than for a stimulated one. They concluded that when the effect of phase redistribution is not severe enough to cause the characteristic pressure distortion (hump), it could lead to a misinterpretation of the reservoir pressure behaviour.

*Olarewaju and Lee* (1989) developed a two-region composite model to determine reservoir parameters, such as permeabilities of the inner and outer zones, radius of the inner zone, and wellbore storage. *Olarewaju and Lee* (1989) stated that for radial flow in an infinite-acting reservoir, the value of the semilog pressure derivative is shifted from 0.5 by a factor equal to the mobility ratio between the outer and the inner zones.

*Ambastha* (1988) presented an analytical study of the transient pressure derivative behaviour of a well in a two-region composite reservoir with a thin skin at the front. *Ambastha* (1988) found that the transition period between the end of the first semilog straight line and the beginning of the second semilog straight line is longer for larger mobility ratios. However, the effect of the storativity ratio on the timing of the semilog straight lines can be assumed as negligible. *Ambastha* (1988) found that the time to the maximum semilog pressure derivative and the magnitude of the maximum pressure derivative are affected by the mobility ratio. He also showed that, although the storativity ratio mildly affects the time to the maximum semilog pressure derivative, the magnitude of the maximum pressure derivative is affected significantly by the storativity ratio.

*Ambastha and Ramey* (1990) investigated the effect of skin at the front on composite reservoirs well tests. They showed how the effects of skin at the front on the transient pressure derivative behaviour are similar to the effects of storativity ratio. *Ambastha and Ramey* (1990) explained how skin at the front may be the cause of a short duration pseudosteady state period corresponding to the inner swept volume, for small mobility and storativity contrasts.

*Olarewaju et al.* (1991) presented type curves from a two-region composite model. They analyzed radially-damaged or -stimulated wells. Their type curves can be used to analyze the extent and magnitude of impairment in a damaged system or the extent or quality of improvement achieved from stimulation. The effect of phase redistribution was also included in their type curves. However, storativity variation was not considered.



### 2.1.2 Numerical Approach

*Bixel and van Poolen* (1967) numerically solved a two-region infinite system in which a well was located at the center of a circular region surrounded by a radial discontinuity. They showed how to estimate the inner region transmissibility by using the slope of the early straight line segment of the drawdown curve. *Bixel and van Poolen* (1967) studied the effect of mobility ratio on transient pressure behaviour. Each set of type curves had a fixed value of storativity ratio. However, the effect of storativity ratio on pressure behaviour was not discussed.

A finite thickness skin zone was treated by *Wattenbarger and Ramey* (1970) as a composite system. They used a numerical technique to obtain pressure transient behaviour for such systems. They concluded that the infinitesimally thin skin concept is applicable for damaged zone dimensionless radii from 1 to about 10. Their work suggested that if the damaged zone dimensionless radius is equal to or larger than 10, two straight lines will be evident on a semi-logarithmic plot.

In 1972, *Kazemi et al.* analyzed simulated pressure falloff tests in reservoirs with fluid banks. They emphasized how wellbore storage can mask the information that can be obtained from the early data of a falloff test. *Kazemi et al.* (1972) studied the two straight lines that can be observed on a falloff test pressure profile. They concluded that the slope ratio of the second straight line to that of the first straight line segment approximates the mobility ratio for the two zones, only when the storativity ratio is near unity. *Kazemi et al.* (1972) stated that when the storativity ratio is greater than one, the ratio of the slopes is

usually greater than the mobility ratio, whereas if the storativity ratio is less than unity, the ratio of the slopes is less than the mobility ratio.

In 1974, *Merrill et al.*, using the same type of simulator as *Kazemi et al.* (1972), investigated the pressure behaviour of two-zone composite systems. *Merrill et al.* (1974) defined what type of information can be obtained from a falloff test, depending on the conditions of the system tested. They concluded that proper analysis of falloff tests from waterflood systems with two contrasting fluid zones can yield information about mobilities and saturations on both sides of the front as well as the distance to the front. Analysis of gas injection systems can give information about the mobility of the first zone and the distance to the front.

*Sosa et al.* (1981) considered the effect of saturation distribution in the swept region on waterflood falloff tests. They used a radial numerical simulator to account for the relative permeability characteristics of the system. Their study showed how the transition region between the water and oil regions affects significantly the falloff test data. *Sosa et al.*'s (1981) analysis provides some qualitative information about waterflooding processes.

*Messner and Williams* (1982) applied the *Walsh et al.* (1981) procedure and used an implicit thermal simulator to analyze falloff data from steam injection projects. The swept volume comparison between the results from the two methods appeared to be favourable. However, thermal efficiencies calculated by the pseudosteady state method tended to be very low, indicating larger than expected overburden heat losses and excessive channelling. *Messner and Williams* (1982) stated that the low thermal efficiencies could also be due to

the inability of the method to accurately assess the reservoir heat content, ahead of the steam zone.

*Fassihi* (1988) numerically simulated falloff tests of steamflood and in-situ combustion processes using areal and radial models. He analyzed whether the swept volume estimated by applying the *Eggenschwiler et al.* (1980) analytical model agreed with the simulated swept volume. In this comparison, the effects of several parameters were studied. These parameters included reservoir and operational characteristics, such as wellbore gridblock size, non-uniform permeability, layering, flowing non-condensable gas, and oil vaporization. *Fassihi* (1988) concluded that, in reservoirs with highly contrasting homogeneous zones, estimated swept volumes from steam falloff tests, using the analytical model, were in good agreement with simulated swept volumes. However, continuously changing the reservoir's physical characteristics may mask the pseudosteady state period, making the analysis impossible. *Fassihi* (1988) also observed that in some in-situ combustion processes, the high mobility of the gases ahead of the front tends to distort the pseudosteady state period, making estimation of the burned volume inaccurate.

*Ziegler* (1990) analyzed pressure falloff data from a steam injection project. He compared results from the *Eggenschwiler et al.* (1980) analytical model and a simulator. *Ziegler* (1990) concluded that the analytical model yields results which are in good agreement with numerical simulation predictions. *Ziegler* (1990) recommended the use of the analytical model to determine reservoir parameters from steam injection falloff tests.

## 2.2 Three-region Composite Models

Solutions for a well located in a radial, three-region reservoir are available. However, very few studies have investigated the transient pressure response from these reservoirs. This section will present some of the most important analysis in this area of well testing.

### 2.2.1 Analytical Approach

*Onyekonwu and Ramey* (1986) developed an analytical solution for three-region, radially infinite, composite reservoirs. They showed, how in a two-region reservoir model, the assumption of a sharp mobility contrast between the zones is not exactly correct. *Onyekonwu and Ramey* (1986) discussed the existing gradation in fluid properties from the swept zone to the unswept zone. They explained that, in a three-region model, the middle zone is used to represent the region where the gradual change in fluid properties between the swept and unswept zones occurs. In their study, *Onyekonwu and Ramey* (1986) also analyzed the effect of the transition zone, mobility ratio and storativity ratio on pressure behaviour. The transition zone causes a departure from pseudosteady state behaviour. This departure is directly proportional to the size of the transition zone. The time of departure from pseudosteady state behaviour is directly proportional to the mobility ratio between the swept and the unswept zones. However, the time of departure from pseudosteady state is independent of the storativity ratio.

*Barua and Horne* (1985) compared analytical solutions for two-region and three-region, radially infinite, composite reservoirs. The three-region model included a transition region between the swept and unswept regions. *Barua and Horne* (1985) used automated type-

curve matching in their analysis. When trying to match the two-region model to the three-region model, they found several data points did not match. They concluded that this failure to match indicated the presence of an intermediate zone between the swept and the unswept zones. *Barua and Horne*'s (1985) work suggests that, by including the intermediate zone in the analysis, the estimates of the discontinuity radii will improve.

*Ambastha and Ramey* (1992) studied the transient pressure response of a well in a three-region composite reservoir. They discussed in detail the effective physical properties of a three-region composite reservoir. *Ambastha and Ramey* (1992) showed how the deviation time method would yield a front radius  $R_1$ , if the mobility ratio and the storativity ratio, at the first discontinuity, are balanced in such a way that a correct deviation time is observed. They also concluded that the pseudosteady state method will yield the second front radius  $R_2$ , if the effective storativity is used in the analysis. *Ambastha and Ramey* (1992) defined a criterion to distinguish apparent pseudosteady state from real pseudosteady state. This criterion uses the effective time to the start of pseudosteady state. When an apparent pseudosteady state is developed, the analysis yields an overestimated value for the second front radius  $R_2$ .

### 2.2.2 Numerical Approach

*Merrill et al.* (1974) used a simulator to study the application of a three-region composite model when analyzing well tests from enhanced oil recovery projects. They used the deviation time concept in their analysis. *Merrill et al.*'s (1974) work includes a tabulation of deviation times for different conditions of three-zone reservoirs. From this table, they obtained an averaged deviation time. They concluded that for three-zone systems, the

average dimensionless deviation time is 0.485. This value of time can be used to estimate the distance to the first discontinuity in the reservoir.

*Onyekonwu et al.* (1984) analyzed in-situ combustion falloff data by using two thermal simulators. He studied how to determine the proper average temperature when using the pseudosteady state concept to estimate the swept volume. *Onyekonwu et al.* (1984) found that the swept volume, determined from pressure analysis, includes both a burned volume and a high gas saturation zone ahead of the front. They emphasized that an effective value of temperature is required for evaluation of compressibility and the formation volume factor. These variables are important for accurate interpretation of falloff data. In their work, *Onyekonwu et al.* (1984) show how the effective temperature is strongly dependent on the wellbore and peak temperatures. They also concluded that this effective temperature is usually lower than the average temperature based on an energy balance.

### 2.3 Multi-region Composite Models

Very little research has been reported about multi-region (more than three regions) composite reservoir models. Normally, multi-region composite models are used to characterize reservoirs with different permeability zones. However, very few studies have investigated the transient pressure response from these reservoirs. The application of multi-region composite models in reservoir characterization will be addressed briefly.

### 2.3.1 Analytical Approach

*Nanba and Horne* (1989) presented a method to estimate water and oil relative permeabilities from pressure transient analysis of water injection well data. In their work, a nonlinear regression algorithm was implemented. *Nanba and Horne's* (1989) solutions were derived based on analytical multicomposite and stepwise(numerical) multicomposite systems. These solutions were compared with the line source moving bank solution and with numerical results. The comparison indicated that multicomposite analytical solutions are appropriate for the analysis of water injection problems. Field examples supported the practicality of the proposed interpretation procedure.

*Abbaszadeh-Dehghani and Kamal* (1989) analyzed pressure transient tests of water injection wells using two-region and multi-region composite reservoir models. They found that the assumption of a stationary front during falloff is generally acceptable, and that waterflooding is better represented by a multi-region composite reservoir. *Abbaszadeh-Dehghani and Kamal* (1989) also studied how the duration of the transition region is increased by storativity contrast between regions.

*Oliver* (1990) presented a process of estimating a permeability distribution from well-test data. He described the relative contribution of the permeability of various regions to the estimate of the average permeability. *Oliver* (1990) showed that permeability estimates using the semilog pressure derivative are some type of volume-averaged reservoir permeability. He concluded that the instantaneous semilog pressure derivative from drawdown pressure data depends upon a weighted average of the permeability within the annular region of the reservoir. *Oliver's* (1990) work only considered the unit storativity

ratio case and the variation of mobility was very small. The maximum mobility ratio considered was five.

### 2.3.2 Numerical Approach

In 1989, *Yeh and Agarwal* simulated a multicomposite model to study how a reservoir mobility profile can be obtained from the reservoir transient pressure behaviour. They defined a term called "instantaneous mobility" which is inversely related to the instantaneous value of the semilog pressure derivative. *Yeh and Agarwal* (1989) also established a relation between instantaneous mobility and the radius of investigation. From simulation runs, they concluded that the instantaneous mobility represents a volumetric average of the true reservoir mobility. They developed an equation to relate the instantaneous mobility to the real reservoir mobility. The theoretical basis for their equations was not explained. *Yeh and Agarwal*'s (1989) characterization method apparently yields satisfactory results when there are low mobility contrasts and storativity is constant within the reservoir.

Using *Oliver*'s (1990) results, *Feitosa et al.* (1993a) expanded *Yeh and Agarwal*'s (1989) algorithm. *Feitosa et al.* (1993a) concluded that *Yeh and Agarwal*'s (1989) method can be improved by establishing a different relationship between instantaneous mobility and the actual reservoir mobility. They considered that the instantaneous mobility represents the harmonic volumetric average of the reservoir's real mobility. *Feitosa et al.*'s (1993a) characterization method seems to yield slightly better results than *Yeh and Agarwal*'s (1989) algorithm. *Feitosa et al.* (1993a) also developed a new characterization method called the inverse solution algorithm (ISA). This algorithm yields similar results to those



obtained from the modified version of *Yeh and Agarwal*'s (1989) method. In all the cases studied, the mobility contrasts were low and storativity remained constant within the reservoir. In the same year, with the purpose of expanding their previous work, *Feitosa et al.* (1993b) included porosity variation in their analysis. They studied porosity variation cases by using the inverse solution algorithm (ISA). *Feitosa et al.* (1993b) concluded that since, in real situations, porosity variations are small compared to permeability variations, the ISA can be applied to obtain a reasonably good approximation to the actual permeability distribution.

## 2.4 Drawdown Analysis

Drawdown tests may provide information about formation permeability, skin factor, and the reservoir volume communicating with the well. Thus, obtaining information from a drawdown test is of great importance. In 1988, *Ambastha* investigated the drawdown pressure derivative response of a two-region composite reservoir. In his work, *Ambastha* (1988) defined the parameters used in a pressure derivative drawdown analysis. When wellbore storage is negligible, the drawdown pressure derivative is not affected by skin at the wellbore. In the absence of wellbore storage, the parameters for the drawdown pressure derivative are the mobility ratio and the storativity ratio. A consideration of wellbore storage introduces two additional parameters: the dimensionless wellbore storage coefficient and the skin factor.

After obtaining drawdown data from a composite reservoir, a dimensionless graph of  $p_{wD}$  versus  $\ln t_D$  may yield two semilog straight lines with a transition period in between. The first semilog straight line develops in an early period and it is related to the inner region mobility. The second semilog straight line develops in a late period and it is related to the outer region mobility. Wellbore storage effects may mask the semilog line corresponding to the inner region mobility. Thus, in composite reservoir well tests, wellbore storage should be minimized. As for the second semilog straight line, this line may be observed as long as the test is run long enough to see the effects of the outer region. However, outer boundary effects may mask the second semilog line.

## **2.5 Estimating Swept Volume in Thermal Recovery Projects**

Many authors have applied different methods to estimate the swept or burned volume from pressure transient analysis. These methods include the deviation time method, the intersection time method, the type-curve matching method and the pseudosteady state method. The correct use of these methods will depend on the conditions of the well test and the reservoir characteristics.

### **2.5.1 Deviation Time Method**

This method states that when falloff test data are being plotted, a graph of pressure vs. time would generate an early semilog straight line corresponding to the inner-region (swept zone) mobility. When the effects of the interface (or front) are felt, a deviation from the straight line can be observed. The time at the end of the semilog straight line is used to

calculate a front radius on the basis of a theoretical dimensionless deviation time. The deviation time method was first used by *van Poolen* (1964) to locate the flood front in an in-situ combustion process.

*Bixel and van Poolen* (1967) found a value of 0.25 for the dimensionless deviation time. *Merrill et al.* (1974), after running several simulation cases, found that the dimensionless deviation time should lie in a range between 0.13 and 1.39. The arithmetic average of this range was 0.389. *Tang* (1982) obtained an approximated value of dimensionless deviation time equal to 0.4. *Ambastha and Ramey* (1989), based on the semilog pressure derivative behaviour, found a value of 0.18 for the dimensionless deviation time.

Many authors have studied the deviation time method obtaining significantly different values for the dimensionless deviation time. This significant difference in values for dimensionless deviation time indicates that an accurate and reliable specification for dimensionless deviation time is required to obtain meaningful results from this method. Another disadvantage of the deviation time method is that the flood front is considered to be cylindrical, which is often not the case for thermal recovery projects, since gravity and/or viscous fingering effects distort the front's shape. Furthermore, it is possible for wellbore storage effects to mask the initial semilog straight line, making the method incapable of producing any results.

### 2.5.2 Intersection Time Method

Following the end of the early semilog straight line, falloff data deviates for a period of time, known as the transition period. After this interval of time, it may be possible to

observe a second semilog straight line, characteristic of the fluid mobility in the outer (unswept) zone. The time at which the two semilog straight lines intersect can be used to estimate a front radius, by using a theoretical dimensionless intersection time as a basis. *Bixel and van Poolen* (1967) proposed this method when discussing the effects of linear and radial discontinuities in composite reservoirs on pressure transient behaviour.

*Odeh* (1969) presented an equation relating the dimensionless discontinuity (or front) radius with the dimensionless intersection time, for equal storativity in both regions. *Merrill et al.* (1974) presented a graphical correlation using a simulator. They showed that for mobility ratios close to or less than unity, the dimensionless intersection time is a constant. However, *Merrill et al.* (1974) observed that for mobility ratios much greater than unity, the dimensionless intersection time is affected by both the mobility ratio and the storativity ratio. *Sosa et al.* (1981) used the intersection method to analyze the effects of mobility ratio on simulated falloff tests. *Ambastha and Ramay* (1989) provided a number of reasons as to why the intersection time method is not suitable for thermal recovery well test analysis. They stated that in most thermal well test cases, the falloff test will not be run long enough to see the second semilog straight line, or the outer boundary effects may mask the second semilog straight line, or wellbore storage and skin may mask the first semilog line.

### 2.5.3 Type-Curve Matching Method

Type curves are dimensionless functions of pressure or pressure derivatives versus time, with mobility and storativity ratios as parameters. Generally, theoretical dimensionless type curves are generated by a mathematical model. The type-curve matching procedure involves fitting the entire well test data to a set of type curves. Once a match is obtained, an

arbitrary point of the data is selected and related to the definition of dimensionless variables of the type curve. By relating data and dimensionless variables definitions, unknown variables are obtained. These variables include important reservoir information, such as permeability, wellbore storage, wellbore skin factor and discontinuity radii. However, the non-uniqueness of the match is still the major disadvantage of type curve matching methods.

Several type curves were developed by *Bixel and van Poolen* (1967) with mobility ratio as a correlating parameter. *Barua and Horne* (1987) successfully used automated type-curve matching to analyze thermal recovery well tests. *Olarewaju and Lee* (1987) used their type curves to analyze field tests exhibiting composite reservoir behaviour. *Olarewaju and Lee's* (1987) type curves include *Fair's* (1981) phase- redistribution parameter. *Ambastha and Ramey* (1989) presented pressure derivative type curves applicable for all front radii, with mobility and storativity ratios as parameters for infinitely-large composite reservoirs. The time match point is used to calculate the front radius, while the pressure derivative match point yields the mobility of the inner (swept) region. Wellbore storage was not considered. *Ambastha and Ramey* (1989) explained that because of enhancement of detail in a pressure derivative graph, improved type-curve matching may be possible by using a pressure derivative type curve.

#### **2.5.4 Pseudosteady State Method**

*Eggenschwiler et al.* (1980) proposed a pseudosteady state method to calculate the inner swept volume for composite reservoirs with large mobility and storativity contrasts

between the swept and unswept regions. They observed that due to these contrasts, the swept region can behave like a closed system for a short duration after the end of the semilog line corresponding to the inner zone mobility. During this time, a pseudosteady Cartesian straight line may originate. The slope of this Cartesian line is inversely proportional to the swept volume. As the pseudosteady state method is independent of the geometry of the swept region, it is not necessary for the flood front to be cylindrical to get a good estimate of the swept volume. *Eggenschwiler et al.* (1980) successfully validated their work against *van Poolen* (1965) and *Kazemi* (1966) falloff data.

*Walsh et al.* (1981) applied the pseudosteady state method to determine swept volume and heat distribution in steamflooding and in-situ combustion wells. They emphasized the use of a two-phase effective compressibility when applying the pseudosteady state method to estimate the swept volume in a steam injection process. The two-phase compressibility accounts for volumetric changes caused by steam condensation. *Satman et al.* (1980) and *Tang* (1982) extended the pseudosteady state method to cases where the pseudosteady state did not develop completely due to insufficient mobility and storativity contrasts between the two regions.

*Onyekonwu et al.* (1984) used the pseudosteady state concept to interpret combustion falloff data. The swept volume calculated by using the pseudosteady state method and simulated swept volume showed a good agreement. *Onyekonwu et al.* (1984) developed correction graphs to relate the burned and swept volumes. *Da Prat et al.* (1985) applied the pseudosteady state method to locate the burning front in an in-situ combustion project. They concluded that the estimated front radius (assuming the front to be cylindrical) was in good agreement with the actual locations of the injection and production wells.

*Issaka and Ambastha* (1992) simulated steam injection falloff tests for a horizontal well. The effects on falloff data of various parameters, such as wellbore grid block sizes, injection time, permeability anisotropy, injection rate and front shape were investigated. Their study showed that swept volume might be overestimated, by 5% to 60%, for horizontal wells. *Issaka and Ambastha* (1992) indicated that longer injection times prior to shut-in may have an adverse effect on the estimated swept volume. The reason for this adverse effect is that for longer injection times, the shape of the swept region is more irregular.

*Sheng* (1992) applied the pseudosteady state method to analyze thermal recovery projects by using the *Stanislav et al.* (1989) approach. He simulated falloff data and studied the effects of parameters such as gravity, dip, permeability anisotropy and irregular shape of the swept volume. *Sheng* (1992) found that all these parameters do not affect the results significantly. He also concluded that, although the estimated swept volume and skin are reasonably calculated by the pseudosteady state method, the permeability might be overestimated by 30% to 40%. His study showed how the estimation of permeabilities and swept volumes depends on the vertical position of a pressure recorder, where pressure falloff data are measured.

## 2.6 Mobility and Storativity Profiles

Previous simulation studies have reported profiles of mobility ratio and storativity ratio, most commonly observed in thermal recovery projects. The mobility ratio and the storativity ratio values used in this study are in a range from 1 to 1000. The characteristic

profiles used in this study are within the range of values given in previous studies from the literature. We refer to some of these studies in this section.

*Fassihi* (1988) simulated several falloff tests to analyze the pressure transient behaviour in steamflood and in-situ combustion processes. His table of estimated physical properties includes values of mobility ratio from 7 to 600 and values of storativity ratio from 23 to 33000.

*Onyekonwu et al.* (1984) made a comparison between analytical and numerical composite reservoir models. They used a three-zone model in the comparison. The estimated value of mobility ratio between the inner region and the transition region was 16 and the estimated value for mobility ratio between the first and the third region was 1840. The storativity ratio between the first and the transition region was 4, while the storativity ratio between the first and the third region was 110.

*Onyekonwu and Ramey* (1986) studied the effect of the transition region on the pressure behaviour of a three-region composite system. The mobility ratio between the first zone and the transition zone was 25, while the mobility ratio between the first and last zone was 1000. Storativity ratios for the first and second discontinuities were 5 and 35, respectively.

## 2.7 Discontinuity Radii

Previous studies have analyzed well tests in enhanced oil recovery operations. These studies have considered cases of injection of fluids to displace and produce oil. Some other



well test analyses have considered cases in which a fraction of oil is burned creating a heat gradient to mobilize and produce oil. Normally, all these types of well test analysis consider the reservoir as a system with multiple banks. Three main banks are considered in these systems. A bank, which represents the injected fluid, is also known as the swept zone. A bank, in which the injected fluid and oil are present, is also known as the transition zone. A bank, which represents the oil region, is termed the unswept zone. Two discontinuities are distinguished within these three banks: a discontinuity between the swept zone and the start of the transition zone, and a discontinuity between the end of transition zone and the unswept zone. The distances from the wellbore to the discontinuities are known as the first and last discontinuity radii, respectively. Although a multi-region composite reservoir may have several discontinuity radii, whenever a ratio of discontinuity radii is mentioned in this study, it will be referring to the ratio between the last and the first discontinuity radii.

Several studies have reported the ratios of discontinuity radii most commonly observed in thermal recovery projects. Some of the ratios of discontinuity radii used in this analysis are: 1.4, 1.9, 2.8 and 10. The ratios of discontinuity radii used in this study are within the range of values given in the studies to be discussed subsequently.

*Merrill et al.* (1974) simulated the pressure behaviour of three-zone composite systems. They analyzed gas injection processes. In their analysis, *Merrill et al.* (1974) used ratios of discontinuity radii of 1.6 and 2.

In 1984, *Onyekonwu et al.* simulated falloff tests to analyze an in-situ combustion project. *Onyekonwu et al.* (1984) reported a table with simulation results. They showed how the

discontinuity radii depend on fluid saturation, temperature and reservoir physical characteristics, such as mobility and storativity. Depending on the interpretation applied to their simulation results, the ratios of discontinuity radii range from 1.6 to 5.6.

*Onyekonwu and Ramey* (1986) simulated an in-situ combustion project to generate data for an analytical model. Their data included a range of ratios of discontinuity radii from 1.1 to 1.4.

In 1989, *Yeh and Agarwal* analyzed injection well test pressure data from reservoirs with multiple fluid banks. They studied reservoirs undergoing a waterflood or chemical injection. They generated simulation results by using a two-phase, two-dimensional numerical model. *Yeh and Agarwal* 's (1989) study used more than 20 sets of relative permeability data and some field tests. Their study included ratios of discontinuity radii of 4.4, 4.8, 10.5 and 20.

## CHAPTER 3

### STATEMENT OF THE PROBLEM

As discussed in the literature review, over the years, the pressure behaviour of composite reservoirs has gained considerable interest and many studies have appeared on this subject. A composite reservoir represents a number of well testing scenarios. Well test scenarios in thermal recovery operations have been typically represented by the use of a two- or three-region composite reservoir model. In some cases, the two- or three-region composite models may not be adequate to describe systems in which the mobility and storativity change continuously within the swept region. For these reservoirs, a multi-region composite model is more suitable. Therefore, this study investigates the pressure and pressure derivative responses of a multi-region, radial composite system. Thus, the main objectives of this study are:

1. To develop an analytical solution, similar to the *Eggenschwiler et al.* (1980) solution, for multi-region, radial composite reservoirs with infinitesimally thin skin at the discontinuities.
2. To develop new pressure derivative type curves for type-curve matching analysis of well tests in either homogeneous or multi-region composite reservoirs.

3. To analyze how previous two-region and three-region composite reservoir solutions compare with the multi-region composite solution.
4. To analyze effective mobility and storativity behaviour in multi-region composite reservoirs.
5. To study how mobility and storativity variations affect the swept volume estimation using the pseudosteady state method.
6. To analyze the possibility of improving previous composite reservoir analysis by means of the multi-region composite model.
7. To study briefly some reservoir characterization methods from the literature.

## **CHAPTER 4**

### **MATHEMATICAL MODEL FOR A MULTI-REGION COMPOSITE RESERVOIR WITH SKIN AT THE DISCONTINUITIES**

A mathematical model developed in this study is presented. This model considers a multi-region radial composite reservoir with wellbore storage and skin at the active (injection or production) well and infinitesimally thin skin at the discontinuities. The surface production (or injection) rate is assumed to be constant. The outer boundary may be infinite, closed or at a constant pressure. The solution for this model is obtained by using the Laplace transformation technique.

Some other assumptions in this model are:

- (1) The formation is homogeneous, horizontal and of uniform thickness.
- (2) The front is of infinitesimal thickness in the radial direction.
- (3) The fluid flowing is considered to be of slight, but constant, compressibility.
- (4) The front can be considered stationary throughout the few hours of a testing period.
- (5) Flow is considered to be single phase, radial and laminar.
- (6) Gravity and capillarity effects are considered negligible.

## 4.1 Mathematical Development

The governing equations and boundary conditions in dimensionless form for a multi-region radial composite reservoir are:

### 4.1.1 Governing Equations:

*first (1) region*

$$\frac{1}{r_D} \frac{\partial}{\partial r_D} \left( r_D \frac{\partial p_{D1}}{\partial r_D} \right) = \frac{\partial p_{D1}}{\partial t_D} \quad \text{for } 1 \leq r_D \leq R_{D1} \quad (4.1)$$

*any (i) region*

for  $i = 2, 3, \dots, n$

$$\frac{1}{r_D} \frac{\partial}{\partial r_D} \left( r_D \frac{\partial p_{Di}}{\partial r_D} \right) = \eta_{i-1} \frac{\partial p_{Di}}{\partial t_D} \quad \text{for } R_{D,i-1} \leq r_D \leq R_{Di} \text{ or } r_{eD} (\text{or } \infty) \quad (4.2)$$

### 4.1.2 Inner Boundary Conditions:

$$C_D \frac{dp_{wD}}{dt_D} - \left( \frac{\partial p_{D1}}{\partial r_D} \right)_{r_D=1} = 1 \quad (4.3)$$

$$p_{wD} = p_{D1} - s \left( \frac{\partial p_{D1}}{\partial r_D} \right)_{r_D=1} \quad (4.4)$$

#### 4.1.3 Conditions at the Discontinuities:

*any discontinuity - regions (i) and (i+1)*

$$r_D \frac{\partial p_{D_i}}{\partial r_D} = - \frac{1}{s_i} (p_{D_i} - p_{D_{i+1}}) \quad \text{for } r_D = R_{D_i} \text{ and } t_D > 0$$

for  $i = 1, 2, \dots, n-1$  (4.5)

$$\frac{\partial p_{D_{i+1}}}{\partial r_D} = M_i \frac{\partial p_{D_i}}{\partial r_D} \quad \text{for } r_D = R_{D_i} \text{ and } t_D > 0$$

for  $i = 1, 2, \dots, n-1$  (4.6)

#### 4.1.4 Outer Boundary Conditions:

*Infinite:*

$$p_{D_n}(r_D, t_D)_{r_D \rightarrow \infty} = 0$$

(4.7)

*Closed:*

$$\left( \frac{\partial p_{D_n}}{\partial r_D} \right)_{r_D = r_{cD}} = 0$$

(4.8)

*Constant pressure:*

$$p_{D_n}(r_{cD}, t_D) = 0$$

(4.9)

#### 4.1.5 Initial Condition:

$$p_{D_i}(r_D, 0) = 0 \quad \text{for } i = 1, 2, \dots, n \quad (4.10)$$

#### 4.1.6 Dimensionless Variables:

Dimensionless variables used in Equations 4.1 through 4.10 are defined as:

*Dimensionless pressure:*

$$p_{D_i} = \frac{2\pi k_1 h}{q \beta \mu_1} (p_o - p_i) \quad \text{for } i = 1, 2, \dots, n \quad (4.11)$$

*Dimensionless pressure at the wellbore*

$$p_{wD} = \frac{2\pi k_1 h}{q \beta \mu_1} (p_o - p_w) \quad (4.12)$$

*Diffusivity ratios:*

$$\eta_i = \frac{(k / \phi \mu c_l)_1}{(k / \phi \mu c_l)_{i+1}} \quad \text{for } i = 1, 2, \dots, n-1 \quad (4.13)$$



**Mobility ratios:**

$$M_i = \frac{(k/\mu)_i}{(k/\mu)_{i+1}} \quad \text{for } i = 1, 2, \dots, n-1 \quad (4.14)$$

**Dimensionless radii:**

$$r_D = \frac{r}{r_w} \quad (4.15)$$

$$r_{eD} = \frac{r_e}{r_w} \quad (4.16)$$

$$R_{Di} = \frac{R_i}{r_w} \quad \text{for } i = 1, 2, \dots, n-1 \quad (4.17)$$

**Dimensionless time:**

$$t_D = \frac{k_1 t}{(\phi \mu c_1)_1 r_w^2} \quad (4.18)$$

**Dimensionless wellbore storage coefficient:**

$$C_D = \frac{C}{2\pi(\phi c_1)_1 h r_w^2} \quad (4.19)$$

**Wellbore skin factor:**

$$s = \frac{2\pi k_1 h}{q \beta \mu_1} \Delta p_s \quad (4.20)$$

**Discontinuity skin factor:**

$$s_{fi} = \frac{2\pi k_1 h}{q_f \beta \mu_1} \Delta p_{fi} \quad \text{for } i = 1, 2, \dots, n-1 \quad (4.21)$$

#### 4.1.7 General Solution

A general solution for the governing equations (Equations 4.1 and 4.2) was obtained by using the Laplace transformation technique with the appropriate initial and boundary conditions. The general solution in Laplace space for each region is:

*first (1) region*

$$\overline{p}_{D1}(r_D, z) = C_1 I_0(r_D \sqrt{z}) + C_2 K_0(r_D \sqrt{z}) \quad \text{for } 1 \leq r_D \leq R_{D1} \quad (4.22)$$

*any (i) region*

for  $i = 2, 3, \dots, n$

$$\overline{p}_{Di}(r_D, z) = C_{2i-1} I_0(r_D \sqrt{\eta_{i-1} z}) + C_{2i} K_0(r_D \sqrt{\eta_{i-1} z}) \quad \text{for } R_{D,i-1} \leq r_D \leq R_{Di} \text{ or } r_{eD} \text{ (or } \infty) \quad (4.23)$$

In Equations 4.22 and 4.23 and in all subsequent equations, the transformed time variable is identified by the symbol  $z$ . The dimensionless wellbore pressure drop in Laplace space is:

$$\overline{p}_{wD}(z) = C_1 [I_0(\sqrt{z}) - s\sqrt{z} I_1(\sqrt{z})] + C_2 [K_0(\sqrt{z}) + s\sqrt{z} K_1(\sqrt{z})] \quad (4.24)$$

#### 4.1.8 Solution's Constants

All constants  $C_1$  through  $C_{2n}$  are obtained by solving the system of equations resulting from the use of boundary conditions (Equations 4.3 through 4.9) in Laplace space:

For example:

from Equations 4.3 and 4.4

$$\alpha_{(1,1)}C_1 + \alpha_{(1,2)}C_2 = 1/z \quad (4.25)$$

from Equation 4.5

$$\alpha_{(2,2-1)}C_{2-1} + \alpha_{(2,2)}C_2 + \alpha_{(2,2+1)}C_{2+1} + \alpha_{(2,2+2)}C_{2+2} = 0 \quad \text{for } i = 1, 2, \dots, n-1 \quad (4.26)$$

from Equation 4.6

$$\alpha_{(2+1,2-1)}C_{2-1} + \alpha_{(2+1,2)}C_2 + \alpha_{(2+1,2+1)}C_{2+1} + \alpha_{(2+1,2+2)}C_{2+2} = 0 \quad \text{for } i = 1, 2, \dots, n-1 \quad (4.27)$$

from Equations 4.7 or 4.8 or 4.9

$$\alpha_{(2n,2n-1)}C_{2n-1} + \alpha_{(2n,2n)}C_{2n} = 0 \quad (4.28)$$

The term  $\alpha_{(i,j)}$  denotes the coefficient of the  $C_j$  in the  $i$  th equation. Equation 4.25 is the first equation, and Equation 4.28 is the last equation in a composite system of  $n$  -regions. The terms  $\alpha_{(i,j)}$  are:

$$\alpha_{(1,1)} = C_{Dz}(I_0(\sqrt{z}) - s\sqrt{z} I_1(\sqrt{z})) - \sqrt{z} I_1(\sqrt{z}) \quad (4.29)$$

$$\alpha_{(1,2)} = C_{DZ} \left( K_0(\sqrt{z}) + s\sqrt{z} K_1(\sqrt{z}) \right) + \sqrt{z} K_1(\sqrt{z}) \quad (4.30)$$

$$\alpha_{(2,1)} = I_0(R_{D1}\sqrt{z}) + s_{f1} R_{D1} \sqrt{z} I_1(R_{D1}\sqrt{z}) \quad (4.31)$$

$$\alpha_{(2,2)} = K_0(R_{D1}\sqrt{z}) - s_{f1} R_{D1} \sqrt{z} K_1(R_{D1}\sqrt{z}) \quad (4.32)$$

$$\alpha_{(3,1)} = M_1 \sqrt{z} I_1(R_{D1}\sqrt{z}) \quad (4.33)$$

$$\alpha_{(3,2)} = -M_1 \sqrt{z} K_1(R_{D1}\sqrt{z}) \quad (4.34)$$

$$\alpha_{(2i,2i-1)} = I_0(R_{D1}\sqrt{z\eta_{i-1}}) + s_{f1} R_{D1} \sqrt{z\eta_{i-1}} I_1(R_{D1}\sqrt{z\eta_{i-1}}) \quad \text{for } i = 2, 3, \dots, n-1 \quad (4.35)$$

$$\alpha_{(2i,2i)} = K_0(R_{D1}\sqrt{z\eta_{i-1}}) - s_{f1} R_{D1} \sqrt{z\eta_{i-1}} K_1(R_{D1}\sqrt{z\eta_{i-1}}) \quad \text{for } i = 2, 3, \dots, n-1 \quad (4.36)$$

$$\alpha_{(2i,2i+1)} = -I_0(R_{D1}\sqrt{z\eta_i}) \quad \text{for } i = 1, 2, \dots, n-1 \quad (4.37)$$

$$\alpha_{(2i,2i+2)} = -K_0(R_{D1}\sqrt{z\eta_i}) \quad \text{for } i = 1, 2, \dots, n-1 \quad (4.38)$$

$$\alpha_{(2i+1,2i-1)} = M_i \sqrt{z\eta_{i-1}} I_1(R_{D1}\sqrt{z\eta_{i-1}}) \quad \text{for } i = 2, 3, \dots, n-1 \quad (4.39)$$

$$\alpha_{(2i+1,2i)} = -M_i \sqrt{z\eta_{i-1}} K_1(R_{D1}\sqrt{z\eta_{i-1}}) \quad \text{for } i = 2, 3, \dots, n-1 \quad (4.40)$$

$$\alpha_{(2i+1,2i+1)} = -\sqrt{z\eta_i} I_1(R_{D1}\sqrt{z\eta_i}) \quad \text{for } i = 1, 2, \dots, n-1 \quad (4.41)$$

$$\alpha_{(2i+1,2i+2)} = \sqrt{z\eta_i} K_1(R_{D1}\sqrt{z\eta_i}) \quad \text{for } i = 1, 2, \dots, n-1 \quad (4.42)$$

The remaining coefficients depend on the specified outer boundary condition and are defined by:

***Infinite outer boundary:***

A bounded solution for  $p_{Dn}(r_D \rightarrow \infty, z)$  is obtained from Equation 4.23 provided that  $C_{2n-1} = 0$ , as  $I_0(r_D \sqrt{\eta_{n-1} z}) \rightarrow \infty$  as  $r_D \rightarrow \infty$ . Therefore,  $\alpha_{(2n-2,2n-1)}$ ,  $\alpha_{(2n-1,2n-1)}$  and  $\alpha_{(2n,2n-1)}$  are set to zero in the system of equations. Also,  $\alpha_{(2n,2n)} = 0$ , as  $K_0(r_D \sqrt{\eta_{n-1} z})$  in Equation 4.23 approaches zero as  $r_D \rightarrow \infty$ . Thus:

$$\alpha_{(2n-2,2n-1)} = \alpha_{(2n-1,2n-1)} = \alpha_{(2n,2n-1)} = \alpha_{(2n,2n)} = 0 \quad (4.43)$$

The values of  $\alpha_{(2n-2,2n-1)}$  and  $\alpha_{(2n-1,2n-1)}$  are to be used based on Equation 4.43 for infinite reservoirs overriding the values corresponding to  $i = n-1$  for these  $\alpha$ 's from Equations 4.37 and 4.41, respectively.

***Closed outer boundary:***

Excepting the coefficients due to the outer boundary condition, all coefficients remain as defined before in Equations 4.29 through 4.42.

$$\alpha_{(2n,2n-1)} = I_1(r_D \sqrt{z \eta_{n-1}}) \quad (4.44)$$

$$\alpha_{(2n,2n)} = -K_1(r_D \sqrt{z \eta_{n-1}}) \quad (4.45)$$

***Constant-pressure outer boundary:***

As in the previous case, the only different coefficients are those due to the outer boundary condition:

$$\alpha_{(2n,2n-1)} = I_0(r_e D \sqrt{z \eta_{n-1}}) \quad (4.46)$$

$$\alpha_{(2n,2n)} = K_0(r_e D \sqrt{z \eta_{n-1}}) \quad (4.47)$$

In this section, the solution to the transient pressure problem for a radial multi-region composite reservoir with skin at the discontinuities has been described. The problem was arranged as a system of  $2n$  equations with  $2n$  unknowns (constants  $C_j$ ). To solve the problem, all the coefficients were grouped in a matrix called  $A$ , all the unknown constants  $C_j$  were grouped in an unknown vector called  $c$  and all right-hand-side terms from Equations 4.25 through 4.28 were arranged in a known vector called  $b$ . Once the system was set in the form  $Ac = b$ , the unknown vector  $c$  was obtained by multiplying the inverse of matrix  $A$  by the known vector  $b$ . After obtaining the values of the constants  $C_j$ , dimensionless transient pressure and dimensionless pressure derivative (semilog and Cartesian) responses in Laplace space were generated. These responses were numerically inverted from the Laplace space to real space by means of the *Stehfest* (1970) algorithm.

Appendix A contains the development of expressions for the physical properties of multi-region composite reservoirs. Appendix B contains the development of the dimensionless form for instantaneous mobility and radius of investigation. Appendix C contains the input

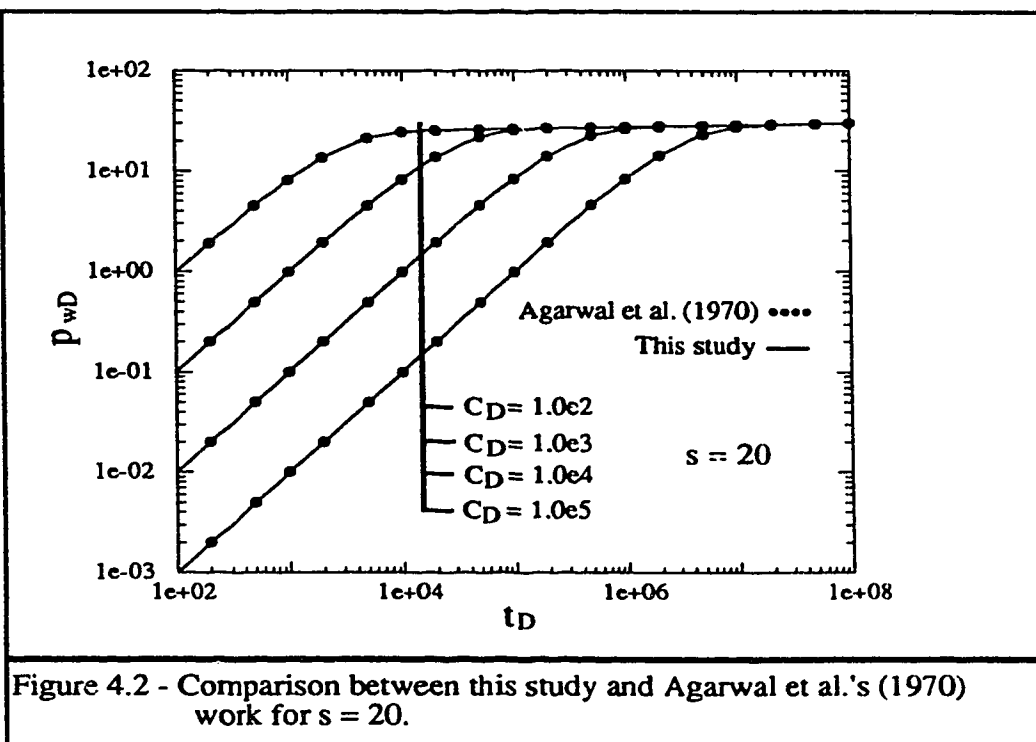
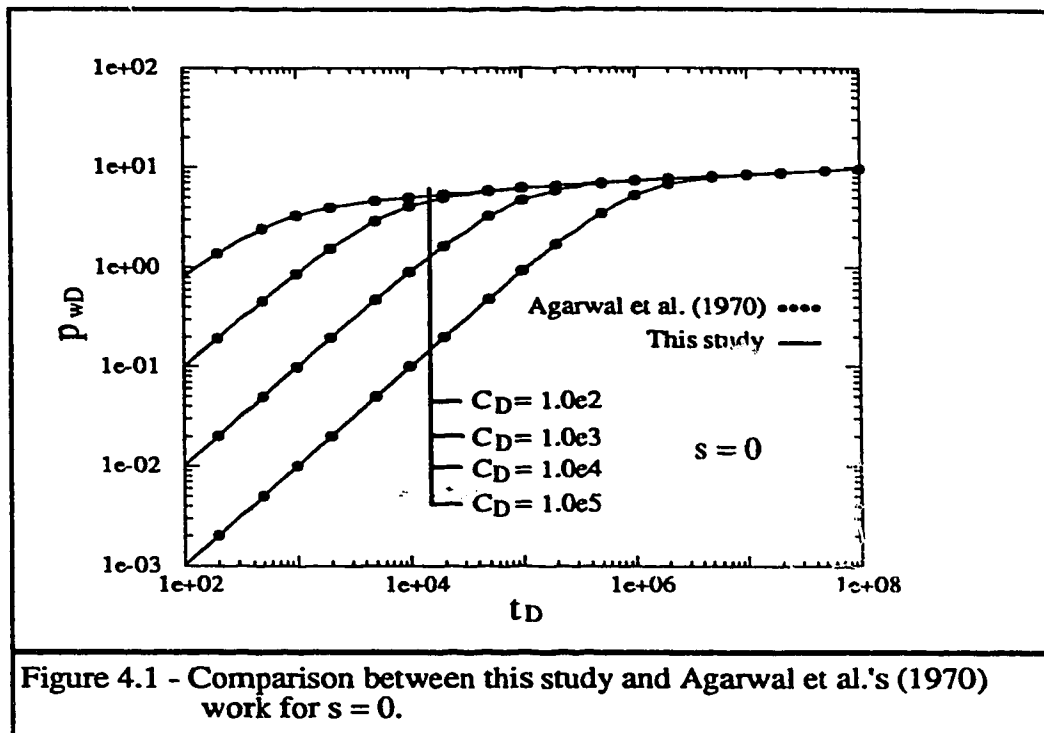
data used to analyze the transient pressure behaviour of multi-region composite reservoirs. Appendix D contains the computer program used in this study.

It is important to note that at very early times ( $t_D = 100$ ), the matrix of coefficients  $A$ , mentioned previously, may become singular or very close to singular (over the working precision limit of the computer). This is because at very early times, there are very small coefficients as well as very large coefficients, which causes the singular behaviour of the matrix. Appendix E explains how the singularity problem was overcome.

Appendix F shows sample results for a particular run of the computer program. Finally, appendix G shows some additional figures for the transient pressure response of multi-region composite reservoirs. These graphs were used during the development of this study, however no discussions have been done about these figures since other figures (Chapter 5) are considered to be more significant for the objectives of this study.

## 4.2 Verification of Solution

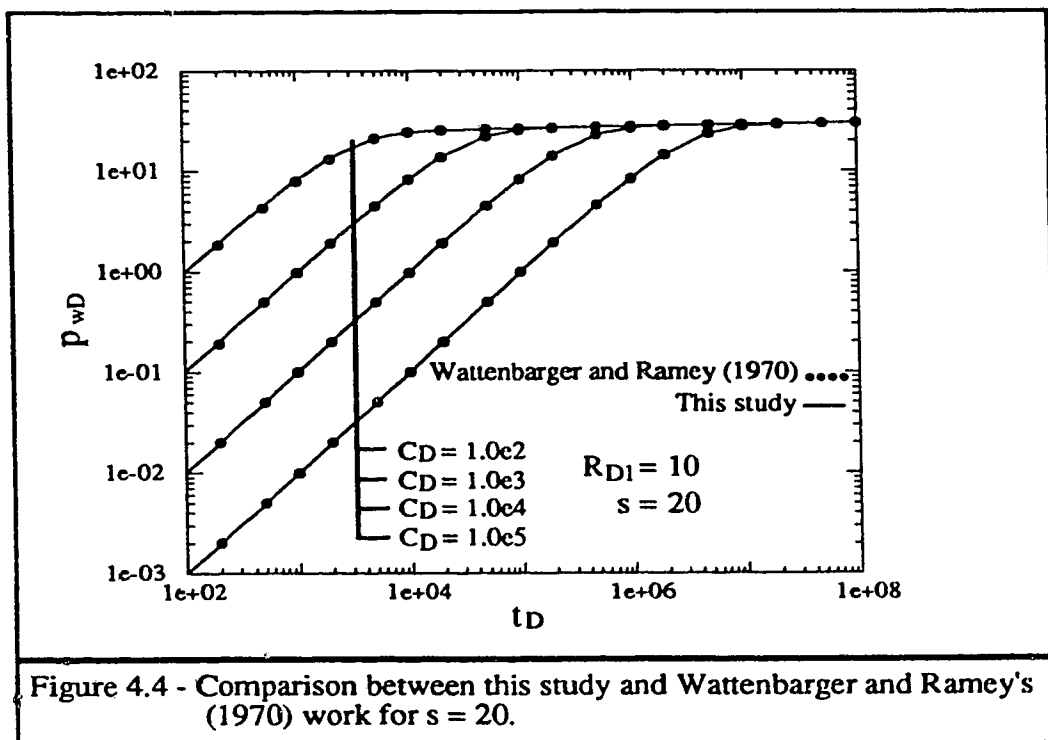
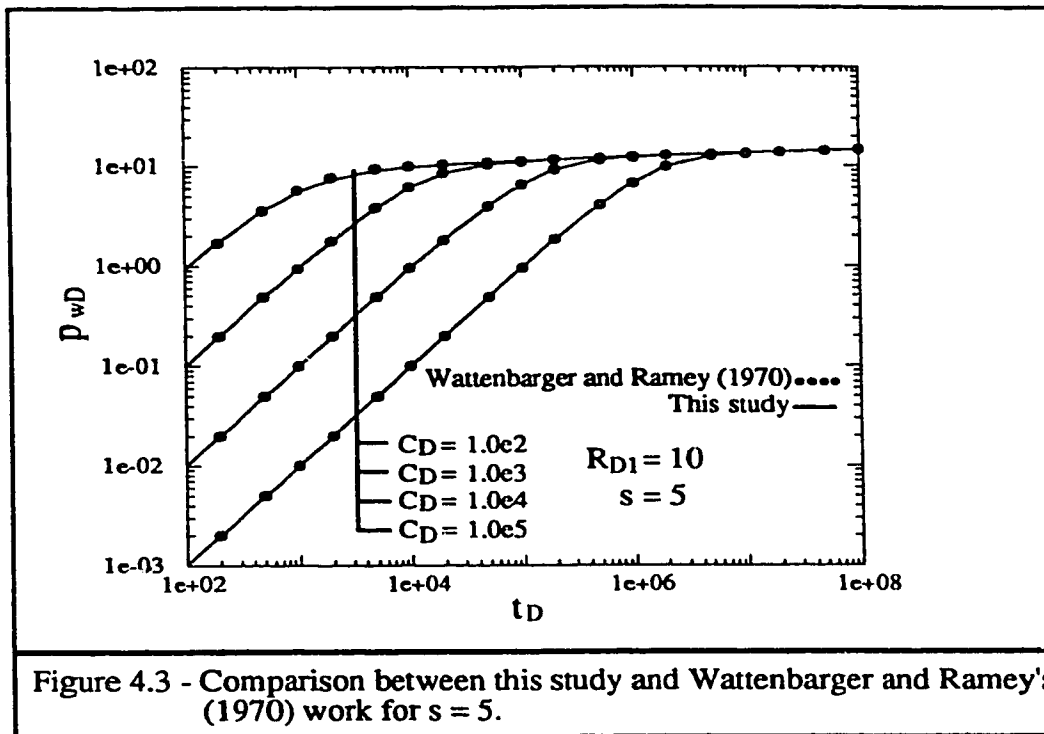
The solution presented in section 4.1 was verified against the *Agarwal et al. (1970)* solution for a well in a homogeneous reservoir with and without skin at the wellbore. To reproduce *Agarwal et al. (1970)* by using this study's solution, the model presented in this work was run as a multi-region (i.e., three, five and ten regions) composite model with no skin at the discontinuities and in which all the mobility and storativity ratios at the discontinuities were equal to unity. The model successfully reproduced the homogeneous reservoir pressure responses (Figures 4.1, 4.2).

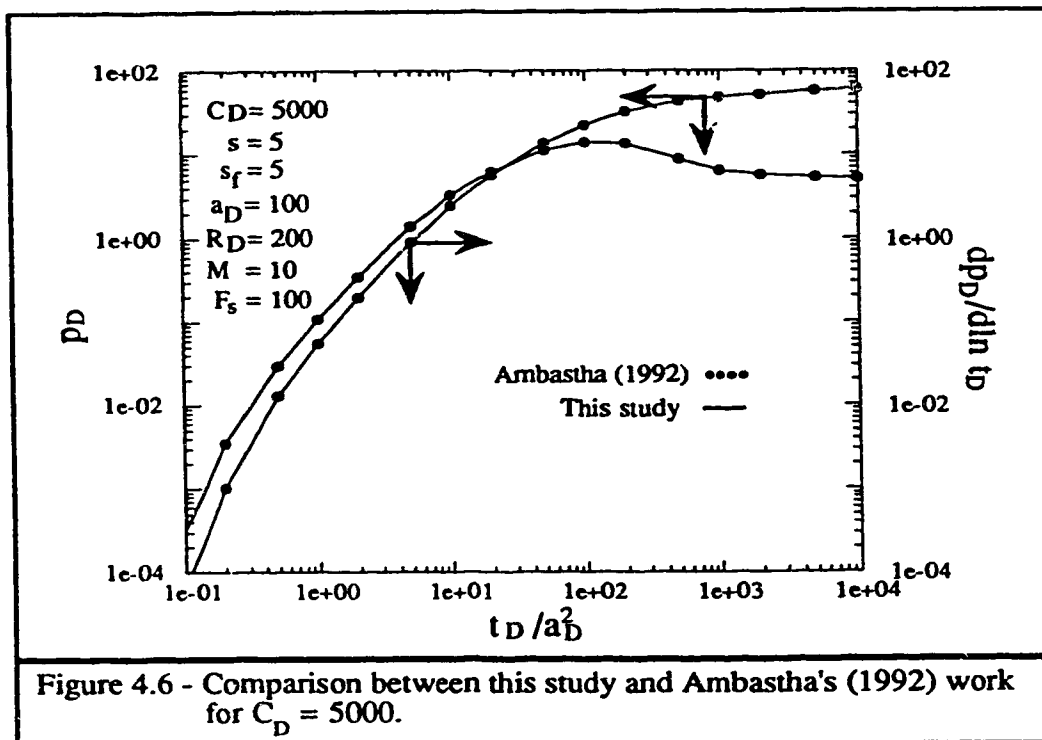
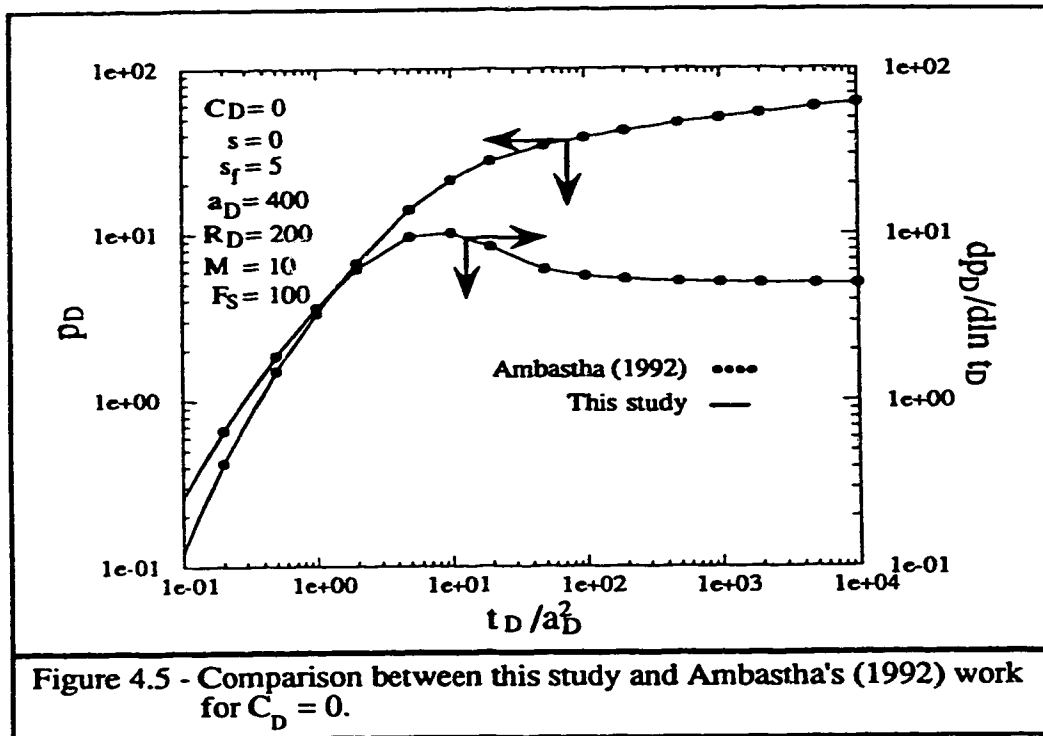




The multi-region composite model was also validated against the *Wattenbarger and Ramey* (1970) solution for a well in a homogeneous reservoir with a finite skin zone. *Wattenbarger and Ramey* (1970) showed how the thick skin concept can be visualized as a zone near the wellbore with a permeability lower or higher than the reservoir's permeability. Thus, a homogeneous reservoir with a thick skin zone is a two-region composite reservoir. *Wattenbarger and Ramey* (1970) presented an equation and a table relating thick skin to the mobility ratio between the two zones as well as the discontinuity radius corresponding to that mobility ratio. To verify the multi-region composite reservoir model against the *Wattenbarger and Ramey* (1970) solution, the model was run as a multi-region (ie. three, five and ten regions) composite model with one value of mobility for the region closest to the wellbore and another value of mobility for the rest of the regions beyond the first discontinuity radius. The multi-region composite reservoir model was run with no skin at the discontinuities, and with unit storativity ratios at the discontinuities. It is important to note that the model was run with no skin at the wellbore, and that the values of skin factor observed in Figures 4.3 and 4.4 are values for the thick skin factor. The multi-region composite reservoir model successfully reproduced *Wattenbarger and Ramey's* (1970) dimensionless pressure responses (Figures 4.3, 4.4).

This study was also verified (Figures 4.5 and 4.6) against *Ambastha's* (1992) two-region radial composite model pressure and pressure derivative responses. The multi-region and two-region model solutions were compared with and without skin at the front, with and without wellbore storage and skin. To reproduce *Ambastha's* (1992) results, the multi-region model was run as reservoirs with three, five and ten regions in which all the mobility and storativity ratios at the discontinuities were equal to unity, except one discontinuity at a specified dimensionless radius.





The multi-region composite reservoir model has also been verified against *Ambastha and Ramey* 's (1992) three-region radial composite model pressure and pressure derivative responses. Same type of previous analysis was employed. The comparison between the two studies was also completely satisfactory (Figures 4.7 and 4.8). No further verification seems necessary.

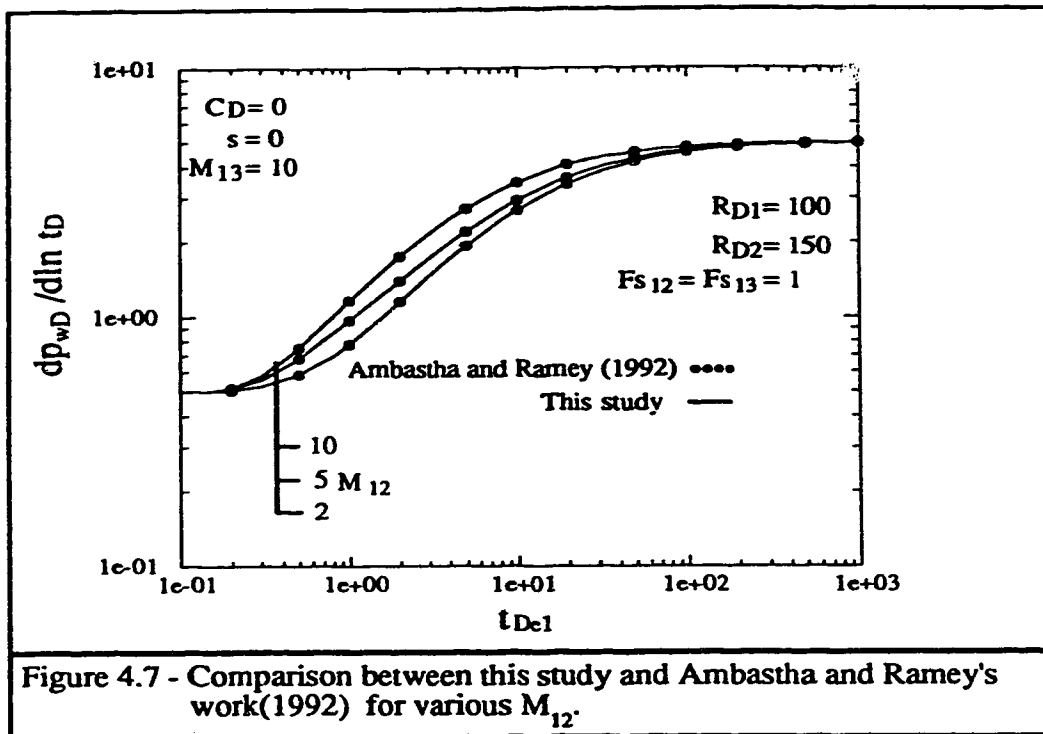


Figure 4.7 - Comparison between this study and Ambastha and Ramey's work(1992) for various  $M_{12}$ .

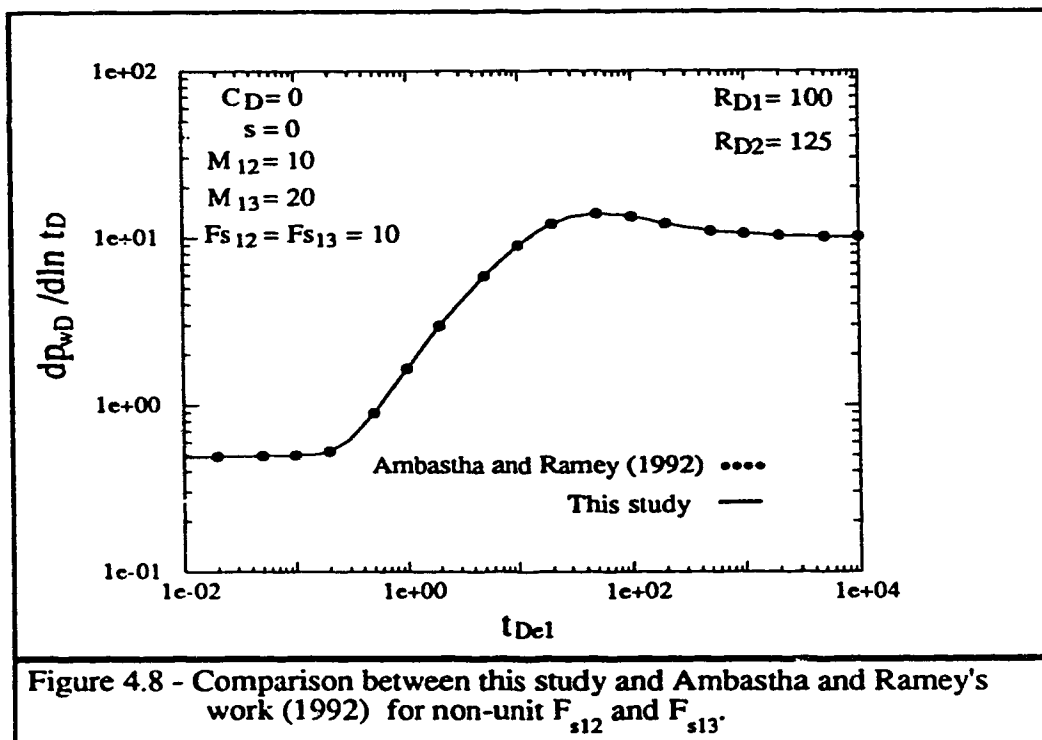


Figure 4.8 - Comparison between this study and Ambastha and Ramey's work (1992) for non-unit  $F_{s12}$  and  $F_{s13}$ .

## **CHAPTER 5**

### **DRAWDOWN TEST ANALYSIS FOR MULTI-REGION COMPOSITE RESERVOIRS**

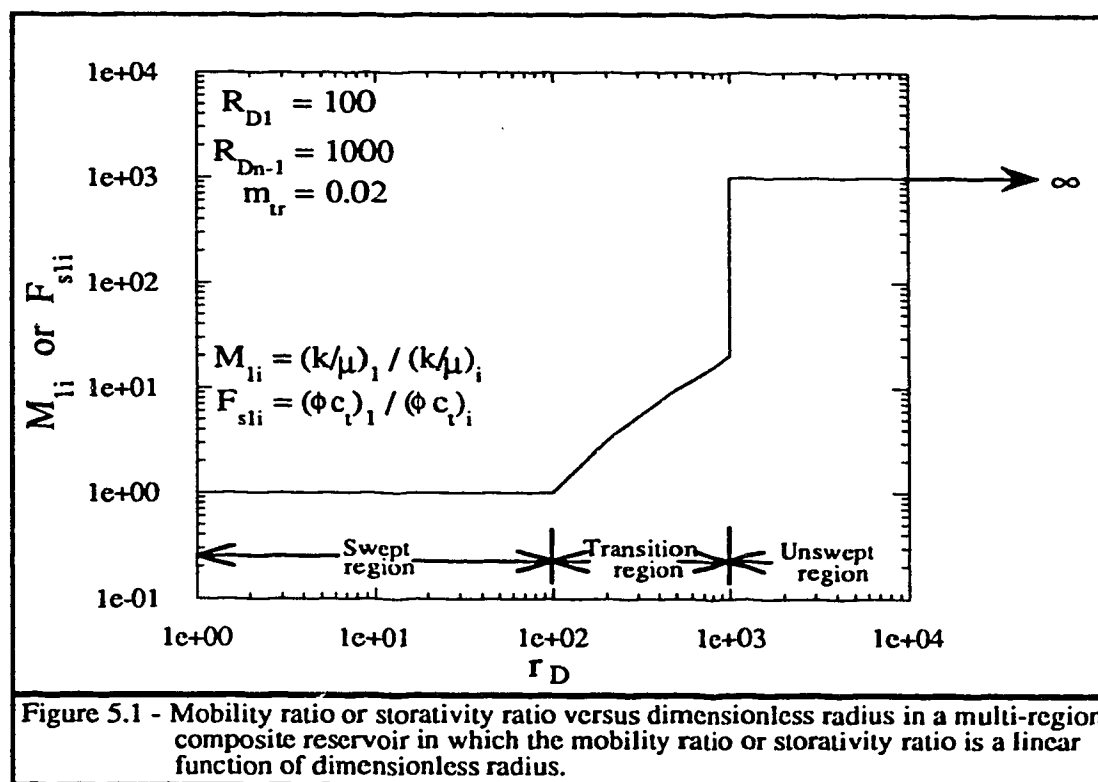
As discussed in Chapter 2, enhanced oil recovery processes, such as in-situ combustion and steam injection, are examples of artificially-created composite systems. In these situations, the reservoir can be viewed as a multi-region system with different rock and/or fluid properties. This study analyzes drawdown test data from a multi-region composite reservoir model representing a reservoir undergoing steam injection.

#### **5.1 Description of a Reservoir undergoing Steam Injection**

A reservoir undergoing steam injection has three characteristic zones. A first inner zone, called the "swept zone", is full of steam and has the greatest values of mobility and storativity. Beyond the inner zone, there exists a second zone in which the mobility and/or the storativity may be continuously changing. This second zone is called the "transition zone". Steam, oil and condensed water are present in the transition zone. At the end of the transition region, towards the reservoir outer boundary, there is a cold heavy oil region called the "unswept zone". This last zone has the lowest mobility and storativity values, and extends as far as the reservoir's outer boundary.

Figure 5.1 represents a mobility ratio and/or storativity ratio profile from a reservoir in which steam is being injected to recover heavy oil. As the pressure transient moves from the swept region to the unswept region, the mobility and storativity will decrease. However, because of the definition of mobility ratio and storativity ratio used in this study, the mobility ratio and the storativity ratio will increase as the pressure transient moves from the swept region to the unswept region. Also, based on the definition, the mobility ratio and storativity ratio of the swept region will be equal to one, while the unswept region will have the largest values for mobility ratio and storativity ratio. The unswept region's mobility ratio and storativity ratio are the overall mobility and storativity ratios. Thus, the swept and unswept regions have well-defined values for mobility ratio and storativity ratio. However, the values for the transition region's mobility ratio or storativity ratio are difficult to define, since mobility and storativity are continuously changing in this region. In the particular case of steam injection, mobility and storativity ratios continuously increase in the transition region. The values for mobility ratio and storativity ratio in the transition region will fall in a range from one to a value lower or equal to the unswept region's ratios.

Though the transition region's mobility and/or storativity ratio profiles can be represented in any suitable manner judged to mimic the real situation, this study analyzes cases in which the transition region's mobility ratio and/or storativity ratio profiles are linear functions of dimensionless radius. Figure 5.1 represents the case of the transition's region linear relationship between mobility and/or storativity ratio versus dimensionless radius. The reason for this transition region's profile not appearing as a straight line is that a Cartesian straight line is being plotted on a log-log scale in Figure 5.1. It is important to note that the definition of mobility ratio in Figure 5.1 is different from the definition in



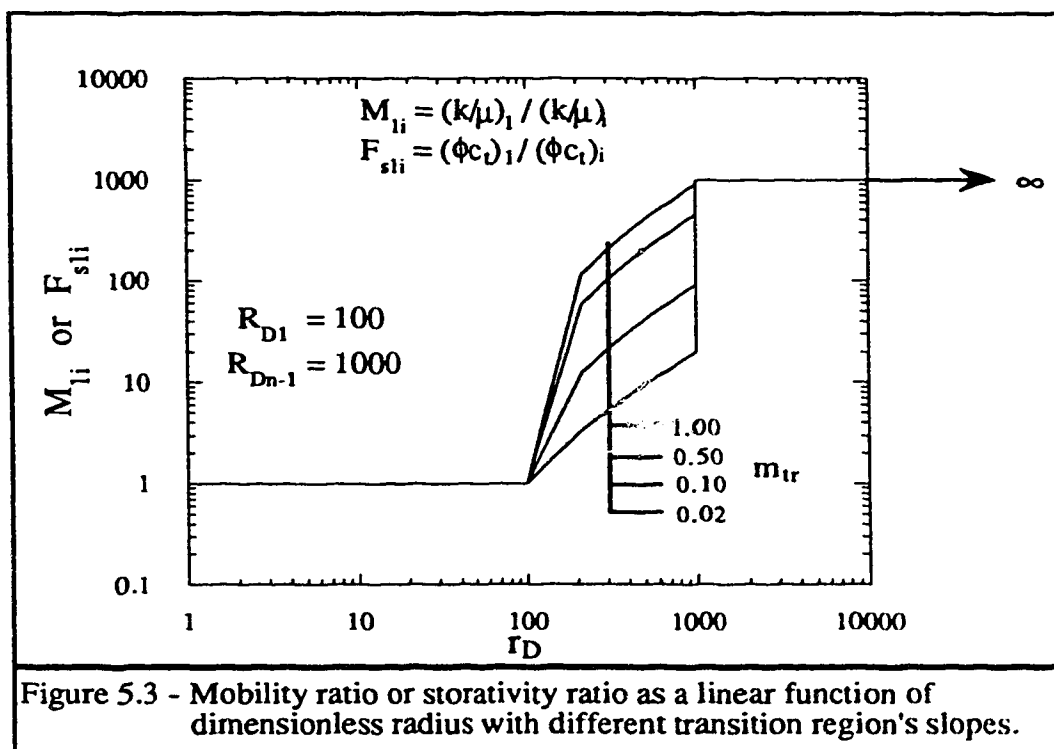
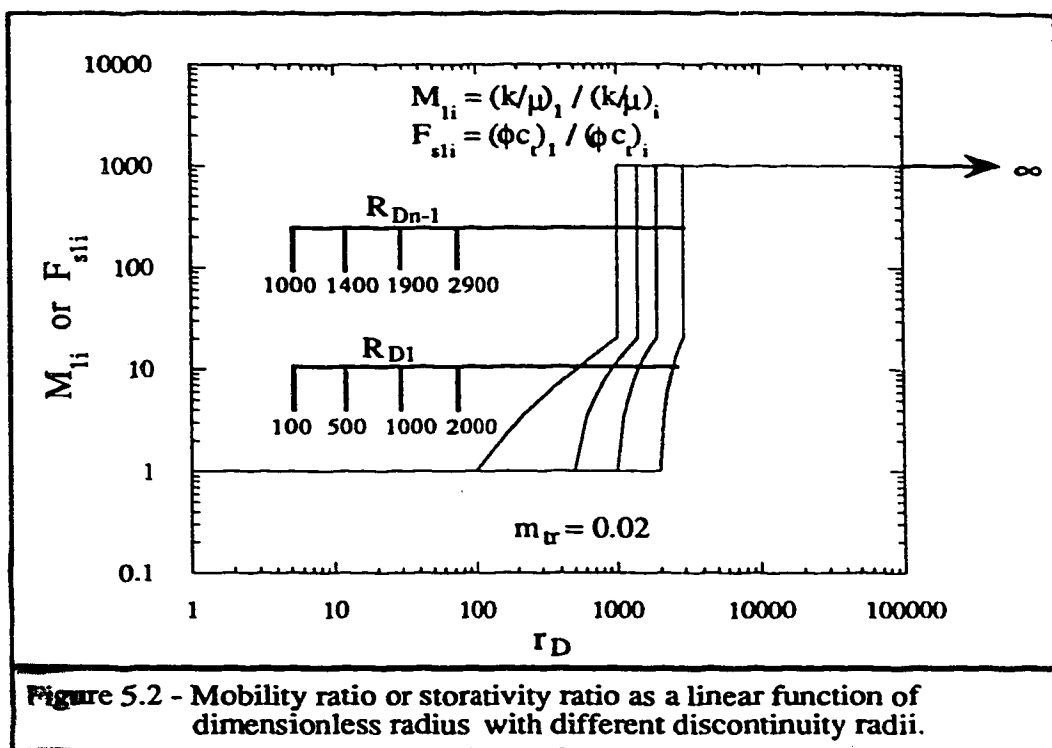


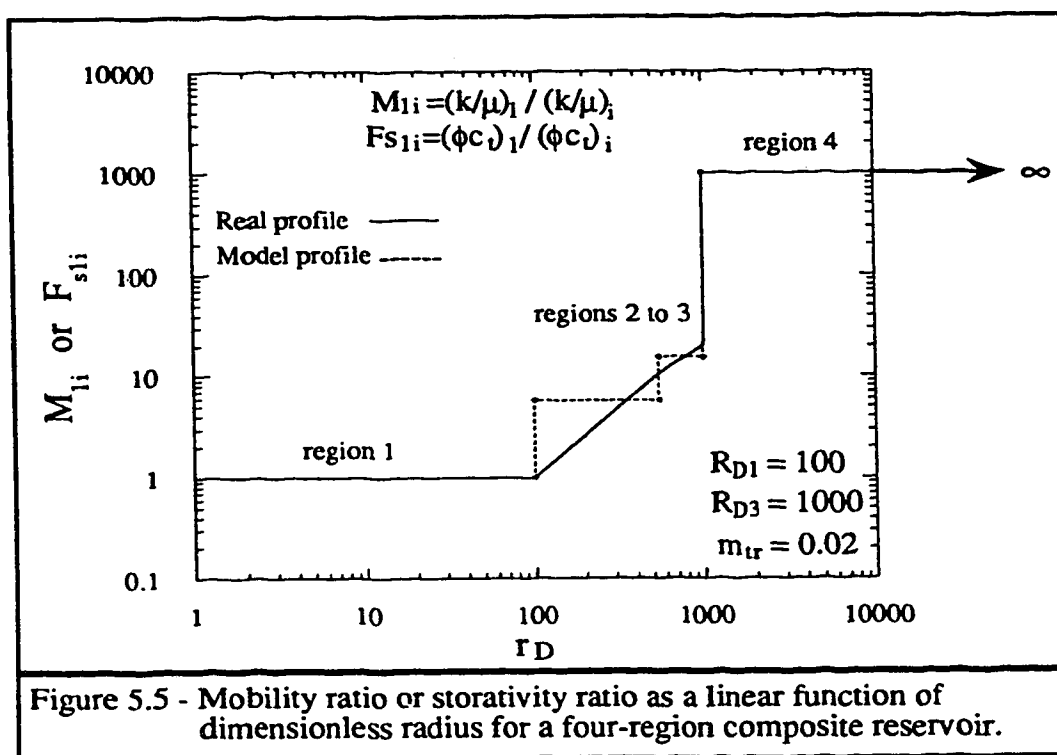
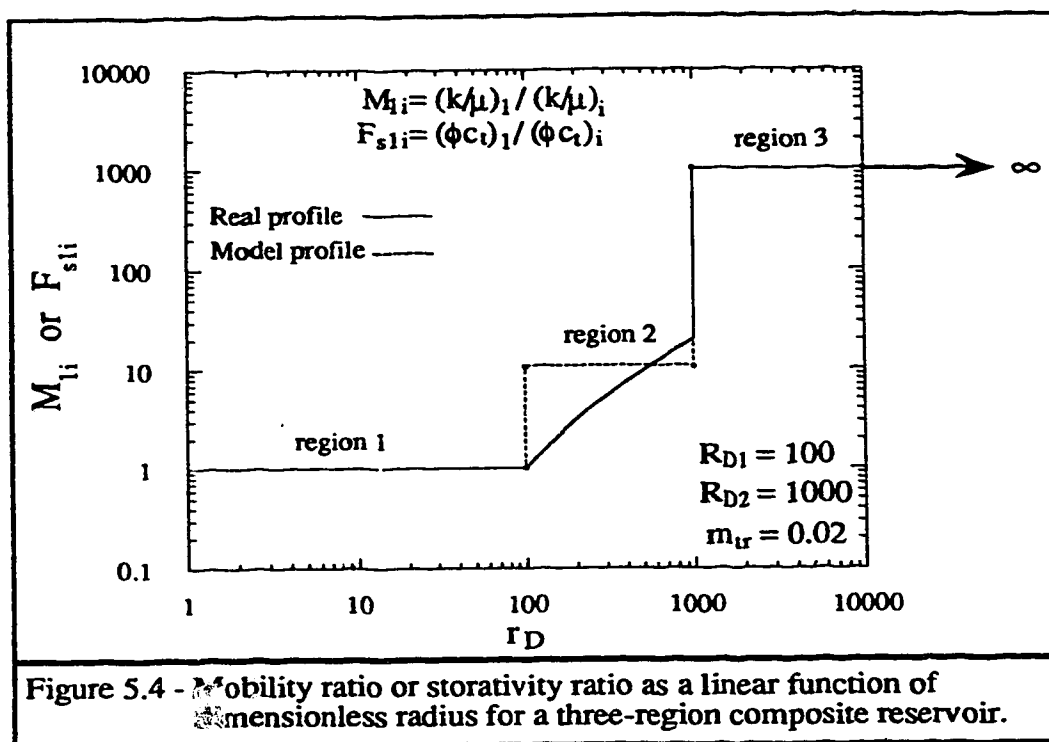
Equation 4.14. This new definition of mobility ratio will be used with the sole purpose of presenting results. There are not any mathematical implications from this new definition of mobility ratio and the mathematical model remains the same as defined in Chapter 4. In Figure 5.1, an arrow and the symbol for infinity are observed. The purpose of the arrow and the infinity symbol is to represent the fact that the unswept region's outer limit is not defined on the graph, since the reservoir has an infinite outer boundary.

Figures 5.2 and 5.3 are the different mobility and storativity ratio profiles considered in this study. In these figures, three variables should be explained:

- 1       $R_{D1}$  is the radius where the inner region ends and the transition region starts.  
 $R_{D1}$  will be referred to as the first discontinuity radius.
- 2       $R_{Dn-1}$  is the radius where the transition region ends and the unswept region starts.  
 $R_{Dn-1}$  will be referred to as the last discontinuity radius.
3.       $m_{tr}$  is the slope of the line that represents the transition region's relationship between the mobility and/or storativity ratios, and the dimensionless radius.  
 $m_{tr}$  will be referred to as the transition region's slope.

The transition region can be represented by one region with an averaged value for mobility ratio and/or storativity ratio or by several regions with different values of mobility ratio and storativity ratio. Both representations are intended to approximate the transition region's profile. Figures 5.4 through 5.8 show different ways of representing the transition region in this study. The composite models used in this analysis vary from a three-region





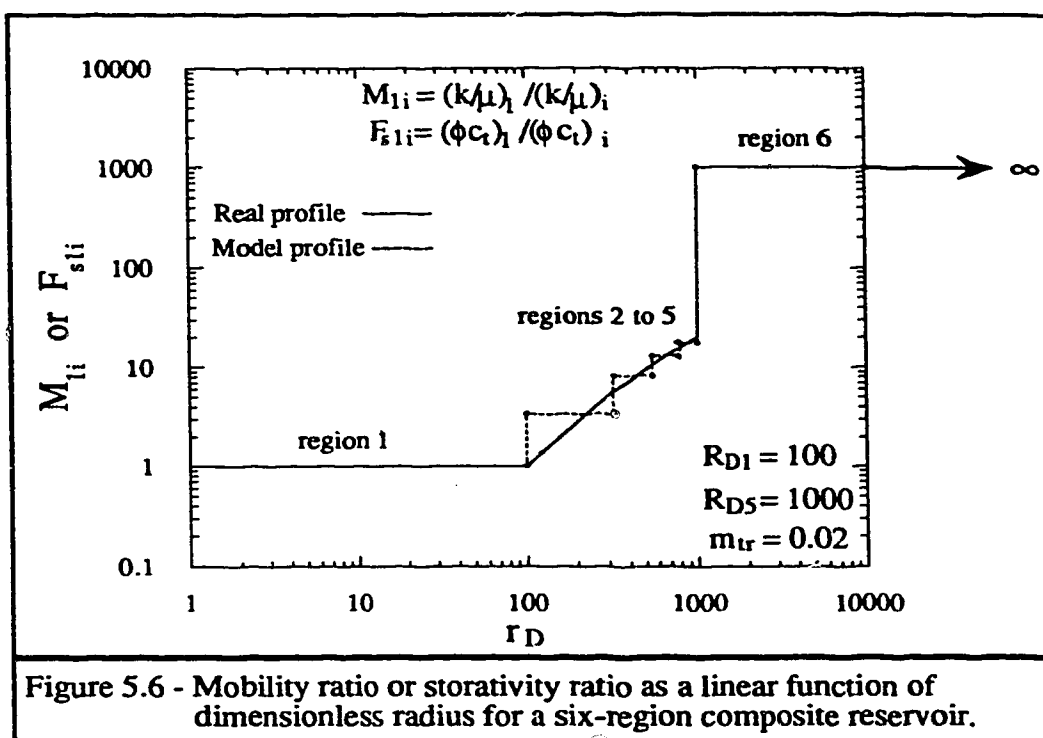


Figure 5.6 - Mobility ratio or storativity ratio as a linear function of dimensionless radius for a six-region composite reservoir.

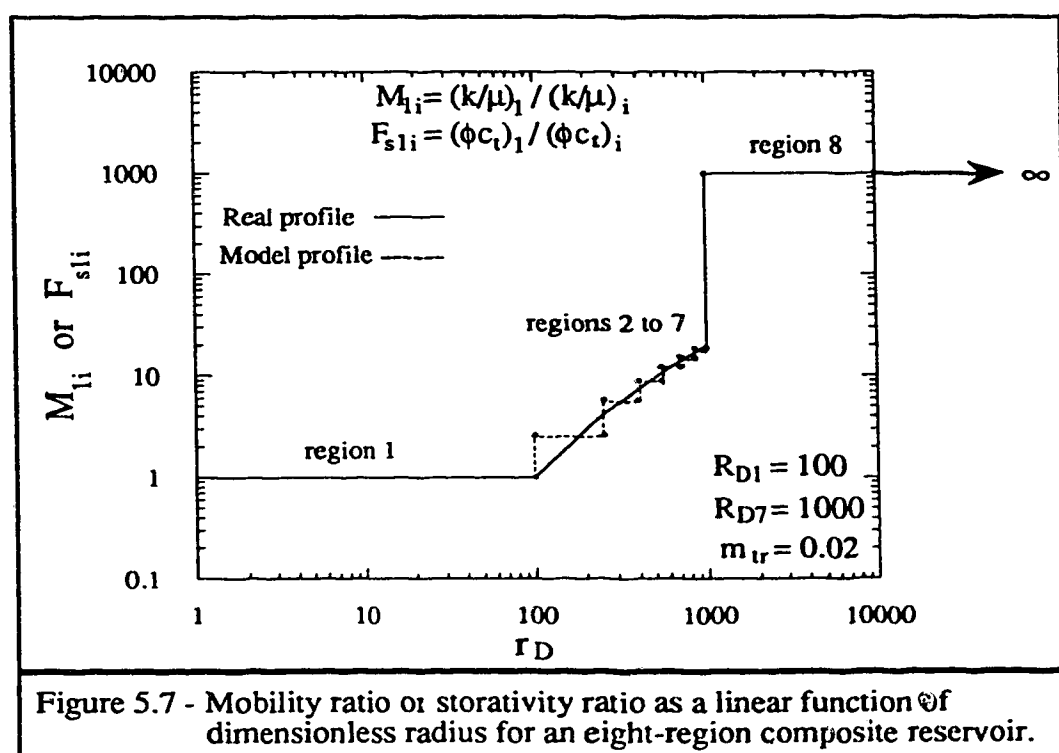


Figure 5.7 - Mobility ratio or storativity ratio as a linear function of dimensionless radius for an eight-region composite reservoir.

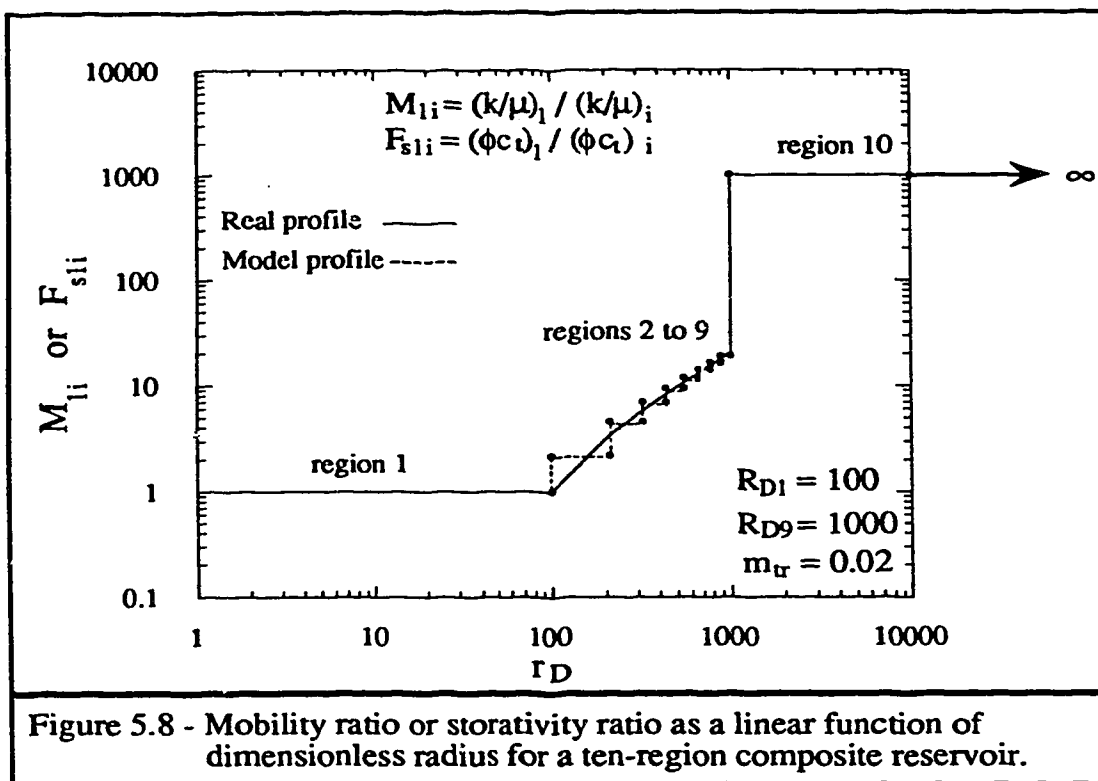


Figure 5.8 - Mobility ratio or storativity ratio as a linear function of dimensionless radius for a ten-region composite reservoir.

composite model to a ten-region composite model. The three-region composite model represents the transition region using one region. The ten-region composite model represents the transition region using eight regions. In all composite models, the swept and the unswept regions are represented by one region each.

The three-region composite model and the ten-region composite model use different values of mobility ratio and/or storativity ratio to represent the transition region's linear profile. To represent this linear profile, a material balance method is used. This method was first proposed by *van Everdingen et al.* (1953) when analyzing the pressure behaviour of an aquifer. Based on this method, there will be two areas between the actual profile line and the value selected. One area is above the actual profile and the other area is under the actual profile line. These areas have triangular shapes (see Figures 5.4 through 5.8). For the case of the three-region composite model, there exists one triangular area above the profile line and one triangular area below the profile line. For the case of a ten-region composite model, there are eight triangular areas above the profile line and eight triangular areas below the profile line. The criterion to select the values representing the transition region is that the areas above the profile should be the same as the areas below the profile line. The smaller the triangular areas, the better is the representation of the straight line profile for mobility and/or storativity variation in the transition region.

Representing a steam injection project by a three-region composite model may yield significantly different pressure transient responses compared to a representation using a ten-region composite model. This study considers such differences in the transient pressure behaviour when the reservoir is represented by a multi-region (three or more regions) composite model.

## 5.2 Steam Injection Pressure Transient Behaviour

Depending on reservoir properties, well conditions and the amount of steam injected, the pressure transient behaviour of a reservoir undergoing steam injection, can be described by different transient flow periods. These periods are:

1. A wellbore storage dominated flow period,
2. An early radial flow period which reflects the mobility of the inner region,
3. An early transition flow period reflecting mobility and/or storativity changes,
4. A pseudosteady state flow period reflecting a large mobility or storativity contrast,
5. A late transition flow period reflecting mobility and/or storativity changes, and
6. A late radial flow period which reflects the mobility of the outer region.

A pressure derivative graph enhances the detail in the information that can be obtained from a well test. Therefore, by using pressure derivative graphs, the pressure transient analysis from a reservoir may be improved. In most of this study, pressure derivative graphs have been used.

A log-log plot of the semilog pressure derivative ( $dp_{wD} / d\ln t_D$ ) versus dimensionless time ( $t_D$ ) may be used to identify the different flow regimes. Various regimes are identified by:

1. A unit slope line for the wellbore dominated period,
2. A zero slope line for for early radial flow in the swept region,
3. A unit slope line for the pseudosteady state flow period, and
4. A zero slope line for the late radial flow in the unswept region.

A log-log plot of the dimensionless Cartesian pressure derivative ( $dp_{wD} / dt_{DA}$ ) versus area-based dimensionless time ( $t_{DA}$ ) may be used to obtain valuable information from a reservoir's pressure transient behaviour. Throughout this study, the area used in the definition of area-based dimensionless time is the area to the last discontinuity radius  $R_{Dn-1}$ . When analyzing a log-log graph of Cartesian pressure derivative versus area-based dimensionless time, various flow regimes are identified by:

1. A zero slope line for the wellbore dominated period,
2. A negative unit slope line for early radial flow in the swept region,
3. A zero slope line for the pseudosteady state flow period, and
4. A negative unit slope line for the late radial flow in the unswept region.

Although the wellbore dominated flow period has been mentioned for completeness sake, this study only considers cases with no wellbore storage. Skin at the wellbore and skin at the discontinuities are also considered to be zero. Since wellbore storage and skin effects have been sufficiently analyzed in previous studies, other features of transient pressure behaviour are considered in this study.

When there is a well defined pseudosteady state period, a log-log graph of the semilog pressure derivative ( $dp_{wD} / d\ln t_D$ ) versus dimensionless time ( $t_D$ ) will exhibit a unit slope line. During the pseudosteady state period, the slope of a Cartesian straight line on a pressure versus time graph is inversely proportional to the volume to the discontinuity at which sharp contrasts in mobility and/or storativity occur. In some cases, after observing the early radial flow and a transition flow period, the semilog pressure derivative data falls



on a straight line, whose slope is less than unity. In such cases, application of the pseudosteady state concept leads to an overestimation of the volume to the last discontinuity radius. *Sheng* (1992) explained that this phenomenon may be caused by a small hot water zone, thermal effects and/or low mobility contrasts between regions. This study further investigates the reasons for this phenomenon.

In a graph of dimensionless Cartesian pressure derivative ( $dp_{wD} / dt_{DA}$ ) versus area-based dimensionless time ( $t_{DA}$ ), a flattening or a zero slope line segment may indicate a pseudosteady state flow period. The condition to be able to see this flattening is a significant mobility and/or storativity contrast between regions. When this flattening occurs at a value of the dimensionless Cartesian pressure derivative equal to  $2\pi$ , the property contrasts observed exist at the radius used to compute the area-based dimensionless time ( $t_{DA}$ ). In this study, the radius used to compute area-based dimensionless time ( $t_{DA}$ ) is the last discontinuity radius  $R_{Dn-1}$ . Thus, if a flattening is observed, when the Cartesian pressure derivative is equal to  $2\pi$ , then there is a significant mobility and/or storativity contrast at the last discontinuity radius  $R_{Dn-1}$ . If a flattening is observed and the value  $m_{cD}$  of the Cartesian pressure derivative is different from  $2\pi$ , then there is a significant mobility and/or storativity contrast at radius  $R_D$  given by:

$$R_D = \frac{R_{Dn-1}}{\sqrt{\frac{m_{cD}}{2\pi}}} \sqrt{\frac{(\phi c_D)_i}{(\phi c_D)_{eff}}} \quad (5.1)$$

For analytical pressure responses shown in this study, Equation 5.1 is useful to check if a correct  $m_{cD}$  occurs with respect to  $R_{D1}$ , as  $R_{Dn-1}$  is an input for data generation

purposes. However, field application of Equation 5.1 is limited because  $R_{Dn-1}$  may not be known accurately. In Equation (5.1), it is important to note that  $(\phi c_D)_{eff}$  is the effective storativity corresponding to the volume up to  $R_D$ .

### 5.3 Analyzing Pressure Transient Responses for a Multi-region Composite Reservoir

This section contains a study of transient pressure responses corresponding to the mobility ratio and storativity ratio profiles shown on Figures 5.4 through 5.8.

Figure 5.9 compares the dimensionless semilog pressure derivative behaviour of several composite models. For all the models, an early and a late radial flow period are observed. The semilog pressure derivative has a value of 0.5 for the early radial flow period and a value of 500 for the late radial flow period. These two values for the semilog pressure derivative represent the swept and unswept region's mobility ratios, respectively. By definition, the mobility ratios of the swept and unswept regions are equal to two times the value of the semilog pressure derivative on the early and late radial flow periods respectively. In our case, the swept region has a mobility ratio of 1, as defined in section 5.2, and the unswept region has a value of 1000.

In Figure 5.9, it can be observed that neither the departure time from the early radial flow period nor the transition region's duration are affected by the number of regions of the composite model. However, the transition region's transient pressure behaviour is affected by the number of regions of the model. Therefore, the information that can be obtained

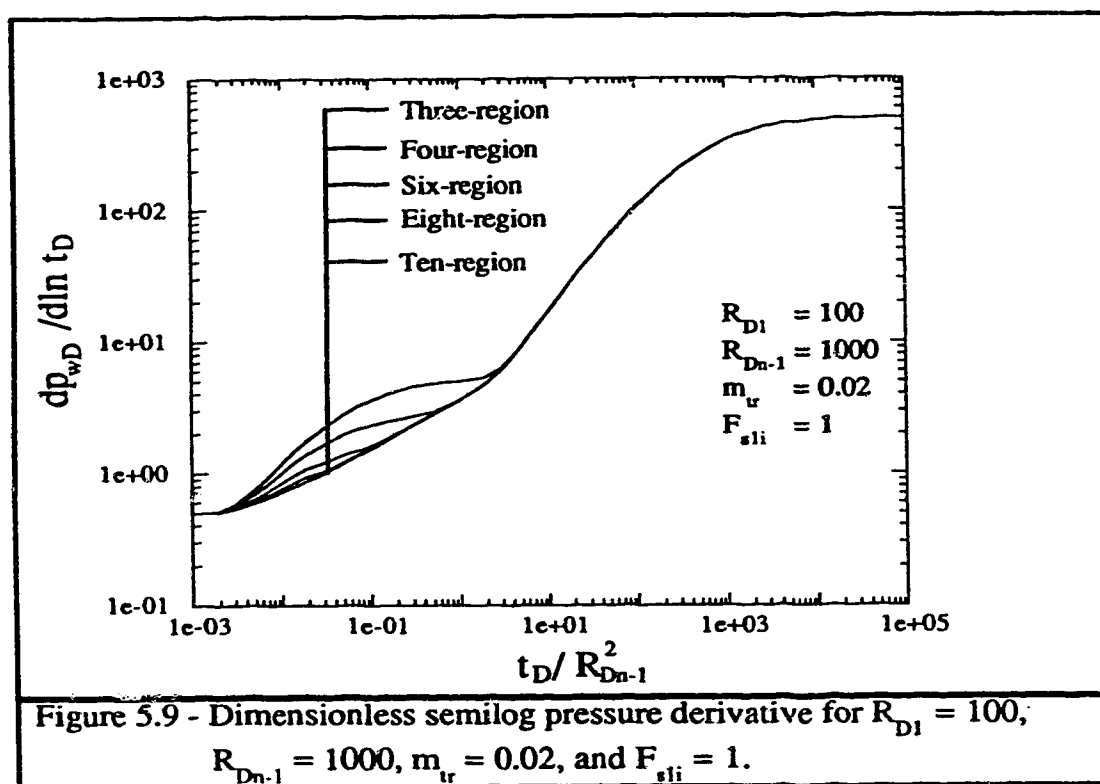


Figure 5.9 - Dimensionless semilog pressure derivative for  $R_{D1} = 100$ ,  $R_{Dn-1} = 1000$ ,  $m_{tr} = 0.02$ , and  $F_{sli} = 1$ .

from the transition region is affected by the number of regions of the model. As observed in Figure 5.9, the transition region's values for the semilog pressure derivative are higher for the three-region composite model than for the ten-region composite model. Thus, this suggests that the value of the transition region's effective mobility ratio for the three-region model is higher than the effective mobility ratio for the ten-region model. Values for the transition region's effective mobility ratio were computed by applying Equation A.9 to the data input values (Tables C2 and C10) of the composite models. A value of 3.07 was obtained for the effective mobility ratio of the ten-region model, while a value of 4.16 was obtained for the effective mobility ratio of the three region composite model. These values confirm the observations from Figure 5.9.

Also, from Figure 5.9, it can be seen that the three-region composite model shows an initial transition period, after the early radial flow, in which the dimensionless semilog pressure derivative falls on a line. This line appears, because of the mobility contrast at the inner region radius. This mobility contrast is the consequence of only one region representing the transition zone. The slope of this line is less than one and suggests a low mobility contrast between regions. The dimensionless Cartesian pressure derivative on Figure 5.10 confirms that there is a low mobility contrast at early times of the pressure transient behaviour. This low mobility contrast is indicated by a deviation of the Cartesian pressure derivative from the negative unit slope line. However, since the mobility contrast is low, the Cartesian pressure derivative does not flatten as it does when there is a high contrast in mobility or storativity. A high contrast in mobility or storativity originates a pseudosteady state period.

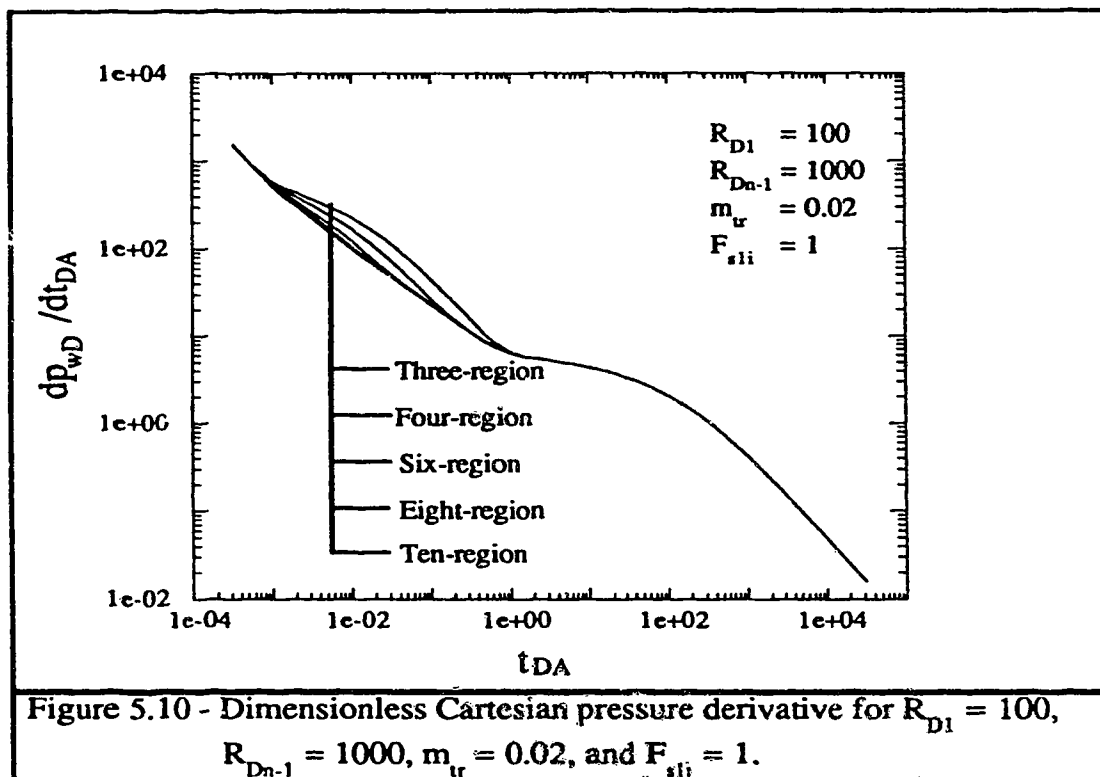
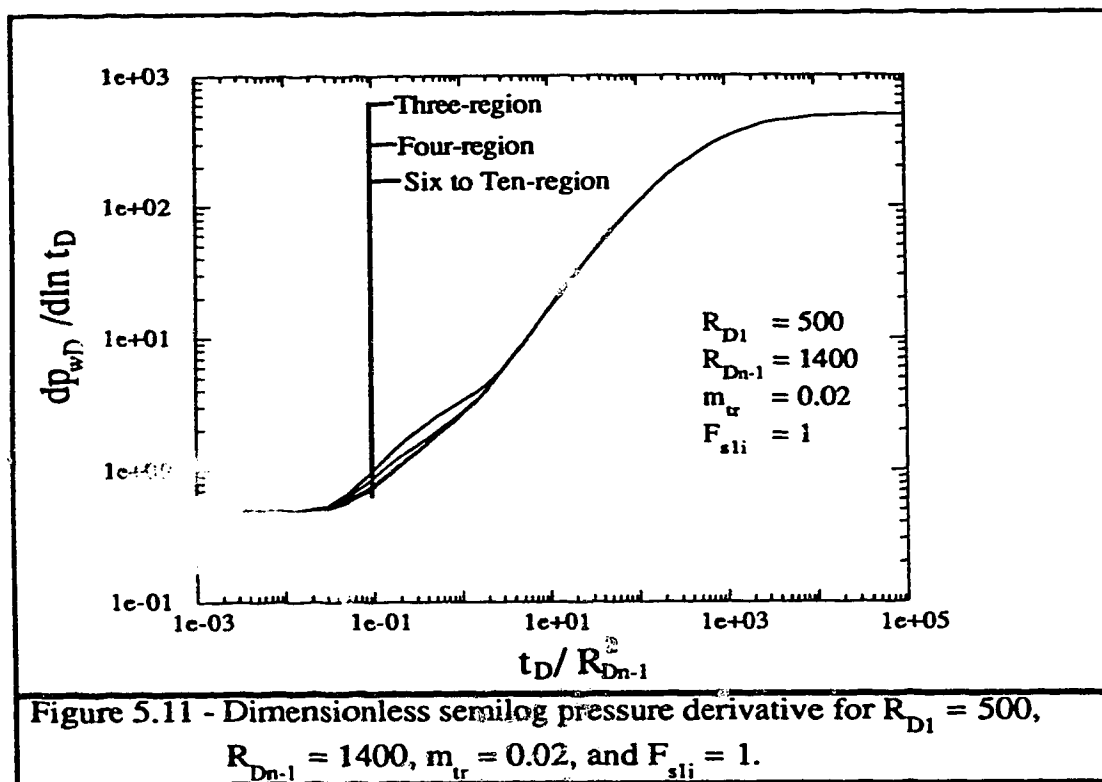


Figure 5.10 shows that all the composite models deviate from the negative unit slope at the same time,  $4 \times 10^{-4}$ , approximately. At this deviation time, the dimensionless Cartesian pressure derivative has a value  $m_{cD}$  of approximately 630. By applying Equation 5.1, a first dimensionless discontinuity radius of approximately 100 was found. This estimated value of first dimensionless discontinuity radius satisfactorily agrees with the input value.

Figure 5.9 shows that there is a time, when, for all of the composite models, the semilog pressure derivative falls on a unit slope straight line. This unit slope straight line indicates a pseudosteady state period due to a high mobility contrast. Figure 5.10 confirms this high contrast by a flattening of the Cartesian pressure derivative. This flattening occurs, when the Cartesian pressure derivative has a value of  $2\pi$ . As explained in Section 5.2, this transient pressure behaviour shows a high mobility contrast at the last discontinuity radius  $R_{Dn-1}$ , as expected.

Figure 5.11 shows the effect of increasing the first discontinuity radius on pressure transient behaviour. Although the input mobility ratios are the same as for Figures 5.9 and 5.10, it seems that changing the first and last discontinuity radii affects the effective mobility ratio of the multi-region (three or more regions) composite systems. By applying Equation A.9 to the input mobility ratios of the three-region composite model, an effective mobility ratio of 2.35 was found, while doing the same thing for the ten-region model yielded an effective mobility ratio of 2.12. This is one likely reason as to why the pressure behaviour for all the composite models are closer to each other than those in the previous case of smaller first discontinuity radius (see Figure 5.9 for comparison).

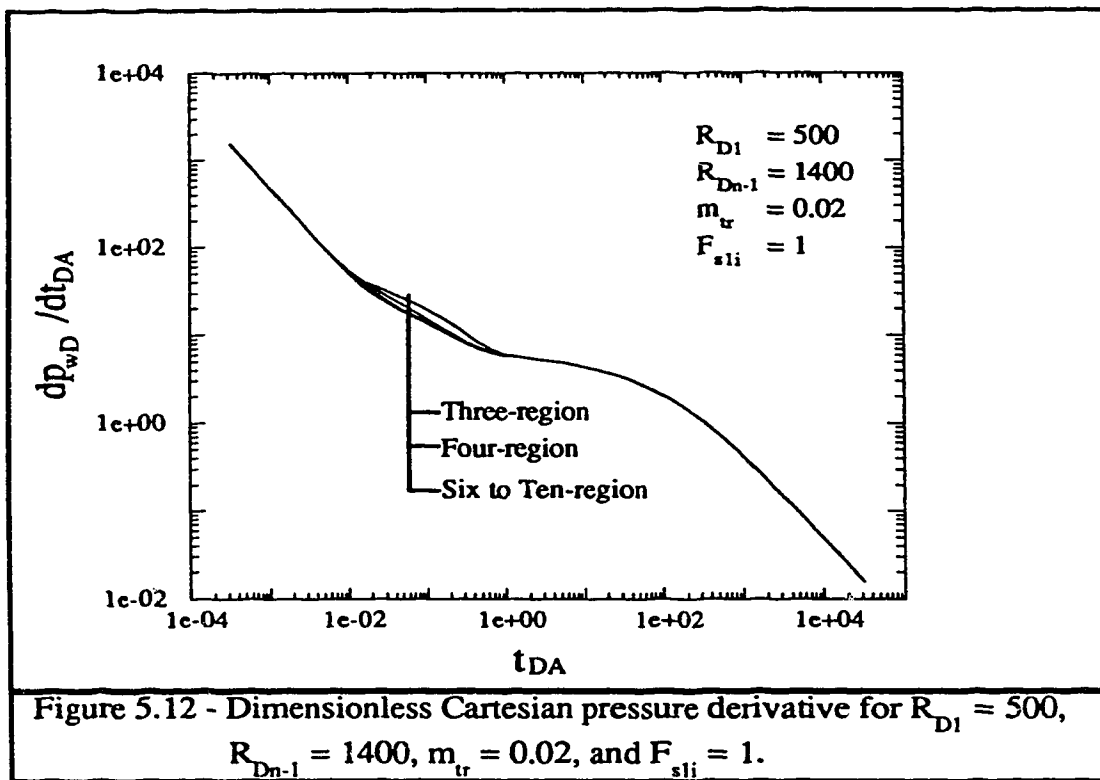


Also, from Figure 5.11, it is observed that the transition region's effects are felt later than the previous case on Figures 5.9 and 5.10, as expected. Thus, increasing the first discontinuity radius increases the deviation time. Another effect of increasing the first discontinuity radius is that the transition region's effects become weaker and the duration of the transition region is shorter.

A general behaviour for all composite models is observed in Figure 5.11. Soon after the end of early radial flow, the semilog pressure derivative falls on a straight line for a short time period. The slope of this straight line is lower than unity. As the number of regions representing the transition region increases, this straight line slope becomes smaller indicating a lower mobility contrast. Thus, more regions in a multi-region composite model, mimicking continuous property variations for an actual reservoir, reduce the possibility of obtaining a unit slope line for the transition pressure behaviour. In theoretical pressure transient models, a unit slope line appears as a consequence of representing a zone with continuously changing mobility or storativity as one region. This one-region representation also erroneously increases the duration of any real pseudosteady state flow period.

At a later period of time in the transition region response, Figure 5.11 shows that all composite models join together and the semilog pressure derivative falls on a straight line. The slope of this straight line is unity, indicating a pseudosteady state period due to a high mobility contrast. Figure 5.12 confirms this high contrast by a flattening of the Cartesian pressure derivative. This flattening occurs, when the Cartesian pressure derivative has a value of  $2\pi$ . This indicates that a large mobility contrast exists at the last discontinuity radius  $R_{Dn-1}$ . By using Equation 5.1, the first dimensionless discontinuity radius can also

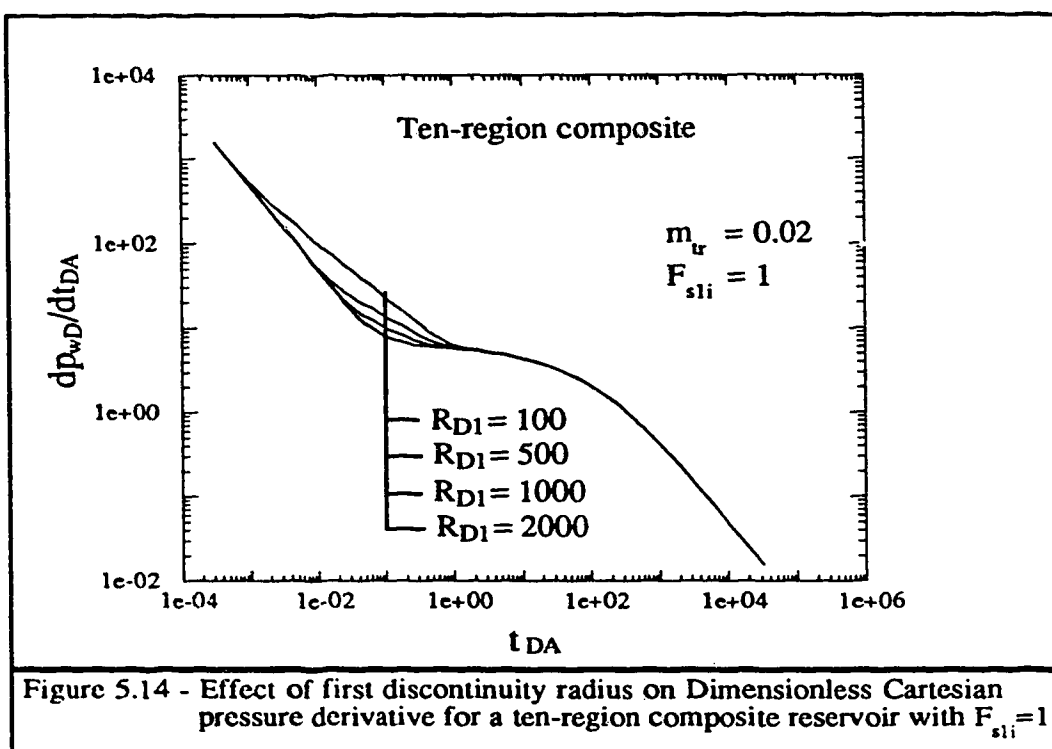
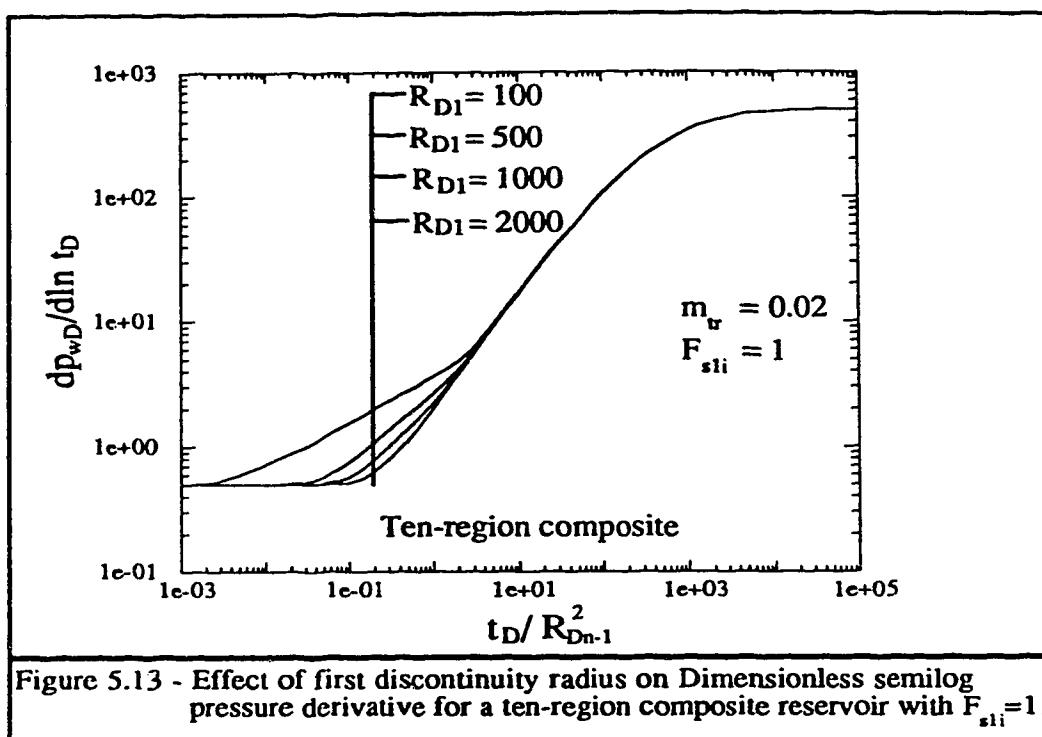


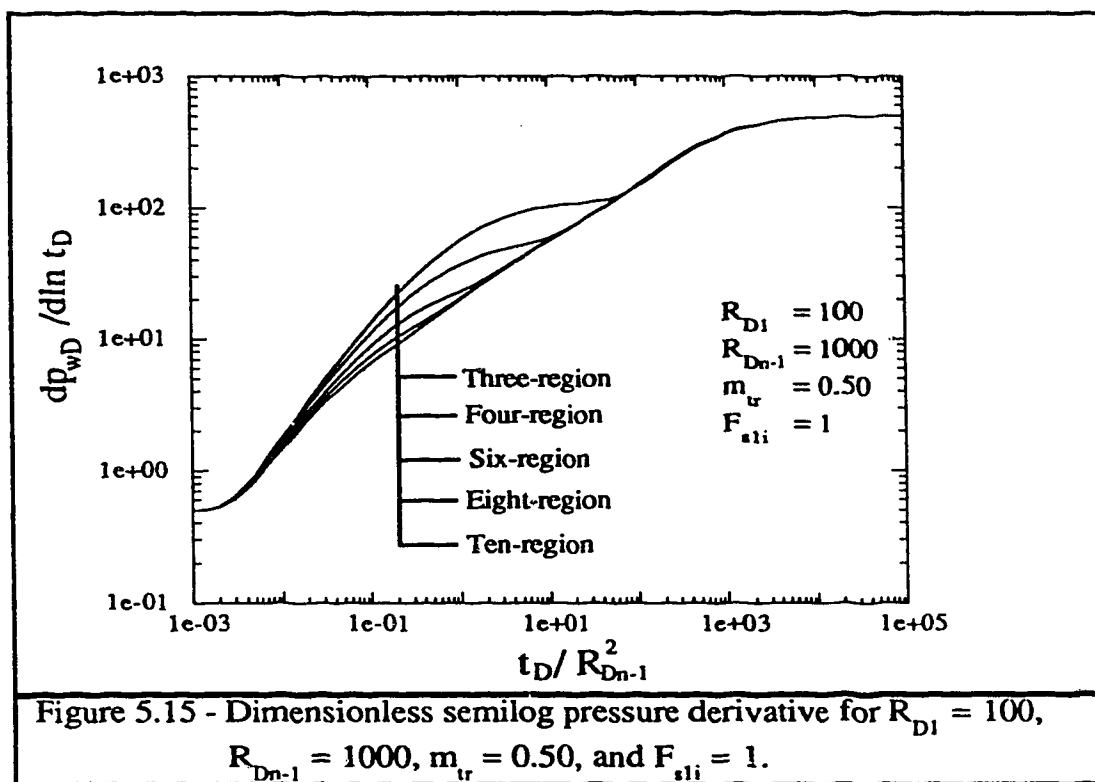


be estimated for the response in Figure 5.12. The first point when the Cartesian pressure derivative deviates from the negative unit slope line indicates a Cartesian pressure derivative value of approximately 49. By applying Equation 5.1 as discussed previously, a value of approximately 500 was obtained for the first dimensionless discontinuity radius. This estimated first dimensionless discontinuity radius is the same as the input value of 500.

Figures 5.13 and 5.14 show the effects of different values of first discontinuity radius on the semilog pressure derivative and the Cartesian pressure derivative behaviour. Figure 5.13 shows that the larger the first discontinuity radius, the larger is the deviation time. Increasing the first discontinuity radius reduces the effects of the transition region on pressure behaviour. The duration of the transition region effects on the pressure behaviour is inversely related to the first discontinuity radius. If the first discontinuity radius is too large compared with the last discontinuity radius, the inner region effects may mask all the transition region effects on the pressure behaviour. Except for the case of totally masked transition region effects, the method based on Equation 5.1 is not affected by the first discontinuity radius.

Figure 5.15 shows the semilog pressure derivative behaviour of another mobility profile. The overall mobility ratio is 1000 as in previous cases. However, a slope( $m_{tr}$ ) of 0.5 is assigned to the transition region's straight line mobility profile. Thus, the mobility ratio at the first discontinuity radius is greater than in previous cases. Increasing the transition region's slope causes a high mobility contrast between the swept region and the transition region. This contrast is observed in Figure 5.15 at the beginning of the transition region effects, when for all the models, the semilog pressure derivative falls on a straight line with a unit slope indicating the pseudosteady state period soon after the end of early radial flow.



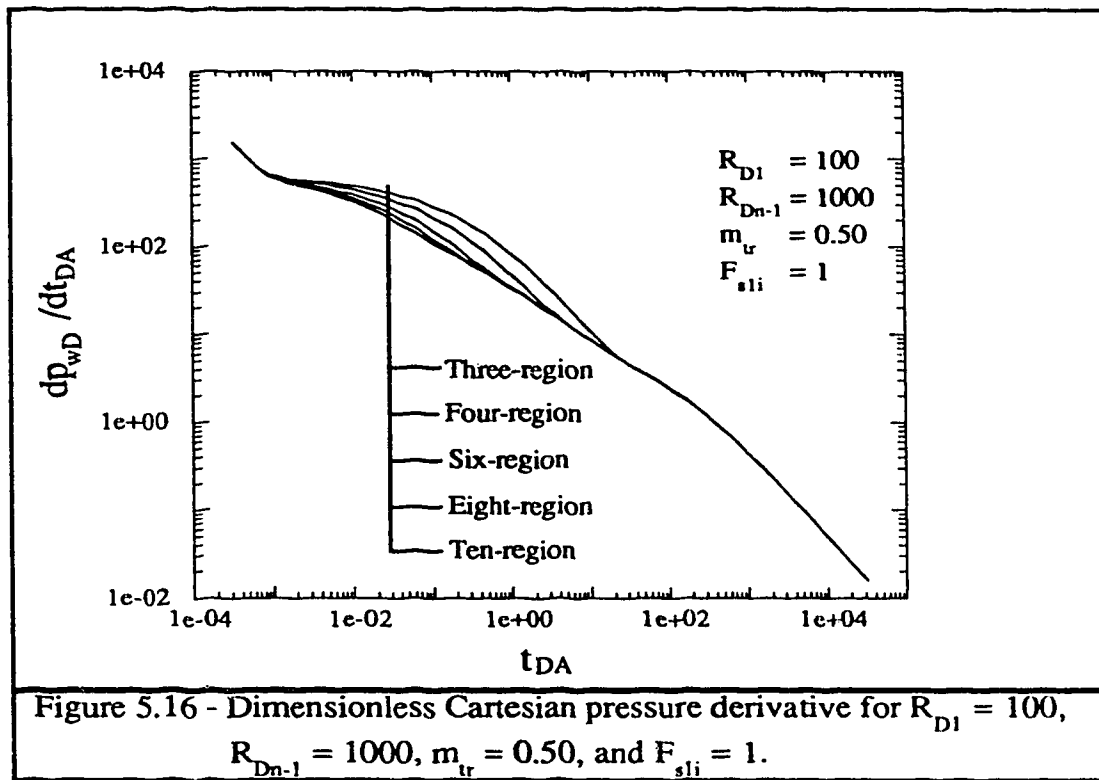


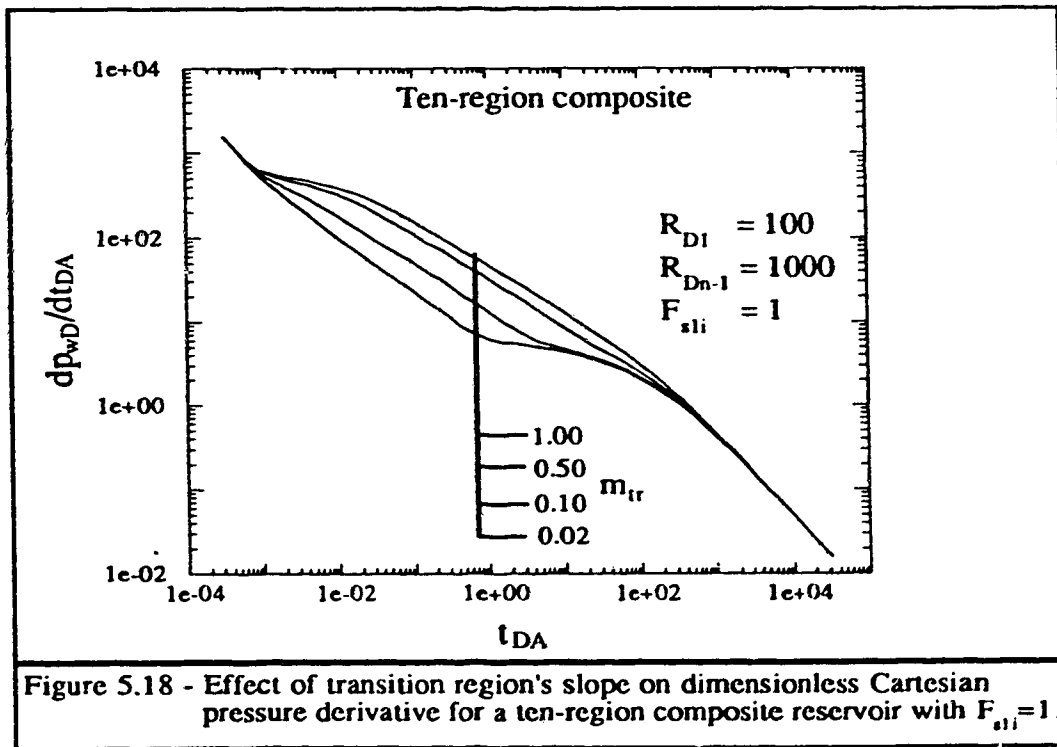
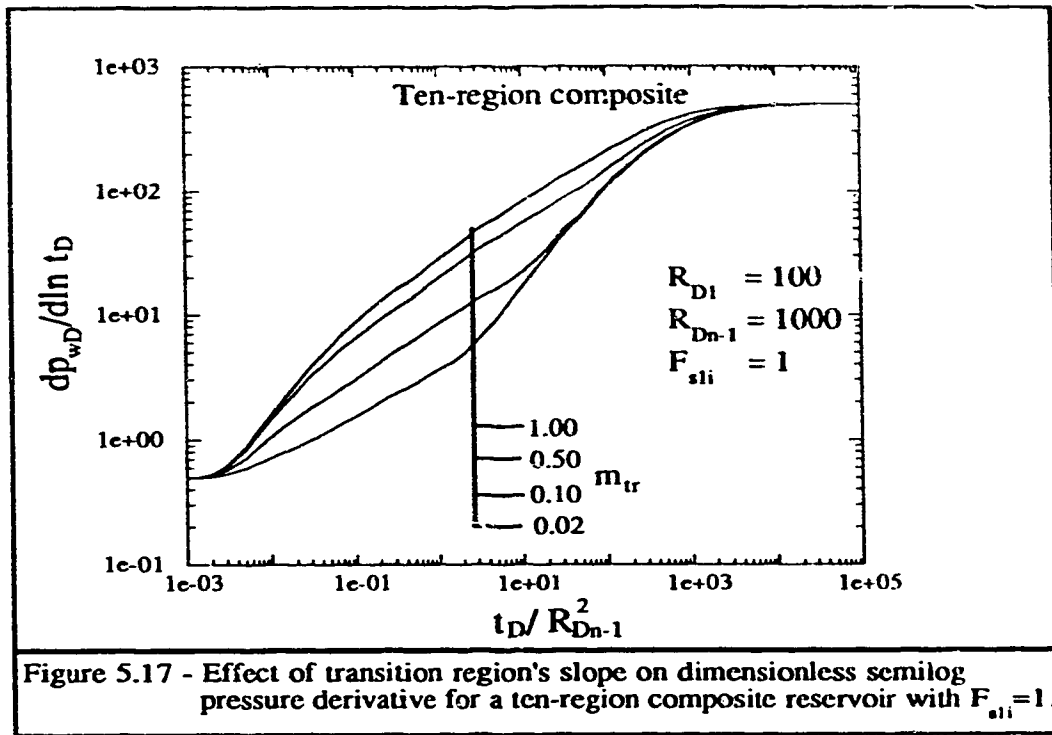
Another effect of increasing the transition region's slope  $m_{tr}$  is that now there is a lower mobility contrast between the transition region and the unswept zone. The effects of this low mobility contrast can be observed in Figure 5.15 at the late transition flow period. This period shows that, for all composite models, the semilog pressure derivative curves fall on a straight line with a slope lower than one. With data from this period of time, the pseudosteady state method may be used to estimate the last discontinuity radius. However, the last discontinuity radius would be overestimated.

Figure 5.16 shows a flattening of the Cartesian pressure derivative, confirming the high contrast in mobility between the swept region and the transition region. Applying Equation 5.1 to the value  $m_{CD}$  of the Cartesian pressure derivative at the first deviation point from the negative unit slope line will yield the first discontinuity radius. The estimated first discontinuity radius is 93, which is slightly lower than the input value of 100.

Figures 5.17 and 5.18 show the effects on the semilog pressure derivative and the Cartesian pressure derivative behaviour of several values of the transition region's slope. In general, increasing the transition region's slope causes an increase in the mobility contrast between the swept and the transition region, while the mobility contrast between the transition region and the unswept region decreases. The higher the mobility contrast, the higher are the chances of existence of a pseudosteady state period.

For low mobility contrasts between the swept and transition regions, Equation 5.1 yields good estimates of the first discontinuity radius. For high mobility contrasts, the pseudosteady state method yields good estimates of the appropriate discontinuity radius, if a correct effective compressibility is used for the analysis. When an adequate flattening in



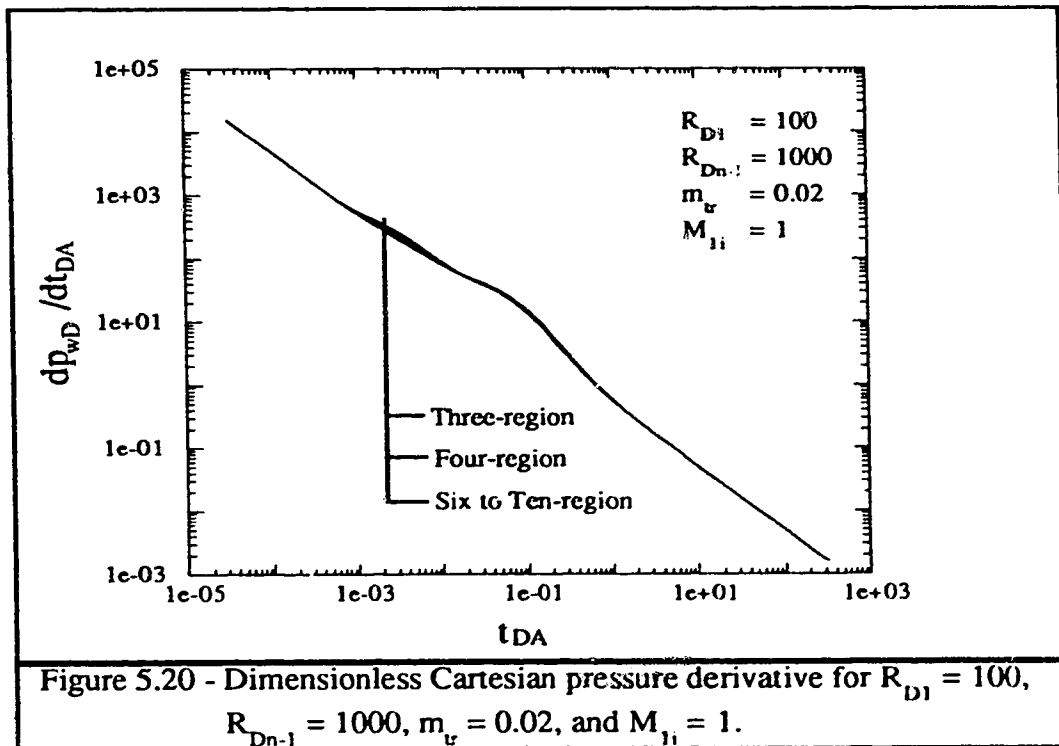
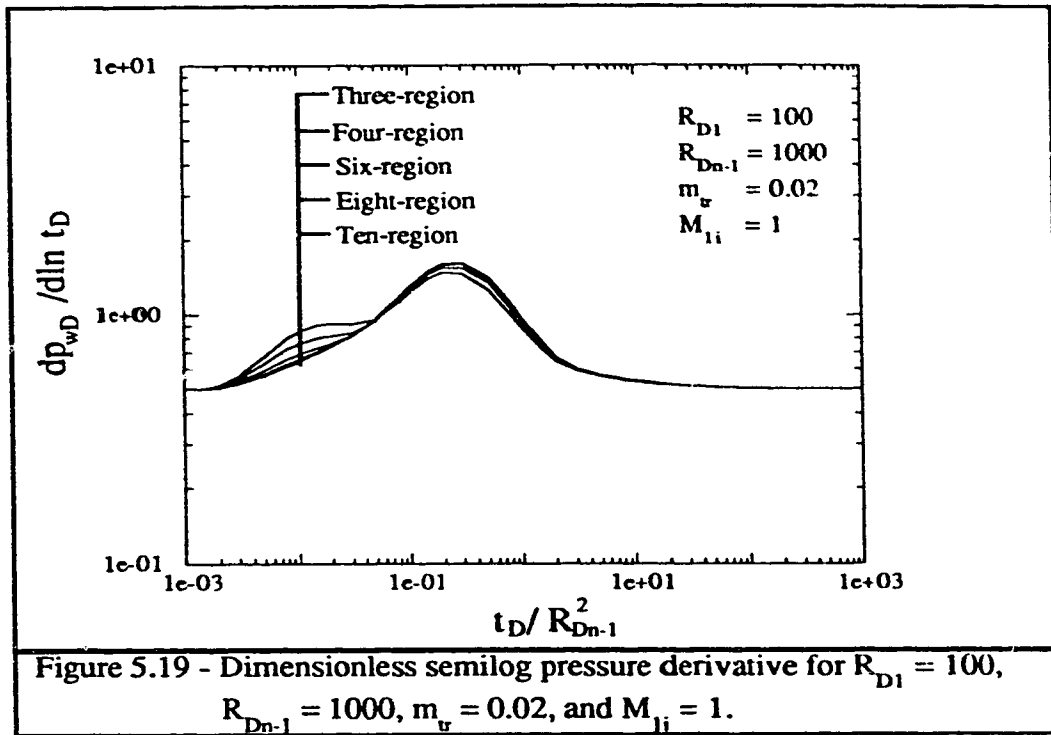


Cartesian pressure derivative is not observed, a discontinuity radius computed using the pseudosteady state method would generally be an overestimated value. This normally occurs when the contrast between the transition region and the unswept region is too low to observe significant flattening on the Cartesian pressure derivative curves.

Figures 5.19 and 5.20 show the semilog pressure derivative and the Cartesian pressure derivative of a reservoir in which storativity in the transition region changes linearly with respect to the dimensionless radius. This profile is shown in Figure 5.2 in which the overall storativity ratio is 1000 and the slope for the transition region profile is 0.02. In this case, a constant mobility throughout the reservoir has been used. Thus, mobility ratio is equal to one everywhere in the reservoir. From Figures 5.19 and 5.20, it can be observed that there is a small difference between the three-region model and the ten-region model. This small difference is directly related to the value of effective storativity in the transition region. By applying Equation A.14 to the input storativity ratios of the ten-region model (Table C10), an effective storativity ratio was computed. An effective storativity ratio of 9.14 was obtained for the ten-region model, while for the three-region model (Table C2), a value of 9.59 was obtained. These results explain small differences, especially for Cartesian pressure derivative (see Figure 5.20), among three- to ten-region representations of storativity variation in the transition region.

Figure 5.19 shows that the number of regions does not affect the deviation time when analyzing a reservoir with a changing storativity profile. Before the semilog pressure derivative reaches its maximum value, for all of the models, the semilog pressure derivative falls on a straight line. This straight line's slope is considerably lower than unity. Thus, if

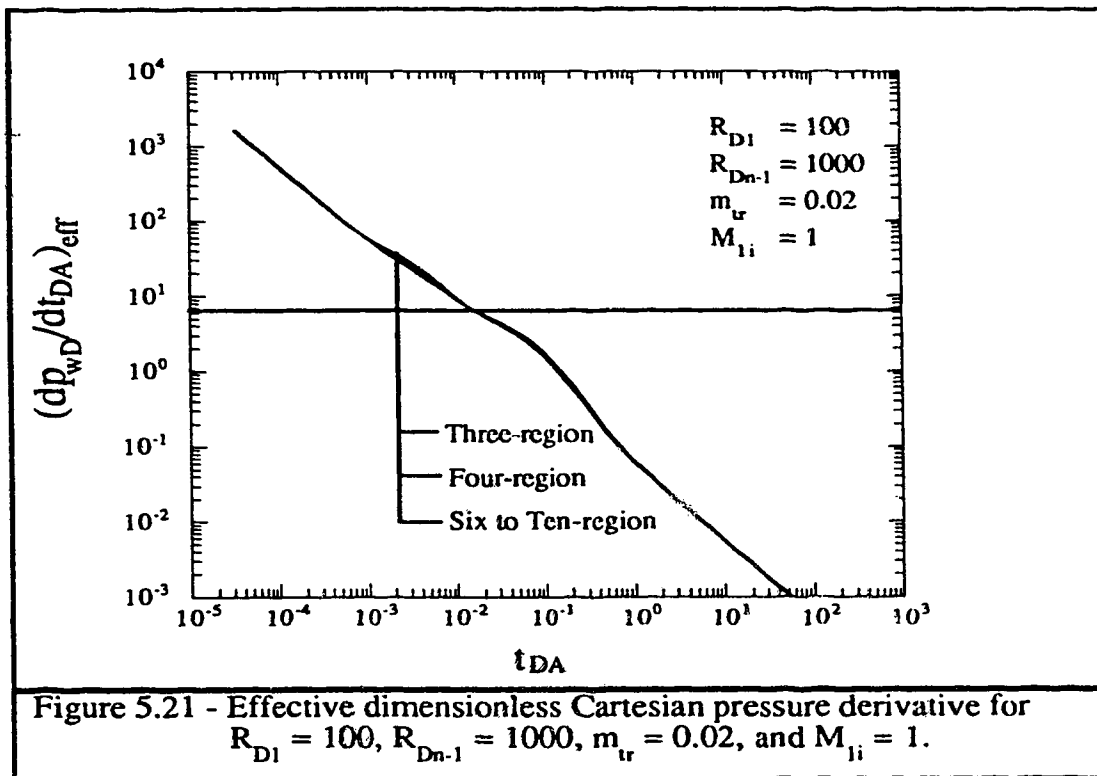




the pseudosteady state method is used with pressure data from this period, the estimated last discontinuity radius would be much higher than the actual one, provided that the correct effective storativity is used for the analysis.

At a dimensionless time  $t_{DA}$  of  $1 \times 10^{-3}$ , the Cartesian pressure derivative on Figure 5.20 shows a slight deviation from a line of slope -1 indicating a very low contrast in storativity. The value of the Cartesian pressure derivative at this first point of deviation is approximately 630. If Equation 5.1 is applied, a value will be computed for the first discontinuity radius. The estimated first discontinuity radius is approximately 100, which agrees with the input value.

At a dimensionless time  $t_{DA}$  of about  $1.8 \times 10^{-2}$ , the Cartesian pressure derivative on Figure 5.20 shows an additional deviation. This deviation shows another low contrast in storativity, since the Cartesian pressure derivative deviates, but does not flatten significantly. Also, Figure 5.20 shows that this deviation occurs for values of the Cartesian pressure derivative greater than  $2\pi$ . This behaviour suggests that estimating the last discontinuity radius by the pseudosteady state method will yield an underestimation of the actual last discontinuity radius. However, this assumption is incorrect since the Cartesian pressure derivative in Figure 5.20 does not account for the effects of effective storativity for multi-region composite reservoirs. Figure 5.21 shows the behaviour of the effective Cartesian pressure derivative for the same storativity profile as in Figure 5.20. The effective Cartesian pressure derivative in Figure 5.21 accounts for the effects of storativity for each of the multi-region composite models. The effective Cartesian pressure derivative on Figure 5.21 shows also as in Figure 5.20, an incomplete flattening at the last discontinuity radius. However, contrary to what was observed in Figure 5.20, the



incomplete flattening of the effective Cartesian pressure derivative on Figure 5.21 has a value lower than  $2\pi$  (horizontal line). This value of effective Cartesian pressure derivative suggests that using the pseudosteady state method to estimate the last discontinuity radius will yield an overestimated value. This is consistent with the observation made in Figure 5.19 for the semilog pressure derivative straight line with a slope lower than unity.

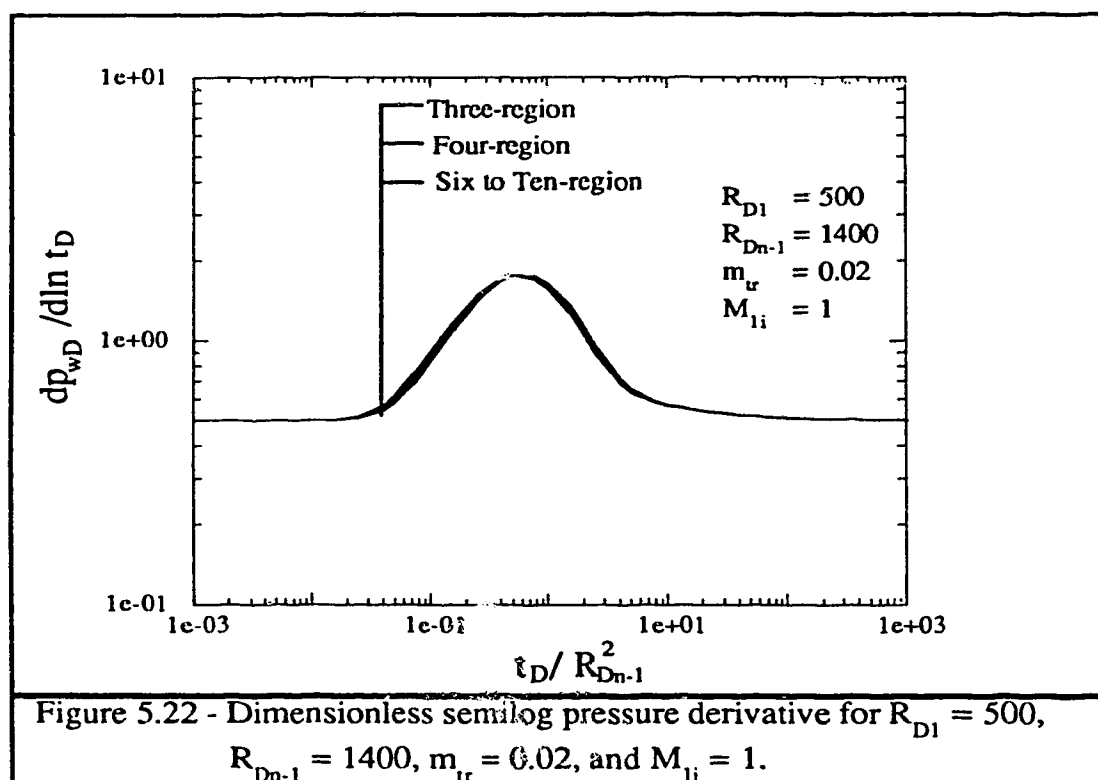
Different possible values were observed for the incomplete flattening (at the last discontinuity radius) of the effective Cartesian pressure derivative on Figure 5.21. These values give an idea of what will be the overestimation of the volume to the last discontinuity radius if the pseudosteady method is used. For this case, the volume to the last discontinuity radius may be overestimated by 25 to 60 per cent.

For Figures 5.10 and 5.20, the discontinuity radii and the slope of the transition region are the same. Both profiles have the same overall ratio in properties. However, for Figure 5.10, mobility changes and storativity is constant, while in Figure 5.20, storativity changes and mobility is constant. In Figure 5.20, the time for the second deviation of the Cartesian pressure derivative is approximately two orders of magnitude smaller than that in Figure 5.10. Thus, the second deviation time due to a storativity variation occurs earlier than a mobility variation of the same magnitude for the transition region of a composite reservoir. However, the first deviation time is independent of mobility and/or storativity variation. The first deviation time depends only on the inner (first) region mobility and the first discontinuity radius. Figures 5.10 and 5.20 also show that a mobility contrast will yield larger and better defined pressure derivative deviations than a storativity contrast of the same magnitude. Thus, mobility contrasts are more likely to develop a pseudosteady state flow period than storativity contrasts.

As observed in Figures 5.19 and 5.20, the greatest difference between the three-region model and the ten-region model is at the beginning of the transition region effects. This difference between the two models is the result of representing the transition region as one or as several regions. When the transition region is represented as one region, the pressure derivative behaviour shows a higher contrast in physical properties than when the transition region is represented by a greater number of regions.

Figure 5.22 shows the semilog pressure derivative for a storativity profile with the same characteristics as the profile for Figures 5.19 and 5.20. However, the first and last discontinuity radii are different. While in Figures 5.19 and 5.20, the profile's first and last dimensionless discontinuity radii are 100 and 1000, respectively, in Figure 5.22, the first and last dimensionless discontinuity radii are 500 and 1400, respectively. Figure 5.22 shows that there is a smaller difference between the three-region model and the ten-region model than it was in Figure 5.19. The reasons for this smaller difference are explained below.

After observing Figures 5.10 through Figure 5.22, a general characteristic for pressure derivative responses is evident. Whenever there is a significant contrast in the reservoir's physical properties, the semilog pressure derivative will show a straight line. For a large property contrast, the slope of this line is unity, showing a pseudosteady state flow period. For a small property contrast, the slope of this line is less than unity. The occurrence of the straight line is also related to the reservoir's volume that this line corresponds to. Thus, for the same contrast in physical properties, this straight line may or may not occur, depending on the reservoir's volume affecting the responses. The early straight line developed at the



beginning of the transition region, in a semilog pressure derivative, reflects the volume of the inner zone. The occurrence of a straight line is inversely related to the reservoir's volume affecting the responses. Thus, if the volume of the inner zone increases and the contrast is still the same, there are less possibilities for this straight line to develop. In Figure 5.22, the difference between the first and the last discontinuity dimensionless radius has not changed from what it was in Figure 5.19. However, the volumes of the inner zone and the transition zone have changed. The volume of the inner zone for Figure 5.22 is 25 times the volume of the inner zone in Figure 5.19. Thus, in Figure 5.22, the semilog pressure derivative does not develop a straight line corresponding to the inner region volume, since the inner region volume is too large in this case. Since no straight line corresponding to the inner region volume develops, no major deviation in the pressure derivative occurs at the beginning of the transition region effects. Since it is at the beginning of the transition region effects that the three-region model and the ten-region model are more different, it follows that both models in Figure 5.22 must show a very similar behaviour.

In Figures 5.22 and 5.19, the semilog pressure derivative develops a straight line at a late period of the transition region effects. This straight line reflects the volume of the swept and the transition region together. The slope of this straight line in Figure 5.22 is larger than the slope in Figure 5.19. In this case, the slope of this line is directly related to the contrast of storativity, since the mobility is constant. This suggests that the storativity contrast between the transition region and the unswept region is greater in Figure 5.22 than in Figure 5.19. Since input storativity ratios are the same in both figures, the discontinuity radii must have affected the value of the effective storativity ratio. Effective storativity ratios for the volume corresponding to the sum of the swept and the transition regions were

computed for storativity profiles for Figures 5.19 and 5.22 using the ten-region model. The computed effective storativity ratio for the profile in Figure 5.19 is 9.14, while the computed effective storativity ratio for the profile in Figure 5.22 is 4.28. The value of the unswept zone storativity ratio is 1000 for both figures. Thus, there is a larger storativity contrast between the transition region and the unswept region in Figure 5.22 than in Figure 5.19. This higher storativity contrast explains why the slope of the straight line in Figure 5.22 is larger than the slope of the straight line in Figure 5.19.

In Figure 5.23, the Cartesian pressure derivative of the same storativity profile as for Figure 5.22 is graphed. A log-log graph of Cartesian pressure derivative appears to be less sensitive than a log-log graph of semilog pressure derivative at early and intermediate times, when the Cartesian pressure derivative values are large. Thus, the difference among the composite models is even smaller than in Figure 5.22, and the responses from all of the models overlap. The Cartesian pressure derivative shows a very low contrast in storativity at a dimensionless time  $t_{DA}$  of  $1 \times 10^{-2}$ . By using Equation 5.1, a value of 500 was found for the first discontinuity radius. The estimated discontinuity radius agrees with the input value. However, the deviation corresponding to the last discontinuity cannot be identified. It seems that all of the effects of the low storativity contrast at the first discontinuity and the higher storativity contrast at the last discontinuity are joined together and the transition region's effects are not distinguishable. However, according to the semilog pressure derivative behaviour in Figure 5.22, the storativity contrast at the last discontinuity radius is the one affecting more the pressure derivative responses. Using the pseudosteady state method in these types of reservoirs may lead to an overestimation of the last discontinuity radius, as explained before.



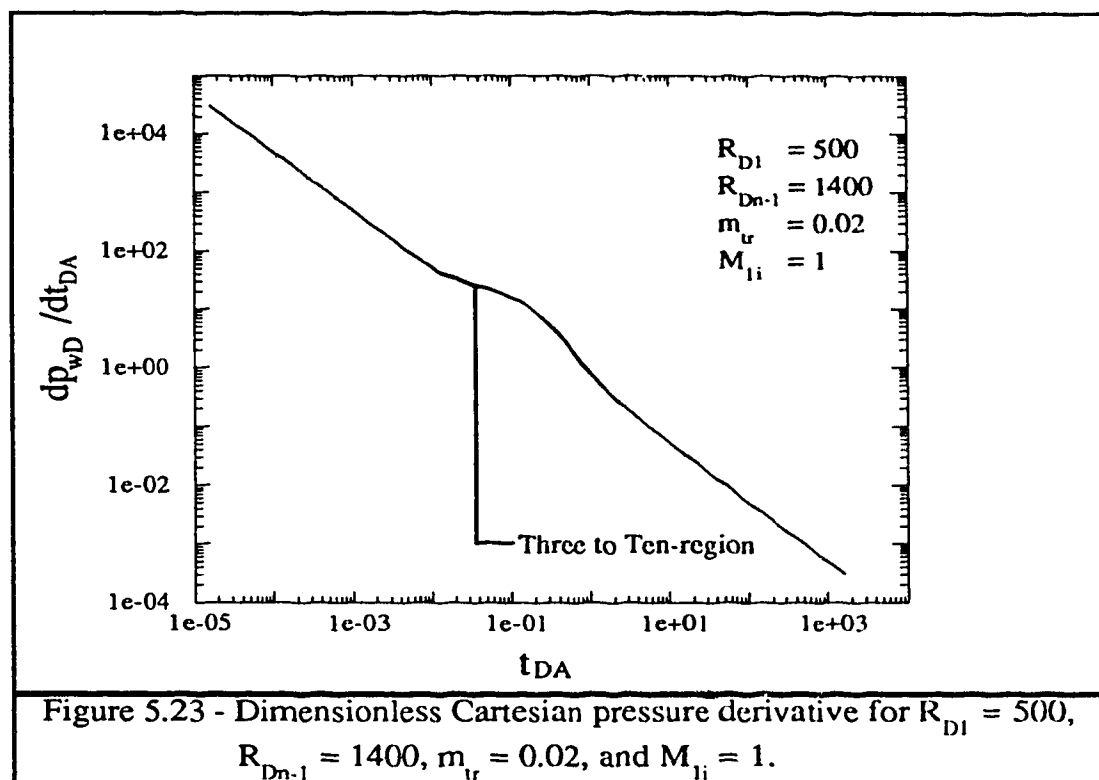
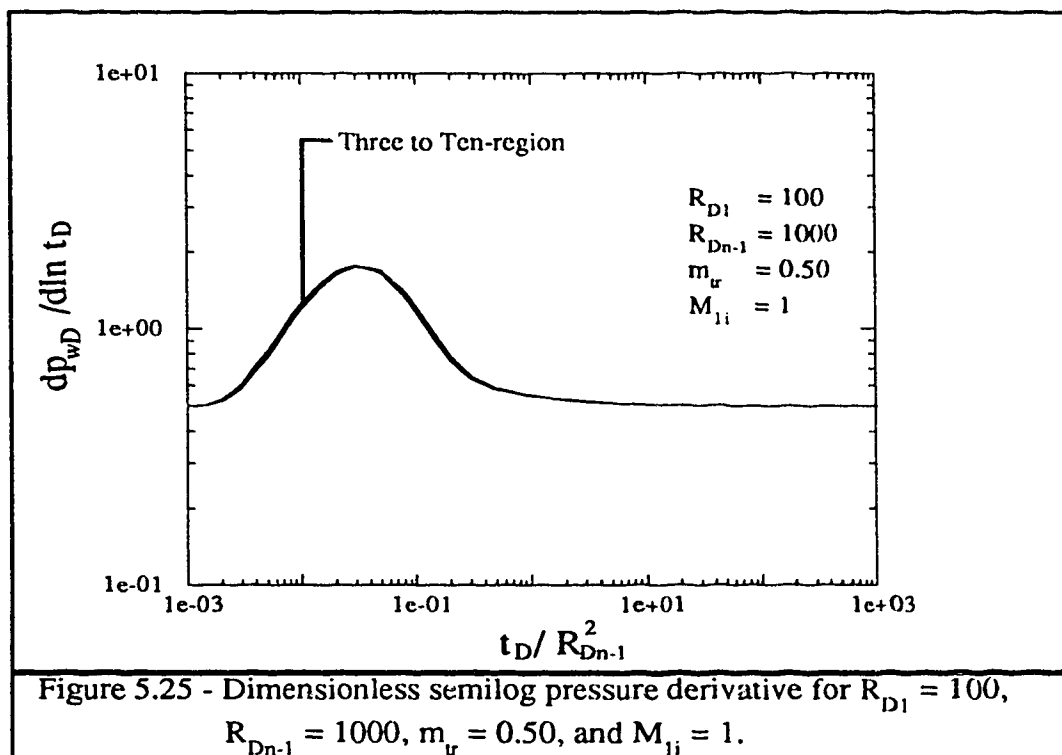
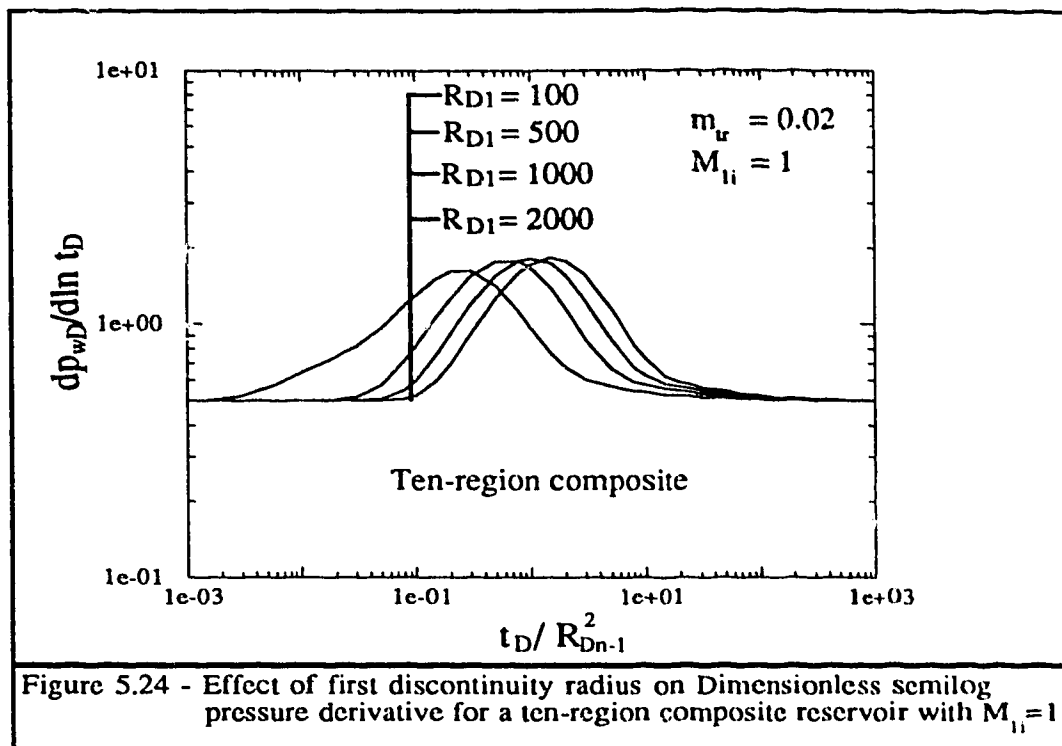


Figure 5.24 shows how the first discontinuity radius and the discontinuity radii ratio affect the semilog pressure derivative behaviour. For all cases,  $R_{Dn-1} = R_{D1} + 900$ . For smaller values of the first discontinuity radius and larger discontinuity radii ratio, the deviation time is earlier, while the transition region's duration is longer. The maximum value of the semilog pressure derivative is mildly affected by the discontinuity radii ratio. The smaller the discontinuity radii ratio, the higher the value of the maximum semilog pressure derivative. This is because the smaller the discontinuity radii ratio, the larger the effective overall storativity ratio.

Figure 5.25 shows the semilog pressure derivative for a reservoir with a first discontinuity radius of 100 and a last discontinuity radius of 1000. Mobility is uniform along the reservoir and storativity within the transition region changes linearly with dimensionless radius. The slope of the storativity linear profile within the transition region is 0.5. Thus, the storativity ratio within the transition region is larger than in the previous cases of Figures 5.19 and 5.20. However, the overall storativity ratio is still 1000 as in previous cases. From Figure 5.25, it can be seen that the contrast between the swept and the transition regions has increased. This first discontinuity contrast is shown when the semilog pressure derivative falls on a straight line in an early period of the transition region. The slope of this straight line is less than one, indicating that this contrast is not too high and that using the pseudosteady state method to estimate a value for the first discontinuity radius will lead to an overestimation of the actual one. Also, from Figure 5.25, there is almost no difference between the three-region model and the ten-region model, indicating that the effective storativity ratio in both models is almost the same. Another observation is that the effects of the storativity contrast at the last discontinuity is not identifiable, which

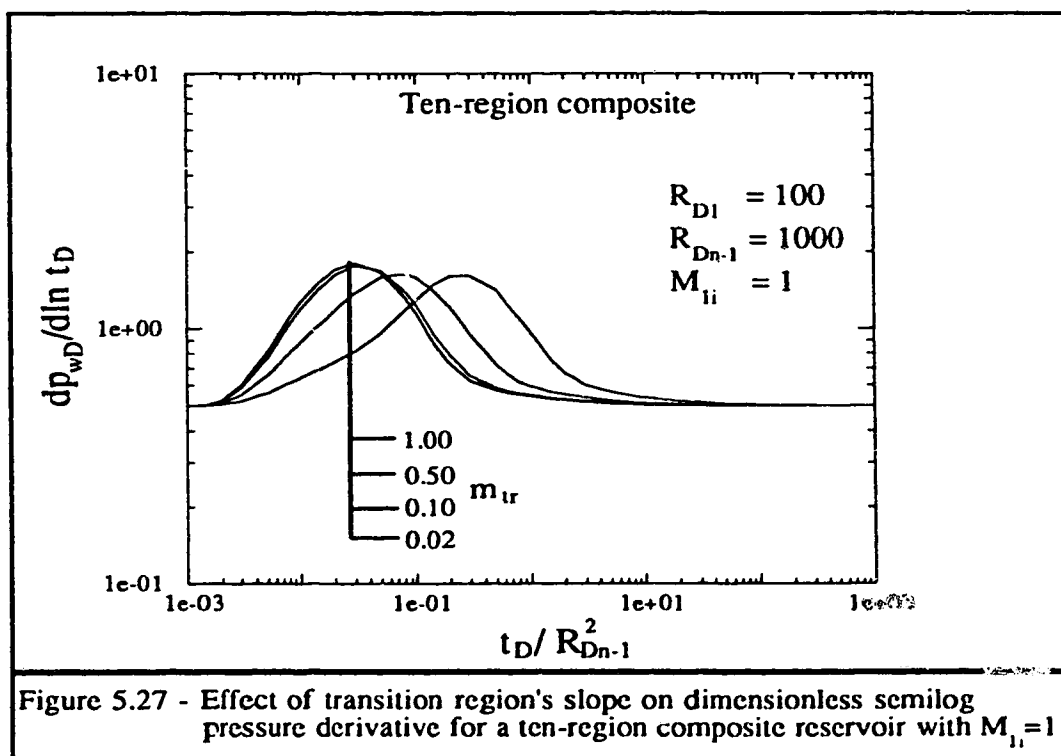
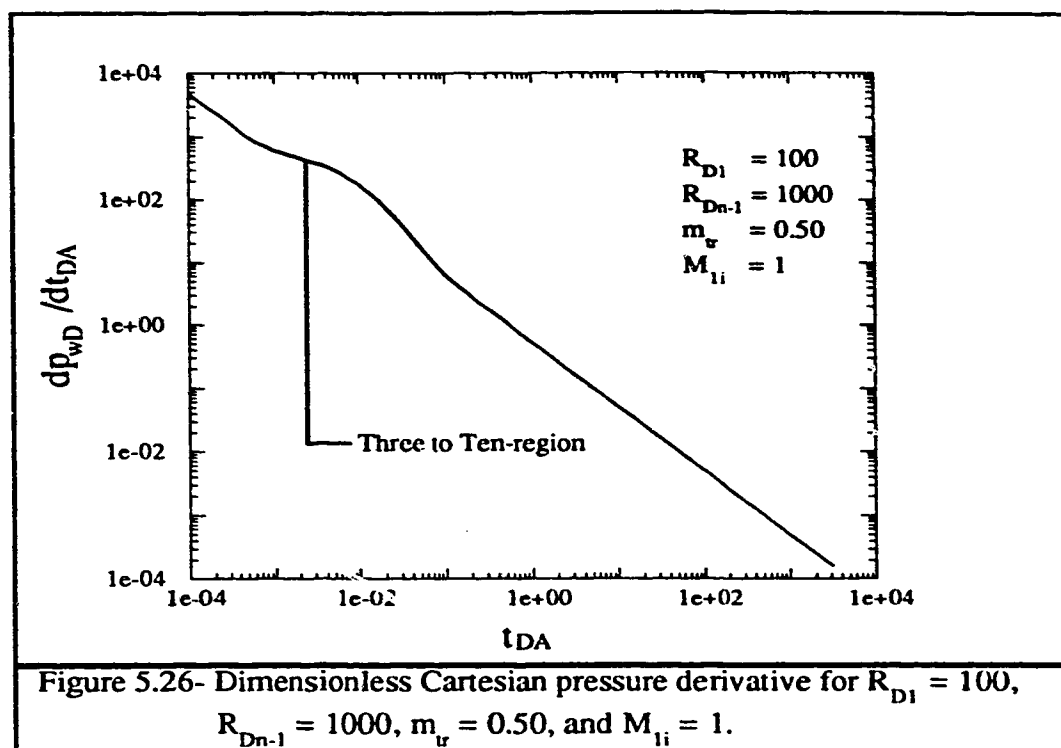


means that the storativity contrast at the last discontinuity is too low to produce any characteristic behaviour.

Figure 5.26 shows the Cartesian pressure derivative for the same storativity profile as for Figure 5.25. There is an early deviation that indicates a low storativity contrast, since the Cartesian pressure derivative does not flatten significantly. By using Equation 5.1, it was found that the first discontinuity radius is 100, as expected from the input value. However, it is impossible to estimate the last discontinuity radius, since the storativity contrast at the last discontinuity is not high enough to produce a characteristic change in the Cartesian pressure derivative behaviour.

Figure 5.27 represents the semilog pressure derivative behaviour of a uniform mobility case, in which the transition region's storativity varies linearly with dimensionless radius. Figure 5.27 shows the effects on the semilog pressure derivative behaviour of several values of the transition region's slope. In general, it can be observed that increasing the transition region's linear profile slope increases the storativity contrast between the swept and the transition region. This happens while the contrast between the transition region and the unswept region decreases. Figure 5.27 shows that increasing the transition region's slope mildly affects the maximum value of the semilog pressure derivative. However, the smaller the transition region's linear profile slope, the larger the transition region's duration. This happens because when the transition region's slope is smaller the contrast at the last discontinuity radius is larger.

Figure 5.28 shows the Cartesian pressure derivative for a reservoir in which the transition region's mobility and storativity change linearly with respect to the dimensionless radius.



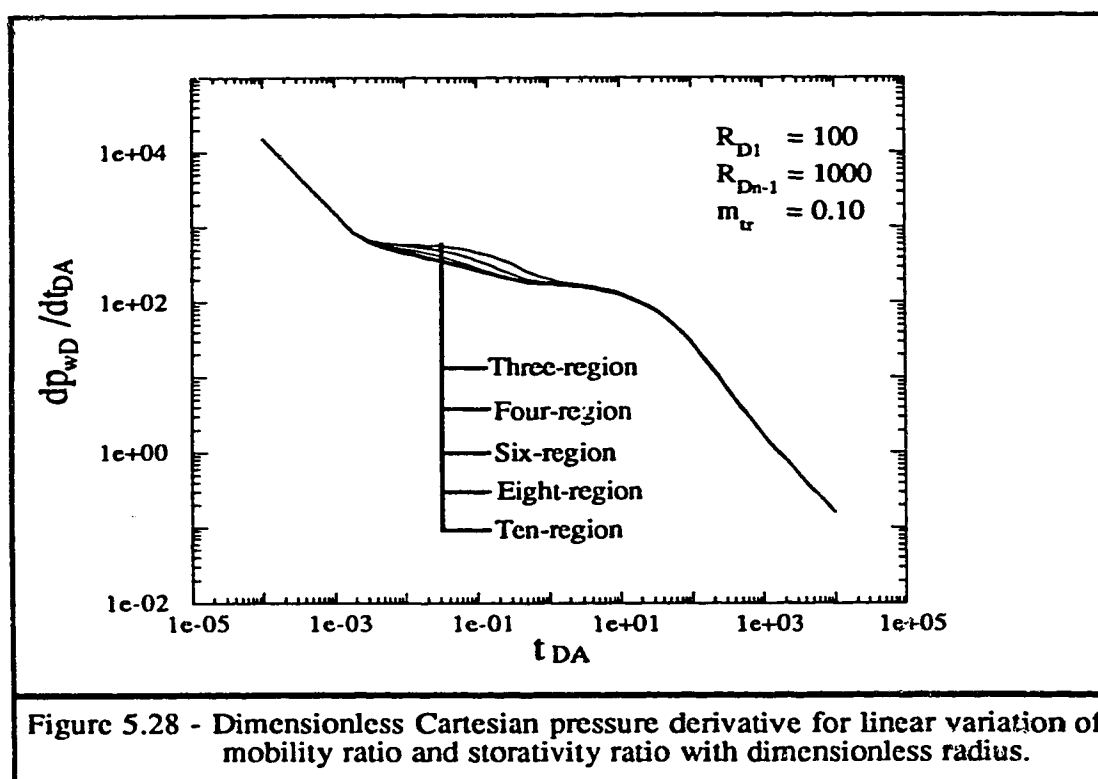
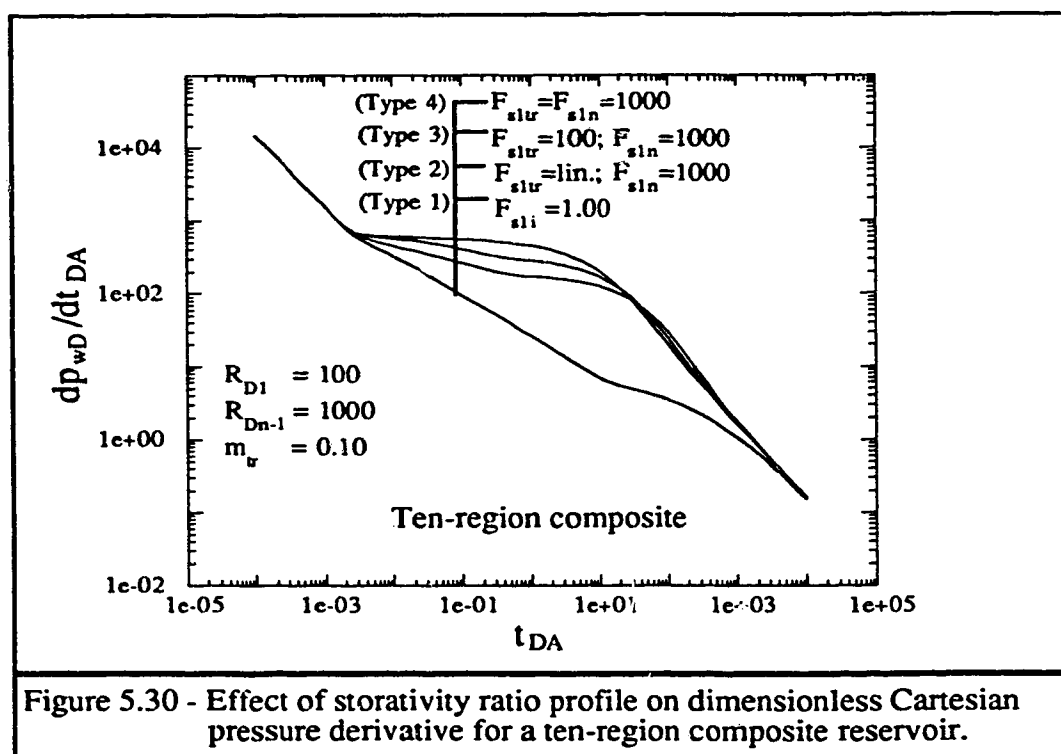
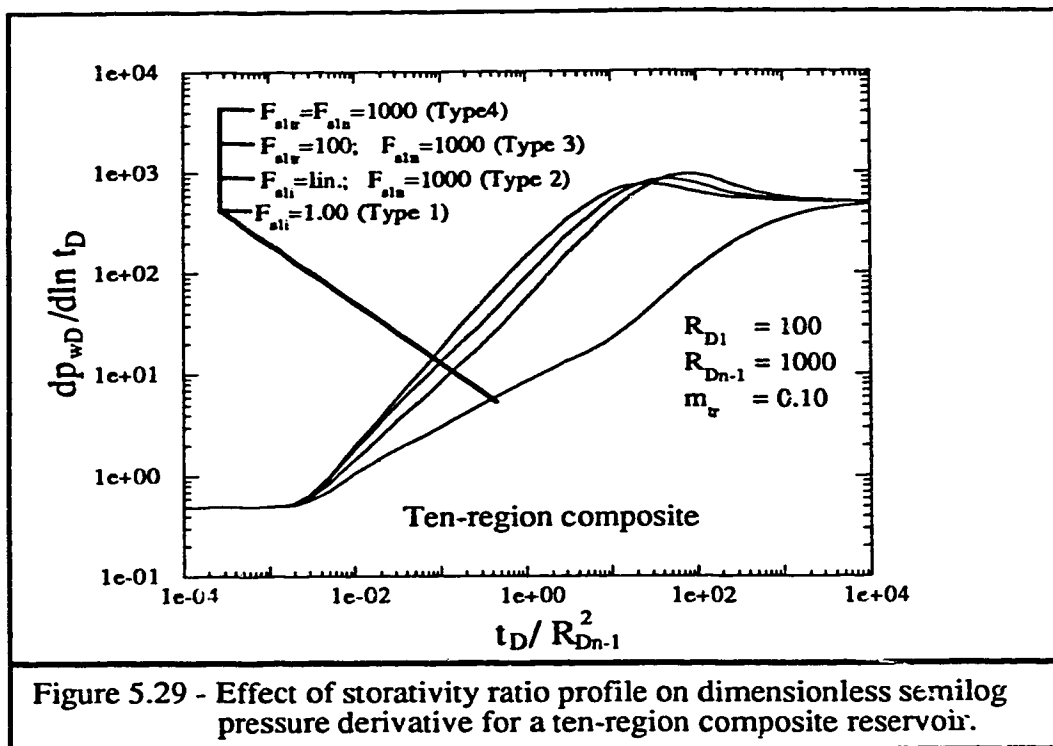


Figure 5.28 - Dimensionless Cartesian pressure derivative for linear variation of mobility ratio and storativity ratio with dimensionless radius.

Figure 5.28 shows, in general, that a slowly changing storativity ratio, as for the ten-region case, reduces the transition region's effects. The Cartesian pressure derivative flattening occurring on Figure 5.28 corresponds to significant mobility and storativity contrasts at appropriate discontinuity radii.

Figures 5.29 and 5.30 show the semilog pressure derivative and the Cartesian pressure derivative for a reservoir in which the transition region's mobility changes linearly with respect to dimensionless radius. The mobility profiles are the same for the four curves on Figures 5.29 and 5.30, while the storativity profiles are different.  $F_{str}$  represents the transition region storativity ratio,  $F_{s1n}$  represents the last region storativity ratio,  $F_{s1i}$  means the storativity ratio at any point in the reservoir and "lin." is an abbreviation meaning that storativity ratio changes linearly with respect to dimensionless radius within the transition region. All the rest of the terms are as defined previously. In Figures 5.29 and 5.30, the profile with a unit storativity ratio will be referred to as Type 1. The profile with a linear variation of storativity will be referred to as Type 2. The profile in which the transition region's storativity ratio is 100 and the unswept region's storativity ratio is 1000 will be referred to as Type 3. Finally, the profile in which the transition region and the unswept region storativity ratios are 1000 will be referred to as Type 4. All the input data used for Figures 5.29 and 5.30 are in Table C11. Figures 5.29 and 5.30 show that intermediate time pressure derivative behaviour can exhibit varied characteristics depending on the magnitude of storativity contrasts at different discontinuity radii.





#### 5.4 Analyzing Characterization Methods

As mentioned previously in Section 2.3.2, *Yeh and Agarwal* (1989) developed a reservoir characterization method in which the reservoir's mobility profile can be obtained from the transient pressure data collected at a well. In their study, they developed relations between the semilog pressure derivative, mobility and radius of investigation. *Yeh and Agarwal's* (1989) equations were in field units. However, this study uses SI units to present their equations. Since all this study has been performed with dimensionless variables, *Yeh and Agarwal's* (1989) equations will also be shown in dimensionless form. Appendix B shows how the dimensionless equations were obtained.

*Yeh and Agarwal* (1989) related "instantaneous mobility",  $\bar{\lambda}_t$ , and the semilog pressure derivative. This relation is:

$$\bar{\lambda}_t = \frac{q\beta}{h \frac{d\Delta p}{d\ln(\Delta t)}} \quad (5.3a)$$

Equation 5.3a, in dimensionless form, is:

$$\bar{M} = 2 \frac{dp_w D}{d\ln t_D} \quad (5.3b)$$

Equation 5.3b defines the relation between "instantaneous mobility ratio",  $\bar{M}$ , and the dimensionless semilog pressure derivative.

From a definition of radius of investigation, *Yeh and Agarwal* (1989) suggested that the radius corresponding to a particular value of "instantaneous mobility",  $\bar{\lambda}_t$ , in Equation 5.3a is:

$$r_i = \left( \frac{\bar{\lambda}_t \Delta t}{\phi c_t} \right)^{0.5} \quad (5.4a)$$

Equation 5.4a, in dimensionless form, is:

$$r_{iD} = 1.5 \left( \frac{t_D}{M} \right)^{0.5} \quad (5.4b)$$

The variable  $r_{iD}$  in Equation 5.4b is a dimensionless radius of investigation.

*Yeh and Agarwal* (1989) explained in their work that the "instantaneous mobility",  $\bar{\lambda}_t$ , represents a volumetric averaged mobility of the actual reservoir mobility profile. However, the theoretical basis for this relation was not explained in their work. *Yeh and Agarwal's* (1989) equation to relate the instantaneous mobility  $\bar{\lambda}_t$  and the real reservoir mobility,  $\lambda_t$ , at the radius  $r_i$  is:

$$\lambda_t = \frac{d(V\bar{\lambda}_t)}{dV} = \frac{r_i}{2} \frac{d\bar{\lambda}_t}{dr_i} + \bar{\lambda}_t \quad (5.5a)$$

Equation 5.5a in dimensionless form is:

$$M = \frac{r_D}{2} \frac{d\left(\frac{1}{M}\right)}{dr_D} + \frac{1}{M} \quad (5.5b)$$

Thus, Equations 5.3a through 5.5a (or Equations 5.3b through 5.5b) are the basis for *Yeh and Agarwal's* (1989) characterization method.

In 1993, *Feitosa et al.*, based on *Oliver's* (1990) work, expanded *Yeh and Agarwal's* (1989) algorithm. *Feitosa et al.* (1993a) explained that *Yeh and Agarwal's* (1989) method may be improved by establishing a different relationship between "instantaneous mobility" and the actual reservoir mobility. They considered that the "instantaneous mobility" represents a harmonic volumetric average of the reservoir's actual mobility profile. Also, as in *Yeh and Agarwal's* (1989) work, no theoretical explanation was given for the relationship between the "instantaneous mobility" and the reservoir's actual mobility. This relationship was developed intuitively based on *Oliver's* (1990) study. *Feitosa et al.'s* (1993a) equation to relate the "instantaneous mobility" and the actual reservoir's mobility at a radius  $r_i$  is:

$$\frac{1}{\lambda_t} = \frac{r_i}{2} \frac{d\left(\frac{1}{\lambda_t}\right)}{dr_i} + \frac{1}{\lambda_t} \quad (5.6a)$$

Equation 5.6a in dimensionless form is:

$$M = \frac{r_D}{2} \frac{d\bar{M}}{dr_D} + \bar{M} \quad (5.6b)$$

The definitions of "instantaneous mobility" and radius of investigation remain the same as in *Yeh and Agarwal*'s (1989) study. Thus, Equations 5.3a, 5.4a and 5.6a (or Equations 5.3b, 5.4b and 5.6b) are the basis for *Feitosa et al.*'s (1993a) characterization method. This method was called the "modified Yeh and Agarwal method" by *Feitosa et al.* (1993a). In this section, a further analysis of both methods is reported.

Figure 5.31 represents the dimensionless form of a permeability profile shown in Figure 1 of *Feitosa et al.* (1993a). Figure 5.31 shows a graph of mobility ratio versus dimensionless radius of investigation for a unit storativity ratio along the reservoir. The continuous line represents the actual mobility ratio profile, while the other symbols represent the mobility ratio profiles from the various characterization methods. The actual profile considered in Figure 5.31 shows a mobility ratio range from 0.5 to 2. This is a relatively small mobility variation. The three methods to obtain the mobility ratio profile seem to perform satisfactorily for this type of mobility ratio variation. The Yeh and Agarwal, and the modified Yeh and Agarwal methods yield better results than the instantaneous mobility profile. Also, the modified Yeh and Agarwal method developed by *Feitosa et al.* (1993a) is the best of the three approaches. For completeness sake, Figure 5.32 shows results for a slightly different profile than in Figure 5.31. However, again, the modified Yeh and Agarwal method yields the best results.

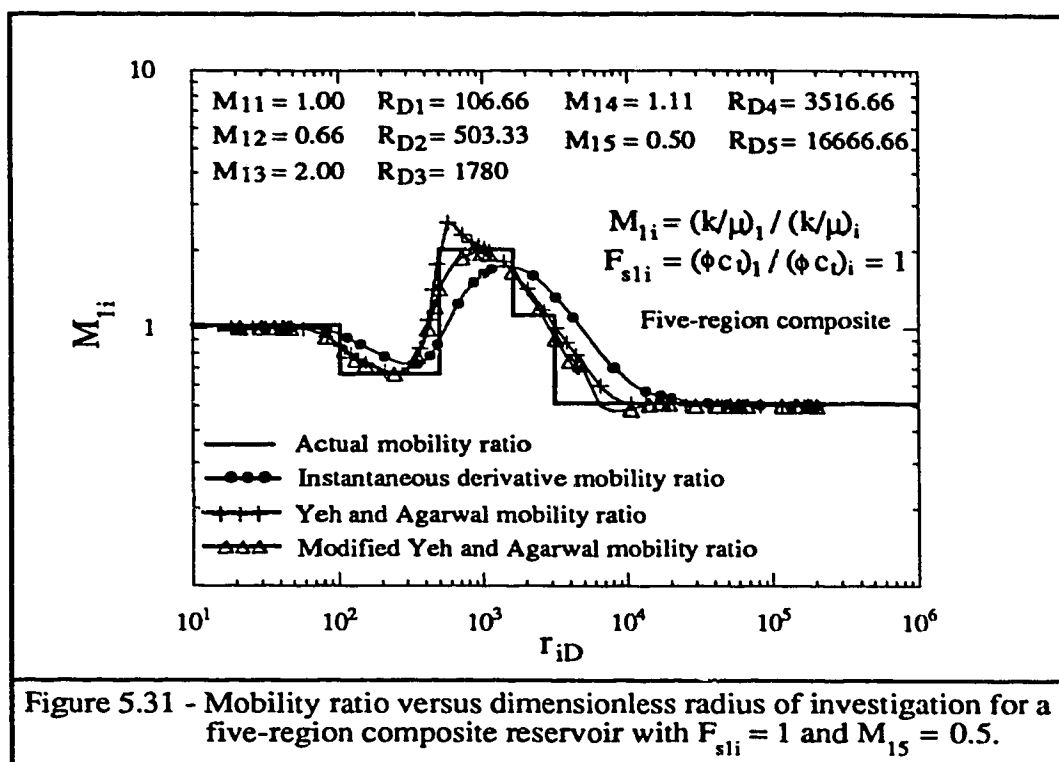


Figure 5.31 - Mobility ratio versus dimensionless radius of investigation for a five-region composite reservoir with  $F_{s1i} = 1$  and  $M_{15} = 0.5$ .

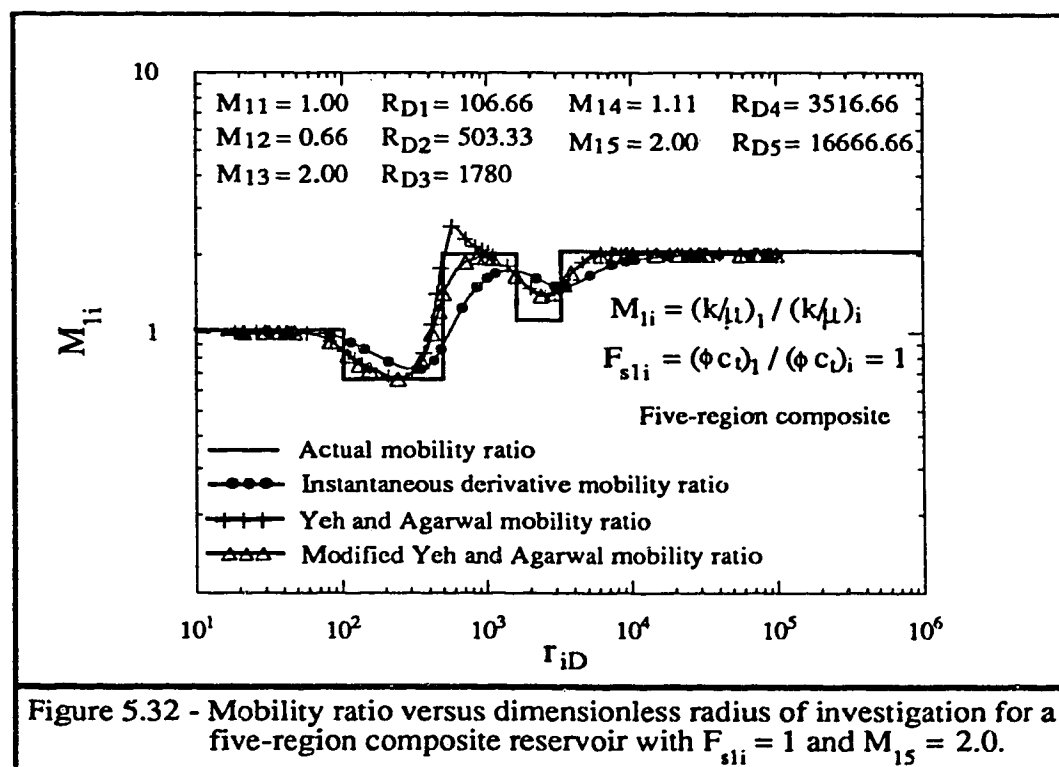
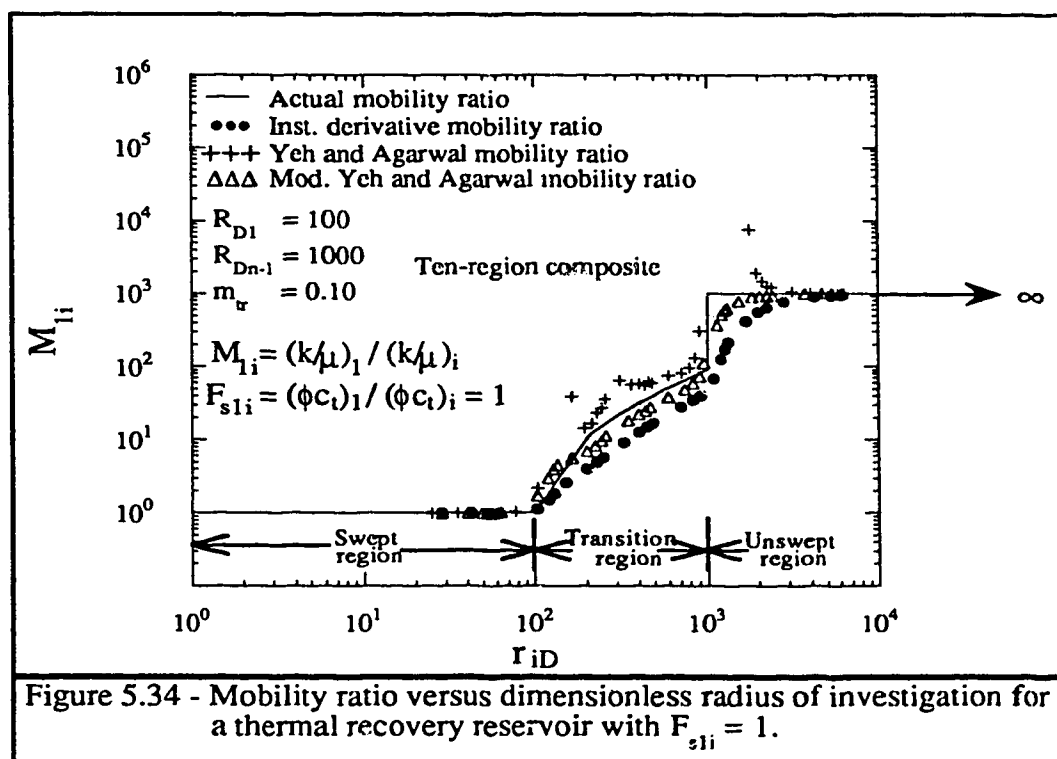
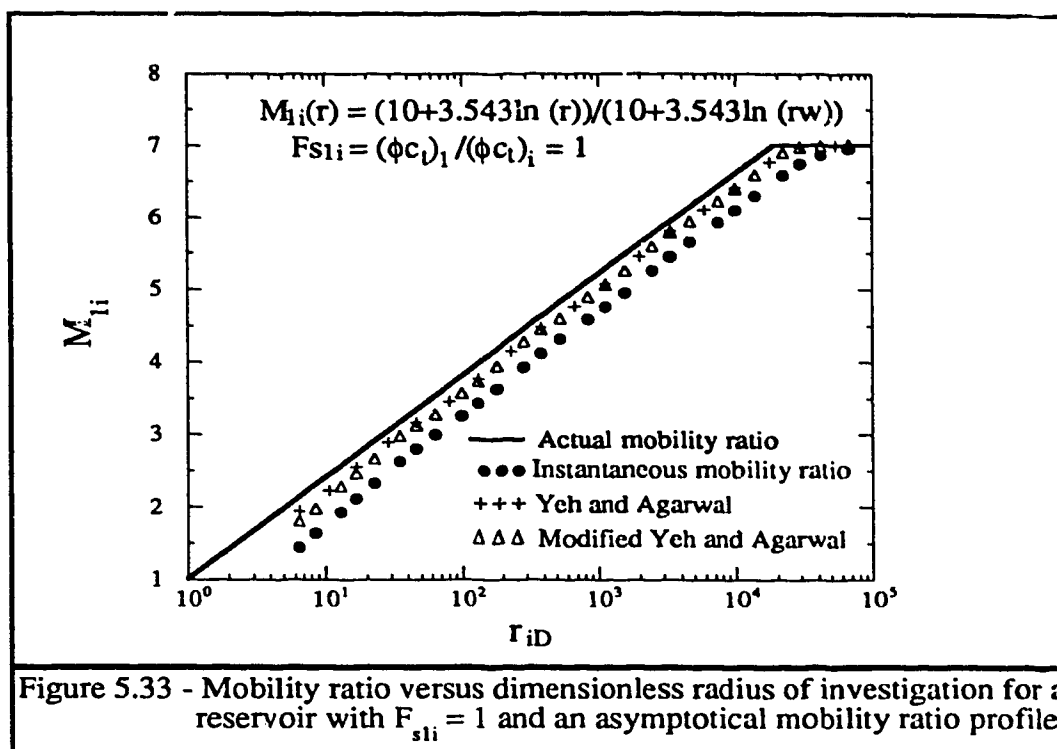


Figure 5.32 - Mobility ratio versus dimensionless radius of investigation for a five-region composite reservoir with  $F_{s1i} = 1$  and  $M_{15} = 2.0$ .

Figure 5.33 represents the dimensionless form of a permeability profile shown in Figure 8 of *Feitosa et al.* (1993a). In Figure 5.33, mobility ratio changes asymptotically with the dimensionless radius of investigation, until it reaches a value of approximately 7. However, storativity remains constant, as in Figures 5.31 and 5.32. Also, as for Figures 5.31 and 5.32, the Yeh and Agarwal method, and the modified Yeh and Agarwal method yield better results than by using the instantaneous mobility concept to represent the reservoir's mobility profile. For this mobility profile, the Yeh and Agarwal method, and the modified Yeh and Agarwal method yield almost the same results. Both methods yield satisfactory results for this particular mobility profile.

Figure 5.34 represents one possible mobility profile from a thermal recovery project, as shown in the previous section. In this figure, the mobility ratio varies considerably as in a thermal recovery processes. However, similar to *Feitosa et al.* (1993a), the storativity ratio along the reservoir,  $F_{s1i}$ , is equal to unity. Also, as in previous cases, the modified Yeh and Agarwal method yields satisfactory results, which are better than the results generated by the instantaneous mobility approach. However, for this case, the Yeh and Agarwal method is not defined for certain sections of the mobility profile, where large contrasts in mobility occur. For these cases of large contrasts in mobility, the first term on the right hand side of Equation 5.5a is negative and larger than the second term on the right hand side of the same equation. Under this condition, Equation 5.5a yields a negative mobility. Thus, the Yeh and Agarwal method is only valid to characterize reservoirs with low mobility contrasts.



Figures 5.31 through 5.34 represent reservoir mobility profiles in which storativity remains constant along the reservoir. However, for actual situations, storativity also varies along the reservoir. Figures 5.35 through 5.38 represent the same mobility profiles as in Figures 5.31 through 5.34, respectively, but with different storativity profiles. All the storativity profiles in these figures are as described in the previous section for thermal well test analysis. There will be a swept region with unit storativity ratio, a transition region with continuously changing storativity ratio and an unswept region with an overall storativity ratio of 1000. As in Section 5.3, the transition region's storativity ratio will change linearly with dimensionless radius. The definition of variables remains the same as in the previous section. In Figures 5.35 and 5.36, the first and last discontinuity radii are 106.66 and 3516.66, respectively. In Figures 5.37 and 5.38, the first and last discontinuity radii are 100 and 1000, respectively. For all Figures 5.35 through 5.38, the slope of the transition region's linear storativity profile is 0.10.

For all Figures 5.35 through 5.38, none of the three approaches to characterize the reservoir's mobility profile worked. This is because, for all the approaches, the reservoir mobility is a function of the semilog pressure derivative. However, the semilog pressure derivative is influenced by both mobility and storativity. Thus, the effect of storativity changes on a reservoir's transient pressure behaviour must be considered, when developing a method for reservoir mobility characterization. The effect of storativity variation on transient pressure behaviour is quite significant for a reservoir undergoing a thermal recovery process, such as in-situ combustion or steam injection.



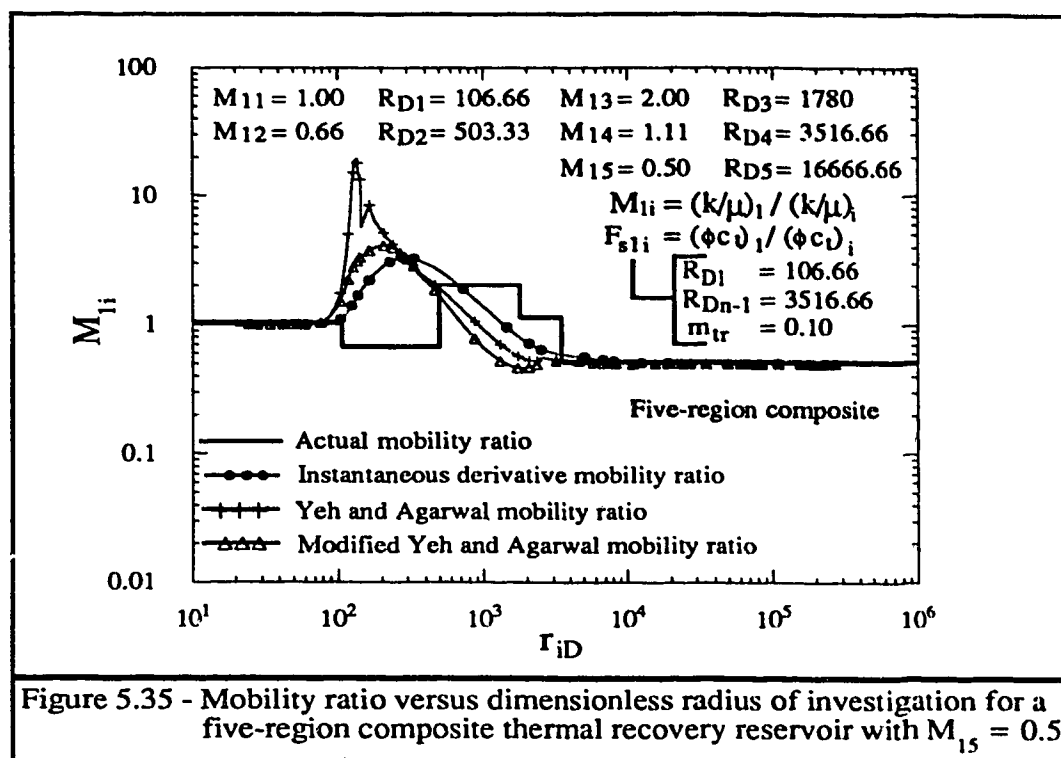


Figure 5.35 - Mobility ratio versus dimensionless radius of investigation for a five-region composite thermal recovery reservoir with  $M_{15} = 0.5$ .

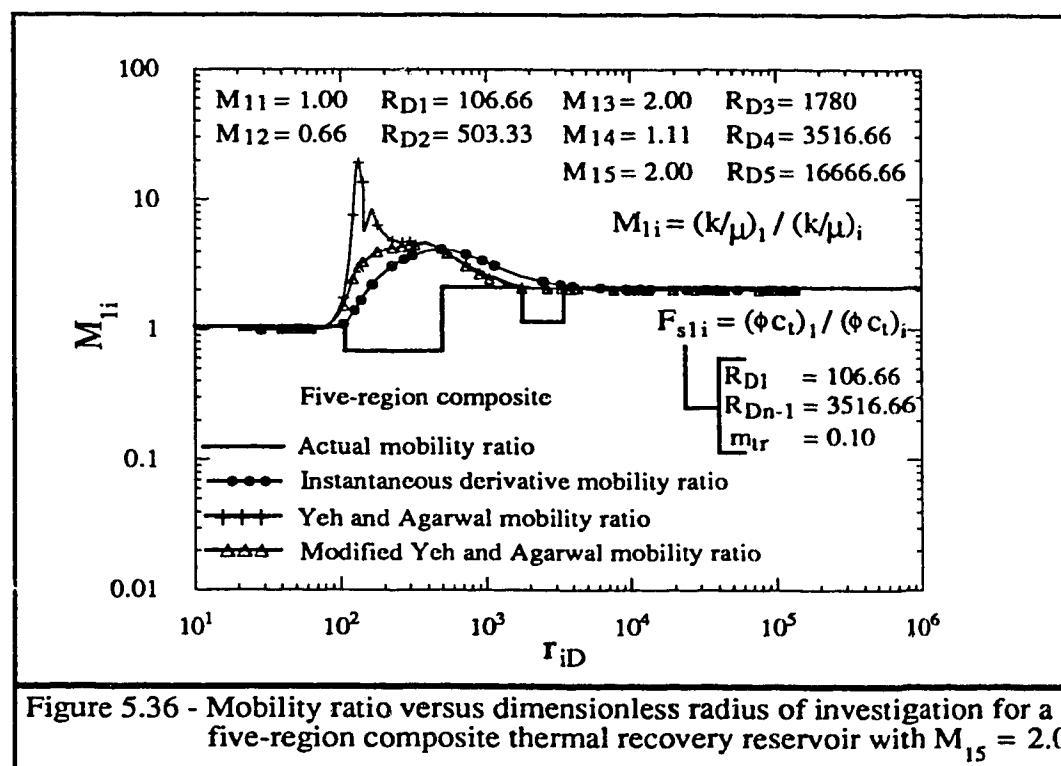


Figure 5.36 - Mobility ratio versus dimensionless radius of investigation for a five-region composite thermal recovery reservoir with  $M_{15} = 2.0$ .

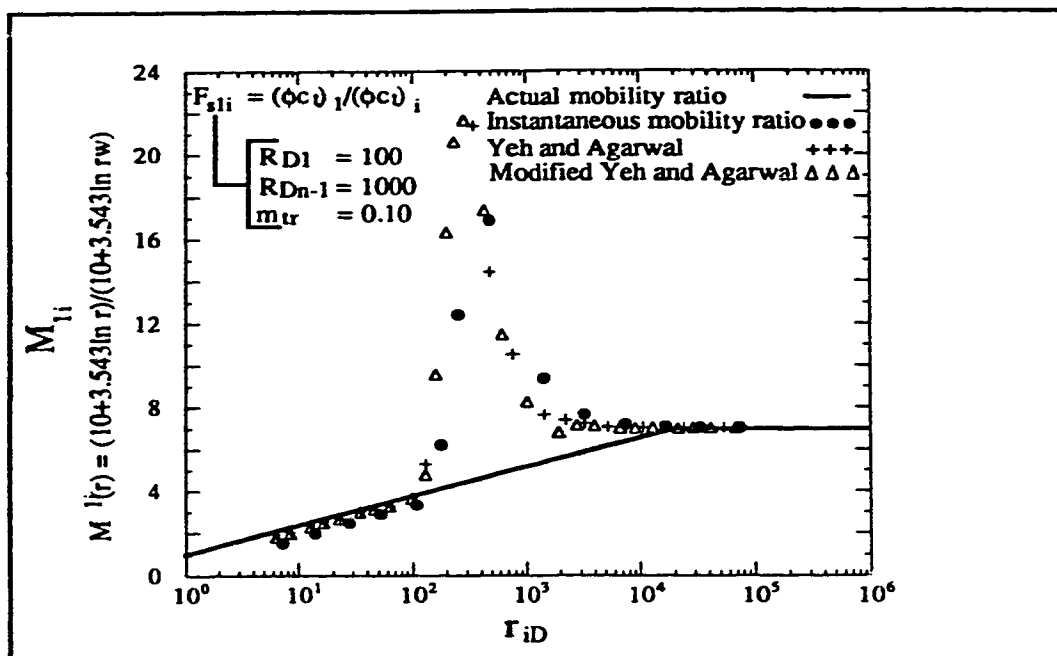


Figure 5.37 - Mobility ratio versus dimensionless radius of investigation for a thermal recovery reservoir with an asymptotical mobility ratio profile.

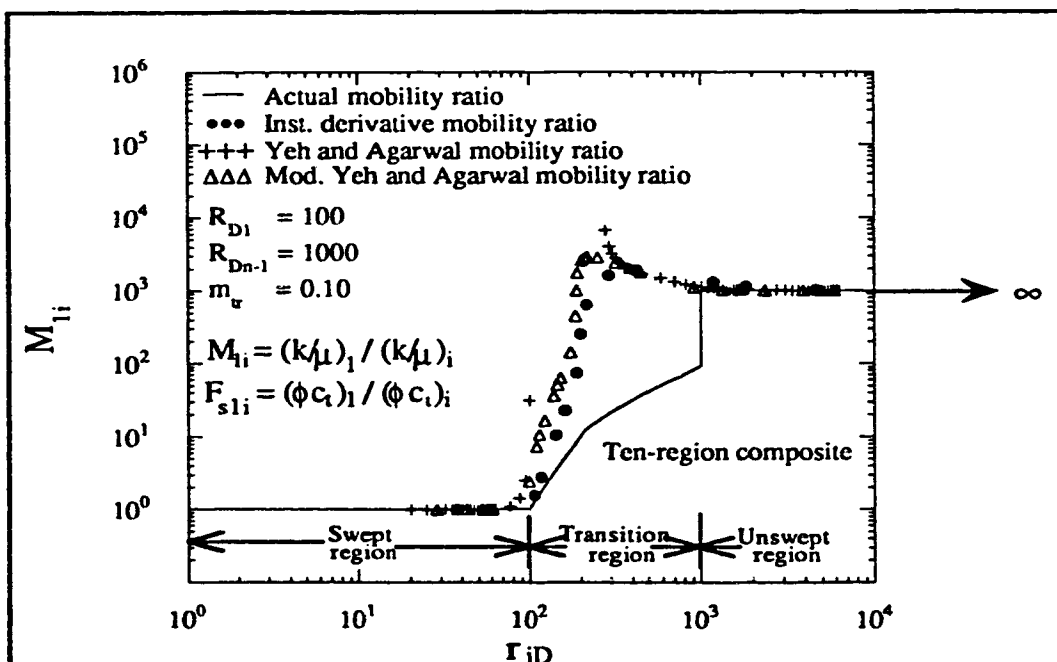


Figure 5.38 - Mobility ratio versus dimensionless radius of investigation for a thermal recovery reservoir with changing storativity ratio.

## **CHAPTER 6**

### **CONCLUSIONS AND RECOMMENDATIONS**

In this study, a multi-region composite reservoir model has been developed. This model has been used to analyze drawdown tests from reservoirs undergoing a thermal recovery process, such as steam injection or in-situ combustion. The effect on pressure derivative behaviour of representing these reservoirs by a different number of regions has been studied. An analysis has been conducted of how discontinuity radii, and mobility and storativity contrasts affect the transient pressure derivative behaviour. A brief evaluation of reservoir characterization methods is also presented. In the following, Section 6.1 presents the conclusions based on this study. Section 6.2 presents recommendations for future studies.

#### **6.1 Conclusions**

By analyzing the drawdown response of multi-region composite reservoirs, the following conclusions may be drawn:

1. Neither the departure time from the early radial flow period nor the duration of the transition region effects are affected by the number of regions of the composite model.

2. The transient pressure derivative behaviour corresponding to the transition zone effects is affected by the number of regions representing the transition zone.
3. Representing the transition zone by one region may generate transient pressure derivative responses which may appear to be due to a higher mobility (or storativity) contrast than what actually exists. Using several regions to represent the transition zone allows a more realistic representation of property variation in the transition region.
4. If the first discontinuity radius is increased while decreasing the discontinuity radii ratio, the deviation time from the early radial flow period becomes larger, while the duration of the transition region effects becomes smaller.
5. Equation 5.1 yields a good estimate for the first discontinuity radius when there is a reasonable contrast in mobility or storativity between the swept and the transition regions. This reasonable property contrast would cause a deviation of the Cartesian pressure derivative from a line of slope equal to -1 on a log-log graph of the Cartesian pressure derivative versus time. Equation 5.1 has, thus, been successfully used to partly verify the accuracy of our solution.
6. For a high contrast in mobility (or storativity), between the swept and the transition regions, the pseudosteady state method may yield a good estimated value for the first discontinuity radius. However, for a low property contrast, the pseudosteady state method may yield an overestimated result.

7. In some cases, during the intermediate time period, the semilog pressure derivative data from a reservoir falls on a straight line whose slope is less than unity. This phenomenon is due to continuously changing mobility or storativity. The transient pressure derivative behaviour from these continuous changes corresponds to the case of small contrasts in mobility or storativity.
8. Using the pseudosteady state method to estimate the last discontinuity radius  $R_{Dn-1}$  will normally yield overestimated results and, in some cases, it may be impossible to use due to insignificant flattening of the Cartesian pressure derivative.
9. Results suggest that a continuously changing storativity profile in the transition region may be approximated by one region with an averaged value of storativity for most cases.
10. A mobility contrast yields a larger and better defined Cartesian pressure derivative flattening than a storativity contrast of the same magnitude. Thus, large mobility contrasts are more likely to yield a pseudosteady state flow period than large storativity contrasts.
11. The smaller the ratio between the last and first discontinuity radii, the higher the value of the maximum semilog pressure derivative. However, the effect of this discontinuity radii ratio on the maximum value of the semilog pressure derivative is mild.

From the study of the two characterization methods, the following conclusions may be drawn:

1. The Modified Yeh and Agarwal method and the Yeh and Agarwal method yield satisfactory results when analyzing reservoirs with low mobility contrasts and constant storativity.
2. For the case of reservoirs with high mobility contrasts and unit storativity ratio, the modified Yeh and Agarwal method yields satisfactory results, while the Yeh and Agarwal method is not defined for certain sections of the mobility profile with large contrasts in mobility. Thus, the Yeh and Agarwal method is only valid to characterize reservoirs with low mobility contrasts.
3. When there is a storativity variation along the reservoir, both methods, the modified Yeh and Agarwal, and the Yeh and Agarwal, fail to characterize the mobility of the reservoir. This is because, for both approaches, the reservoir mobility is considered to be the only variable affecting the semilog pressure derivative. However, the semilog pressure derivative is influenced by both mobility and storativity.

## **6.2 Recommendations**

1. Future studies should consider effective pressure derivative behaviour versus effective dimensionless time in multi-region composite reservoirs.
2. The effect of storativity changes on the transient pressure derivative behaviour should be considered when developing future methods for reservoir characterization.
3. The transient pressure derivative behaviour of the multi-region composite reservoirs with a constant pressure outer boundary and/or closed outer boundary should be studied.

## REFERENCES

- Abbaszadeh-Dehghani, M. and Kamal, M.M.: "Pressure-Transient Testing of Water Injection Wells," *SPE Reservoir Engineering* (Feb. 1989) 115-24.
- Abramowitz, M. and Stegun, I.A. (ed.): "*Handbook of Mathematical Functions with Formulas, Graphs and Mathematical Tables* " National Bureau of Standards Applied Mathematics series-55 (June 1964) 227-253.
- Agarwal, R.G., Al-Hussainy, R., and Ramey, H.J., Jr.: "An Investigation of Wellbore Storage and Skin Effect in Unsteady Liquid Flow: I. Analytical Treatment," *SPE Journal* (Sept. 1970) 279-90.
- Ambastha, A.K.: *Pressure Transient Analysis for Composite Systems*, Ph.D. Thesis, Stanford University (Oct. 1988) 193 pp.
- Ambastha, A.K. and Ramey, H.J., Jr.: "Thermal Recovery Well Test Design and Interpretation," *SPE Formation Evaluation* (June 1989) 173-180.
- Ambastha, A.K. and Ramey, H.J., Jr.: "Effects of a Thin Skin at the Front on Composite Reservoir Well Tests," *J. Cdn. Pet. Tech.* (March-April 1990) 98-104.
- Ambastha, A.K. and Ramey, H.J., Jr.: "Pressure Transient Analysis for a Three-Region Composite Reservoir," paper SPE 24378 presented at the SPE Rocky Mountain Regional Meeting in Casper, Wyoming (May 18-21, 1992).
- Ambastha, A.K.: "Interference Testing in a Two-Region Composite Reservoir with a Frontal Skin," paper CIM 92-41 presented at the CIM Annual Technical Conference in Calgary, Alberta (June 7-10, 1992).



Barua, J. and Horne, R.N.: "*Computer Analysis of Thermal Recovery Well Test Data*," SUPRI-A Tech. Rept. 45, DOE Rept. No. DOE/SF/11564-10 (March 1985).

Barua, J. and Horne, R.N.: "Computerized Analysis of Thermal Recovery Well Test Data," *SPE Formation Evaluation* (December 1987) 560-566.

Bixel, H.C., and van Poolen, H.K.: "Pressure Drawdown and Buildup in the Presence of Radial Discontinuities," *SPE Journal* (Sept. 1967) 301-09.

Brown, L.P.: "Pressure Transient Behavior of the Composite Reservoir," paper SPE 14316 presented at the 60th Annual Meeting. of SPE of AIME, Las Vegas, Nevada (Sept. 22-25, 1985).

Carter, R.D. "Pressure Behavior of a Limited Circular Composite Reservoir," *SPE Journal* (Dec 1966) 328-34.

Carslaw, H.S and Jaegar, J.C.: *Conduction of Heat in Solids*, Second Edition, Oxford at the Clarendon Press, Oxford, England, Ch. 15, 1959.

Craft, B.C. and Hawkins, M.H.: *Applied Petroleum Reservoir Engineering*, Prentice Hall Inc., Englewood Cliffs, New Jersey (1959).

Da Prat, G., Bockh, A., and Prado, L.: "Use of Pressure Falloff Tests to Locate the Burning Front in the Miga Field, Eastern Venezuela," paper SPE 13667 presented at the California Regional Meeting of SPE of AIME, Bakersfield, CA (March 27-29, 1985).

Earlougher, R.C., Jr.: "*Advances in Well Test Analysis*," Monograph Volume 5, SPE of AIME, Dallas, Texas (1977).

Eggenschwiler, M., Ramey, H.J., Jr., Satman, A., and Cinco-Ley, H.: "Interpretation of Injection Well Pressure Transient Data in Thermal Oil Recovery," paper SPE 8908 presented at the 50th Annual California Regional Meeting of SPE of AIME, Los Angeles, California (April 9-11, 1980).

Fair, W.B., Jr.: "Pressure Buildup Analysis with Wellbore Phase Redistribution Effects," *SPE Journal* (April 1981) 259-270.

Fassihi, M.R.: "Evaluation of An Analytic Technique for Estimating Swept Volume from Thermal Pressure Falloff Tests in Heterogeneous Systems," *SPE Formation Evaluation* (June 1988) 449-58.

Feitosa, G.S., Chu, L., Thompson, L.G., and Reynolds, A.C.: "Determination of Permeability Distribution From Well Test Pressure Data," paper SPE 26047 presented at the SPE Western Regional Meeting, Anchorage, Alaska (May 26-28, 1993a).

Feitosa, G.S., Chu, L., Thompson, L.G., and Reynolds, A.C.: "Determination of Permeability Distributions From Pressure Buildup Data," paper SPE 26457 presented at the 68th Annual Meeting of SPE of AIME, Houston, Texas (Oct. 3-6, 1993b).

Hazebroek, P., Rainbow, H., and Mathews, C.S.: "Pressure Falloff in Water Injection Wells," *Trans.*, AIME (1958) 213, 250-60.

Horne, R.N., Satman, A., and Grant, M.A.: "Pressure Transient Analysis of Geothermal Wells with Phase Boundaries," paper SPE 9274 presented at the 55th Annual Meeting of SPE of AIME, Dallas, Texas (Sept. 21-24, 1980).

Hurst, W.: "Interference Between Oil Fields," *Trans.*, AIME (1960) 219, 175-92.

Issaka, M.B.: "*Horizontal Well Testing Under Thermal and Non-Thermal Situations*," M.Sc. Thesis, University of Alberta, Edmonton, Alberta (Nov. 1991) 133 pp.

Issaka, M.B. and Ambastha A.K.: "Thermal Well Testing for a Horizontal Well," paper CIM 92-24 presented at the CIM Annual Tech. Conf., Calgary, Alberta (June 7-10, 1992).

Jaeger, J.C.: "Some Problems Involving Line Sources in Conduction of Heat," *Phil. Mag.* (1944) Vol. 35, 169.

Johnson, P.W.: "The Relationship Between Radius of Drainage and Cumulative Production," *SPE Formation Evaluation* (March 1988) 267-270.

Jones, P.: "Reservoir Limit Test on Gas Wells," *Journal of Petroleum Technology* (June, 1962) 613-619.

Kazemi, H.: "Locating Burning Front by Pressure Transient Measurements," *Journal of Petroleum Technology* (Feb. 1966) 227-232.

Kazemi, H., Merrill, L.S., and Jargon, J.R.: "Problems in Interpretation of Pressure Falloff Tests in Reservoirs with and without Fluid Banks," *Journal of Petroleum Technology* (Sept. 1972) 1147-56.

Larkin, B.K.: "Solution to the Diffusion Equation for a Region Bounded by a Circular Discontinuity," *SPE Journal* (June, 1963) 113-115.

Loucks, T.L., and Guerrero, E.T.: "Pressure Drop in a Composite Reservoir," *SPE Journal* (Sept. 1961) 170.

Merrill, L.S., Kazemi, H., and Gogarty, W.B.: "Pressure Falloff Analysis in Reservoirs with Fluid Banks," *Journal of Petroleum Technology* (July 1974) 809-18.

Messner, G.L. and Williams, R.L.: "Application of Pressure Transient Analysis in Steam Injection Wells," paper SPE 10781 presented at the California Regional Meeting of SPE of AIME, San Francisco, California (March 24-26, 1982).

Nanba, T. and Horne, R.N.: "Estimation of Water and Oil Relative Permeabilities From Pressure Transient Analysis of Water Injection Well Data," paper SPE 19829 presented at the 64th Annual Technical Conference and Exhibition of SPE, San Antonio, Texas (Oct. 8-11, 1989).

Odeh, A.S.: "Flow Test Analysis for a Well With Radial Discontinuity," *JPT* (Feb. 1969) 207-10; *Trans.*, AIME, 246.

- Olarewaju, J.S. and Lee, W.J.: "An Analytical Model for Composite Reservoirs Produced at Either Constant Bottomhole Pressure or Constant Rate," paper SPE 16763 presented at the Annual Meeting of SPE of AIME in Dallas, Texas (Sept. 27-30, 1987b).
- Olarewaju, J.S. and Lee, W.J.: "A Comprehensive Application of a Composite Reservoir Model to Pressure-Transient Analysis," *SPE Reservoir Engineering* (August 1989) 325-331.
- Olarewaju, J.S., Lee, W.J. and Lancaster, D.E.: "Type- and decline Curve Analysis with Composite Models," *SPE Formation Evaluation* (March 1991) 79-85.
- Oliver, D.S.: "The Averaging Process in Permeability Estimation From Well-Test Data ," *SPE Formation Evaluation* (September 1990) 319-324.
- Onyekonwu, M.O., Ramey, H.J., Jr., Brigham, W.E., and Jenkins, R.M.: "Interpretation of Simulated Falloff Tests," paper SPE 12746 presented at the California Regional Meeting of SPE of AIME, Long Beach, California (April 11-13, 1984).
- Onyekonwu, M.O. and Ramey, H.J.: "*Interpretation of In-situ Combustion Thermal Oil Recovery Falloff Test*," SUPRI TR-50, DOE Report No. DOE/SF/11564-14 (March 1986).
- Rosa, A.J. and Horne, R.N.: "Automated Type-Curve Matching in Well Test Analysis Using Laplace Space Determination of Parameter Gradients," paper SPE 12131 presented at the 1983 Annual Technical Conference and Exhibition, San Francisco, Oct. 5-8.
- Satman, A.: "An Analytical Study of Transient Flow in Stratified Systems with Fluid Banks," paper SPE 10264 presented at the Annual Meeting of SPE of AIME in San Antonio, Texas (Oct. 5-7, 1981).
- Satman, A. and Oskay, M.M.: "Effect of a Tilted Front on Well Test Analysis," paper SPE 14701 available from SPE (1985).

- Satman, A., Eggenschwiler, M., Tang, R.W., and Ramey, H.J., Jr.: "An Analytical Study of Transient Flow in Systems with Radial Discontinuities," paper SPE 9399 presented at the 55th Annual Meeting of SPE of AIME, Dallas, Texas (Sept. 21-24, 1980).
- Sosa, A., Raghavan, R., and Limon, T.J.: "Effect of Relative Permeability and Mobility Ratio on Pressure Falloff Behaviour," *Journal of Petroleum Technology* (June 1981) 1125-35.
- Sheng, J.J.: "*Thermal Well Testing for Non-Dipping and Dipping Reservoirs*," M.Sc. Thesis, University of Alberta, Edmonton, Alberta (Nov. 1992) 153 pp.
- Stanislav, J.F., Easwaran, C.V. and Kokal, S.L.: "Interpretation of Thermal Well Falloff Testing," *SPE Formation Evaluation* (June 1989) 181-186.
- Stehfest, H.: "Algorithm 368, Numerical Inversion of Laplace Transforms," D-5, *Communications of ACM* (Jan. 1970) vol. 13, No. 1, 49.
- Tang, R.W.: *Transient Pressure Analysis in Composite Reservoirs*, topical report, U.S. DOE (Aug. 1982) 125pp.
- van Everdingen, A.F., Timmerman, E.H. and McMahon, J.J.: "Application of the Material Balance Equation to a Partial Water-Drive Reservoir," *Trans. AIME* (1953) 198-51.
- van Poolen, H.K.: "Radius of Drainage and Stabilization Time Equations," *Oil and Gas Journal* (Sept. 14, 1964) 138-43.
- van Poolen, H.K.: "Transient Test Finds Fire Front in an In-situ Combustion Project," *Oil and Gas Journal* (Feb. 1, 1965) 78-80.
- Walsh, J.W., Jr., Ramey, H.J., Jr. and Brigham, W.E.: "Thermal Injection Well Falloff Testing," paper SPE 10227 presented at the 56th Annual Meeting of SPE of AIME, San Antonio, Texas (Oct. 5-7, 1981).

Wattenbarger, R.A. and Ramey, H.J., Jr.: "An Investigation of Wellbore Storage and Skin Effects in Unsteady Liquid Flow: II. Finite Difference Treatment," *SPE Journal* (Sept. 1970) 291-97.

Yeh, N.S. and Agarwal, R.G.: "Pressure Transient Analysis of Injection Wells in Reservoirs With Multiple Fluid Banks," paper SPE 19775, presented at the 1989 SPE Annual Technical Conference and Exhibition, San Antonio, Texas (Oct. 8-11, 1989).

Ziegler, V.M.: "Injection Well Testing in a Light Oil Steamflood, Buena Vista Hills Field, California" *SPE Production Engineering* (Nov. 1990) 394-402.

## **APPENDIX A**

**Development of expressions for effective physical properties for  
multi-region composite reservoirs.**

## APPENDIX A

### Development of expressions for effective physical properties for multi-region composite reservoirs.

This appendix contains the equations obtained for the effective mobility and the effective storativity of multi-region composite reservoirs.

#### 1. Effective mobility of a multi-region composite reservoir

One can obtain the effective mobility of a multi-region composite reservoir by starting from the principles of pressure behaviour in a radial reservoir. The difference in pressure between two points in a radial reservoir may be expressed by the steady-state radial flow equation:

$$(P_{i+1} - P_i) = \frac{q\beta\mu_{avg}/n \left( \frac{r_{i+1}}{r_i} \right)}{2\pi h k_{avg}} \quad (A.1)$$

The difference in pressure between the wellbore and the last region "n" of a multi-region composite system is equal to the sum of all the pressure differentials between the regions of the system. Thus,

$$(P_n - P_w) = (P_1 - P_w) + (P_2 - P_1) + \dots + (P_{i+1} - P_i) + \dots + (P_{n-1} - P_{n-2}) + (P_n - P_{n-1}) \quad (A.2)$$

Substituting Equation A.1 in Equation A.2 leads to:

$$\frac{q\beta\mu_{eff}/n \left( \frac{r_n}{r_w} \right)}{2\pi h k_{eff}} = \frac{q\beta\mu_1/n \left( \frac{r_1}{r_w} \right)}{2\pi h k_1} + \frac{q\beta\mu_2/n \left( \frac{r_2}{r_1} \right)}{2\pi h k_2} + \dots + \frac{q\beta\mu_{i+1}/n \left( \frac{r_{i+1}}{r_i} \right)}{2\pi h k_{i+1}} + \dots + \frac{q\beta\mu_{n-1}/n \left( \frac{r_{n-1}}{r_{n-2}} \right)}{2\pi h k_{n-1}} + \frac{q\beta\mu_n/n \left( \frac{r_n}{r_{n-1}} \right)}{2\pi h k_n} \quad (A.3)$$



Note that:

$$R_{Dn} = \frac{r_n}{r_w} \quad (\text{A.4})$$

$$R_{D1} = \frac{r_1}{r_w} \quad (\text{A.5})$$

Substituting Equations A.4 and A.5 in Equation A.3, and simplifying yields:

$$\frac{\mu_{\text{eff}}}{k_{\text{eff}}} \ln(R_{Dn}) = \frac{\mu_1}{k_1} \ln(R_{D1}) + \frac{\mu_2}{k_2} \ln\left(\frac{r_2}{r_1}\right) + \dots + \frac{\mu_{i+1}}{k_{i+1}} \ln\left(\frac{r_{i+1}}{r_i}\right) + \dots + \frac{\mu_{n-1}}{k_{n-1}} \ln\left(\frac{r_{n-1}}{r_{n-2}}\right) + \frac{\mu_n}{k_n} \ln\left(\frac{r_n}{r_{n-1}}\right) \quad (\text{A.6})$$

Re-arranging Equation A.6 yields the effective mobility for a multi-region composite reservoir:

$$\left(\frac{k}{\mu}\right)_{\text{eff}} = \frac{\ln(R_{Dn})}{\left(\frac{\mu}{k}\right)_1 \ln(R_{D1}) + \left(\frac{\mu}{k}\right)_2 \ln\left(\frac{r_2}{r_1}\right) + \dots + \left(\frac{\mu}{k}\right)_{i+1} \ln\left(\frac{r_{i+1}}{r_i}\right) + \dots + \left(\frac{\mu}{k}\right)_{n-1} \ln\left(\frac{r_{n-1}}{r_{n-2}}\right) + \left(\frac{\mu}{k}\right)_n \ln\left(\frac{r_n}{r_{n-1}}\right)} \quad (\text{A.6})$$

Mobility ratio is defined as:

$$M_{li} = \frac{\left(\frac{k}{\mu}\right)_1}{\left(\frac{k}{\mu}\right)_i} \quad (\text{A.7})$$

Thus, the effective mobility ratio for a multi-region composite reservoir is defined as:

$$M_{\text{eff}} = \frac{\left(\frac{k}{\mu}\right)_1}{\left(\frac{k}{\mu}\right)_{\text{eff}}} \quad (\text{A.8})$$

Now multiplying both sides of Equation A.6 by  $\frac{1}{\left(\frac{k}{\mu}\right)_1}$ , and transforming to dimensionless form the radii involved in the ratios of the natural log function, we obtain:

$$\frac{1}{M_{eff}} = \frac{\ln(R_{Dn})}{\ln(R_{D1}) + M_{12} \ln\left(\frac{R_{D2}}{R_{D1}}\right) + \dots + M_{1i+1} \ln\left(\frac{R_{Di+1}}{R_{D1}}\right) + \dots + M_{1n-1} \ln\left(\frac{R_{Dn-1}}{R_{Dn-2}}\right) + M_{1n} \ln\left(\frac{R_{Dn}}{R_{Dn-1}}\right)} \quad (A.9)$$

The inverse of both sides of Equation A.9 yields the effective mobility ratio for a multi-region composite reservoir.

## 2. Effective storativity of a multi-region composite reservoir

The effective storativity of a multi-region composite reservoir is defined as a volume-averaged storativity. Thus,

$$(\phi c_i)_{eff} = \frac{(\phi c_i)_1 h \pi R_1^2 + (\phi c_i)_2 h \pi (R_2^2 - R_1^2) + \dots + (\phi c_i)_{i+1} h \pi (R_{i+1}^2 - R_i^2) + \dots + (\phi c_i)_n h \pi (R_n^2 - R_{n-1}^2)}{h \pi R_n^2} \quad (A.10)$$

Simplifying Equation A.10, we have:

$$(\phi c_i)_{eff} = \frac{(\phi c_i)_1 R_1^2 + (\phi c_i)_2 (R_2^2 - R_1^2) + \dots + (\phi c_i)_{i+1} (R_{i+1}^2 - R_i^2) + \dots + (\phi c_i)_n (R_n^2 - R_{n-1}^2)}{R_n^2} \quad (A.10)$$

Equation A.10 defines the effective storativity for a multi-region composite system. The storativity ratio is defined as:

$$F_{s1i} = \frac{(\phi c_i)_1}{(\phi c_i)_i} \quad (A.11)$$

Obviously, the effective storativity ratio is defined as:

$$F_{s_{\text{eff}}} = \frac{(\phi c_l)_1}{(\phi c_l)_{\text{eff}}} \quad (\text{A.12})$$

Dividing both sides of Equation A.10 by  $(\phi c_l)_1 R_1^2$  and using Equation A.11 yields:

$$\frac{(\phi c_l)_{\text{eff}} R_n^2}{(\phi c_l)_1 R_1^2} = 1 + \frac{1}{F_{s_{12}}} \left( \frac{R_2^2}{R_1^2} - 1 \right) + \dots + \frac{1}{F_{s_{i+1}}} \left( \frac{R_{i+1}^2 - R_i^2}{R_1^2} \right) + \dots + \frac{1}{F_{s_{n-1}}} \left( \frac{R_{n-1}^2 - R_{n-2}^2}{R_1^2} \right) + \frac{1}{F_{s_n}} \left( \frac{R_n^2 - R_{n-1}^2}{R_1^2} \right) \quad (\text{A.13})$$

Using dimensionless radii in Equation A.13 and substituting Equation A.12 into the resulting equation yields:

$$\frac{1}{F_{s_{\text{eff}}}} \frac{R_n^2}{R_1^2} = 1 + \frac{1}{F_{s_{12}}} \left( \frac{R_{D2}^2}{R_{D1}^2} - 1 \right) + \dots + \frac{1}{F_{s_{i+1}}} \left( \frac{R_{Di+1}^2 - R_{Di}^2}{R_{D1}^2} \right) + \dots + \frac{1}{F_{s_{n-1}}} \left( \frac{R_{Dn-1}^2 - R_{Dn-2}^2}{R_{D1}^2} \right) + \frac{1}{F_{s_n}} \left( \frac{R_{Dn}^2 - R_{Dn-1}^2}{R_{D1}^2} \right) \quad (\text{A.14})$$

An obvious re-arrangement of Equation A.14 yields the effective storativity ratio for a multi-region composite reservoir.

**APPENDIX B**

Development of the dimensionless form of *Yeh and Agarwal's* (1989) equations.

## APPENDIX B

### Dimensionless form of instantaneous mobility and radius of Investigation

The purpose of this appendix is to show how expressions for instantaneous mobility ratio and dimensionless radius of investigation were obtained by transforming *Yeh and Agarwal's* (1989) equations.

#### 1. Instantaneous mobility ratio

*Yeh and Agarwal* (1989) defined instantaneous mobility as:

$$\lambda_t = \frac{70.62 \, q\beta}{h \, \Delta p'} \quad (\text{B.1})$$

where,

$$\Delta p' = \frac{d \, \Delta p}{d \, \ln t} \quad (\text{B.2})$$

Start from the following definition (field units) of dimensionless wellbore pressure for multi-region composite reservoirs:

$$p_{wD} = \frac{k_1 h \, \Delta p}{141.2 \, q\beta\mu_1} \quad (\text{B.3})$$

A re-arrangement of Equation B.3 yields:

$$\Delta p = \frac{141.2 q \beta \mu_1 p_{wD}}{k_1 h} \quad (B.4)$$

Differentiating both sides of Equation B.4 with respect to time, we have:

$$\frac{d\Delta p}{dt} = \frac{141.2 q \beta \mu_1}{k_1 h} \frac{dp_{wD}}{dt} \quad (B.5)$$

The left side of Equation B.5 is expressed in terms of the semilog pressure derivative as:

$$\frac{d\Delta p}{dt} = \frac{1}{t} \frac{d\Delta p}{d \ln t} \quad (B.6)$$

Equation B.5 in view of B.6 is:

$$\frac{d\Delta p}{d \ln t} = \frac{141.2 q \beta \mu_1 t}{k_1 h} \frac{dp_{wD}}{dt} \quad (B.7)$$

The definition of dimensionless time in a multi-region composite reservoir is:

$$t_D = \frac{0.006328 k_1 t}{(\phi c_i \mu)_1 r_w^2} \quad (B.8)$$

Re-arranging Equation B.8 yields:

$$t = \frac{(\phi c_i \mu)_1 r_w^2 t_D}{0.006328 k_1} \quad (B.9)$$

Differentiating both sides of Equation B.9 with respect to time and re-arranging results in:

$$dt = \frac{(\phi c_i \mu)_1 r_w^2}{0.006328 k_1} dt_D \quad (B.10)$$

Equation B.7 in view of Equations B.9 and B.10 is:

$$\frac{d\Delta p}{d \ln t} = \frac{141.2 q \beta \mu_1 \frac{(\phi c_i \mu)_1 r_w^2 t_D}{0.006328 k_1}}{k_1 h} \frac{dp_{wD}}{\frac{(\phi c_i \mu)_1 r_w^2}{0.006328 k_1} dt_D} \quad (B.11)$$

Simplifying and re-arranging Equation B.11 results in:

$$\frac{d\Delta p}{d \ln t} = \frac{141.2 q \beta \mu_1}{k_1 h} \frac{t_D dp_{wD}}{dt_D} \quad (B.12)$$

Note that :

$$t_D \frac{dp_{wD}}{dt_D} = \frac{dp_{wD}}{d \ln t_D} \quad (B.13)$$

Equation B.12 in view of Equation B.13 is:

$$\frac{d\Delta p}{d \ln t} = \frac{141.2 \, q\beta\mu_1}{k_1 h} \frac{dp_{wD}}{d \ln t_D} \quad (B.14)$$

Equation B.1 in view of Equations B.2 and B.14 is:

$$\lambda_t = \frac{70.62 \, q\beta}{h \frac{141.2 \, q\beta\mu_1}{k_1 h} \frac{dp_{wD}}{d \ln t_D}} \quad (B.15)$$

Simplifying and re-arranging Equation B.15 yields:

$$\lambda_t = 0.5 \frac{\left(\frac{k}{\mu}\right)_1}{\frac{dp_{wD}}{d \ln t_D}} \quad (B.16)$$

Let's represent instantaneous mobility  $\lambda_t$  by:

$$\lambda_t = \overline{\left(\frac{k}{\mu}\right)} \quad (B.17)$$



Re-arranging Equation B.16 in view of Equation B17 results in:

$$\bar{M} = \frac{\left(\frac{k}{\mu}\right)_1}{\left(\frac{k}{\mu}\right)} = 2 \frac{dp_w D}{d \ln t_D} \quad (\text{B.18})$$

The term  $\bar{M}$  in Equation B.18 is referred to as instantaneous mobility ratio.

## 2. Dimensionless radius of investigation

*Yeh and Agarwal* (1989) defined radius of investigation as:

$$r_i = 0.02436 \left[ \left(\frac{k}{\mu}\right)_{\frac{t}{\phi c_t}} \right]^{0.5} \quad (\text{B.19})$$

In Equation B.19 time "t" is in hours. If time is measured in days, the numerical constant 0.02436 should be changed to 0.1193. Thus:

$$r_i = 0.1193 \left[ \left(\frac{k}{\mu}\right)_{\frac{t}{\phi c_t}} \right]^{0.5} \quad (\text{B.20})$$

Equation B.20 in view of Equation B.9 is:

$$r_i = 0.1193 \left[ \overline{\left( \frac{k}{\mu} \right)} \frac{(\phi c_t \mu)_1 r_w^2 t_D}{0.006328 k_1 \phi c_t} \right]^{0.5} \quad (\text{B.21})$$

Simplifying and re-arranging Equation B.21 assuming  $\phi c_t = (\phi c_t)_1$ , we have:

$$r_i = 1.5 r_w \sqrt{\frac{\overline{\left( \frac{k}{\mu} \right)}}{\left( \frac{k}{\mu} \right)_1} t_D} \quad (\text{B.22})$$

Using Equation B.22, dimensionless radius of investigation  $r_{iD}$  is:

$$r_{iD} = \frac{r_i}{r_w} = 1.5 \sqrt{\frac{t_D}{M}} \quad (\text{B.23})$$

If the "conventional" (see *van Poollen* (1965)) definition of radius of investigation would have been used, the constant in Equation B.19 would have been 0.1590, instead of 0.1193, for time in days, and the constant 1.5 in Equation B.23 would have been changed to 2. Thus, the "conventional" definition of dimensionless radius of investigation is:

$$r_{iD} = 2 \sqrt{\frac{t_D}{M}} \quad (\text{B.24})$$

## **APPENDIX C**

Data used to analyze the transient pressure response for a multi-region composite reservoir.

## APPENDIX C

**Multi-region composite reservoir in which the transition region properties are a linear function of dimensionless radius.**

This appendix lists some of the data sets used to analyze the transient pressure behaviour of multi-region composite reservoirs. In these systems, the mobility and/or storativity within the transition zone changes linearly with respect to dimensionless radius.

**Table C1: Discontinuity radii data for a multi-region composite reservoir visualized as a three-region composite reservoir**

Discontinuity radii ( $R_{Di}$ ) for			
$R_{D1} = 100$	$R_{D1} = 500$	$R_{D1} = 1000$	$R_{D1} = 2000$
1 (well)	1 (well)	1 (well)	1 (well)
100	500	1000	2000
1000	1400	1900	2900

**Table C2: Physical properties data for a multi-region composite reservoir visualized as a three-region composite reservoir**

Mobility ratio ( $M_{1i}$ ) and/or Storativity ratio ( $F_{s1i}$ ) for			
$m_{tr} = 0.02$	$m_{tr} = 0.10$	$m_{tr} = 0.50$	$m_{tr} = 1.00$
1	1	1	1
10.5	46	226	451
1000	1000	1000	1000

**Table C3: Discontinuity radii data for a multi-region composite reservoir visualized as a four-region composite reservoir**

Discontinuity radii ( $R_{Di}$ ) for			
$R_{D1} = 100$	$R_{D1} = 500$	$R_{D1} = 1000$	$R_{D1} = 2000$
1 (well)	1 (well)	1 (well)	1 (well)
100	500	1000	2000
550	950	1450	2450
1000	1400	1900	2900

**Table C4: Physical properties data for a multi-region composite reservoir visualized as a four-region composite reservoir**

Mobility ratio ( $M_{1i}$ ) and/or Storativity ratio ( $F_{s1i}$ ) for			
$m_{tr} = 0.02$	$m_{tr} = 0.10$	$m_{tr} = 0.50$	$m_{tr} = 1.00$
1	1	1	1
5.75	23.50	113.50	226
15.25	68.50	338.50	676
1000	1000	1000	1000

**Table C5: Discontinuity radii data for a multi-region composite reservoir visualized as a six-region composite reservoir**

Discontinuity radii ( $R_{Di}$ ) for			
$R_{D1} = 100$	$R_{D1} = 500$	$R_{D1} = 1000$	$R_{D1} = 2000$
1 (well)	1 (well)	1 (well)	1 (well)
100	500	1000	2000
325	725	1225	2225
550	950	1450	2450
775	1175	1675	2675
1000	1400	1900	2900

**Table C6: Physical properties data for a multi-region composite reservoir visualized as a six-region composite reservoir**

Mobility ratio ( $M_{1i}$ ) and/or Storativity ratio ( $F_{s1i}$ ) for			
$m_{tr} = 0.02$	$m_{tr} = 0.10$	$m_{tr} = 0.50$	$m_{tr} = 1.00$
1	1	1	1
3.38	12.25	57.25	113.50
8.13	34.75	169.75	338.50
12.88	57.25	282.25	563.50
17.63	79.75	394.75	788.50
1000	1000	1000	1000

**Table C7: Discontinuity radii data for a multi-region composite reservoir visualized as a eight-region composite reservoir**

Discontinuity radii ( $R_{Di}$ ) for			
$R_{D1} = 100$	$R_{D1} = 500$	$R_{D1} = 1000$	$R_{D1} = 2000$
1 (well)	1 (well)	1 (well)	1 (well)
100	500	1000	2000
250	650	1150	2150
400	800	1300	2300
550	950	1450	2450
700	1100	1600	2600
850	1250	1750	2750
1000	1400	1900	2900

**Table C8: Physical properties data for a multi-region composite reservoir visualized as a eight-region composite reservoir**

Mobility ratio ( $M_{1i}$ ) and/or Storativity ratio ( $F_{s1i}$ ) for			
$m_{tr} = 0.02$	$m_{tr} = 0.10$	$m_{tr} = 0.50$	$m_{tr} = 1.00$
1	1	1	1
2.58	8.50	38.50	76
5.75	23.50	113.50	226
8.92	38.50	188.50	376
12.08	53.50	263.50	526
15.25	68.50	338.50	676
18.42	83.50	413.50	826
1000	1000	1000	1000

**Table C9: Discontinuity radii data for a multi-region composite reservoir visualized as a ten-region composite reservoir**

Discontinuity radii ( $R_{D1}$ ) for			
$R_{D1} = 100$	$R_{D1} = 500$	$R_{D1} = 1000$	$R_{D1} = 2000$
1 (well)	1 (well)	1 (well)	1 (well)
100	500	1000	2000
212.5	612.5	1112.5	2212.5
325	725	1225	2225
437.5	837.5	1337.5	2337.5
550	950	1450	2450
662.5	1062.5	1562.5	2562.5
775	1175	1675	2675
887.5	1287.5	1787.5	2787.5
1000	1400	1900	2900

**Table C10: Physical properties data for a multi-region composite reservoir visualized as a ten-region composite reservoir**

Mobility ratio ( $M_{1i}$ ) and/or Storativity ratio ( $F_{s1i}$ ) for			
$m_{tr} = 0.02$	$m_{tr} = 0.10$	$m_{tr} = 0.50$	$m_{tr} = 1.00$
1	1	1	1
2.19	6.63	29.13	57.25
4.56	17.88	85.38	169.75
6.94	29.13	141.63	282.25
9.31	40.38	197.88	394.75
11.68	51.63	254.13	507.25
14.06	62.88	310.38	619.75
16.44	74.13	366.63	732.25
18.81	85.38	422.88	844.75
1000	1000	1000	1000



**Table C1i: Physical properties data for a multi-region composite reservoir for a particular ten-region case (Figures 5.29 and 5.30).**

<b>R<sub>D</sub>i</b>	<b>M<sub>1i</sub></b>	<b>F<sub>s1i</sub> Type 1</b>	<b>F<sub>s1i</sub> Type 2</b>	<b>F<sub>s1i</sub> Type 3</b>	<b>F<sub>s1i</sub> Type 4</b>
1	1	1	1	1	1
100	6.63	1	6.63	100	1000
212.5	17.88	1	17.88	1000	1000
325	29.13	1	29.13	1000	1000
437.5	40.38	1	40.38	1000	1000
550	51.63	1	51.63	1000	1000
662.5	62.88	1	62.88	1000	1000
775	74.13	1	74.13	1000	1000
887.5	85.38	1	85.38	1000	1000
1000	1000	1	1000	1000	1000

## **APPENDIX D**

**Program to obtain the transient pressure response for a multi-region composite reservoir.  
A reservoir characterization subroutine is also included.**

**Name:** Luis Guillermo Acosta  
**Date:** January 4, 1994.

**Wellbore storage and skin at the well are allowed. Skin at the front of each interphase between regions is accounted. Well produces at a constant rate.**

**The outer boundary may be infinite, closed or at a constant pressure.**

## VARIABLE IDENTIFICATION LIST

% A	= Matrix of coefficients
% B	= Known vector from the boundary conditions
% C	= Constants used in the solution of the system
% c	= Constant postmultiplying the results obtained from the system of eqs.
% CD	= Wellbore storage dimensionless coefficient
% dPwD	= Semilog pressure derivative (with respect to $(tD/rDn^2)$ )
% dPwDca	= Cartesian pressure derivative (with respect to $tDAn$ )
% Fs	= Storativity ratio, defined as: $Fs = (\phi \cdot ct) / (\phi \cdot ct)_i$
% Io	= Modified Bessel function of the first kind, zero order
% I1	= Modified Bessel function of the first kind, first order
% Ko	= Modified Bessel function of the second kind, zero order
% K1	= Modified Bessel function of the second kind, first order
% M	= Mobility ratio, defined as: $M = (k/u)_i / (k/u)_{i+1}$
% Mi	= Mobility ratio, defined as: $M_i = (k/u) / (k/u)_i$
% Mins	= Instantaneous mobility ratio
% MM	= Parameter of the Stehfest algorithm
% Mmya	= Modified Yeh and Agarwal mobility ratio
% Mya	= Yeh and Agarwal mobility ratio
% N	= Iteration parameter of the Stehfest algorithm
% Nc	= Number of time log cycles desired
% Nr	= Number of regions of the reservoir
% n	= Difussivity ratio, defined as: $n = M_i / Fs$
% OBCode	= Outer boundary code
% PwD	= Dimensionless wellbore pressure
% rD	= Dimensionless radius

```

% rDins      = Dimensionless radius of investigation
% reD        = Dimensionless reservoir outer radius
% S          = Skin at the wellbore
% Sf         = Skin at the discontinuities
% TD1        = First value of dimensionless time
% tDAn       = Dimensionless time vector based on the area to the last discontinuity
% tD         = Dimensionless time vector
% Zm         = Argument of the Bessel functions
% z          = Laplace space parameter
% zbb        = Argument of the exponential numbers that premultiply the coefficients

```

```

%%%%%%%%%%%%%%%%%%%%%%%%%%%%%%%%%%%%%%%%%%%%%%%%%%%%%%%%%%%%%%%%%%%%%%%%

```

```

% The Main program calls the subroutine with all the data, DATA.m.

```

```

    DATA

```

```

% The Main program calls the Stehfest algorithm subroutine, STEHFEST.m.
% The Stehfest algorithm inverts the solution from Laplace space to real space.

```

```

    STEHFEST

```

```

% The Main program will call, if desired, a reservoir characterization
% subroutine called CHARAC.m.

```

```

disp(' Do you want to use a characterization subroutine?')
disp('')
disp('          1 YES')
disp('          0 NO')
disp('')

```

```

Characode = input (' Select the number and press enter for the option selected:')

```

```

if Characode == 1

```

```

% If the characterization method is desired, it will inquire what type of
% definition of radius of investigation is desired.

```

```

disp(' Do you want to use the conventional (see van Poollen (1965)) definition of radius ')
disp(' of investigation or you prefer to use Yeh and Agarwal (1989) definition?')
disp('')
disp(' The radius of investigation codes are:')
disp('')
disp('          0 to use the conventional definition')
disp('          1 to use Yeh and Agarwal(1989) definition')
disp('')
rinvcde = input ('Select the number and press enter for the option selected:')

```

```

end

```

```
disp ( '          !!! THE PROGRAM IS NOW RUNNING - WAIT FOR RESULTS !!!  ' )
```

```
% The program obtains the pressure behaviour for each dimensionless time value.
```

```
for I=1:tDlast
```

```
% The Main program calls a subroutine which is actually part of the Stehfest  
% algorithm, it is a numerical iterative subroutine, NUMAPROX.m.
```

```
    NUMAPROX
```

```
% The NUMAPROX.m subroutine also calls a subroutine called LAPLACE.m, which  
% contains the solution to the problem in Laplace space.
```

```
% The LAPLACE.m subroutine also calls a subroutine called CONSTANTS.m, which  
% contains a linear equation solver that yields the constants required to compute the  
% solution to the problem. The CONSTANTS.m subroutine also calls a subroutine called  
% BESSEL.m which computes the Modified Bessel functions of first and second kind that  
% are required to solve the problem.  
% Finally after going through all these subroutines the program obtains the  
% pressure behaviour for a multi-region composite reservoir.
```

```
end
```

```
if Characode == 1  
    CHARAC  
end
```

```
disp(' This is the transient pressure behaviour for a multi-region composite reservoir      ' )  
disp(' in which the number of regions "Nr" is:                                           ' )
```

```
    Nr
```

```
disp(' The dimensionless wellbore storage coefficient "CD" is:                           ' )
```

```
    CD
```

```
disp(' The skin factor at the wellbore "S" is:                                           ' )
```

```
    S
```

```
disp(' The dimensionless radii, physical characteristics ratios and skin at the          ' )  
disp(' discontinuities are:                                                                ' )  
disp('                                                                                      ' )  
disp(' _____ ' )  
disp('    rD      Mi      Fs      n      Sf ' )  
disp(' _____ ' )  
disp(' [ rD      Mi      Fs      n      Sf ] ' )  
disp(' _____ ' )
```

```
disp('')
disp('')
```

```
disp('')
disp('tD    tD/rDn^2    tDAn    PwD    dPwD/dlntD    dPwD/dtDAn')
disp('')
Ans1
disp('')
```

```
if Characode == 1
```

```
disp('')
disp('tD    dPwD/dlntD    rDins    Mins    Mya    Mmya')
disp('')
Ans2
disp('')
```

```
end
```

```

%%%%%%%%%%%%%%%%%%%%%%%%%%%%%%%%%%%%%%%%%%%%%%%%%%%%%%%%%%%%%%%%%%%%%%%%
%
%
%   DATA SUBROUTINE - DATA.m
%
%   The purpose of this subroutine is to provide the data required to analyze the
%   transient pressure response of a well in a multi-region composite reservoir.
%   There are two ways of providing the required data:
%   a) from a previously edited file or b) from the keyboard.
%
%%%%%%%%%%%%%%%%%%%%%%%%%%%%%%%%%%%%%%%%%%%%%%%%%%%%%%%%%%%%%%%%%%%%%%%%

```

```

clear
disp(' This program obtains the pressure behaviour for multi-region composite ')
disp(' reservoirs. The program also includes, if desired, a reservoir characterization ')
disp(' subroutine which yields satisfactory results if the storativity contrasts within ')
disp(' the reservoir are low or negligible. ')
disp(' ')
disp(' Wellbore storage and skin at the well are allowed. Skin at the front of each ')
disp(' interphase between regions is accounted. Well produces at a constant rate. ')
disp(' ')
disp(' The outer boundary may be infinite, closed or constant pressure. ')
disp(' ')
disp(' The outer boundary selection codes are: ')
disp(' ')
disp('          1  for infinite outer boundary ')
disp('          2  for closed outer boundary ')
disp('          3  for constant pressure outer boundary ')
disp(' ')

```

```

OBcode = input (' Select the number and press enter for the outer boundary code: ')

```

```

format short e

```

```

disp(' Do you want to use a data file previously edited or do you prefer to ')
disp(' input the data from the keyboard? ')
disp(' ')
disp(' The data file selection codes are: ')
disp(' ')
disp('          1  to use a previously edited data file ')
disp('          0  to input data from the keyboard ')
disp(' ')
Datcode = input (' Select the number and press enter for the option selected: ')

```

```

if Datcode~=0
DATAFILE
end

```

```

if Datcode==0

```





```

Nr = input('Enter the number of regions required:      ')

format short e

disp('')
disp('          Now enter the data at each INTERPHASE')
disp('')

rD(1,1)=1;
Mi(1,1)=1;
Fs(1,1)=1;
Sf(1,1)=0;

for I = 1:(Nr-1)
    INTERPHASE = I
    rD(I+1,1)= input('Enter the value for dimensionless radius rD at this interphase:');
    Mi(I+1,1)= input('Enter mobility ratio Mi at this interphase:      ');
    Fs(I+1,1)= input('Enter storativity ratio Fs at this interphase:   ');
    Sf(I+1,1)= input('Enter front skin factor Sf at this interphase:   ');
    disp('')
    disp('')
end

disp(' The data you just entered is:      ')
disp('')
disp('-----')
disp('   rD   Mi   Fs   Sf                      ')
disp('-----')
disp(' [ rD   Mi   Fs   Sf ]                    ')
disp('-----')

end

if OBcode ~= 1
    reD = input(' Enter the value for dimensionless reservoir radius reD:      ')
end

end

% The data subroutine defines the Stehfest algorithm parameters.

N      = 8;
MM     = 7;

% This program generates 13 data points per log cycle.
% The data subroutine generates the tD vector.

Im = 0;

```

```

for I=1:Nc
    tD(lm+1,1) = TD1;
    tD(lm+2,1) = 1.5*TD1;
    tD(lm+3,1) = 2.0*TD1;
    tD(lm+4,1) = 2.5*TD1;
    tD(lm+5,1) = 3.0*TD1;
    tD(lm+6,1) = 3.5*TD1;
    tD(lm+7,1) = 4.0*TD1;
    tD(lm+8,1) = 4.5*TD1;
    tD(lm+9,1) = 5.0*TD1;
    tD(lm+10,1) = 6.0*TD1;
    tD(lm+11,1) = 7.0*TD1;
    tD(lm+12,1) = 8.0*TD1;
    tD(lm+13,1) = 9.0*TD1;

    lm = lm+13;
    TD1 = TD1*10;
end

tD(lm+1) = TD1;

```

% The data subroutine counts how many values of each variable are available.  
 % The purpose of counting the values is to use these numbers in logical cycles.

```

N1 = size(rD);
N2 = size(tD);
rDlast = N1(1,1);
tDlast = N2(1,1);

```

% The data subroutine defines different types of dimensionless times.

```

for I = 1:tDlast
    tD2(I,1) = tD(I,1)/(rD(rDlast,1)^2);
    tD3(I,1) = tD2(I,1)/pi;
end

```

% The data subroutine redefines mobility ratio according to the definition of  
 % the mathematical model.

```

M(1,1) = 1;
for ii = 2:N1
    M(ii,1) = Mi(ii,1)/ Mi(ii-1,1);
end

```

% The data subroutine defines diffusivity ratio according to the definition of  
 % the mathematical model.

```
n(1,1) = 1;  
for j = 2:N1  
    n(j,1) = Mi(j,1)/ Fs(j,1);  
end
```

$$\begin{aligned} \text{Nr} &= 10; \\ \text{TDI} &= 100; \\ \text{Nc} &= 8; \\ \text{CD} &= 0; \\ \text{S} &= 0; \end{aligned}$$

```

if OBcode ~= 1
    reD = 5000;
end

```

```

%%%%%%%%%%%%%%%%%%%%%%%%%%%%%%%%%%%%%%%%%%%%%%%%%%%%%%%%%%%%%%%%%%%%%%%%%%%%%%
%
%
%   THE STEHFEST ALGORITHM SUBROUTINE - STEHFEST.m
%
%   The purpose of this subroutine is to invert the solution to the system from
%   Laplace space to real space. This subroutine computes numerically the Laplace
%   transform inverse of  $F(z)$ .
%
%%%%%%%%%%%%%%%%%%%%%%%%%%%%%%%%%%%%%%%%%%%%%%%%%%%%%%%%%%%%%%%%%%%%%%%%%%%%%%

```

```

% If the array V(i) was computed before (N = MM), the program goes directly to the
% end of the subroutine to calculate F(z).

```

```

while N ~= MM

```

```

    MM = N;
    Dlogtw = 0.6931471805599;
    Nh = N/2;

```

```

    % The factorials from 1 to N are calculated into array G.

```

```

    G(1) = 1;
    clear i
    for i = 2:N
        G(i) = G(i-1)*i;
    end

```

```

    % Terms with k only are calculated into array HH.

```

```

    HH(1) = 2/G(Nh-1);
    clear j

```

```

    for j = 2:Nh

```

```

        Fi = j;
        vr = j - Nh;

```

```

        if vr < 0
            HH(j) = (Fi^Nh)*G(2*j)/(G(Nh-j)*G(j)*G(j-1));
        end

```

```

        if vr == 0
            HH(j) = (Fi^Nh)*G(2*j)/(G(j)*G(j-1));
        end

```

```

    end

```

```

% The terms  $(-1)^{(N_h+1)}$  are calculated.
% First the term for  $i = 1$ 

Sn = - 1;

% The rest of Sn's are calculated in the main routine.

% The array V(ii) is calculated.

clear ii

for ii = 1:N

    % First set  $V(ii,1) = 0$ .

    V(ii,1) = 0;

    % The limits for k are established.
    % The lower limit is  $k1 = \text{Integ}((ii+1)/2)$ 
    % The command "floor" in Matlab is equivalent to the command
    % "Integer" in Fortran.

    k1 = floor((ii+1)/2);

    % The upper limit is  $k2 = \text{Min}(ii, N_h)$ 

    k2 = min(ii, N_h);

    clear kk

    for kk = k1:k2;

        vr3 = 2*kk - ii;
        vr4 = ii - kk;

        if vr3 ~= 0 & vr4 ~= 0
            V(ii,1) = V(ii,1) + HH(kk)/(G(vr4)*G(2*kk-ii));
        end

        if vr3 ~= 0 & vr4 == 0
            V(ii,1) = V(ii,1) + HH(kk)/G(2*kk-ii);
        end

        if vr3 == 0
            V(ii,1) = V(ii,1) + HH(kk)/G(vr4);
        end

    end

    % The V(ii) array is finally calculated by weighting according
    % to Sn.

```

```
V(ii,1) = Sn*V(ii,1);
```

```
% The term changes its sign in each iteration.
```

```
Sn = Sn*(-1);
```

```
end
```

```
end
```

```

%%%%%%%%%%%%%%%%%%%%%%%%%%%%%%%%%%%%%%%%%%%%%%%%%%%%%%%%%%%%%%%%%%%%%%%%%%%%%%
%
%
%   NUMERICAL ITERATIVE SUBROUTINE - NUMAPROX.m
%
%   This subroutine calculates the numerical approximation of a function called F(z).
%   This approximation is actually a part of the Stehfest algorithm.
%
%%%%%%%%%%%%%%%%%%%%%%%%%%%%%%%%%%%%%%%%%%%%%%%%%%%%%%%%%%%%%%%%%%%%%%%%%%%%%%

```

```

a = Dlogtw/tD(I,1);
PwD = 0;
dPwD = 0;

```

```

clear jj

```

```

    for jj = 1:N

```

```

        z = a*jj;

```

```

        % Laplace subroutine: it contains the solution to the problem
        % in Laplace Space.

```

```

        LAPLACE

```

```

        PwD = PwD + V(jj)*PwDl;
        dPwD = dPwD + V(jj)*dPwDl;

```

```

    end

```

```

PwD(I,1) = PwD*a;
dPwDc(I,1) = dPwD*a;
dPwD(I,1) = dPwDc(I,1)*tD(I,1);
dPwDcA(I,1) = dPwDc(I,1)*pi*(rD(rDlast,1))^2;

```

```

% The matrix Ans1 contains all the main program transient pressure behavior results.

```

```

Ans1(I,1) = tD(I,1);
Ans1(I,2) = tD2(I,1);
Ans1(I,3) = tD3(I,1);
Ans1(I,4) = PwD(I,1);
Ans1(I,5) = dPwD(I,1);
Ans1(I,6) = dPwDcA(I,1);

```



```

%%%%%%%%%%%%%%%%%%%%%%%%%%%%%%%%%%%%%%%%%%%%%%%%%%%%%%%%%%%%%
%
%
%      LAPLACE SPACE SUBROUTINE - LAPLACE.m
%
%      The purpose of this subroutine is to provide the solution in
%      Laplace space.
%
%
%
%%%%%%%%%%%%%%%%%%%%%%%%%%%%%%%%%%%%%%%%%%%%%%%%%%%%%%%%%%%%%

```

```

% The program calls a subroutine called CONSTANTS.m, which, as its name indicates,
% provides the constants required to compute the solution to the problem in Laplace space.

```

#### CONSTANTS

```

Pwdl = C(1,1)*(Io1-S*sqrt(z*n(1,1))*I11) + C(2,1)*(Ko1+S*sqrt(z*n(1,1))*K11);
dPwdl = z*Pwdl;

```

```

%%%%%%%%%%%%%%%%%%%%%%%%%%%%%%%%%%%%%%%%%%%%%%%%%%%%%%%%%%%%%%%%%%%%%%%%
%
%      CONSTANTS SUBROUTINE - CONSTANTS.m
%
%      The purpose of this subroutine is to provide the constants required for the
%      general solution of the problem.
%
%%%%%%%%%%%%%%%%%%%%%%%%%%%%%%%%%%%%%%%%%%%%%%%%%%%%%%%%%%%%%%%%%%%%%%%%

```

```

%      The subroutine defines a limit of the Bessel functions argument. This limit is
%      called Plim.

```

```

Plim = 600;
rf = 0.5;

```

```

%      The subroutine defines the argument of the Bessel functions called Zm.

```

```

Zm(I,1) = rD(1,1)*sqrt(z*n(1,1));

```

```

%      The subroutine defines the argument of an exponential function that will premultiply
%      the coefficients so that the matrix obtained is not singular. This argument is
%      called zbb.

```

```

zbb1(I,1) = rD(1,1)*sqrt(z*n(1,1));
zbb2(I,1) = rD(2,1)*sqrt(z*n(1,1));
zbb(I,1) = rf*(zbb1(I,1)+zbb2(I,1));

```

```

if Zm(I,1) > Plim;
    Zm(I,1) = Plim;
end

```

```

if zbb(I,1) > Plim
    zbb(I,1) = Plim;
end

```

```

%      The subroutine defines the numbers that will postmultiply the results obtained from
%      solving the set of linear equations.

```

```

c(1,1) = exp(-zbb(I,1));
c(2,1) = exp(zbb(I,1));

```

```

%      The subroutine CONSTANTS.m calls the subroutine BESSEL.m, which
%      provides the Modified Bessel functions of the first and second kind required
%      to compute the solution to the problem.

```

```

BESSEL

```

% The subroutine defines the first two coefficients of the equations.

```

A(1,1) = (CD*z*(Io - S*sqrt(z*n(1,1))*I1) - sqrt(z*n(1,1))*I1)*exp(-zbb(I,1));
- A(1,2) = (CD*z*(Ko + S*sqrt(z*n(1,1))*K1) + sqrt(z*n(1,1))*K1)*exp(zbb(I,1));;

Io1 = Io;
I11 = I1;
Ko1 = Ko;
K11 = K1;
clear Z

```

for k = 1:(Nr-1)

```

    Zm(I,1) = rD(k+1,1)*sqrt(n(k,1)*z);

```

```

    zbb1(I,1) = rD(k,1)*sqrt(n(k,1)*z);
    zbb2(I,1) = rD(k+1,1)*sqrt(n(k,1)*z);
    zbb(I,1) = rf*(zbb1(I,1)+zbb2(I,1));

```

```

    if Zm(I,1) > Plim
        Zm(I,1) = Plim;
    end

```

```

    if zbb(I,1) > Plim
        zbb(I,1) = Plim;
    end

```

BESSEL

% The subroutine defines another group of coefficients of the equations.

```

A(2*k,(2*k-1)) = (Io + Sf(k+1,1)*rD(k+1,1)*sqrt(n(k,1)*z)*I1)*exp(-zbb(I,1));
A(2*k,2*k)      = (Ko - Sf(k+1,1)*rD(k+1,1)*sqrt(n(k,1)*z)*K1)*exp(zbb(I,1));
A(2*k+1,2*k-1) = (M(k+1,1)*sqrt(n(k,1)*z)*I1)*exp(-zbb(I,1));
A(2*k+1,2*k)   = (-M(k+1,1)*sqrt(n(k,1)*z)*K1)*exp(zbb(I,1));

```

```

clear Z
end

```

for k = 1:(Nr-1)

```

    Zm(I,1) = rD(k+1,1)*sqrt(n(k+1,1)*z);
    zbb1(I,1) = rD(k+1,1)*sqrt(n(k+1,1)*z);

```

```

    if k == (Nr-1)
        zbb2(I,1) = zbb1(I,1);

```

```

    else
        zbb2(I,1) = rD(k+2,1)*sqrt(n(k+1,1)*z);

```

```

    end

```

```
zbb(I,1) = rf*(zbb1(I,1)+zbb2(I,1));
```

```
if Zm(I,1) > Plim
    Zm(I,1) = Plim;
end
```

```
if zbb(I,1) > Plim
    zbb(I,1) = Plim;
end
```

```
if k ~= (Nr-1)
    c(2*k+1,1) = exp(-zbb(I,1));
    c(2*k+2,1) = exp(zbb(I,1));;
end
```

```
if k == (Nr-1)
    if OBcode ~= 1
        c(2*k+1,1) = exp(-zbb(I,1));
        c(2*k+2,1) = exp(zbb(I,1));;
    else
        c(2*k+1,1) = exp(zbb(I,1));
    end
end
```

BESSEL

% The subroutine defines the final group of coefficients of the equations

```
if k ~= (Nr-1)

    A(2*k,2*k+1) = -Io*exp(-zbb(I,1));
    A(2*k+1,2*k+1) = (-sqrt(n(k+1,1)*z)*I1)*exp(-zbb(I,1));
    A(2*k,2*k+2) = -Ko*exp(zbb(I,1));
    A(2*k+1,2*k+2) = (sqrt(n(k+1,1)*z)*K1)*exp(zbb(I,1));

end
```

```
if k == (Nr-1)

    if OBcode == 1

        A(2*k,2*k+1) = -Ko*exp(zbb(I,1));
        A(2*k+1,2*k+1) = (sqrt(n(k+1,1)*z)*K1)*exp(zbb(I,1));

    else
```

```

    A(2*k,2*k+1) = -Io*exp(-zbb(I,1));
    A(2*k+1,2*k+1) = (-sqrt(n(k+1,1)*z)*I1)*exp(-zbb(I,1));
    A(2*k,2*k+2) = -Ko*exp(zbb(I,1));
    A(2*k+1,2*k+2) = (sqrt(n(k+1,1)*z)*K1)*exp(zbb(I,1));

    end

end

clear Z
end

% The subroutine considers the other (different from infinite outer boundary)
% types of outer boundary. This will be the last row of the coefficients matrix.
% In the case of infinite outer boundary, this row will not exist.

if OBcode == 2 | OBcode == 3
    Zm(I,1) = sqrt(n(Nr,1)*z)*reD;

    if Zm(I,1) > Plim;
        Zm(I,1) = Plim;
    end

    if zbb(I,1) > Plim
        zbb(I,1) = Plim;
    end

    BESSEL

    % Closed outer boundary case.

    if OBcode == 2
        A(2*Nr,(2*Nr-1)) = I1*exp(-zbb(I,1));
        A(2*Nr,2*Nr) = K1*exp(zbb(I,1));
        clear Z
    end

    % Constant pressure outer boundary case.

    if OBcode == 3
        A(2*Nr,(2*Nr-1)) = Io*exp(-zbb(I,1));
        A(2*Nr,2*Nr) = Ko*exp(zbb(I,1));
        clear Z
    end

end

end

```

% The "known vector" B is defined.

B(1,1) = 1/z;

if OBcode == 1

    Bcount = (2\*Nr)-1;

else

    Bcount = 2\*Nr;

end

for II = 2:Bcount

    B(II,1)=0;

end

% The subroutine obtains the solution to the system of linear equations.

C = A\B;

% The subroutine postmultiplies the results obtained from the system of linear  
% equations.

C = C.\*c;

```

%%%%%%%%%%%%%%%%%%%%%%%%%%%%%%%%%%%%%%%%%%%%%%%%%%%%%%%%%%%%
%
%
%      BESSEL FUNCTIONS SUBROUTINE - BESSEL.m
%
%      The purpose of this subroutine is to provide the Modified Bessel functions
%      required for the general solution of the problem.
%
%
%%%%%%%%%%%%%%%%%%%%%%%%%%%%%%%%%%%%%%%%%%%%%%%%%%%%%%%%%%%%%%%%%%%%%%%%

```

```

%      This subroutine follows the development of Abramowitz and Stegun(1964),
%      "Handbook of Mathematical Functions". This subroutine has proved to have
%      the same accuracy as the built-in Modified Bessel functions of Matlab version 4.0a.
%      However, it seems that using this subroutine saves computing time compared with
%      the built-in subroutine of Matlab version 4.0a.

```

```

format short e
Z = Zm(I,1);
tm(I,1) = Zm(I,1)/3.75;
t = tm(I,1);

```

```

if Z >= -3.75 & Z <= 3.75

```

```

    Ilo(I,1) = 1 + 3.5156229*(t^2) + 3.0899424*(t^4) + 1.2067492*(t^6) + ...
               0.2659732*(t^8) + 0.0360768*(t^10) + 0.0045813*(t^12);
    elo(I,1) = exp(-Z)*Ilo(I,1);
    lo(I,1) = Ilo(I,1);

```

```

end

```

```

if Z >= 3.75 & Z < Inf

```

```

    Ilo(I,1) = 0.39894228 + 0.01328592*(t^(-1)) + 0.00225319*(t^(-2)) - ...
               0.00157565*(t^(-3)) + 0.00916281*(t^(-4)) - 0.02057706*(t^(-5)) + ...
               0.02635537*(t^(-6)) - 0.01647633*(t^(-7)) + 0.00392377*(t^(-8));
    elo(I,1) = Ilo(I,1)/(sqrt(Z));
    lo(I,1) = elo(I,1)/exp(-Z);

```

```

end

```

```

if Z >= -3.75 & Z <= 3.75

```

```

    II1(I,1) = 0.5 + 0.87890594*(t^2) + 0.51498869*(t^4) + 0.15084934*(t^6) + ...
               0.02658733*(t^8) + 0.00301532*(t^10) + 0.00032411*(t^12);
    eI1(I,1) = exp(-Z)*II1(I,1)*Z;
    I1(I,1) = eI1(I,1)/exp(-Z);

```

```

end

```

if  $Z \geq 3.75$  &  $Z < \text{Inf}$

$$\begin{aligned} \text{II1}(I,1) = & 0.39894228 - 0.03988024*(t^{(-1)}) - 0.00362018*(t^{(-2)}) + \dots \\ & 0.00163801*(t^{(-3)}) - 0.01031555*(t^{(-4)}) + 0.02282967*(t^{(-5)}) - \dots \\ & 0.02895312*(t^{(-6)}) + 0.01787654*(t^{(-7)}) - 0.00420059*(t^{(-8)}); \\ \text{eI1}(I,1) = & \text{II1}(I,1)/(\text{sqrt}(Z)); \\ \text{I1}(I,1) = & \text{eI1}(I,1)/\exp(-Z); \end{aligned}$$

end

if  $Z > 0$  &  $Z \leq 2$

$$\begin{aligned} \text{KKo}(I,1) = & -\log(Z/2)*\text{Io}(I,1) - 0.57721566 + 0.42278420*(Z/2)^2 + \dots \\ & 0.23069756*(Z/2)^4 + 0.03488590*(Z/2)^6 + 0.00262698*(Z/2)^8 + \dots \\ & 0.00010750*(Z/2)^{10} + 0.00000740*(Z/2)^{12}; \end{aligned}$$

$$\begin{aligned} \text{eKo}(I,1) &= \text{KKo}(I,1)*\exp(Z); \\ \text{Ko}(I,1) &= \text{KKo}(I,1); \end{aligned}$$

end

if  $Z \geq 2$  &  $Z < \text{Inf}$

$$\begin{aligned} \text{KKo}(I,1) = & 1.25331414 - 0.07832358*(2/Z) + 0.02189568*(2/Z)^2 - \dots \\ & 0.01062446*(2/Z)^3 + 0.00587872*(2/Z)^4 - 0.00251540*(2/Z)^5 + \dots \\ & 0.00053208*(2/Z)^6; \end{aligned}$$

$$\begin{aligned} \text{eKo}(I,1) &= \text{KKo}(I,1)/(\text{sqrt}(Z)); \\ \text{Ko}(I,1) &= \text{eKo}(I,1)/\exp(Z); \end{aligned}$$

end

if  $Z > 0$  &  $Z \leq 2$

$$\begin{aligned} \text{KK1}(I,1) = & Z*\log(Z/2)*\text{I1}(I,1) + 1 + 0.15443144*(Z/2)^2 - \dots \\ & 0.67278579*(Z/2)^4 - 0.18156897*(Z/2)^6 - 0.01919402*(Z/2)^8 - \dots \\ & 0.00110404*(Z/2)^{10} - 0.00004686*(Z/2)^{12}; \end{aligned}$$

$$\begin{aligned} \text{eK1}(I,1) &= \text{KK1}(I,1)*\exp(Z)/Z; \\ \text{K1}(I,1) &= \text{KK1}(I,1)/Z; \end{aligned}$$

end

if  $Z \geq 2$  &  $Z < \text{Inf}$

$$\begin{aligned} \text{KK1}(I,1) = & 1.25331414 + 0.23498619*(2/Z) - 0.03655620*(2/Z)^2 + \dots \\ & 0.01504268*(2/Z)^3 - 0.00780353*(2/Z)^4 + 0.00325614*(2/Z)^5 - \dots \\ & 0.00068245*(2/Z)^6; \end{aligned}$$



```
eK1(I,1) = KK1(I,1)/sqrt(Z);
K1(I,1)  = eK1(I,1)/exp(Z);
```

```
end
```

```
if Z == 0
eKo(I,1) = Inf;
eK1(I,1) = Inf;
Ko(I,1)  = Inf;
K1(I,1)  = Inf;
end
```

```
Io = Io(I,1);
I1 = I1(I,1);
Ko = Ko(I,1);
K1 = K1(I,1);
```

```

%%%%%%%%%%%%%%%%%%%%%%%%%%%%%%%%%%%%%%%%%%%%%%%%%%%%%%%%%%%%%%%%%%%%%%%%%%%%%%
%
%
%   RESERVOIR CHARACTERIZATION SUBROUTINE - CHARAC.m
%
%   The purpose of this subroutine to characterize the reservoir mobility ratio
%   according to two methods from the Petroleum Engineering literature. The
%   two methods are: Yeh and Agarwal(1989) and Feitosa et al.(1993a).
%
%
%%%%%%%%%%%%%%%%%%%%%%%%%%%%%%%%%%%%%%%%%%%%%%%%%%%%%%%%%%%%%%%%%%%%%%%%%%%%%%

```

```
for I=1:tDlast
```

```
% Instantaneous mobility ratio is defined.
```

```
Mins(I,1) = 2*di_vD(I,1);
```

```
% Dimensionless radius of investigation is defined.
```

```
if rinvcod == 0
```

```
  rDins(I,1) = 1.5*sqrt(tD(I,1)/Mins(I,1));
end
```

```
if rinvcod == 1
```

```
  rDins(I,1) = 2*sqrt(tD(I,1)/Mins(I,1));
end
```

```
end
```

```

% For the first value of instantaneous mobility ratio and the first value of dimensionless
% radius of investigation, the subroutine uses "forward difference" to obtain a mobility
% ratio derivative required. For all the rest of values, excepting the last values of mobility
% ratio and dimensionless radius of investigation, the subroutine uses "central difference"
% to obtain mobility ratio derivatives. For the last value of instantaneous mobility ratio and
% the last value of dimensionless radius of investigation, the subroutine uses "backward
% difference" to obtain the mobility ratio derivative required.

```

```
for I = 1:tDlast
```

```
  if I == 1
```

```
    DerMinv(I,1) = (((1/Mins(I+1,1)) - (1/Mins(I,1)))/(rDins(I+1,1) - rDins(I,1)));
    DerMi(I,1)   = ((Mins(I+1,1) - Mins(I,1))/(rDins(I+1,1) - rDins(I,1)));
  end
```

```
  if I~=1 & I~=tDlast
```

```
    DerMinv(I,1) = (((1/Mins(I+1,1)) - (1/Mins(I-1,1)))/(rDins(I+1,1) - rDins(I-1,1)));
    DerMi(I,1)   = ((Mins(I+1,1) - Mins(I-1,1))/(rDins(I+1,1) - rDins(I-1,1)));
  end
```

```

if I == tDlast
DerMinv(I,1) = (((1/Mins(I,1)) - (1/Mins(I-1,1)))/(rDins(I,1) - rDins(I-1,1)));
DerMi(I,1) = ((Mins(I,1) - Mins(I-1,1))/(rDins(I,1) - rDins(I-1,1)));
end

```

% Yeh and Agarwal's(1989) mobility ratio is defined.

```
Mya(I,1) = 1/(0.5*rDins(I,1)*DerMinv(I,1) + 1/(Mins(I,1)));
```

% Feitosa et al.'s(1993a) mobility ratio is defined.

```
Mmya(I,1) = (0.5*rDins(I,1)*DerMi(I,1) + Mins(I,1));
```

% All the results from this subroutine are arranged in a matrix called Ans2.

```

Ans2(I,1) = tD(I,1);
Ans2(I,2) = dPwD(I,1);
Ans2(I,3) = rDins(I,1);
Ans2(I,4) = Mins(I,1);
Ans2(I,5) = Mya(I,1);
Ans2(I,6) = Mmya(I,1);

```

```
end
```

```

%%%%%%%%%%%%%%%%%%%%%%%%%%%%%%%%%%%%%%%%%%%%%%%%%%%%%%%%%%%%%%%%%%%%%%%%
%
%
%   RESULTS FILE SUBROUTINE - MULTITEST.m
%
%   The purpose of this subroutine is to create a file of results after running the
%   main program and obtaining the transient pressure response of a well in a
%   multi-region composite reservoir. And if desired, this file will also include
%   results from the reservoir characterization subroutine for a particular case.
%
%
%%%%%%%%%%%%%%%%%%%%%%%%%%%%%%%%%%%%%%%%%%%%%%%%%%%%%%%%%%%%%%%%%%%%%%%%

```

diary MULTIRESULTS.m

```

disp ('          MULTICOM PROGRAM - diary MULTIRESULTS.m  ')
disp ('          ')
disp ('          MULTI-REGION COMPOSITE RESERVOIR MODEL    ')
disp ('          ')
disp ('          ')

```

MULTICOM

diary off

## **APPENDIX E**

**Overcoming the matrix singularity problem.**

## APPENDIX E

### Overcoming the matrix singularity problem

As briefly explained in Chapter 4, at early times ( $t_D = 100$ ), the matrix of coefficients  $A$  becomes singular or very close to singular with respect to the working precision limit of the computer. This is because, at these times, there are very small and very large coefficients. The main factor that contributes to the magnitude of these coefficients is the modified Bessel functions of first and second kind. The arguments of these modified Bessel functions are the product of dimensionless radius and the square root of the product of the Laplace parameter and the diffusivity ratio. At early times, the Laplace parameter has a large magnitude which causes large arguments of the modified Bessel functions. These large arguments cause certain modified Bessel functions to be very small and certain modified Bessel functions to be very large, which causes the singularity problem. However, these large arguments cannot be altered without altering the nature of the problem. Thus, an alternative solution had to be looked for.

To overcome the problem, the modified Bessel functions are multiplied by a variable such that it will reduce the large modified Bessel functions and it will increase the small modified Bessel functions. The idea to select this variable came from the definition and the behaviour of the exponentially scaled modified Bessel functions. According to the exponentially-scaled modified Bessel functions definition, the modified Bessel functions that yield large values ( $I_0$  and  $I_1$ ) for large arguments are multiplied by the negative exponentiated form of its argument and the modified Bessel functions that yield small values ( $K_0$  and  $K_1$ ) for large arguments are multiplied by the exponentiated form of its argument.

The exponentially-scaled modified Bessel functions yield reasonable (not so large, not so small and not so far apart) values, irrespective of the argument magnitude.

The matrix of coefficients is structured in such a form that it has some columns composed only of modified Bessel functions that generate large numbers for large arguments and it has other columns composed only of modified Bessel functions that generate small numbers for large arguments. Thus, the matrix becomes ideally suitable to apply exponentially-scaled modified Bessel functions. However, in each column, there are two types of arguments for the modified Bessel functions, and we can only multiply each column by one number. Thus, exponentially-scaled modified Bessel functions cannot be directly employed in the system of coefficients, since these functions require a multiplication of each modified Bessel function by the exponentiated form of its argument. However, it was observed by trial and error that if each column is multiplied by the exponentiated form of the arithmetic average of the two arguments in each column, the singularity problem is overcome. Then, the solution vector components (the required constants) are systematically multiplied by the same numbers that multiplied the matrix of coefficients.

## **APPENDIX F**

**Transient pressure response for a multi-region composite reservoir.  
(Sample results for a particular run)**



## MULTICOM PROGRAM - diary MULTIRESULTS.m

## MULTI-REGION COMPOSITE RESERVOIR MODEL

This program obtains the pressure behaviour for multi-region composite reservoirs. The program also includes, if desired, a reservoir characterization subroutine which yields satisfactory results if the storativity contrasts within the reservoir are low or negligible.

Wellbore storage and skin at the well are allowed. Skin at the front of each interphase between regions is accounted. Well produces at a constant rate.

The outer boundary may be infinite, closed or constant pressure.

The outer boundary selection codes are:

- |   |                                      |
|---|--------------------------------------|
| 1 | for infinite outer boundary          |
| 2 | for closed outer boundary            |
| 3 | for constant pressure outer boundary |

Select the number and press enter for the outer boundary code: 1

OBcode = 1

Do you want to use a data file previously edited or do you prefer to input the data from the keyboard?

The data file selection codes are:

- |   |                                      |
|---|--------------------------------------|
| 1 | to use a previously edited data file |
| 0 | to input data from the keyboard      |

Select the number and press enter for the option selected: 1

Datcode = 1

Do you want to use a characterization subroutine?

- |   |     |
|---|-----|
| 1 | YES |
| 0 | NO  |

Select the number and press enter for the option selected: 1

Characode = 1

Do you want to use the conventional definition of radius of investigation or you prefer to use Yeh and Agarwal (1989) definition?

The radius of investigation codes are:

0 to use the conventional definition  
 1 to use Yeh and Agarwal(1989) definition

Select the number and press enter for the option selected: 1

rinvcode = 1

!!! THE PROGRAM IS NOW RUNNING - WAIT FOR RESULTS !!!

This is the pressure behaviour of a multi-region composite reservoir  
 in which the number of regions "Nr" is:

Nr = 10

The dimensionless wellbore storage coefficient "CD" is:

CD = 0

The skin factor at the wellbore "S" is:

S = 0

The dimensionless radii, physical characteristics ratios and skin at the discontinuities are:

rD	Mi	Fs	n	Sf
1.0000e+00	1.0000e+00	1.0000e+00	1.0000e+00	0
1.0000e+02	6.6250e+00	6.6250e+00	1.0000e+00	0
2.1250e+02	1.7875e+01	1.7875e+01	1.0000e+00	0
3.2500e+02	2.9125e+01	2.9125e+01	1.0000e+00	0
4.3750e+02	4.0375e+01	4.0375e+01	1.0000e+00	0
5.5000e+02	5.1625e+01	5.1625e+01	1.0000e+00	0
6.6250e+02	6.2875e+01	6.2875e+01	1.0000e+00	0
7.7500e+02	7.4125e+01	7.4125e+01	1.0000e+00	0
8.8750e+02	8.5375e+01	8.5375e+01	1.0000e+00	0
1.0000e+03	1.0000e+03	1.0000e+03	1.0000e+00	0

$tD$	$tD/rDn^2$	$tDAn$	$PwD$	$dPwD/d\ln tD$	$dPwD/dtDAn$
1.0000e+02	1.0000e-04	3.1831e-05	2.7228e+00	4.8682e-01	1.5294e+04
1.5000e+02	1.5000e-04	4.7746e-05	2.9210e+00	4.9047e-01	1.0272e+04
2.0000e+02	2.0000e-04	6.3662e-05	3.0624e+00	4.9246e-01	7.7356e+03
2.5000e+02	2.5000e-04	7.9577e-05	3.1724e+00	4.9374e-01	6.2045e+03
3.0000e+02	3.0000e-04	9.5493e-05	3.2625e+00	4.9463e-01	5.1798e+03
3.5000e+02	3.5000e-04	1.1141e-04	3.3388e+00	4.9530e-01	4.4458e+03
4.0000e+02	4.0000e-04	1.2732e-04	3.4050e+00	4.9583e-01	3.8942e+03
4.5000e+02	4.5000e-04	1.4324e-04	3.4635e+00	4.9625e-01	3.4645e+03
5.0000e+02	5.0000e-04	1.5915e-04	3.5158e+00	4.9659e-01	3.1202e+03
6.0000e+02	6.0000e-04	1.9099e-04	3.6065e+00	4.9708e-01	2.6027e+03
7.0000e+02	7.0000e-04	2.2282e-04	3.6832e+00	4.9734e-01	2.2321e+03
8.0000e+02	8.0000e-04	2.5465e-04	3.7497e+00	4.9745e-01	1.9535e+03
9.0000e+02	9.0000e-04	2.8648e-04	3.8083e+00	4.9752e-01	1.7367e+03
1.0000e+03	1.0000e-03	3.1831e-04	3.8608e+00	4.9767e-01	1.5635e+03
1.5000e+03	1.5000e-03	4.7746e-04	4.0628e+00	5.0346e-01	1.0544e+03
2.0000e+03	2.0000e-03	6.3662e-04	4.2092e+00	5.2346e-01	8.2224e+02
2.5000e+03	2.5000e-03	7.9577e-04	4.3291e+00	5.5822e-01	7.0148e+02
3.0000e+03	3.0000e-03	9.5493e-04	4.4347e+00	6.0430e-01	6.3282e+02
3.5000e+03	3.5000e-03	1.1141e-03	4.5321e+00	6.5791e-01	5.9054e+02
4.0000e+03	4.0000e-03	1.2732e-03	4.6242e+00	7.1611e-01	5.6243e+02
4.5000e+03	4.5000e-03	1.4324e-03	4.7125e+00	7.7680e-01	5.4231e+02
5.0000e+03	5.0000e-03	1.5915e-03	4.7980e+00	8.3863e-01	5.2693e+02
6.0000e+03	6.0000e-03	1.9099e-03	4.9628e+00	9.6257e-01	5.0400e+02
7.0000e+03	7.0000e-03	2.2282e-03	5.1209e+00	1.0843e+00	4.8664e+02
8.0000e+03	8.0000e-03	2.5465e-03	5.2739e+00	1.2028e+00	4.7233e+02
9.0000e+03	9.0000e-03	2.8648e-03	5.4224e+00	1.3179e+00	4.6002e+02
1.0000e+04	1.0000e-02	3.1831e-03	5.5671e+00	1.4297e+00	4.4914e+02
1.5000e+04	1.5000e-02	4.7746e-03	6.2466e+00	1.9512e+00	4.0867e+02
2.0000e+04	2.0000e-02	6.3662e-03	6.8735e+00	2.4309e+00	3.8185e+02
2.5000e+04	2.5000e-02	7.9577e-03	7.4643e+00	2.8836e+00	3.6237e+02
3.0000e+04	3.0000e-02	9.5493e-03	8.0282e+00	3.3164e+00	3.4730e+02
3.5000e+04	3.5000e-02	1.1141e-02	8.5706e+00	3.7333e+00	3.3510e+02
4.0000e+04	4.0000e-02	1.2732e-02	9.0955e+00	4.1367e+00	3.2489e+02
4.5000e+04	4.5000e-02	1.4324e-02	9.6053e+00	4.5284e+00	3.1614e+02
5.0000e+04	5.0000e-02	1.5915e-02	1.0102e+01	4.9098e+00	3.0849e+02
6.0000e+04	6.0000e-02	1.9099e-02	1.1063e+01	5.6456e+00	2.9560e+02
7.0000e+04	7.0000e-02	2.2282e-02	1.1987e+01	6.3503e+00	2.8500e+02
8.0000e+04	8.0000e-02	2.5465e-02	1.2880e+01	7.0284e+00	2.7600e+02
9.0000e+04	9.0000e-02	2.8648e-02	1.3747e+01	7.6832e+00	2.6819e+02
1.0000e+05	1.0000e-01	3.1831e-02	1.4590e+01	8.3174e+00	2.6130e+02
1.5000e+05	1.5000e-01	4.7746e-02	1.8533e+01	1.1253e+01	2.3568e+02
2.0000e+05	2.0000e-01	6.3662e-02	2.2141e+01	1.3936e+01	2.1891e+02
2.5000e+05	2.5000e-01	7.9577e-02	2.5523e+01	1.6494e+01	2.0727e+02
3.0000e+05	3.0000e-01	9.5493e-02	2.8747e+01	1.8999e+01	1.9896e+02
3.5000e+05	3.5000e-01	1.1141e-01	3.1857e+01	2.1491e+01	1.9290e+02
4.0000e+05	4.0000e-01	1.2732e-01	3.4885e+01	2.3986e+01	1.8839e+02
4.5000e+05	4.5000e-01	1.4324e-01	3.7851e+01	2.6493e+01	1.8496e+02
5.0000e+05	5.0000e-01	1.5915e-01	4.0771e+01	2.9013e+01	1.8229e+02
6.0000e+05	6.0000e-01	1.9099e-01	4.6508e+01	3.4085e+01	1.7847e+02
7.0000e+05	7.0000e-01	2.2282e-01	5.2147e+01	3.9182e+01	1.7585e+02

$tD$	$tD/rDn^2$	$tD\Delta n$	$PwD$	$dPwD/d\ln tD$	$dPwD/dtD\Delta n$
8.0000e+05	8.0000e-01	2.5465e-01	5.7716e+01	4.4284e+01	1.7390e+02
9.0000e+05	9.0000e-01	2.8648e-01	6.3232e+01	4.9375e+01	1.7235e+02
1.0000e+06	1.0000e+00	3.1831e-01	6.8702e+01	5.4443e+01	1.7104e+02
1.5000e+06	1.5000e+00	4.7746e-01	9.5523e+01	7.9277e+01	1.6604e+02
2.0000e+06	2.0000e+00	6.3662e-01	1.2163e+02	1.0316e+02	1.6205e+02
2.5000e+06	2.5000e+00	7.9577e-01	1.4714e+02	1.2615e+02	1.5852e+02
3.0000e+06	3.0000e+00	9.5493e-01	1.7211e+02	1.4830e+02	1.5530e+02
3.5000e+06	3.5000e+00	1.1141e+00	1.9658e+02	1.6969e+02	1.5232e+02
4.0000e+06	4.0000e+00	1.2732e+00	2.2060e+02	1.9038e+02	1.4953e+02
4.5000e+06	4.5000e+00	1.4324e+00	2.4418e+02	2.1041e+02	1.4690e+02
5.0000e+06	5.0000e+00	1.5915e+00	2.6736e+02	2.2982e+02	1.4440e+02
6.0000e+06	6.0000e+00	1.9099e+00	3.1257e+02	2.6691e+02	1.3976e+02
7.0000e+06	7.0000e+00	2.2282e+00	3.5637e+02	3.0188e+02	1.3549e+02
8.0000e+06	8.0000e+00	2.5465e+00	3.9887e+02	3.3492e+02	1.3152e+02
9.0000e+06	9.0000e+00	2.8648e+00	4.4014e+02	3.6617e+02	1.2782e+02
1.0000e+07	1.0000e+01	3.1831e+00	4.8028e+02	3.9578e+02	1.2434e+02
1.5000e+07	1.5000e+01	4.7746e+00	6.6595e+02	5.2276e+02	1.0949e+02
2.0000e+07	2.0000e+01	6.3662e+00	8.3060e+02	6.2170e+02	9.7656e+01
2.5000e+07	2.5000e+01	7.9577e+00	9.7815e+02	6.9944e+02	8.7895e+01
3.0000e+07	3.0000e+01	9.5493e+00	1.1114e+03	7.6074e+02	7.9664e+01
3.5000e+07	3.5000e+01	1.1141e+01	1.2325e+03	8.0904e+02	7.2619e+01
4.0000e+07	4.0000e+01	1.2732e+01	1.3432e+03	8.4696e+02	6.6520e+01
4.5000e+07	4.5000e+01	1.4324e+01	1.4447e+03	8.7650e+02	6.1192e+01
5.0000e+07	5.0000e+01	1.5915e+01	1.5383e+03	8.9926e+02	5.6502e+01
6.0000e+07	6.0000e+01	1.9099e+01	1.7049e+03	9.2917e+02	4.8651e+01
7.0000e+07	7.0000e+01	2.2282e+01	1.8491e+03	9.4404e+02	4.2368e+01
8.0000e+07	8.0000e+01	2.5465e+01	1.9752e+03	9.4875e+02	3.7257e+01
9.0000e+07	9.0000e+01	2.8648e+01	2.0865e+03	9.4659e+02	3.3042e+01
1.0000e+08	1.0000e+02	3.1831e+01	2.1854e+03	9.3981e+02	2.9525e+01
1.5000e+08	1.5000e+02	4.7746e+01	2.5538e+03	8.7804e+02	1.8390e+01
2.0000e+08	2.0000e+02	6.3662e+01	2.7963e+03	8.1268e+02	1.2766e+01
2.5000e+08	2.5000e+02	7.9577e+01	2.9715e+03	7.5922e+02	9.5406e+00
3.0000e+08	3.0000e+02	9.5493e+01	3.1064e+03	7.1778e+02	7.5166e+00
3.5000e+08	3.5000e+02	1.1141e+02	3.2151e+03	6.8593e+02	6.1569e+00
4.0000e+08	4.0000e+02	1.2732e+02	3.3056e+03	6.6128e+02	5.1936e+00
4.5000e+08	4.5000e+02	1.4324e+02	3.3830e+03	6.4195e+02	4.4817e+00
5.0000e+08	5.0000e+02	1.5915e+02	3.4504e+03	6.2660e+02	3.9370e+00
6.0000e+08	6.0000e+02	1.9099e+02	3.5636e+03	6.0409e+02	3.1630e+00
7.0000e+08	7.0000e+02	2.2282e+02	3.6563e+03	5.8868e+02	2.6420e+00
8.0000e+08	8.0000e+02	2.5465e+02	3.7348e+03	5.7761e+02	2.2683e+00
9.0000e+08	9.0000e+02	2.8648e+02	3.8028e+03	5.6931e+02	1.9873e+00
1.0000e+09	1.0000e+03	3.1831e+02	3.8628e+03	5.6287e+02	1.7683e+00
1.5000e+09	1.5000e+03	4.7746e+02	4.0875e+03	5.4435e+02	1.1401e+00
2.0000e+09	2.0000e+03	6.3662e+02	4.2426e+03	5.3510e+02	8.4054e-01
2.5000e+09	2.5000e+03	7.9577e+02	4.3610e+03	5.2930e+02	6.6514e-01
3.0000e+09	3.0000e+03	9.5493e+02	4.4568e+03	5.2522e+02	5.5001e-01
3.5000e+09	3.5000e+03	1.1141e+03	4.5372e+03	5.2217e+02	4.6870e-01
4.0000e+09	4.0000e+03	1.2732e+03	4.6065e+03	5.1978e+02	4.0824e-01
4.5000e+09	4.5000e+03	1.4324e+03	4.6674e+03	5.1786e+02	3.6154e-01

tD	tD/rDn^2	tDAn	PwD	dPwD/dlntD	dPwD/dtDAn
5.0000e+09	5.0000e+03	1.5915e+03	4.7217e+03	5.1628e+02	3.2439e-01
6.0000e+09	6.0000e+03	1.9099e+03	4.8154e+03	5.1383e+02	2.6904e-01
7.0000e+09	7.0000e+03	2.2282e+03	4.8942e+03	5.1201e+02	2.2979e-01
8.0000e+09	8.0000e+03	2.5465e+03	4.9623e+03	5.1061e+02	2.0052e-01
9.0000e+09	9.0000e+03	2.8648e+03	5.0223e+03	5.0950e+02	1.7785e-01
1.0000e+10	1.0000e+04	3.1831e+03	5.0758e+03	5.0860e+02	1.5978e-01
1.5000e+10	1.5000e+04	4.7746e+03	5.2812e+03	5.0582e+02	1.0594e-01
2.0000e+10	2.0000e+04	6.3662e+03	5.4264e+03	5.0439e+02	7.9230e-02
2.5000e+10	2.5000e+04	7.9577e+03	5.5388e+03	5.0353e+02	6.3275e-02
3.0000e+10	3.0000e+04	9.5493e+03	5.6306e+03	5.0294e+02	5.2668e-02
3.5000e+10	3.5000e+04	1.1141e+04	5.7081e+03	5.0252e+02	4.5107e-02
4.0000e+10	4.0000e+04	1.2732e+04	5.7751e+03	5.0221e+02	3.9444e-02
4.5000e+10	4.5000e+04	1.4324e+04	5.8343e+03	5.0197e+02	3.5044e-02
5.0000e+10	5.0000e+04	1.5915e+04	5.8872e+03	5.0177e+02	3.1527e-02
6.0000e+10	6.0000e+04	1.9099e+04	5.9786e+03	5.0148e+02	2.6257e-02
7.0000e+10	7.0000e+04	2.2282e+04	6.0559e+03	5.0127e+02	2.2497e-02
8.0000e+10	8.0000e+04	2.5465e+04	6.1229e+03	5.0111e+02	1.9679e-02
9.0000e+10	9.0000e+04	2.8648e+04	6.1819e+03	5.0099e+02	1.7488e-02
1.0000e+11	1.0000e+05	3.1831e+04	6.2347e+03	5.0089e+02	1.5736e-02

tD	dPwD/dlntD	rDins	Mins	Mya	Mmya
1.0000e+02	4.8682e-01	1.5202e+01	9.7363e-01	9.9038e-01	9.9022e-01
1.5000e+02	4.9047e-01	1.8549e+01	9.8094e-01	9.9827e-01	9.9791e-01
2.0000e+02	4.9246e-01	2.1375e+01	9.8493e-01	9.9826e-01	9.9807e-01
2.5000e+02	4.9374e-01	2.3867e+01	9.8748e-01	9.9850e-01	9.9837e-01
3.0000e+02	4.9463e-01	2.6121e+01	9.8926e-01	9.9879e-01	9.9870e-01
3.5000e+02	4.9530e-01	2.8195e+01	9.9060e-01	9.9910e-01	9.9903e-01
4.0000e+02	4.9583e-01	3.0126e+01	9.9166e-01	9.9936e-01	9.9930e-01
4.5000e+02	4.9625e-01	3.1940e+01	9.9250e-01	9.9949e-01	9.9944e-01
5.0000e+02	4.9659e-01	3.3656e+01	9.9319e-01	9.9888e-01	9.9885e-01
6.0000e+02	4.9708e-01	3.6850e+01	9.9415e-01	9.9865e-01	9.9863e-01
7.0000e+02	4.9734e-01	3.9792e+01	9.9468e-01	9.9733e-01	9.9732e-01
8.0000e+02	4.9745e-01	4.2535e+01	9.9491e-01	9.9638e-01	9.9637e-01
9.0000e+02	4.9752e-01	4.5112e+01	9.9505e-01	9.9695e-01	9.9694e-01
1.0000e+03	4.9767e-01	4.7545e+01	9.9533e-01	1.0176e+00	1.0174e+00
1.5000e+03	5.0346e-01	5.7895e+01	1.0069e+00	1.0946e+00	1.0898e+00
2.0000e+03	5.2346e-01	6.5562e+01	1.0469e+00	1.4062e+00	1.3213e+00
2.5000e+03	5.5822e-01	7.0981e+01	1.1164e+00	2.4925e+00	1.7421e+00
3.0000e+03	6.0430e-01	7.4733e+01	1.2086e+00	3.0748e+00	2.3763e+00
3.5000e+03	6.5791e-01	7.7362e+01	1.3158e+00	-2.9326e+00	3.2216e+00
4.0000e+03	7.1611e-01	7.9272e+01	1.4322e+00	-1.4905e+00	4.2311e+00
4.5000e+03	7.7680e-01	8.0729e+01	1.5536e+00	-1.0825e+00	5.3189e+00
5.0000e+03	8.3863e-01	8.1899e+01	1.6773e+00	-9.1510e-01	6.7288e+00
6.0000e+03	9.6257e-01	8.3741e+01	1.9251e+00	-8.4538e-01	8.1172e+00
7.0000e+03	1.0843e+00	8.5221e+01	2.1686e+00	-8.7756e-01	9.5813e+00

tD	dPwD/dlntD	rDins	Mins	Mya	Mmya
8.0000e+03	1.2028e+00	8.6502e+01	2.4056e+00	-9.6329e-01	1.0715e+01
9.0000e+03	1.3179e+00	8.7652e+01	2.6357e+00	-1.0735e+00	1.1653e+01
1.0000e+04	1.4297e+00	8.8708e+01	2.8593e+00	-1.4872e+00	1.3373e+01
1.5000e+04	1.9512e+00	9.2996e+01	3.9025e+00	-1.5701e+00	1.6319e+01
2.0000e+04	2.4309e+00	9.6207e+01	4.8618e+00	-2.0580e+00	2.0427e+01
2.5000e+04	2.8836e+00	9.8759e+01	5.7672e+00	-2.4568e+00	2.4485e+01
3.0000e+04	3.3164e+00	1.0088e+02	6.6329e+00	-2.8213e+00	2.8388e+01
3.5000e+04	3.7333e+00	1.0270e+02	7.4665e+00	-3.1752e+00	3.2099e+01
4.0000e+04	4.1367e+00	1.0430e+02	8.2734e+00	-3.5290e+00	3.5609e+01
4.5000e+04	4.5284e+00	1.0573e+02	9.0568e+00	-3.8873e+00	3.8926e+01
5.0000e+04	4.9098e+00	1.0704e+02	9.8196e+00	-4.5054e+00	4.2932e+01
6.0000e+04	5.6456e+00	1.0934e+02	1.1291e+01	-4.9127e+00	4.7723e+01
7.0000e+04	6.3503e+00	1.1136e+02	1.2701e+01	-5.6977e+00	5.3054e+01
8.0000e+04	7.0284e+00	1.1316e+02	1.4057e+01	-6.5057e+00	5.7939e+01
9.0000e+04	7.6832e+00	1.1480e+02	1.5366e+01	-7.3318e+00	6.2476e+01
1.0000e+05	8.3174e+00	1.1630e+02	1.6635e+01	-1.0354e+01	7.0825e+01
1.5000e+05	1.1253e+01	1.2246e+02	2.2506e+01	-1.0701e+01	8.6435e+01
2.0000e+05	1.3936e+01	1.2706e+02	2.7872e+01	-1.3419e+01	1.0984e+02
2.5000e+05	1.6494e+01	1.3058e+02	3.2988e+01	-1.4266e+01	1.3933e+02
3.0000e+05	1.8999e+01	1.3328e+02	3.7999e+01	-1.3884e+01	1.7744e+02
3.5000e+05	2.1491e+01	1.3536e+02	4.2981e+01	-1.2969e+01	2.2595e+02
4.0000e+05	2.3986e+01	1.3697e+02	4.7972e+01	-1.1938e+01	2.8622e+02
4.5000e+05	2.6493e+01	1.3823e+02	5.2986e+01	-1.0979e+01	3.5907e+02
5.0000e+05	2.9013e+01	1.3924e+02	5.8026e+01	-9.9698e+00	4.8258e+02
6.0000e+05	3.4085e+01	1.4072e+02	6.8170e+01	-9.1065e+00	6.3420e+02
7.0000e+05	3.9182e+01	1.4177e+02	7.8365e+01	-8.4945e+00	8.6619e+02
8.0000e+05	4.4284e+01	1.4256e+02	8.8568e+01	-8.3416e+00	1.1036e+03
9.0000e+05	4.9375e+01	1.4320e+02	9.8750e+01	-8.5658e+00	1.3223e+03
1.0000e+06	5.4443e+01	1.4375e+02	1.0889e+02	-1.0799e+01	1.7026e+03
1.5000e+06	7.9277e+01	1.4590e+02	1.5855e+02	-1.3488e+01	1.9659e+03
2.0000e+06	1.0316e+02	1.4768e+02	2.0633e+02	-2.1858e+01	2.2303e+03
2.5000e+06	1.2615e+02	1.4932e+02	2.5229e+02	-3.2552e+01	2.3748e+03
3.0000e+06	1.4830e+02	1.5086e+02	2.9660e+02	-4.5206e+01	2.4794e+03
3.5000e+06	1.6969e+02	1.5233e+02	3.3939e+02	-5.9769e+01	2.5617e+03
4.0000e+06	1.9038e+02	1.5374e+02	3.8077e+02	-7.6277e+01	2.6283e+03
4.5000e+06	2.1041e+02	1.5511e+02	4.2083e+02	-9.4797e+01	2.6830e+03
5.0000e+06	2.2982e+02	1.5645e+02	4.5965e+02	-1.2691e+02	2.7185e+03
6.0000e+06	2.6691e+02	1.5903e+02	5.3383e+02	-1.5930e+02	2.7958e+03
7.0000e+06	3.0188e+02	1.6151e+02	6.0377e+02	-2.1694e+02	2.8443e+03
8.0000e+06	3.3492e+02	1.6393e+02	6.6984e+02	-2.8570e+02	2.8776e+03
9.0000e+06	3.6617e+02	1.6629e+02	7.3234e+02	-3.6734e+02	2.8997e+03
1.0000e+07	3.9578e+02	1.6860e+02	7.9156e+02	-7.6156e+02	2.7643e+03
1.5000e+07	5.2276e+02	1.7967e+02	1.0455e+03	-1.0537e+03	2.9210e+03
2.0000e+07	6.2170e+02	1.9024e+02	1.2434e+03	-3.3599e+03	2.8550e+03
2.5000e+07	6.9944e+02	2.0053e+02	1.3989e+03	-1.2581e+05	2.7663e+03
3.0000e+07	7.6074e+02	2.1063e+02	1.5215e+03	6.6889e+03	2.6708e+03
3.5000e+07	8.0904e+02	2.2061e+02	1.6181e+03	4.0543e+03	2.5752e+03
4.0000e+07	8.4696e+02	2.3050e+02	1.6939e+03	3.2020e+03	2.4826e+03
4.5000e+07	8.7650e+02	2.4033e+02	1.7530e+03	2.7783e+03	2.3944e+03
5.0000e+07	8.9926e+02	2.5010e+02	1.7985e+03	2.3949e+03	2.2496e+03

iD	dPwD/dlntD	rDins	Mins	Mya	Mmya
6.0000e+07	9.2917e+02	2.6953e+02	1.8583e+03	2.2405e+03	2.1700e+03
7.0000e+07	9.4404e+02	2.8882e+02	1.8881e+03	2.0494e+03	2.0351e+03
8.0000e+07	9.4875e+02	3.0800e+02	1.8975e+03	1.9184e+03	1.9180e+03
9.0000e+07	9.4659e+02	3.2705e+02	1.8932e+03	1.8189e+03	1.8163e+03
1.0000e+08	9.3981e+02	3.4598e+02	1.8796e+03	1.6776e+03	1.6666e+03
1.5000e+08	8.7804e+02	4.3839e+02	1.7561e+03	1.4910e+03	1.4468e+03
2.0000e+08	8.1268e+02	5.2618e+02	1.6254e+03	1.3281e+03	1.2581e+03
2.5000e+08	7.5922e+02	6.0864e+02	1.5184e+03	1.2289e+03	1.1564e+03
3.0000e+08	7.1778e+02	6.8571e+02	1.4356e+03	1.1649e+03	1.0983e+03
3.5000e+08	6.8593e+02	7.5765e+02	1.3719e+03	1.1224e+03	1.0643e+03
4.0000e+08	6.6128e+02	8.2493e+02	1.3226e+03	1.0940e+03	1.0443e+03
4.5000e+08	6.4195e+02	8.8804e+02	1.2839e+03	1.0747e+03	1.0326e+03
5.0000e+08	6.2660e+02	9.4748e+02	1.2532e+03	1.0698e+03	1.0410e+03
6.0000e+08	6.0409e+02	1.0571e+03	1.2082e+03	1.0443e+03	1.0166e+03
7.0000e+08	5.8868e+02	1.1566e+03	1.1774e+03	1.0372e+03	1.0171e+03
8.0000e+08	5.7761e+02	1.2483e+03	1.1552e+03	1.0335e+03	1.0186e+03
9.0000e+08	5.6931e+02	1.3336e+03	1.1386e+03	1.0314e+03	1.0199e+03
1.0000e+09	5.6287e+02	1.4137e+03	1.1257e+03	1.0472e+03	1.0431e+03
1.5000e+09	5.4435e+02	1.7607e+03	1.0887e+03	1.0181e+03	1.0119e+03
2.0000e+09	5.3510e+02	2.0506e+03	1.0702e+03	1.0167e+03	1.0135e+03
2.5000e+09	5.2930e+02	2.3051e+03	1.0586e+03	1.0137e+03	1.0116e+03
3.0000e+09	5.2522e+02	2.5349e+03	1.0504e+03	1.0111e+03	1.0094e+03
3.5000e+09	5.2217e+02	2.7460e+03	1.0443e+03	1.0090e+03	1.0077e+03
4.0000e+09	5.1978e+02	2.9424e+03	1.0396e+03	1.0073e+03	1.0063e+03
4.5000e+09	5.1786e+02	3.1266e+03	1.0357e+03	1.0061e+03	1.0052e+03
5.0000e+09	5.1628e+02	3.3008e+03	1.0326e+03	1.0064e+03	1.0058e+03
6.0000e+09	5.1383e+02	3.6245e+03	1.0277e+03	1.0034e+03	1.0027e+03
7.0000e+09	5.1201e+02	3.9218e+03	1.0240e+03	1.0025e+03	1.0021e+03
8.0000e+09	5.1061e+02	4.1983e+03	1.0212e+03	1.0020e+03	1.0016e+03
9.0000e+09	5.0950e+02	4.4578e+03	1.0190e+03	1.0016e+03	1.0012e+03
1.0000e+10	5.0860e+02	4.7031e+03	1.0172e+03	1.0042e+03	1.0041e+03
1.5000e+10	5.0582e+02	5.7759e+03	1.0116e+03	9.9952e+02	9.9934e+02
2.0000e+10	5.0439e+02	6.6789e+03	1.0088e+03	9.9984e+02	9.9975e+02
2.5000e+10	5.0353e+02	7.4737e+03	1.0071e+03	9.9994e+02	9.9988e+02
3.0000e+10	5.0294e+02	8.1918e+03	1.0059e+03	9.9998e+02	9.9994e+02
3.5000e+10	5.0252e+02	8.8518e+03	1.0050e+03	9.9999e+02	9.9997e+02
4.0000e+10	5.0221e+02	9.4659e+03	1.0044e+03	1.0000e+03	9.9998e+02
4.5000e+10	5.0197e+02	1.0043e+04	1.0039e+03	1.0000e+03	9.9999e+02
5.0000e+10	5.0177e+02	1.0588e+04	1.0035e+03	1.0002e+03	1.0002e+03
6.0000e+10	5.0148e+02	1.1602e+04	1.0030e+03	9.9996e+02	9.9995e+02
7.0000e+10	5.0127e+02	1.2534e+04	1.0025e+03	9.9998e+02	9.9997e+02
8.0000e+10	5.0111e+02	1.3402e+04	1.0022e+03	9.9999e+02	9.9999e+02
9.0000e+10	5.0099e+02	1.4216e+04	1.0020e+03	1.0000e+03	1.0000e+03
1.0000e+11	5.0089e+02	1.4987e+04	1.0018e+03	9.9988e+02	9.9987e+02

## **APPENDIX G**

**Figures for transient pressure responses for multi-region composite reservoirs .**



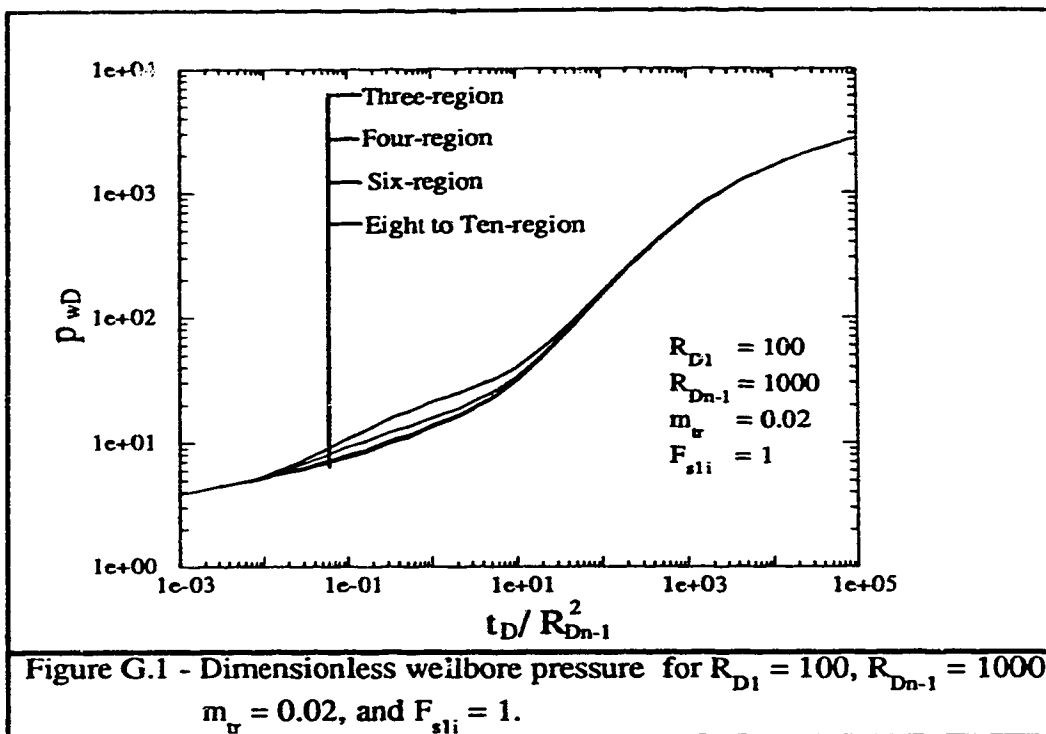


Figure G.1 - Dimensionless wellbore pressure for  $R_{D1} = 100$ ,  $R_{Dn-1} = 1000$ ,  $m_u = 0.02$ , and  $F_{sli} = 1$ .

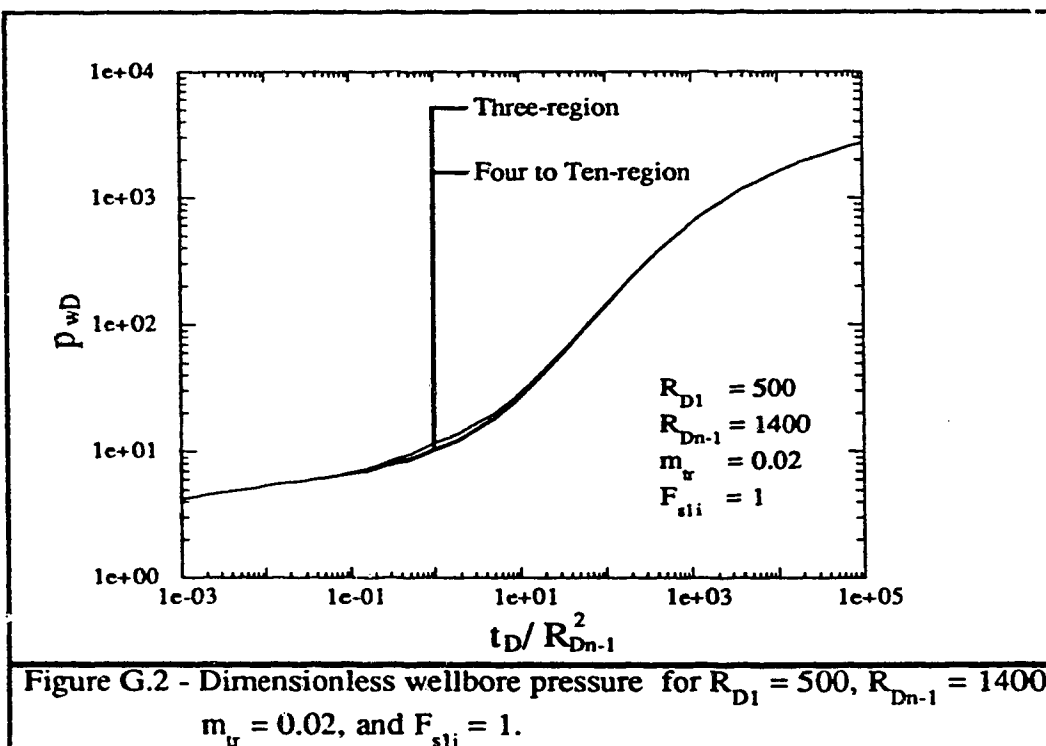
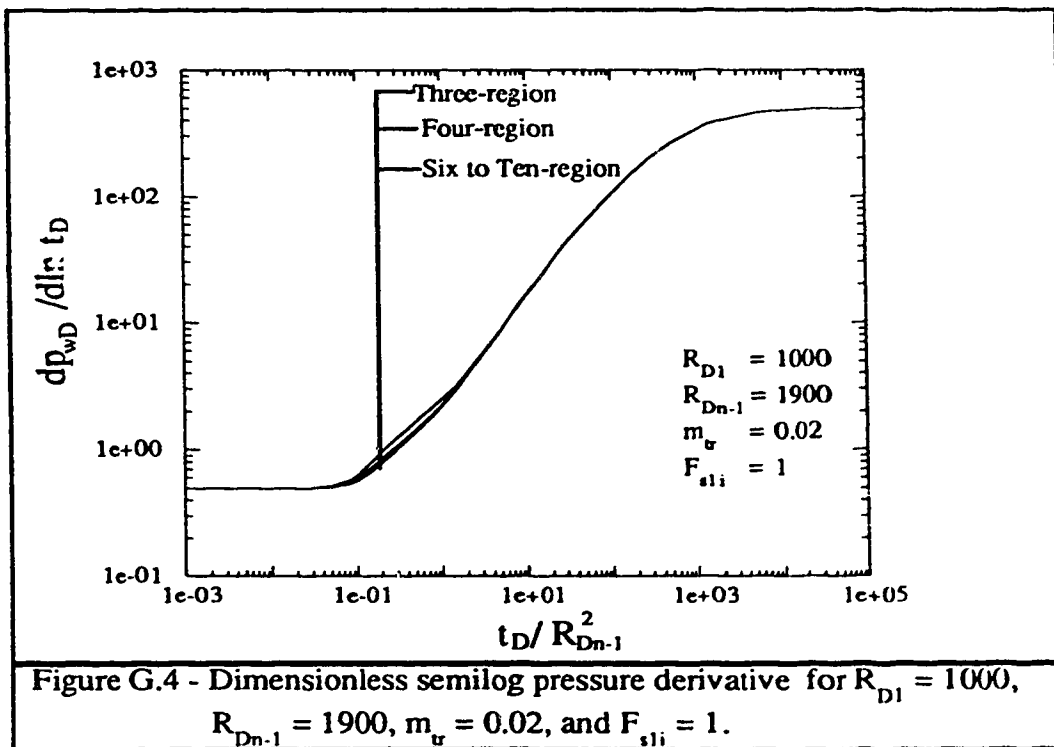
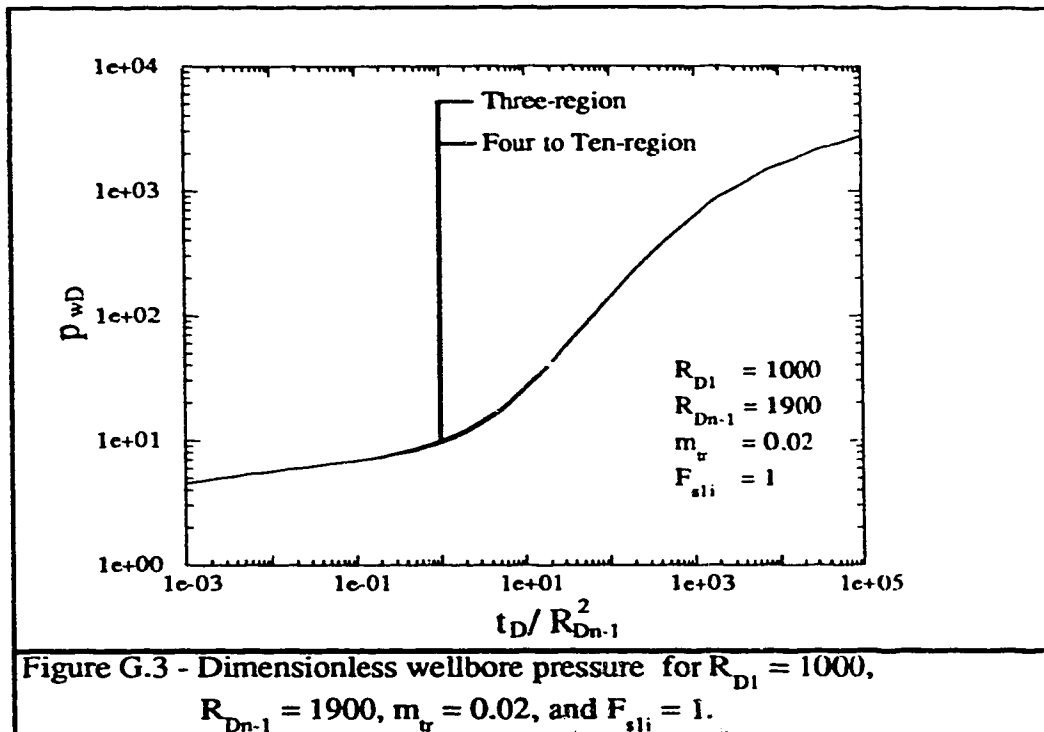


Figure G.2 - Dimensionless wellbore pressure for  $R_{D1} = 500$ ,  $R_{Dn-1} = 1400$ ,  $m_u = 0.02$ , and  $F_{sli} = 1$ .



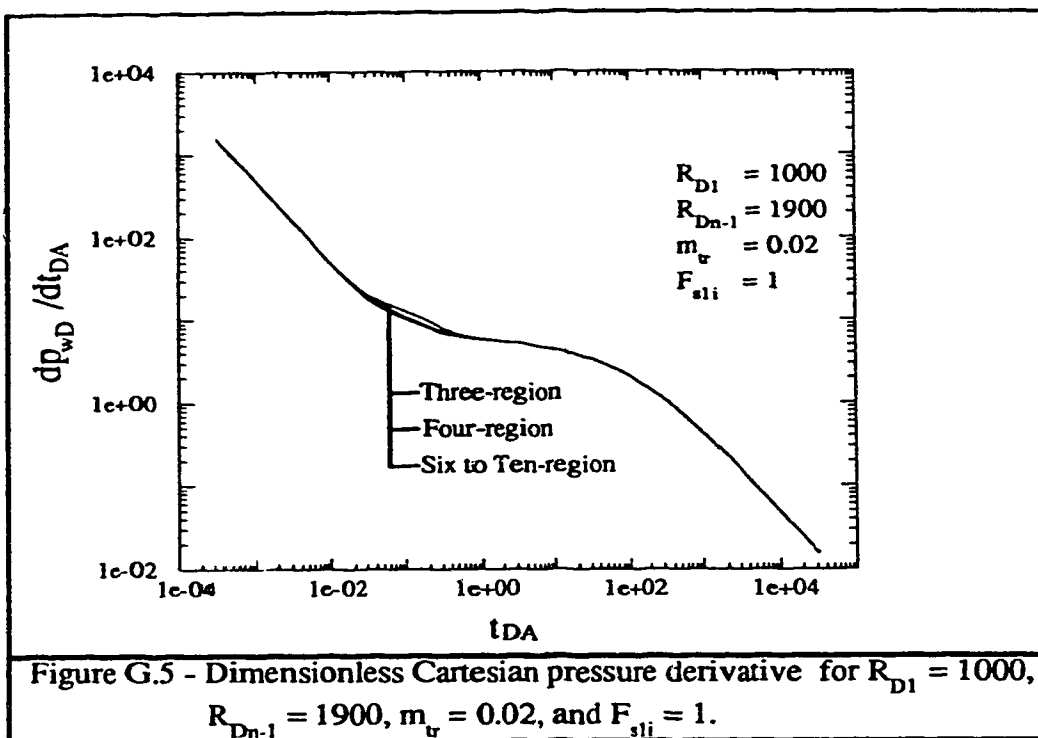


Figure G.5 - Dimensionless Cartesian pressure derivative for  $R_{D1} = 1000$ ,  $R_{Dn-1} = 1900$ ,  $m_u = 0.02$ , and  $F_{sli} = 1$ .

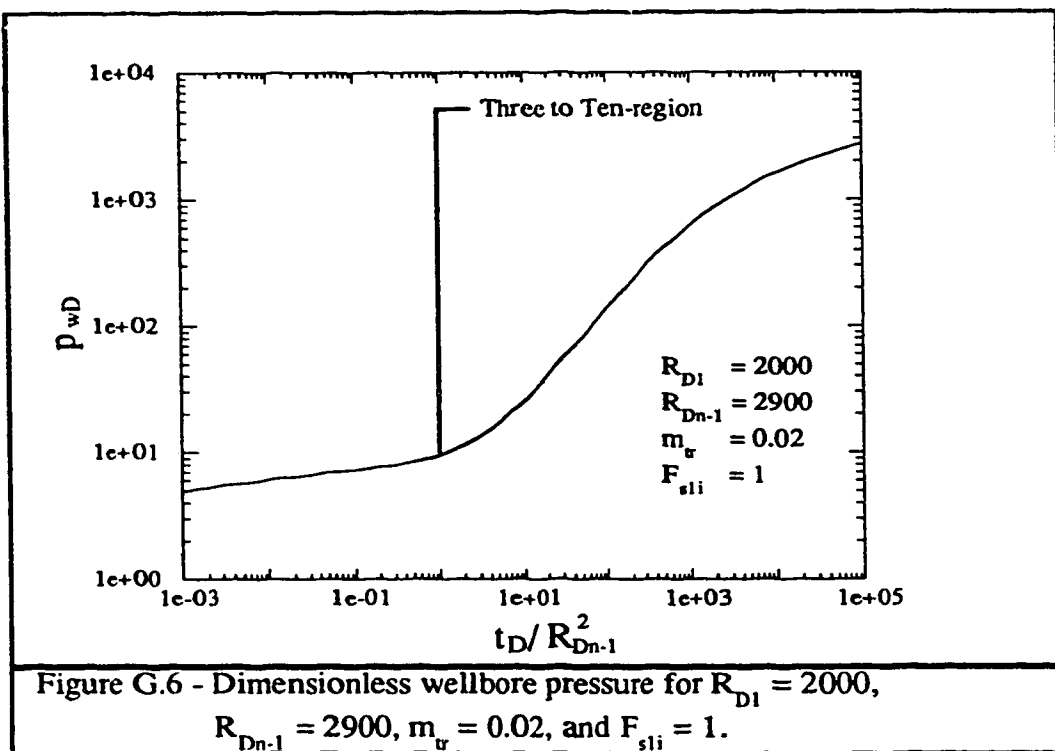
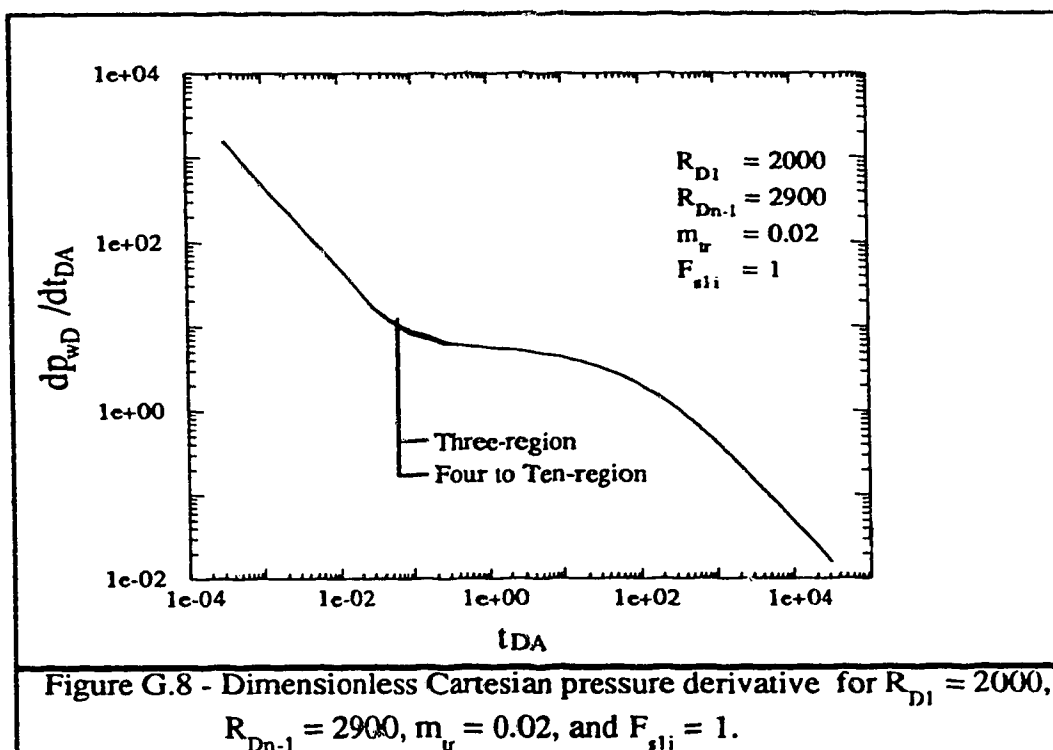
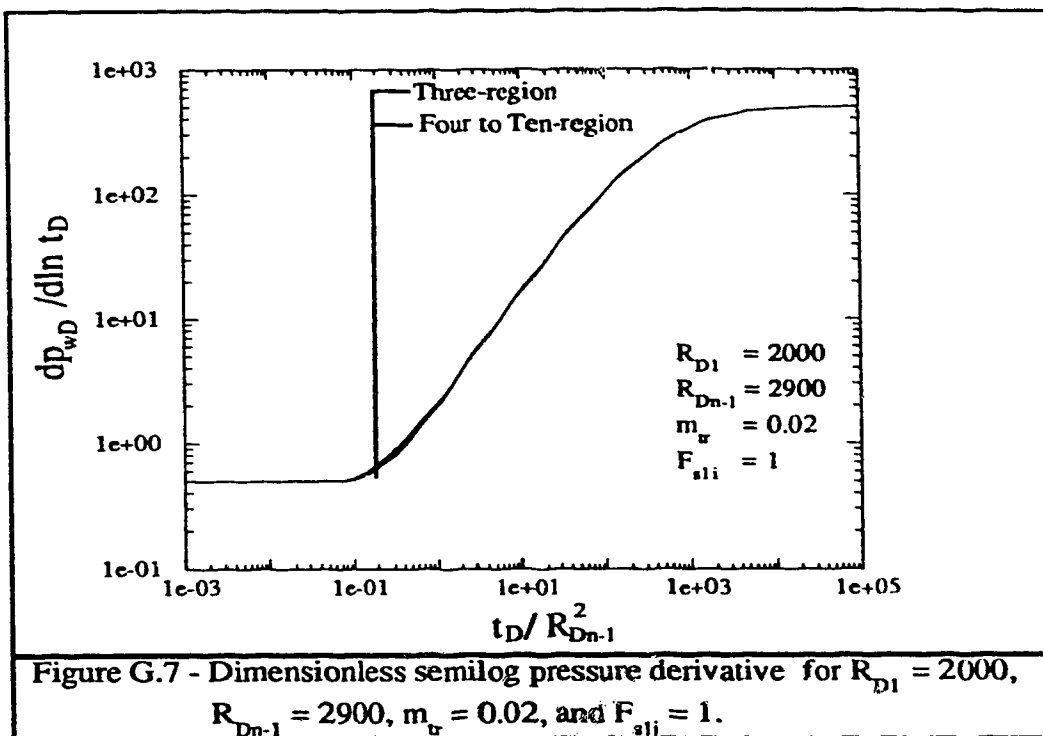
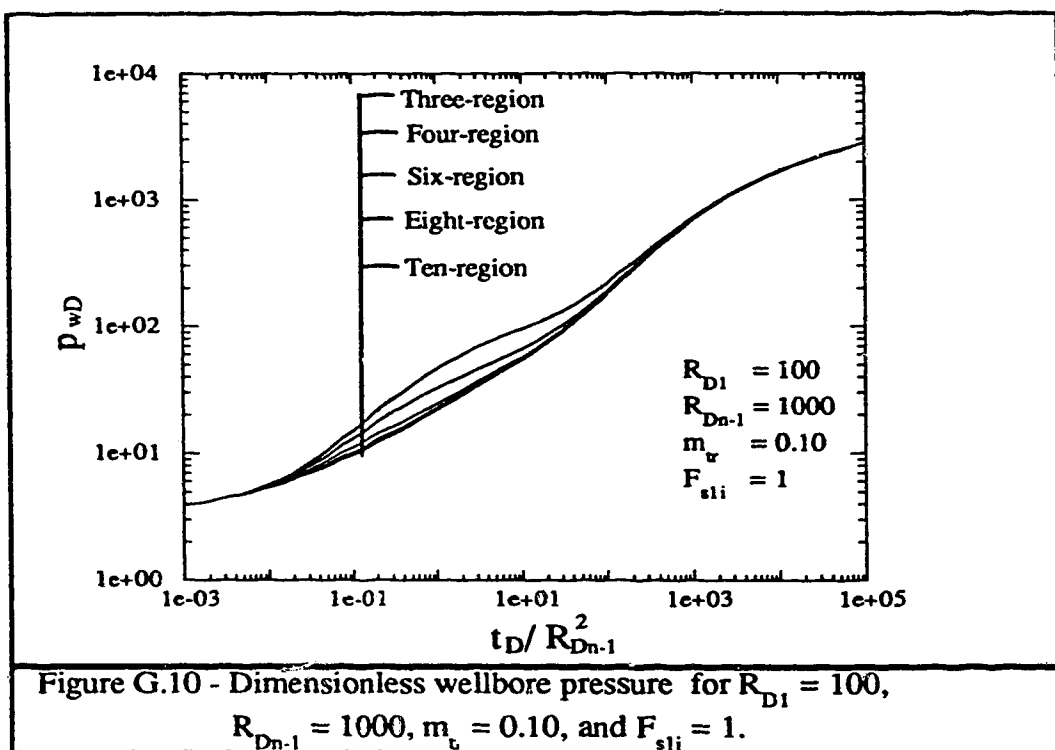
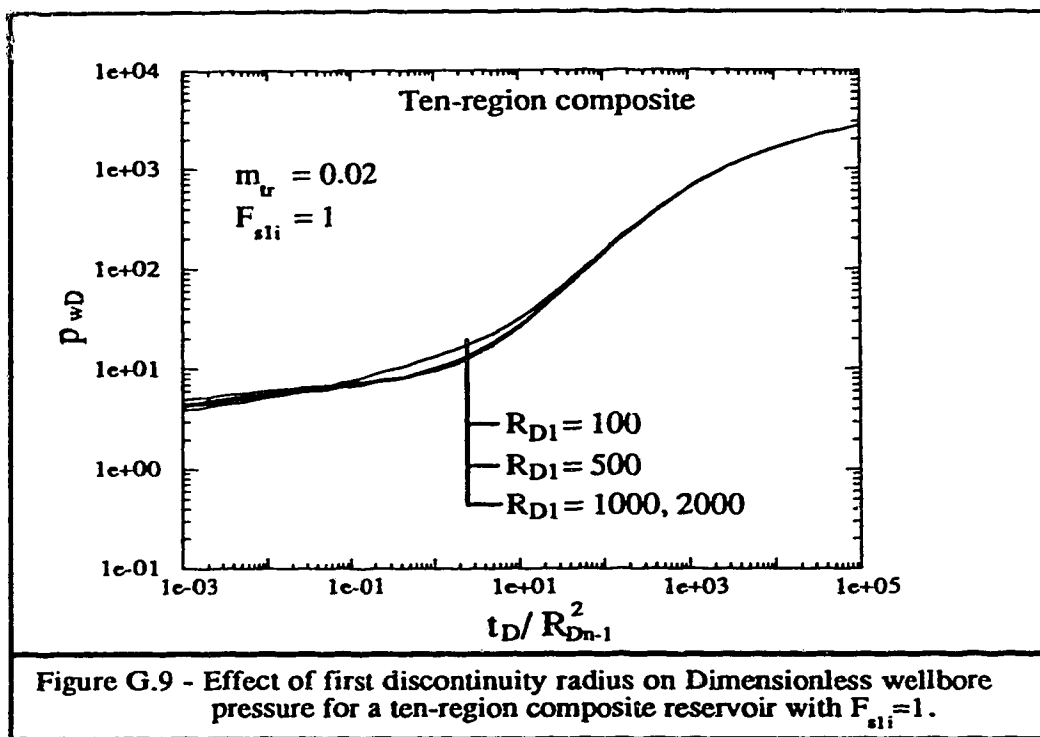
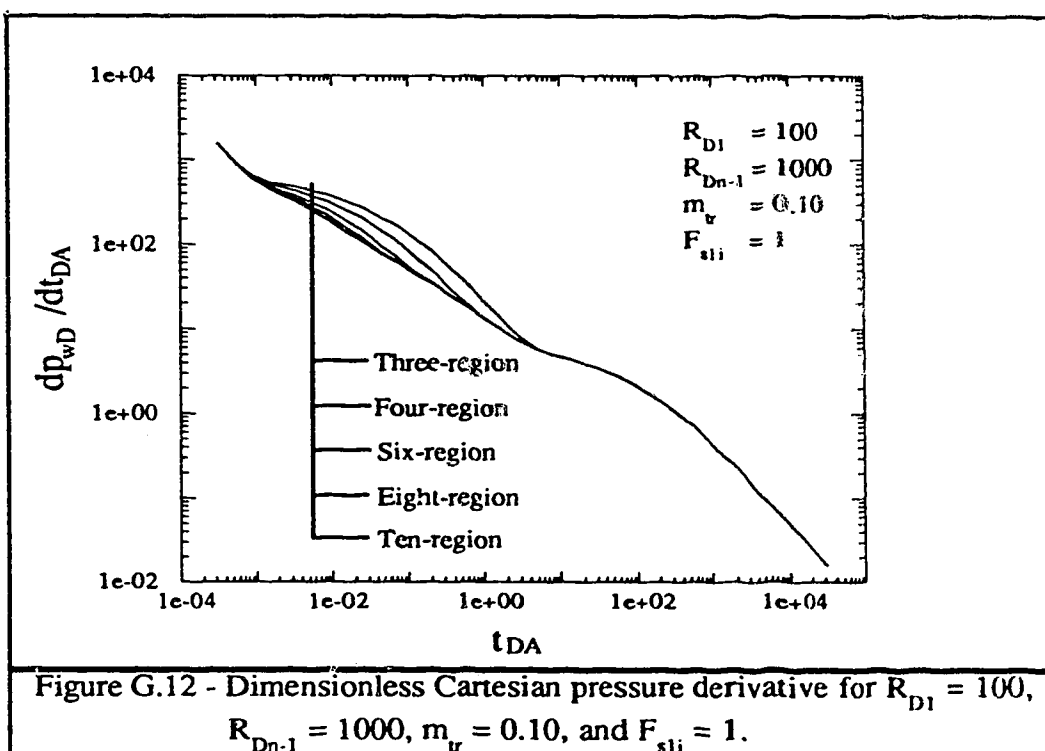
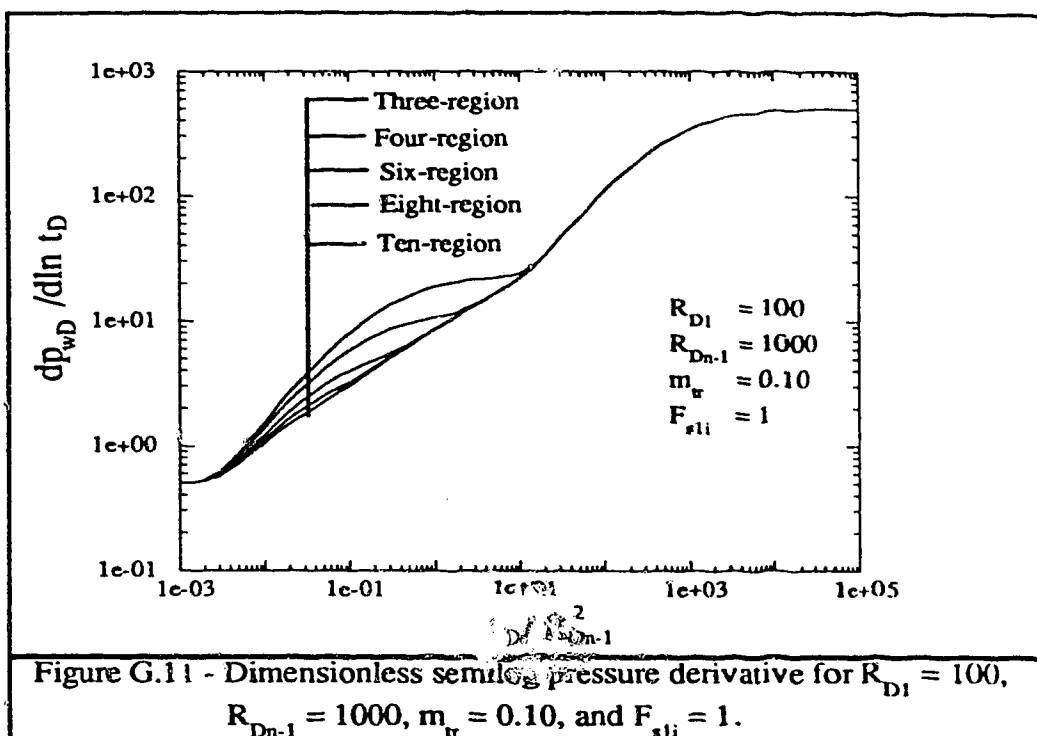
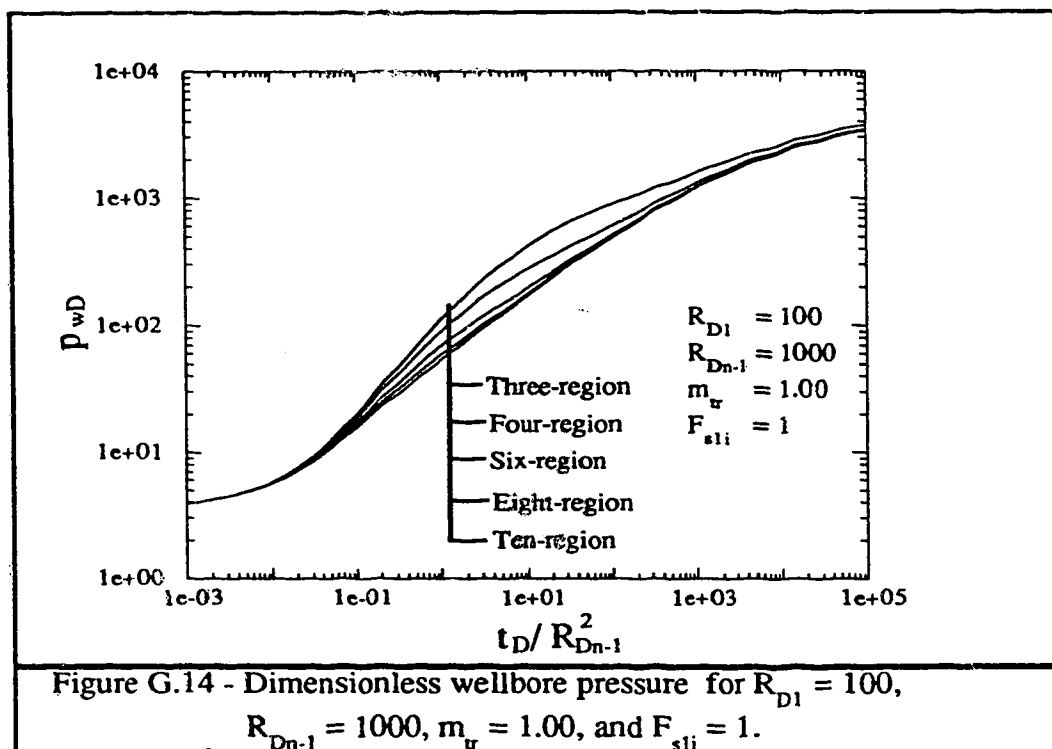
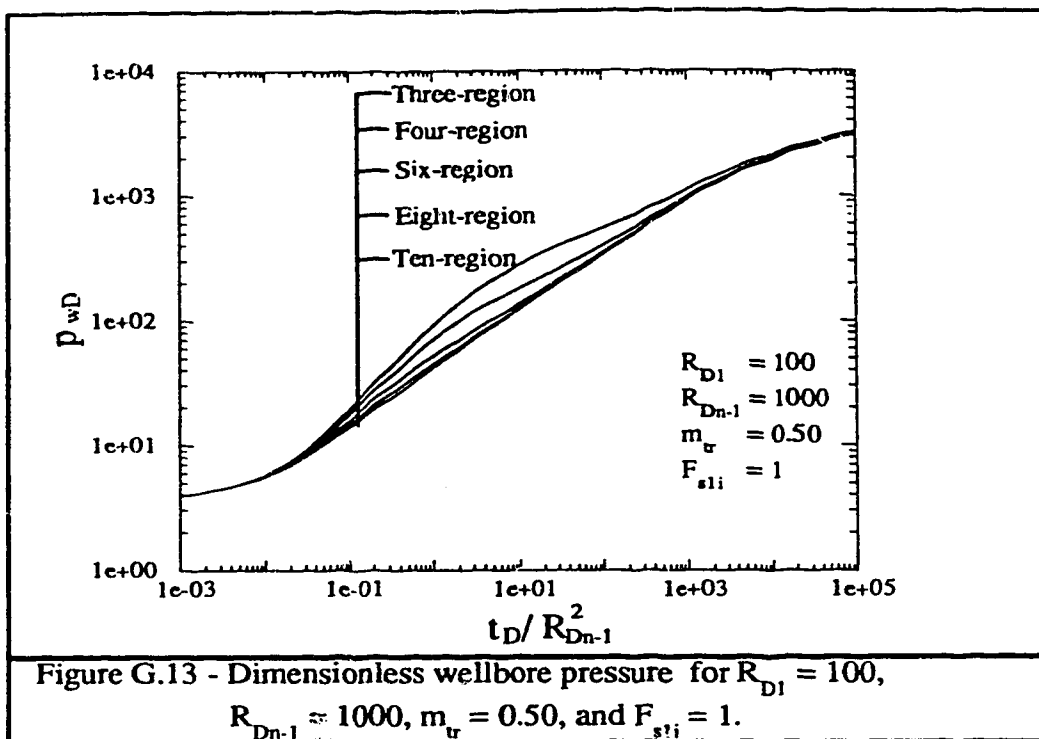


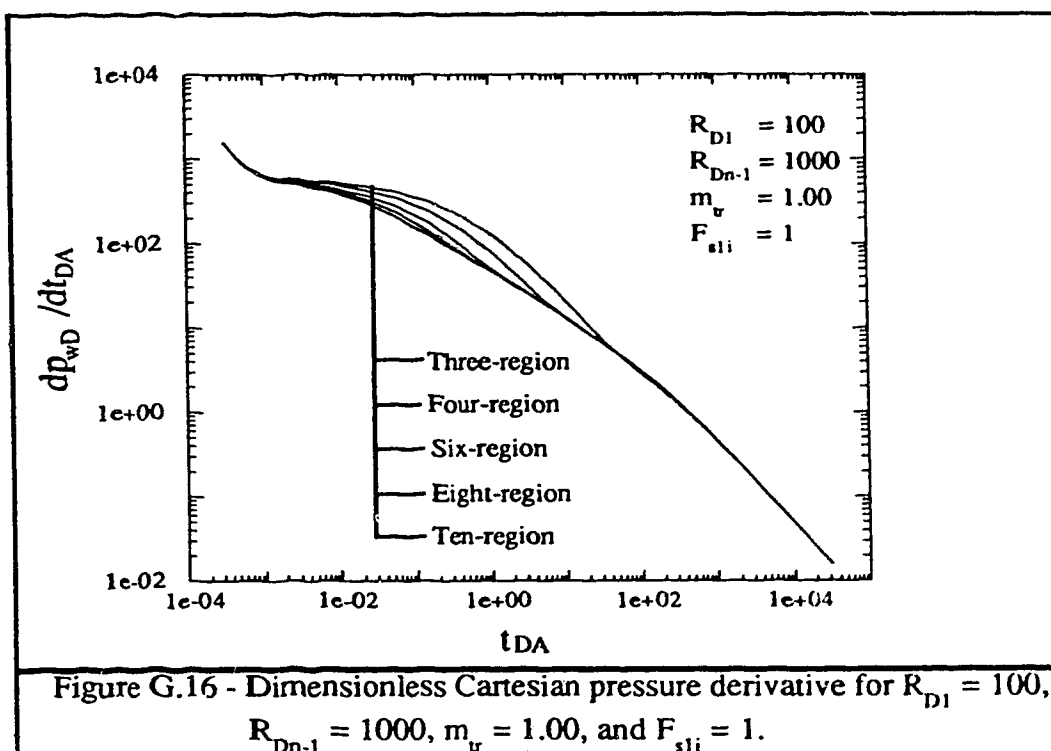
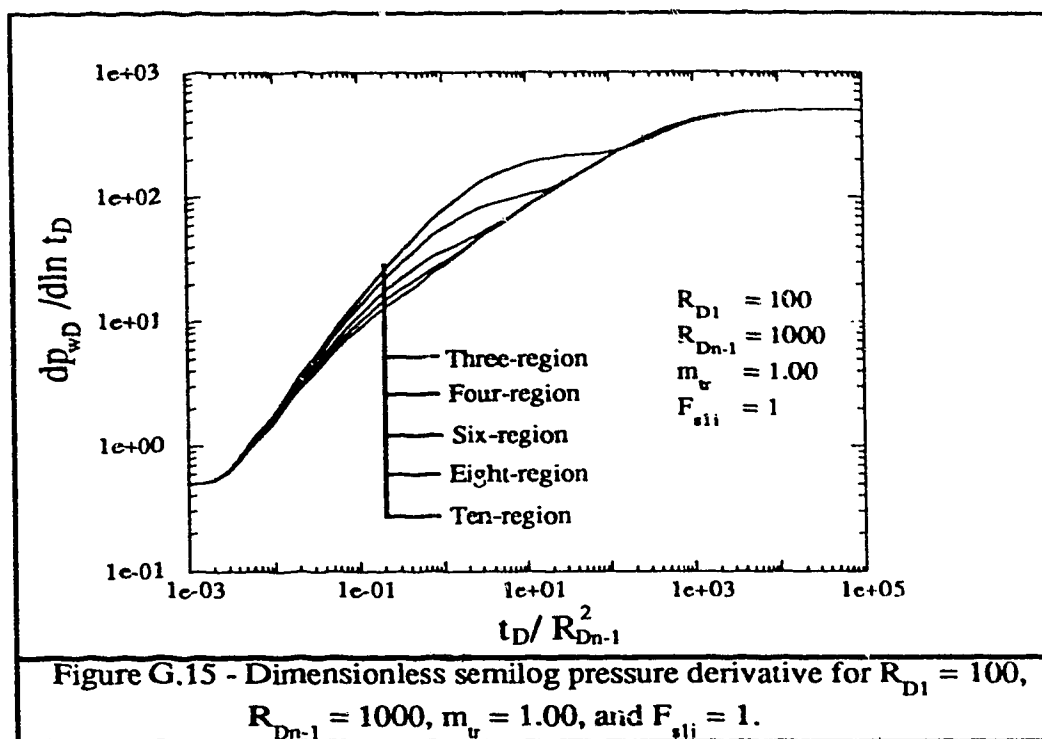
Figure G.6 - Dimensionless wellbore pressure for  $R_{D1} = 2000$ ,  $R_{Dn-1} = 2900$ ,  $m_u = 0.02$ , and  $F_{sli} = 1$ .



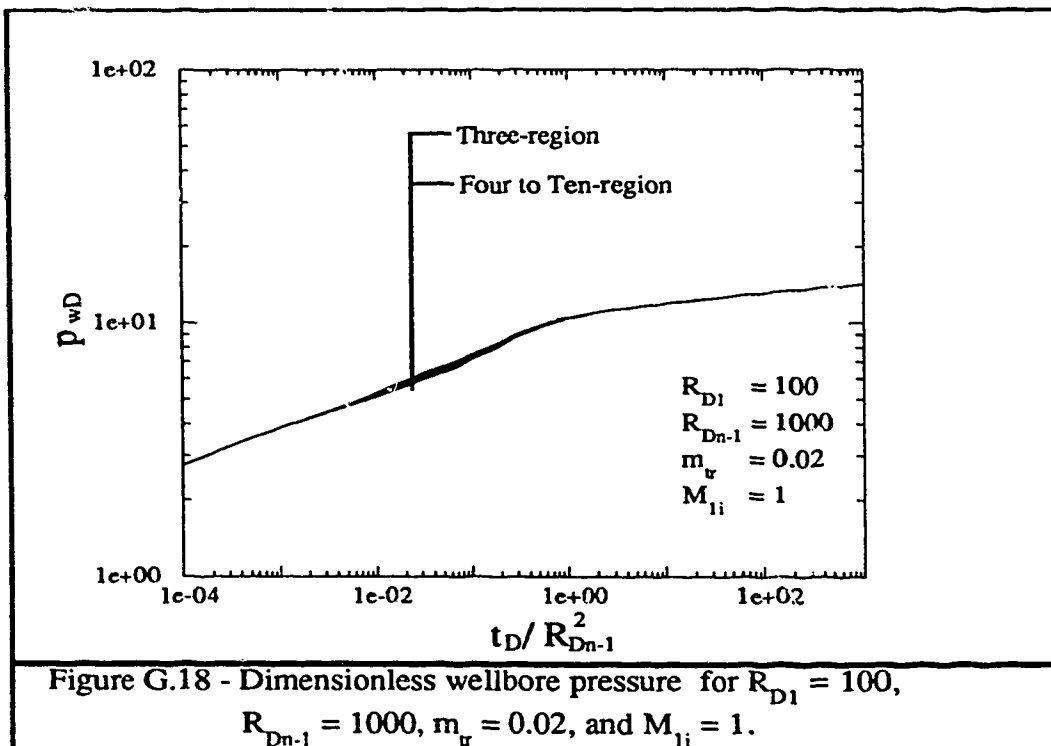
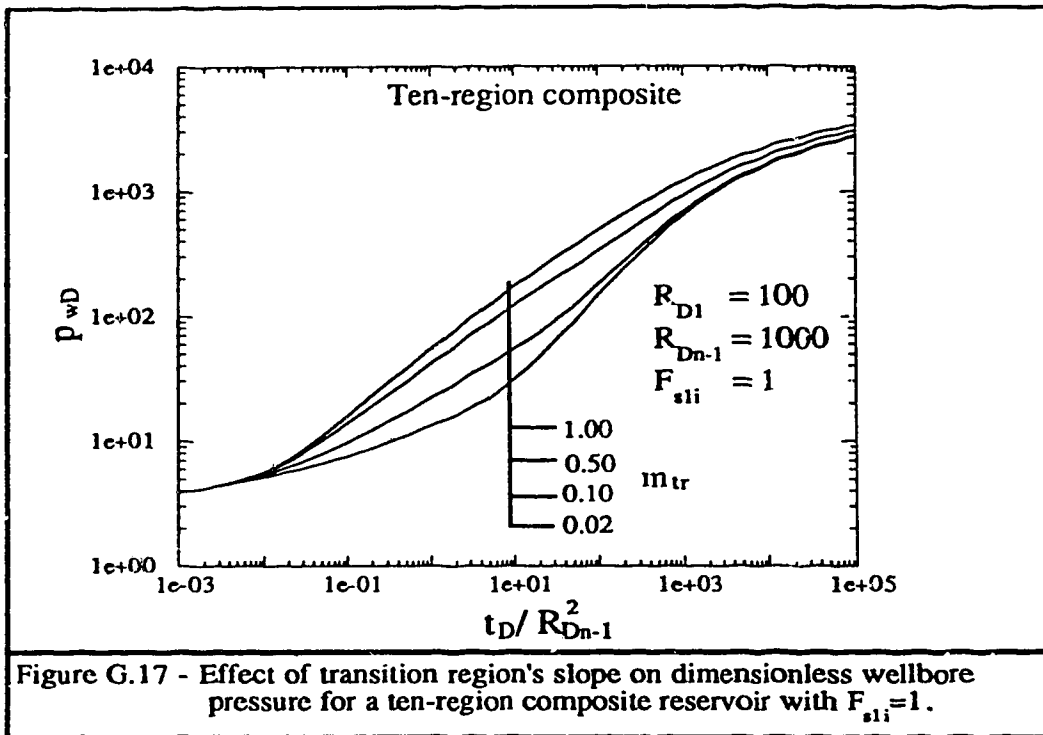












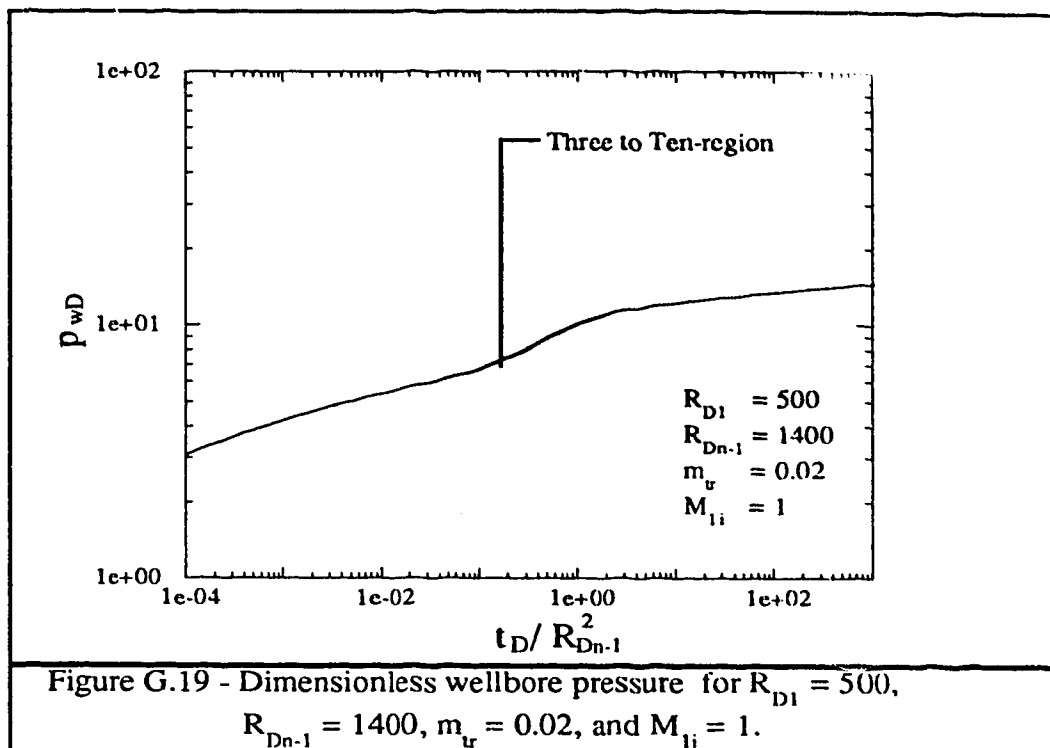


Figure G.19 - Dimensionless wellbore pressure for  $R_{D1} = 500$ ,  $R_{Dn-1} = 1400$ ,  $m_u = 0.02$ , and  $M_{li} = 1$ .

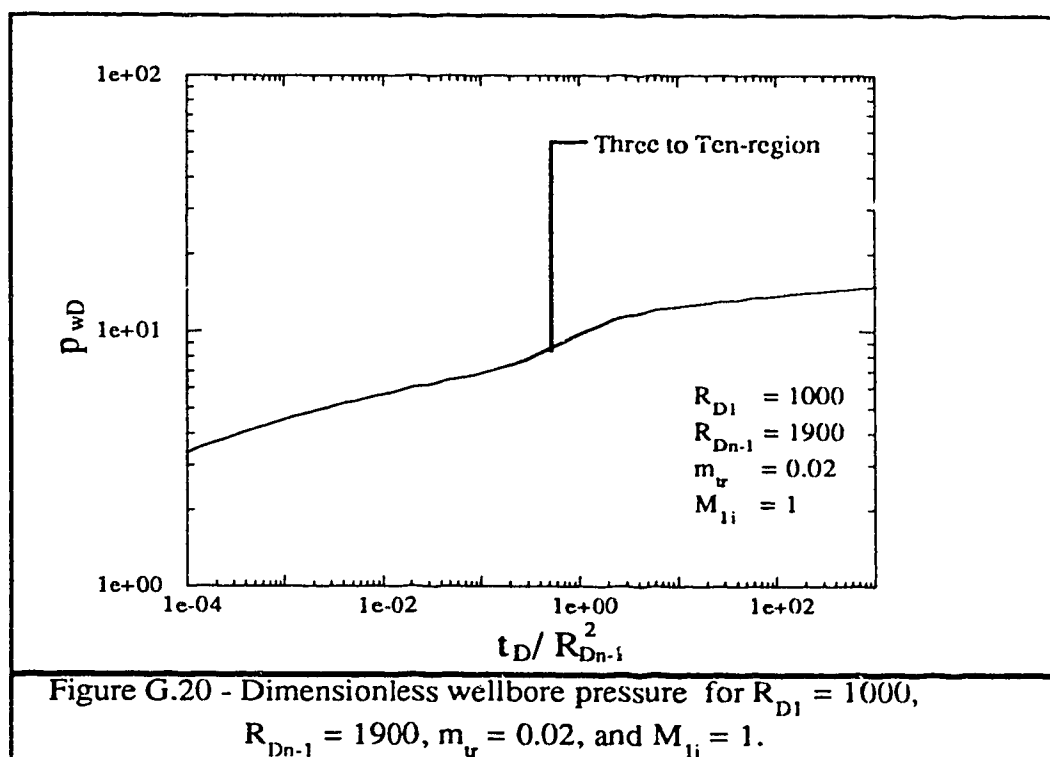
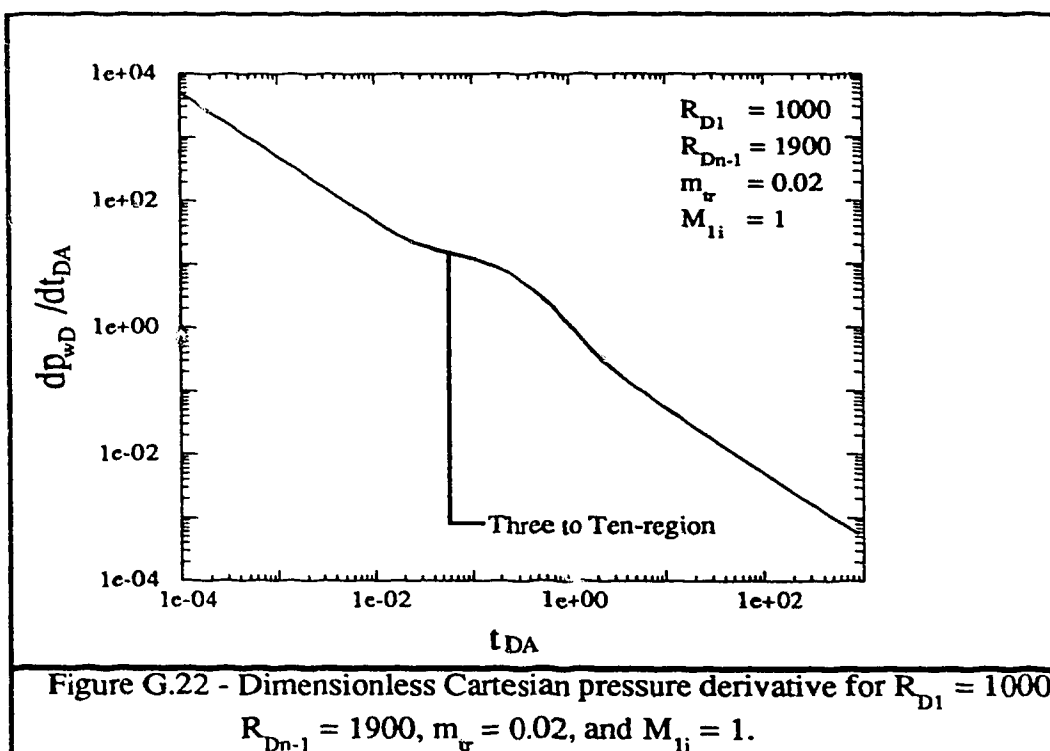
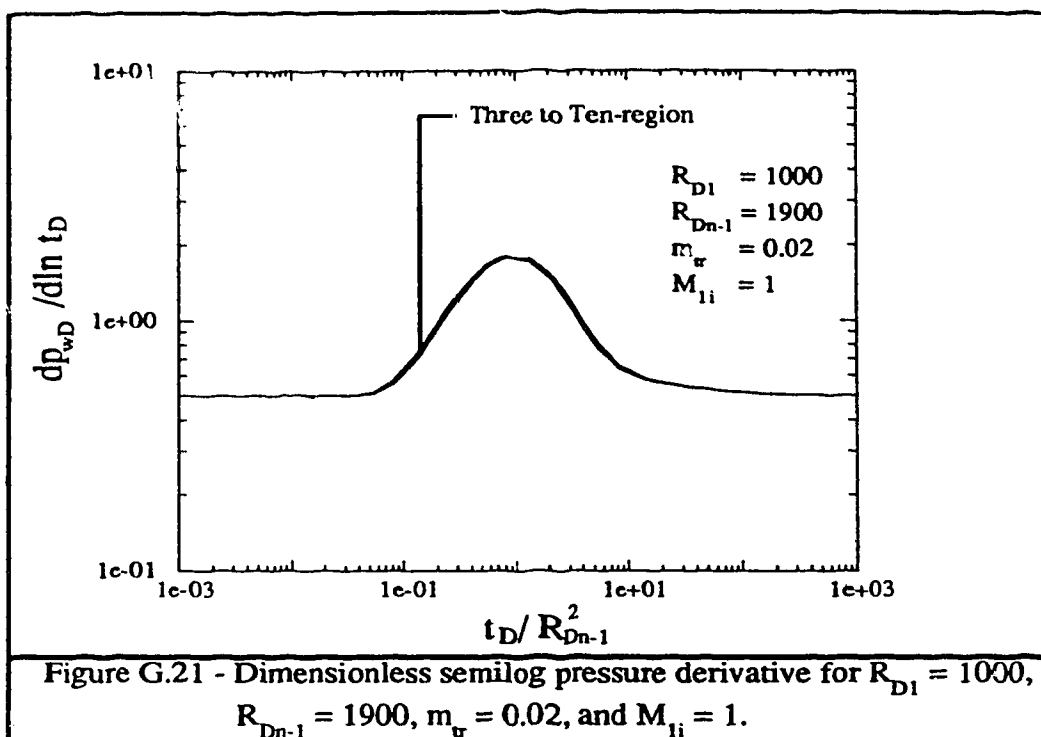
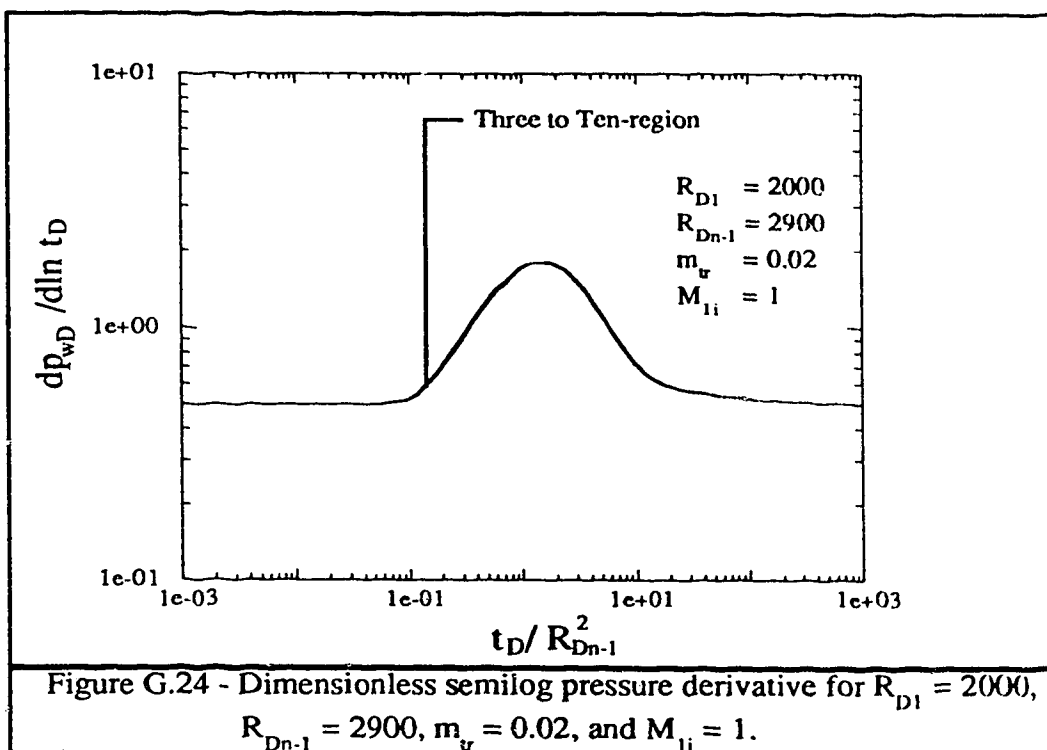
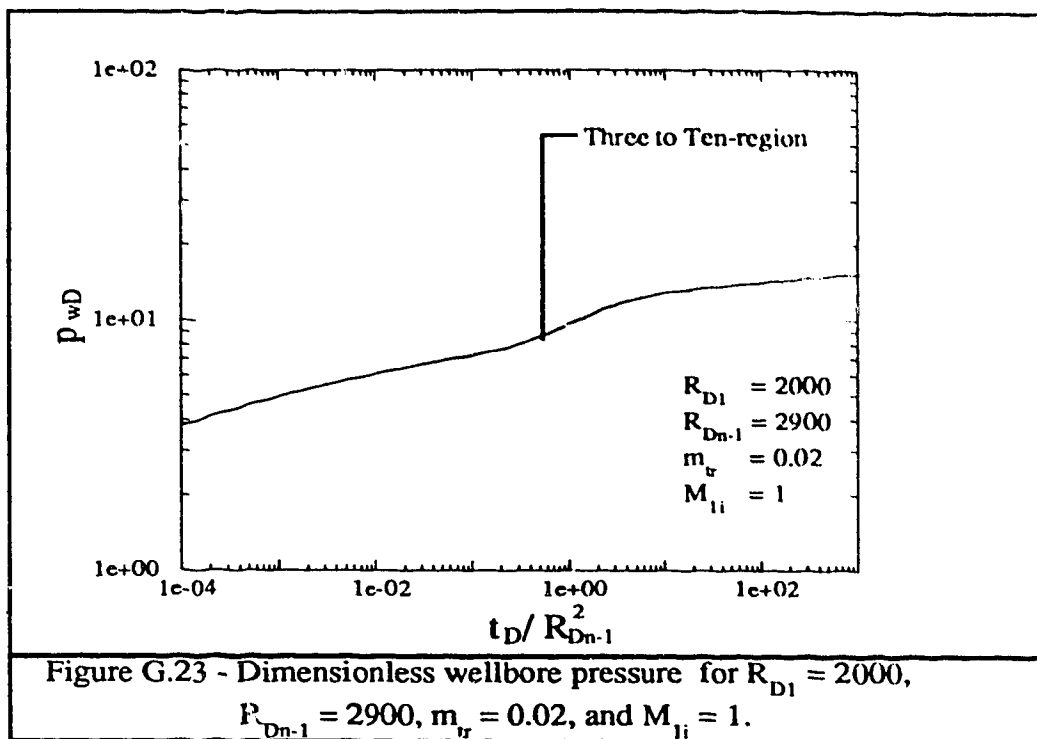
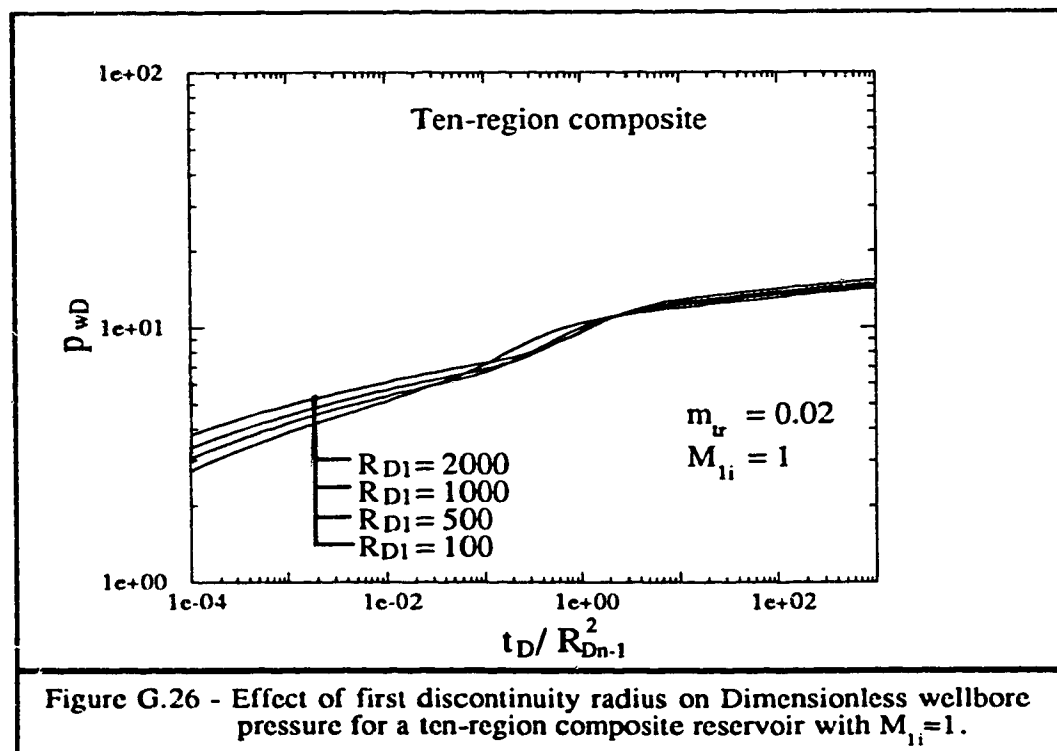
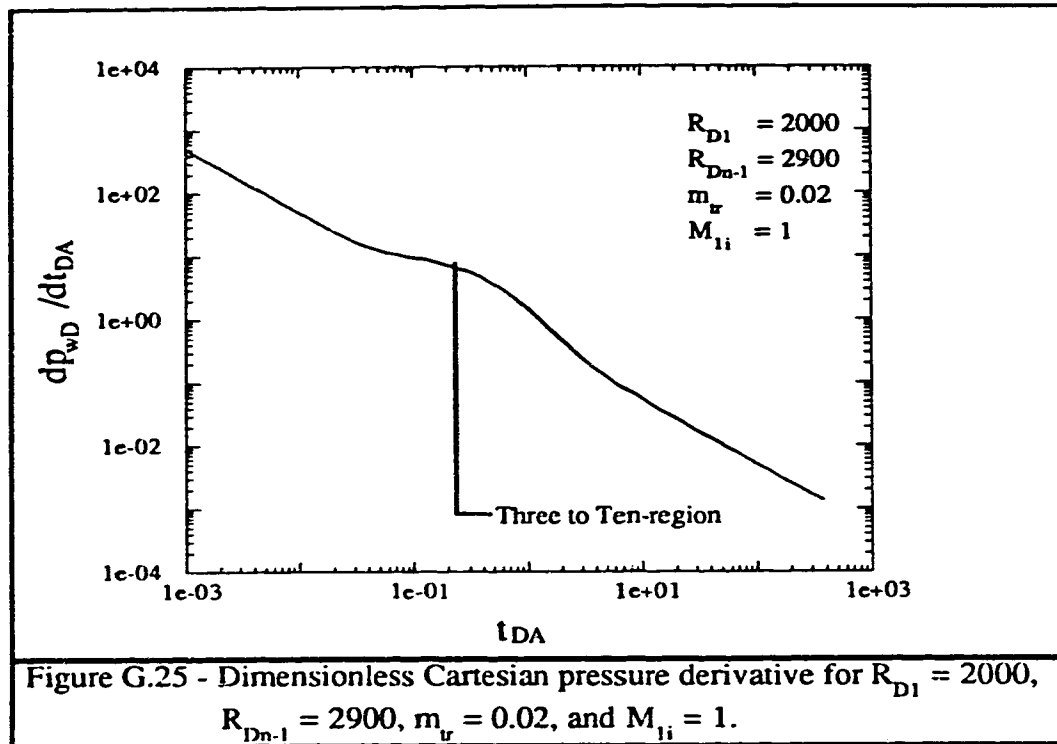
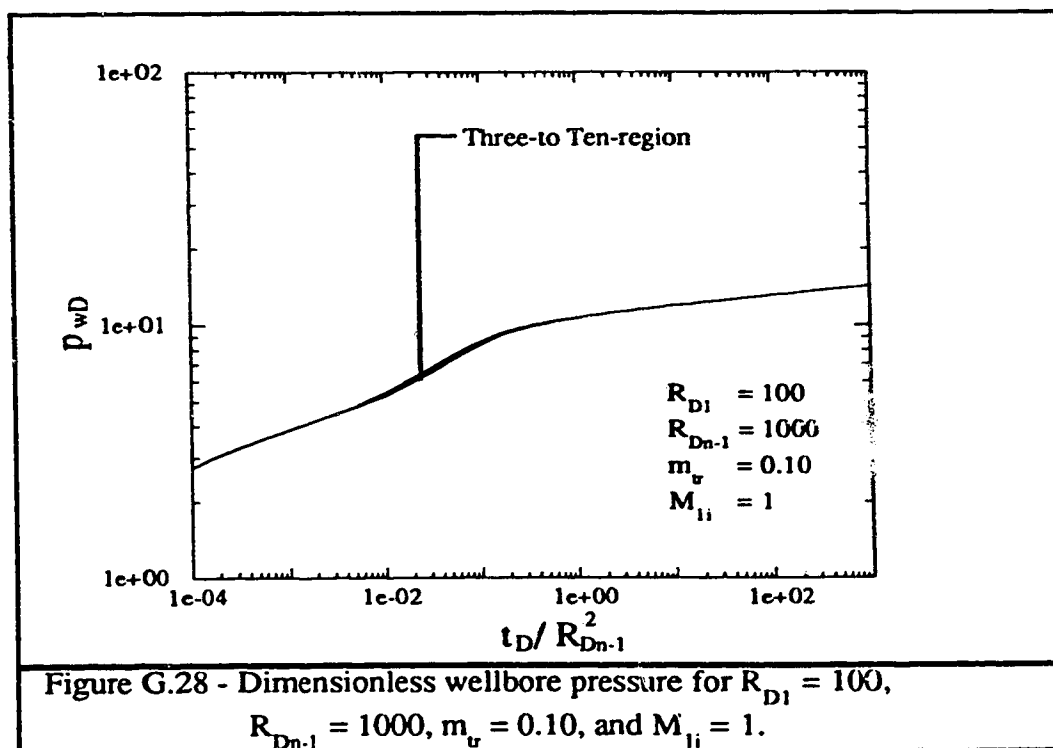
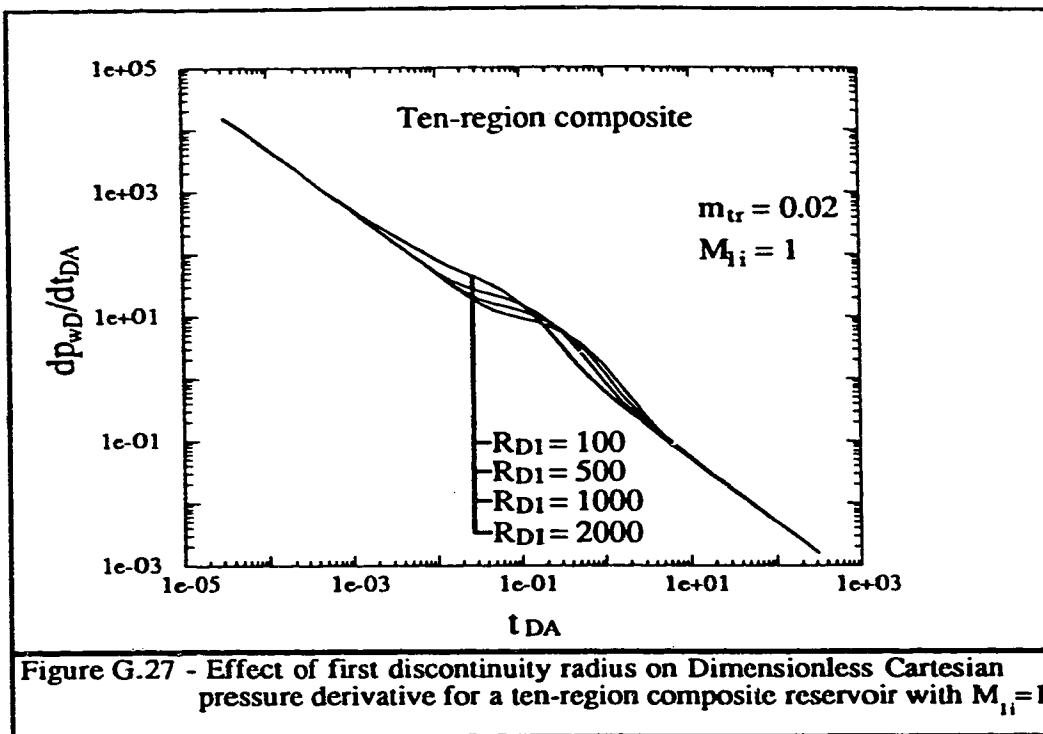


Figure G.20 - Dimensionless wellbore pressure for  $R_{D1} = 1000$ ,  $R_{Dn-1} = 1900$ ,  $m_u = 0.02$ , and  $M_{li} = 1$ .









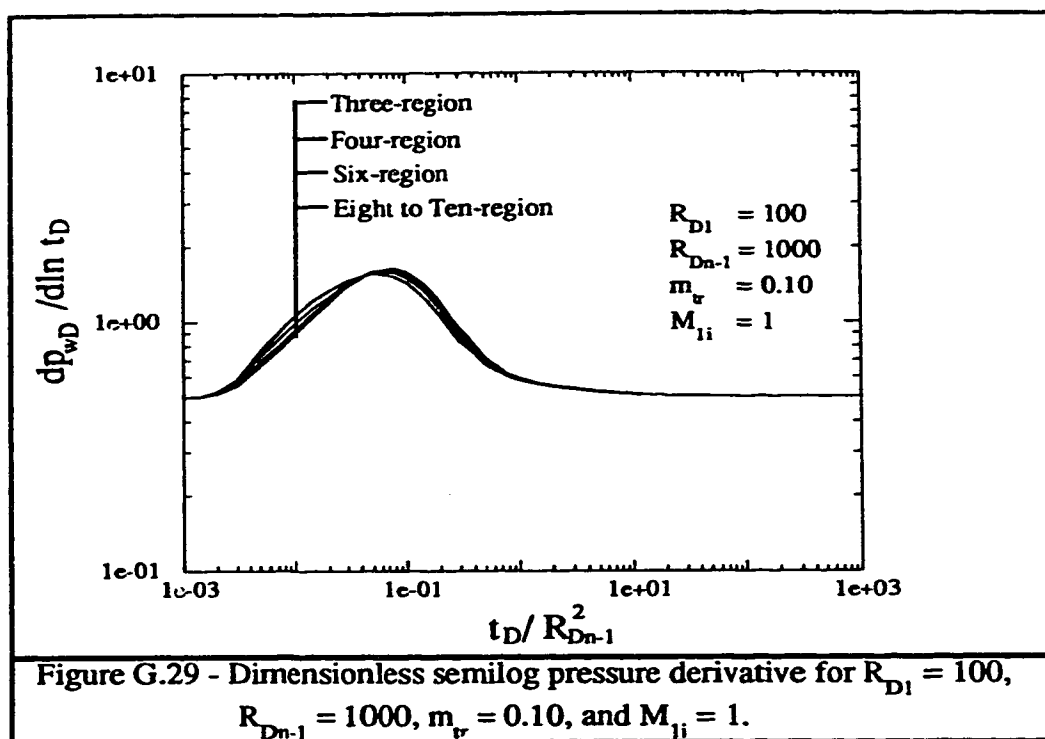


Figure G.29 - Dimensionless semilog pressure derivative for  $R_{D1} = 100$ ,  $R_{Dn-1} = 1000$ ,  $m_v = 0.10$ , and  $M_{li} = 1$ .

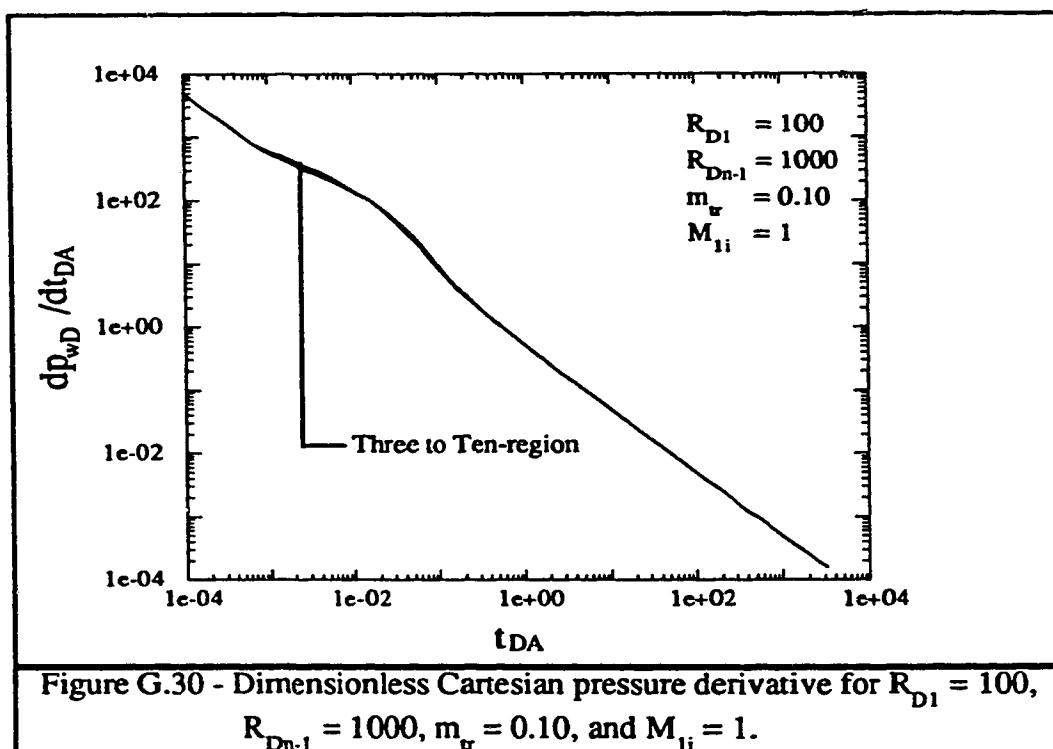
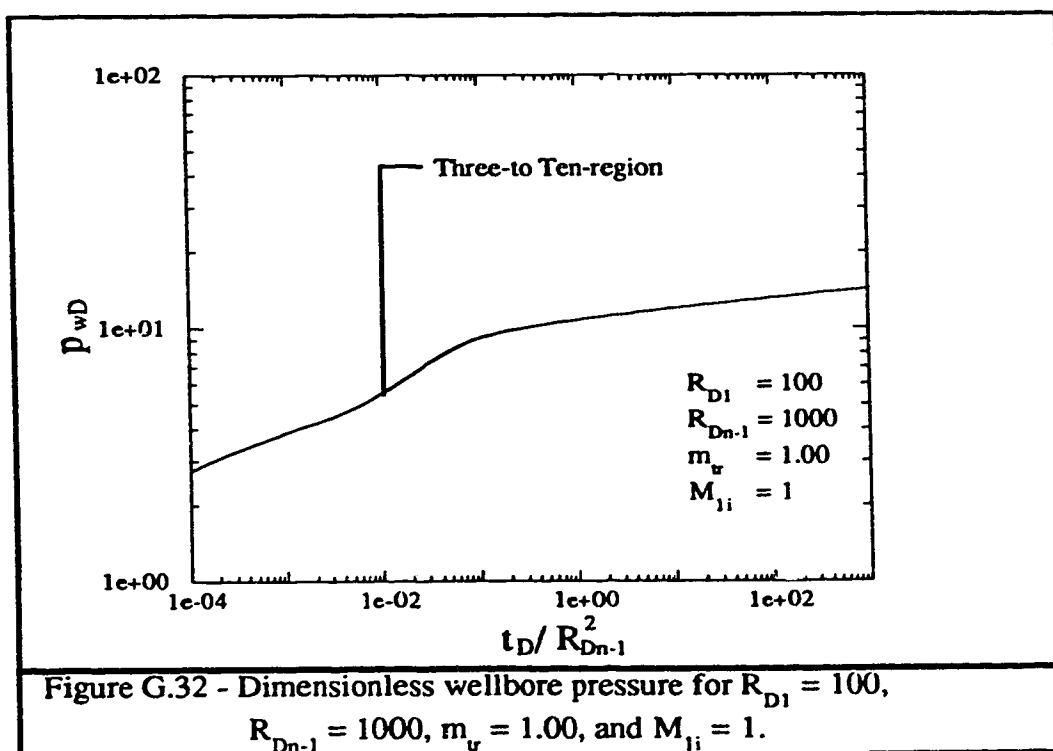
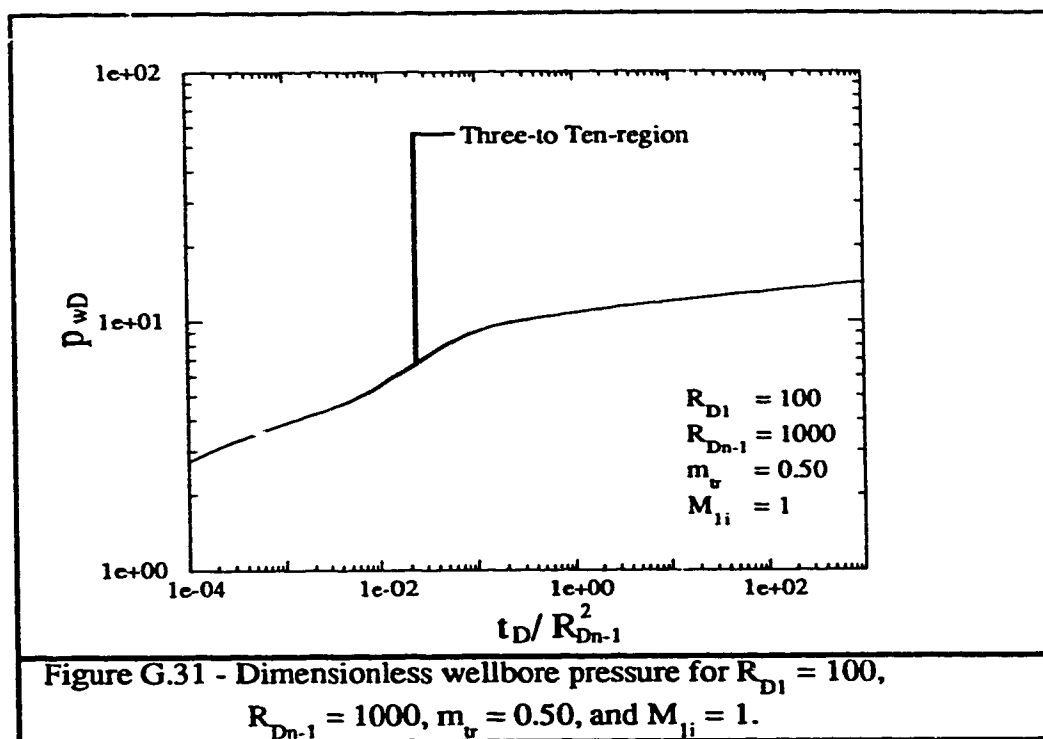
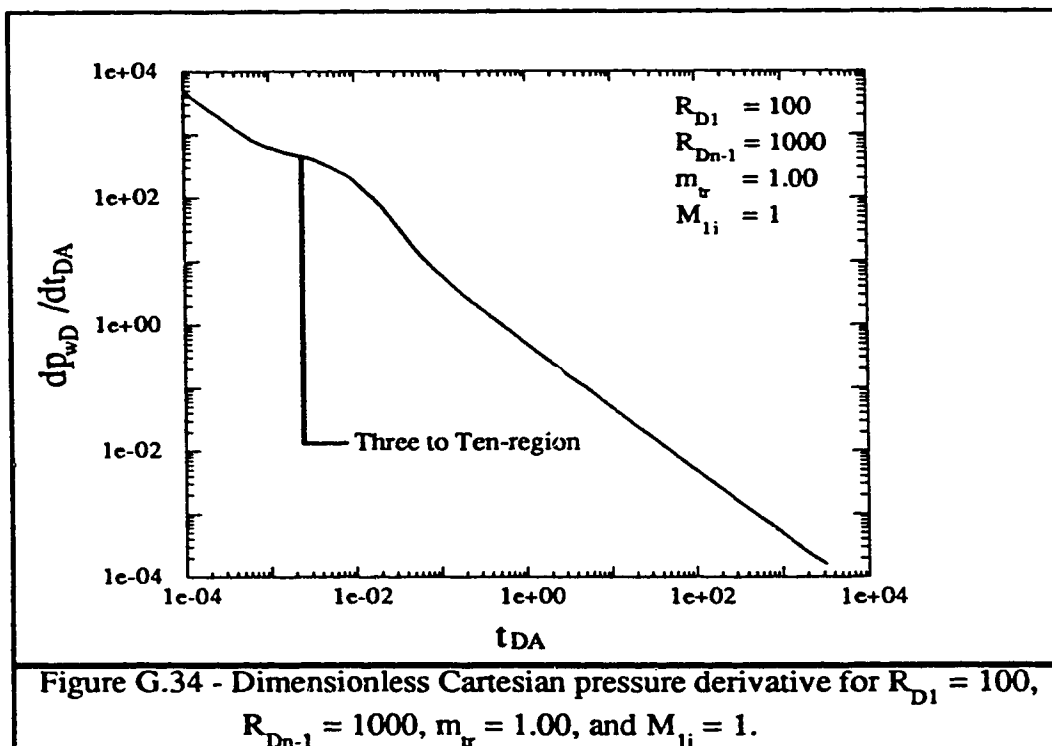
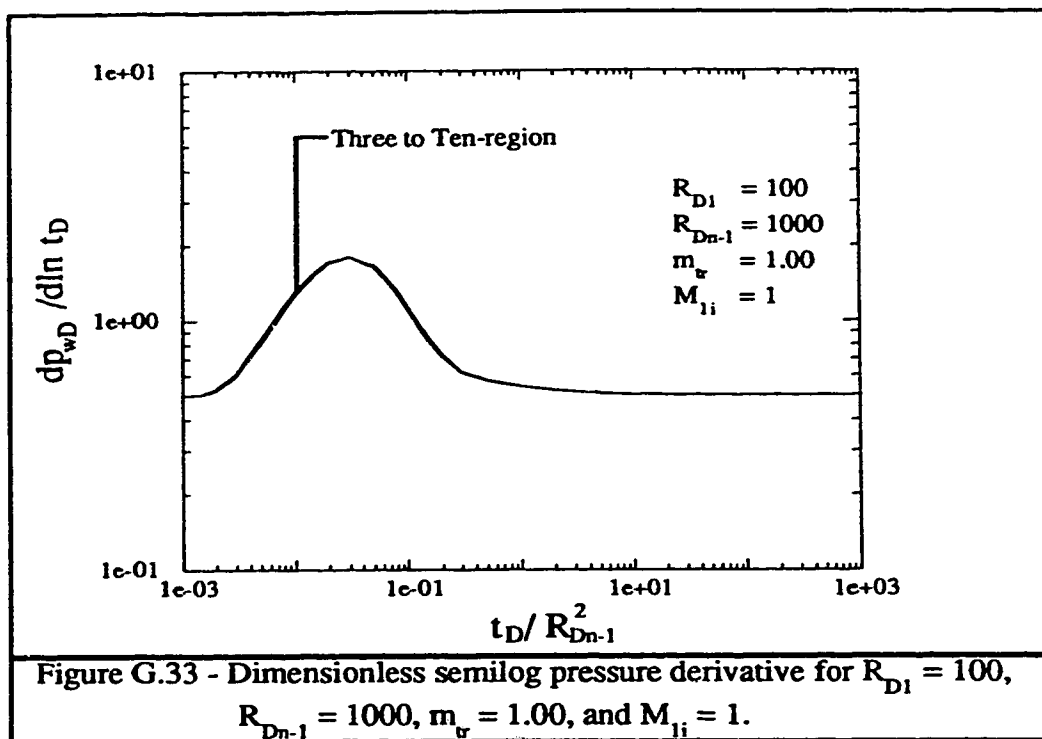
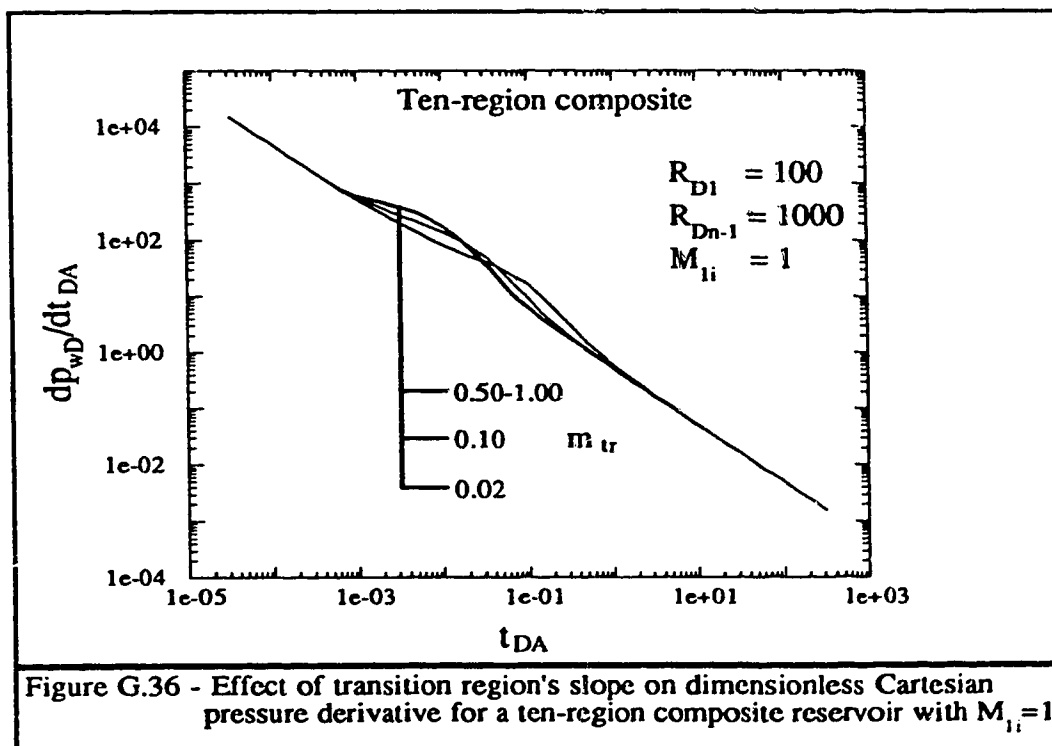
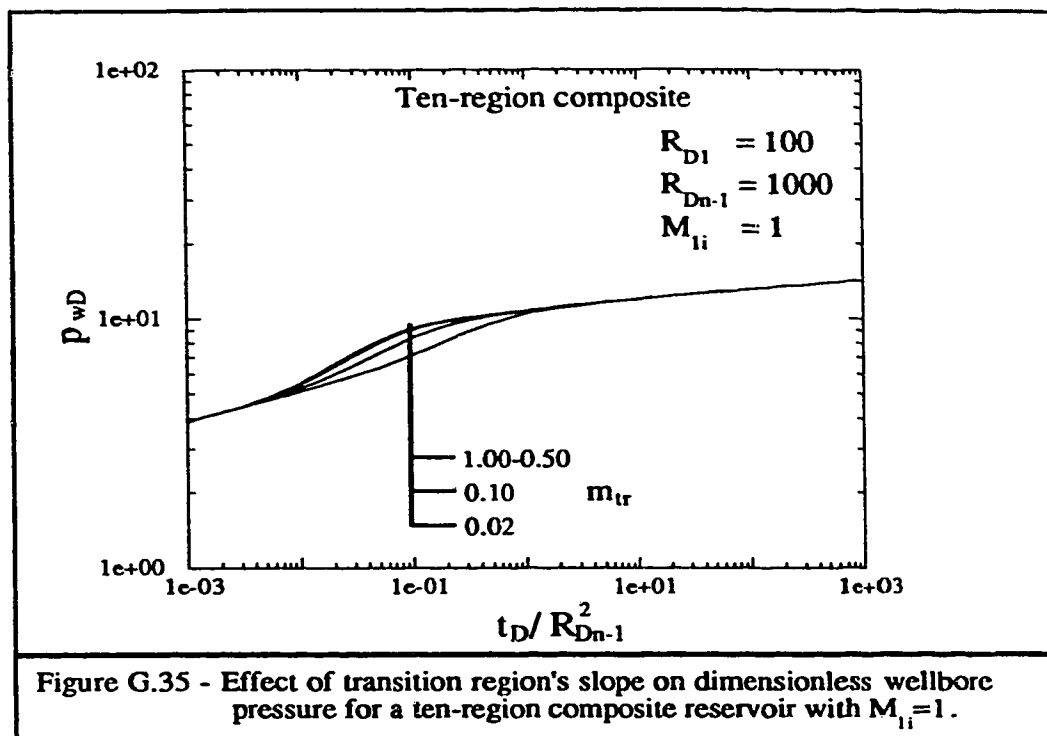


Figure G.30 - Dimensionless Cartesian pressure derivative for  $R_{D1} = 100$ ,  $R_{Dn-1} = 1000$ ,  $m_v = 0.10$ , and  $M_{li} = 1$ .









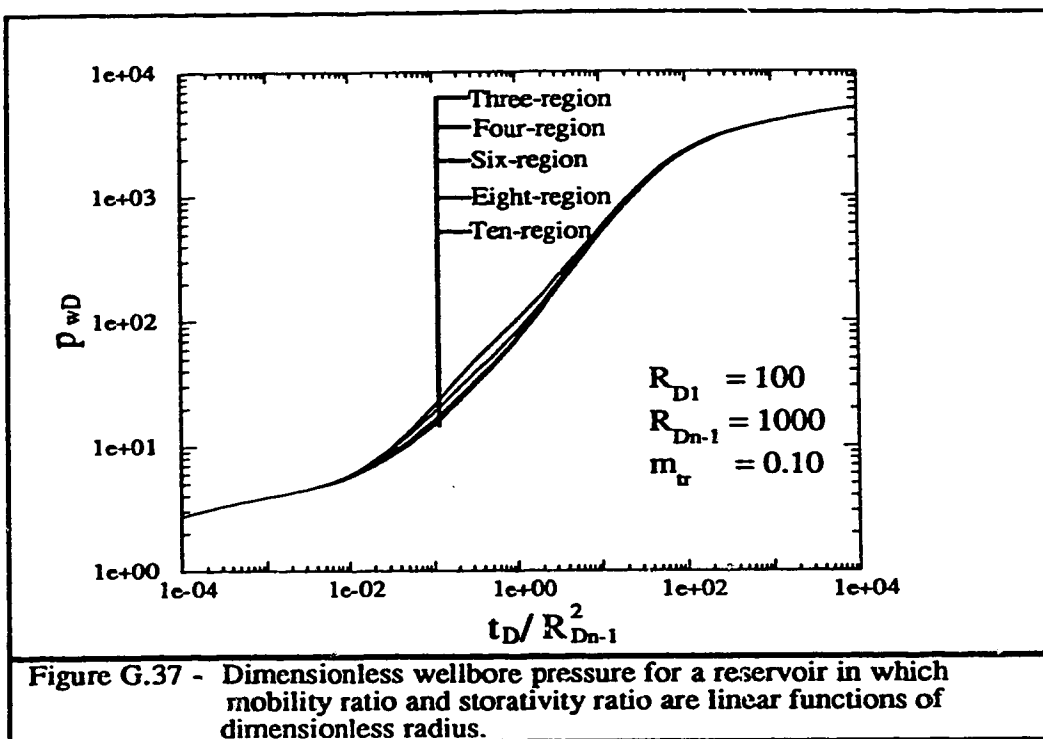


Figure G.37 - Dimensionless wellbore pressure for a reservoir in which mobility ratio and storativity ratio are linear functions of dimensionless radius.

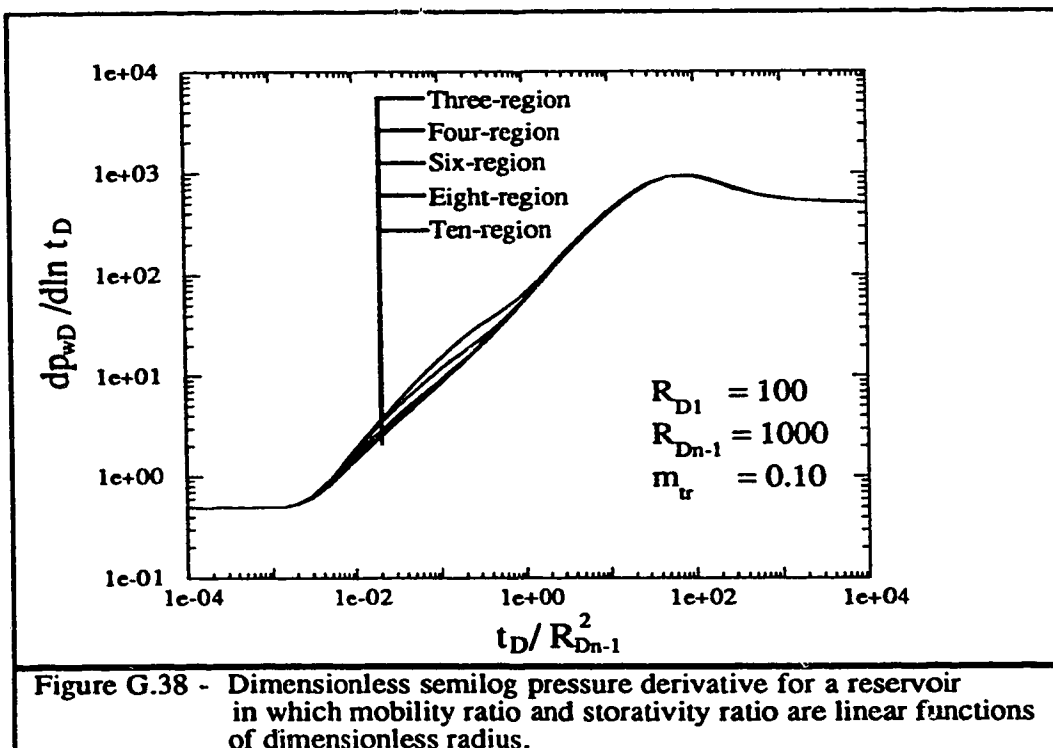


Figure G.38 - Dimensionless semilog pressure derivative for a reservoir in which mobility ratio and storativity ratio are linear functions of dimensionless radius.

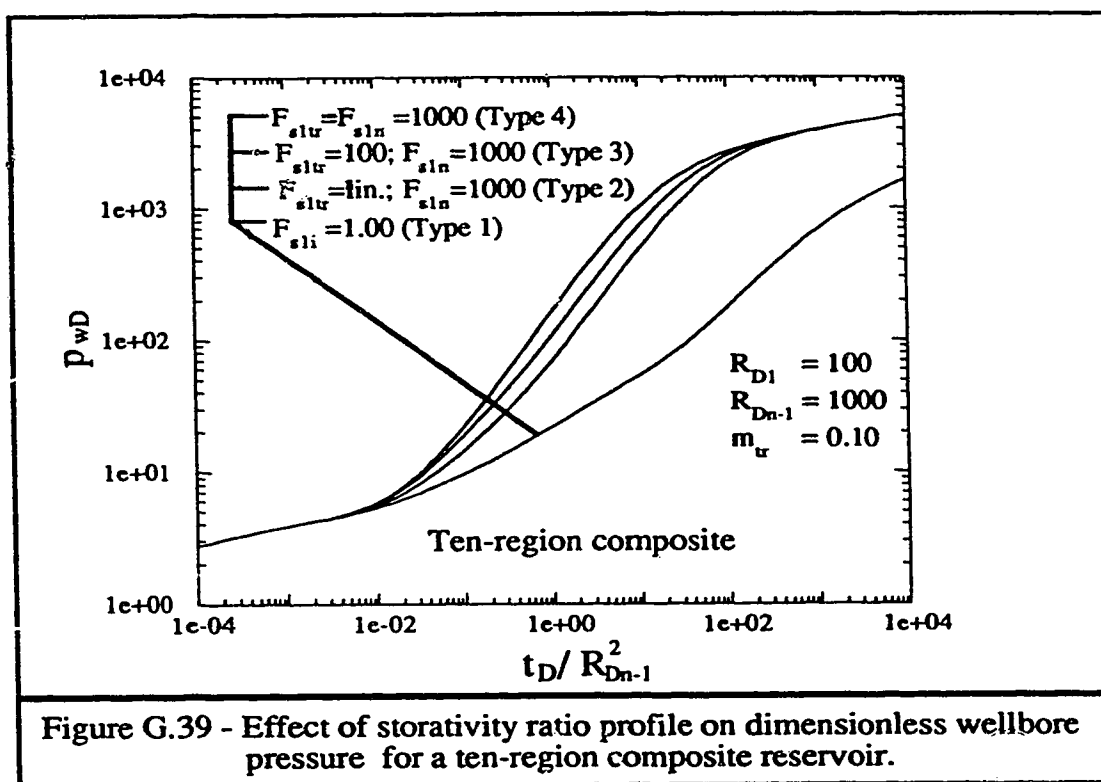


Figure G.39 - Effect of storativity ratio profile on dimensionless wellbore pressure for a ten-region composite reservoir.

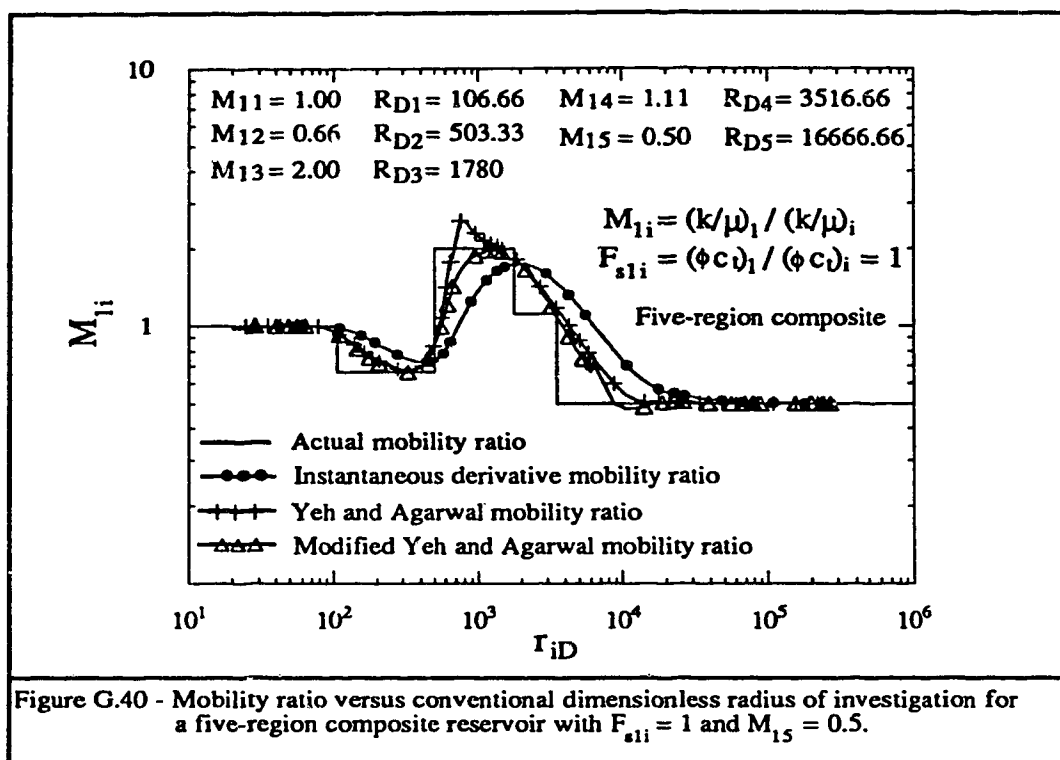


Figure G.40 - Mobility ratio versus conventional dimensionless radius of investigation for a five-region composite reservoir with  $F_{s1i} = 1$  and  $M_{15} = 0.5$ .

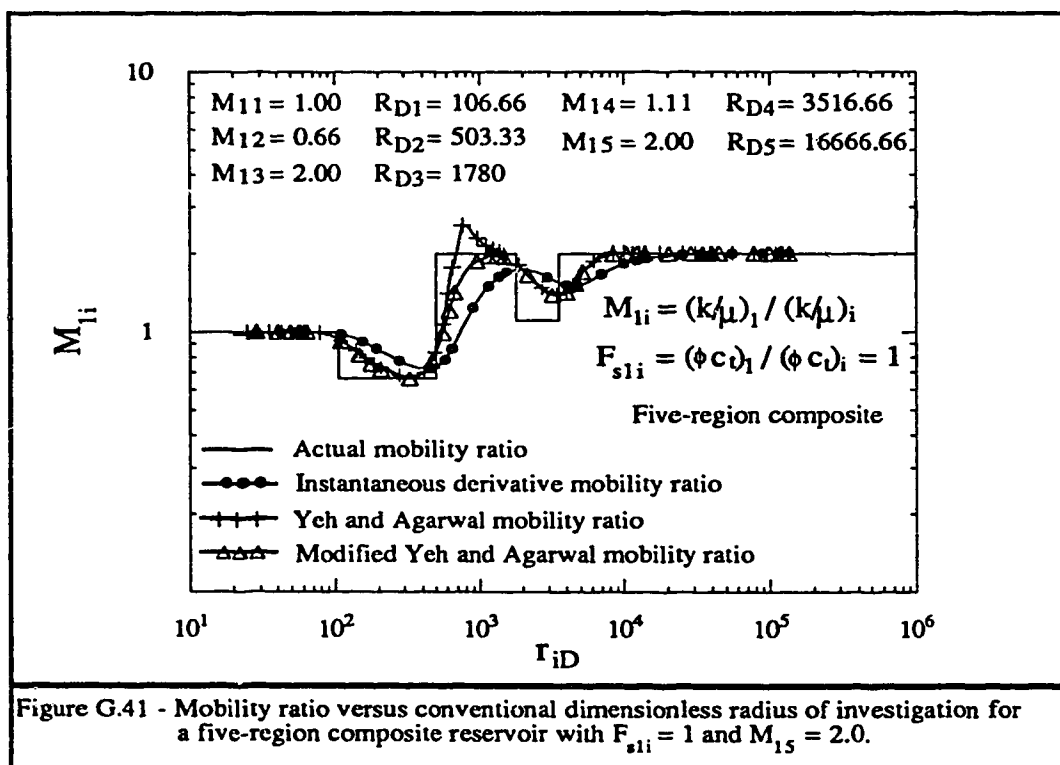


Figure G.41 - Mobility ratio versus conventional dimensionless radius of investigation for a five-region composite reservoir with  $F_{s1i} = 1$  and  $M_{15} = 2.0$ .

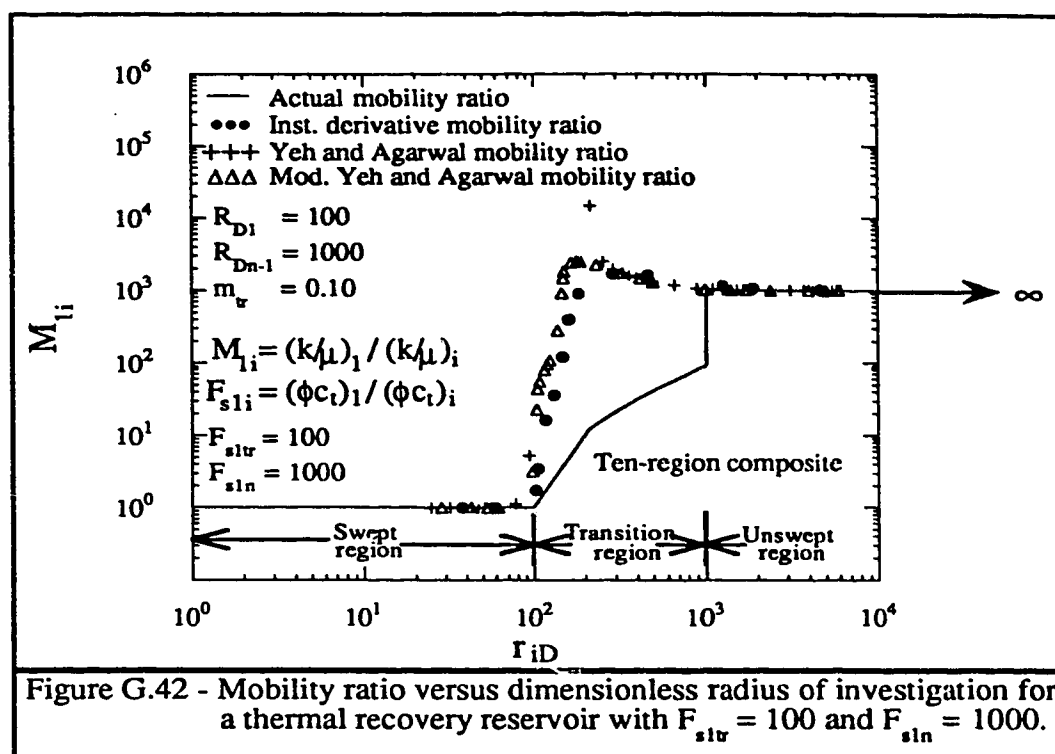


Figure G.42 - Mobility ratio versus dimensionless radius of investigation for a thermal recovery reservoir with  $F_{str} = 100$  and  $F_{sln} = 1000$ .

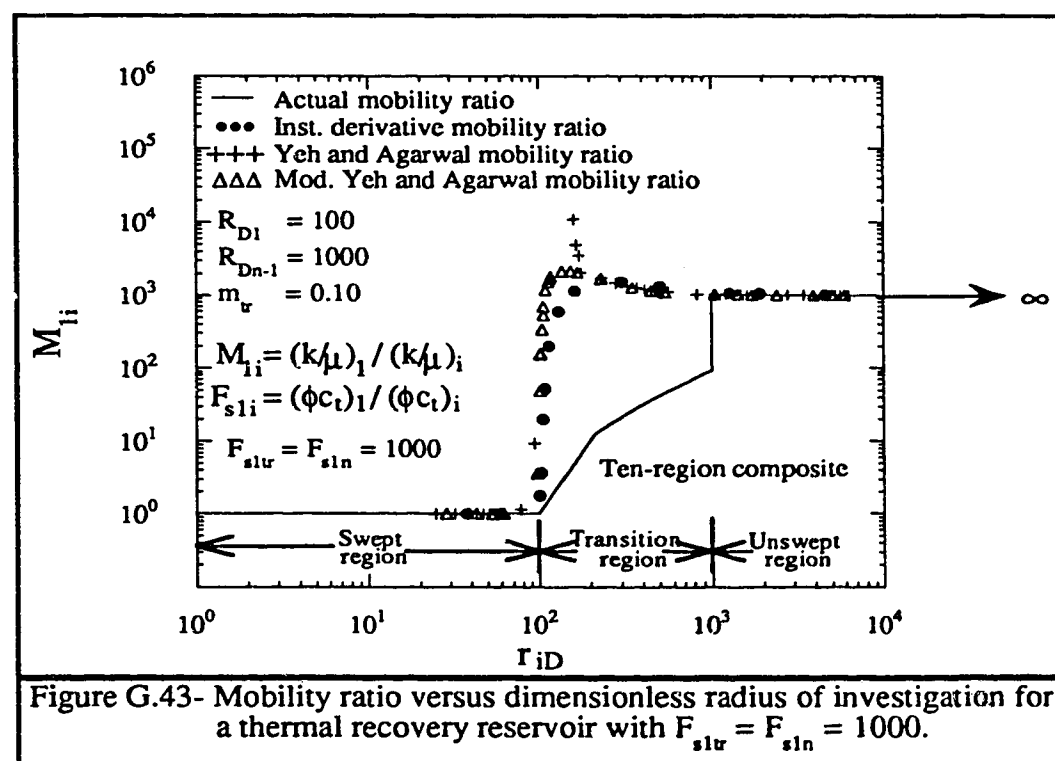


Figure G.43- Mobility ratio versus dimensionless radius of investigation for a thermal recovery reservoir with  $F_{str} = F_{sln} = 1000$ .